FACULTY OF ENGINEERING
AND ARCHITECTURE

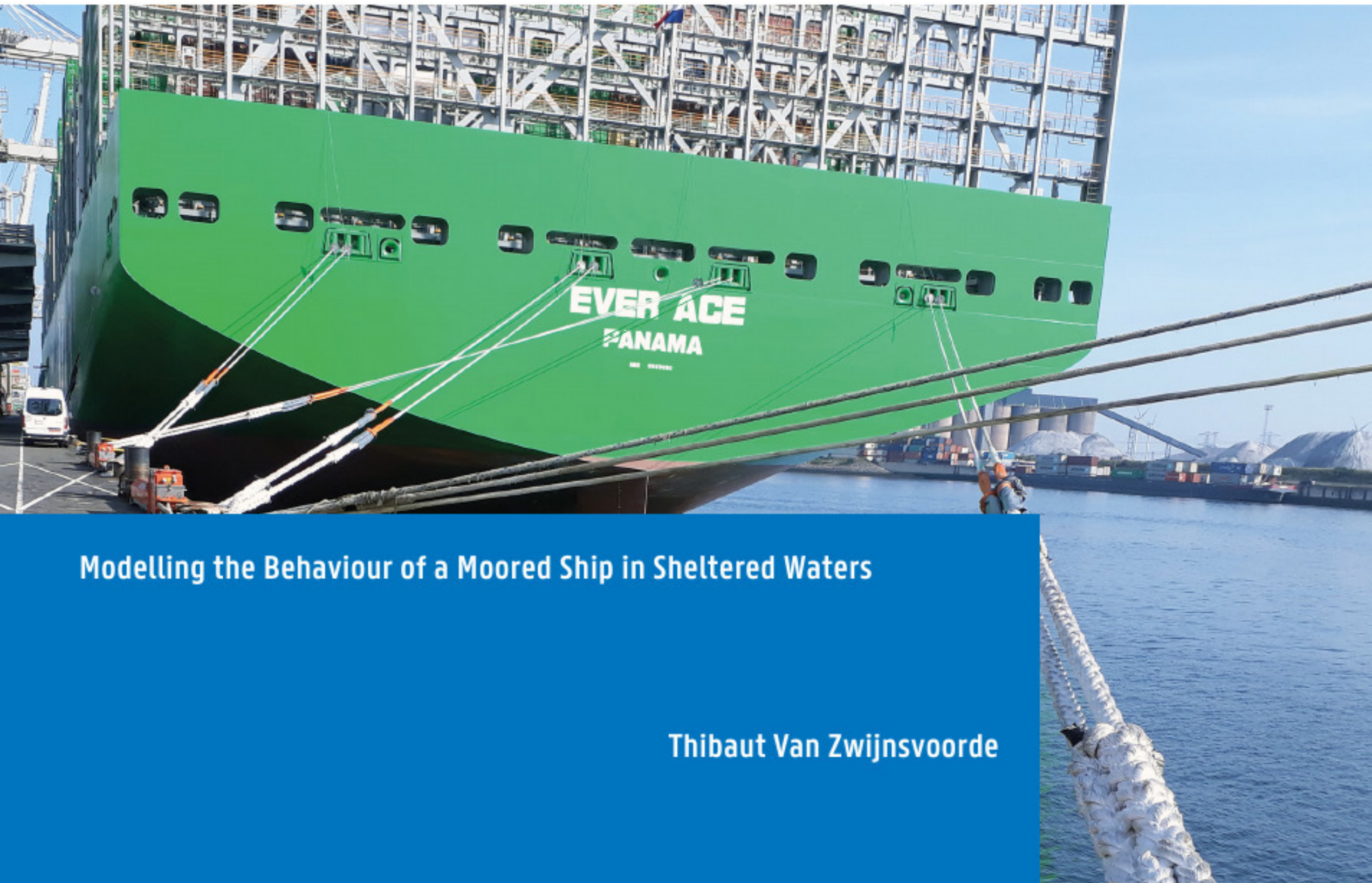

Modelling the Behaviour of a Moored Ship in Sheltered Waters

Thibaut Van Zwijnsvoorde

Doctoral dissertation submitted to obtain the academic degree of
Doctor of Maritime Engineering

Supervisors

Prof. Evert Lataire, PhD - Prof. Em. Marc Vantorre, PhD

Department of Civil Engineering
Faculty of Engineering and Architecture, Ghent University

February 2022

GHENT
UNIVERSITY

FACULTY OF ENGINEERING AND ARCHITECTURE

Modelling the Behaviour of a Moored Ship in Sheltered Waters

Thibaut Van Zwijnsvoorde

Doctoral dissertation submitted to obtain the academic degree of
Doctor of Maritime Engineering

Supervisors
Prof. Evert Lataire, PhD - Prof. Em. Marc Vantorre, PhD

Department of Civil Engineering
Faculty of Engineering and Architecture, Ghent University

February 2022

GHENT UNIVERSITY

ISBN 978-94-6355-572-2
NUR 969, 974
Wettelijk depot: D/2022/10.500/13

Members of the Examination Board

Chair

Prof. Patrick De Baets, PhD, Ghent University

Other members entitled to vote

Djahida Boucetta, PhD, Ghent University
Prof. Guillaume Delefortrie, PhD, Ghent University
Tim Gourlay, PhD, Perth Hydro, Australia
Prof. Em. Jo Pinkster, PhD, Pinkster Marine Hydrodynamics, the Netherlands
Prof. Kurt Stockman, PhD, Ghent University

Supervisors

Prof. Evert Lataire, PhD, Ghent University
Prof. Em. Marc Vantorre, PhD, Ghent University

Preface

Ghent, 2022/02/08
Thibaut Van Zwijnsvoorde

It has been quite the ride. What started with a 23 year old fresh graduate trying to figure out the road he wants to follow, ended up with the completion of this book, almost 8 years later. The pivotal figure in this process is Prof. Marc Vantorre.
Marc, it is difficult to describe the impact you had on my life in a few sentences. Ever since my start at the Maritime Technology Division, you took me under your wings. Your intellect and the ability to explain difficult material, 10 times if needed, is unprecedented. Your warm personality is however what really stands out. Thank you for offering me countless opportunities.
'Assistant' Lataire, and later Prof. Lataire, has created an environment where a great team of researchers, supporting and motivating each other, but also just being good friends. This great atmosphere made my decision to leave UGent after completing my PhD ever so difficult. Evert, you are a great motivator, who always sticks up for your researchers, a perfect profile to lead the Maritime Technology Division for many years (decades?) to come.
I am glad that i was also there to witness the exponential expansion of the division. With every new face joining, new insights are brought to the group. What I appreciated most is the cultural diversity, providing endless card game variates to play over lunch. I don't know why *Briscolla* topped all others, but i can only congratulate Luca for that.
Thanks to all of you for being there for me. Maxim, Changyuan, Ajie, Luca, Bernhard, Marc M. and Ellen, you have been there with me for the whole ride. Thanks for being a source of inspiration, discussion, laughter and parties. Manasés, you have been a role model to me in 'being a researcher'. The phrase *if you are frustrated, you are learn-*

ing, you should be happy really helps out when times get tough.
To Bjorn, Natalia, Paula and Yury, I guess you need to go and find you a new *Wolowitz*. Thanks for being there, understanding that (finishing) a PhD can be difficult and can make you frustrated and grumpy.
Keyser, your personal motivation and bravery, combined with your eagerness to learn, set an example for me. The little trip to visit you in Berlin last year provided me with a needed mental pause before starting on the last stretch towards submission of my PhD.
Ceunick, Charlotte, KJ, Eveline, whether it was a barbecue, poker evening or Pokémon community day, you gave me many moments to cherish and an escape from my research when needed.
Lijie, Farid, Cornelia, for most of my PhD research, you were already in different parts of the world. Your warmth, and the countless dinner and party evenings at Farid's, however showed how rich your life is as a PhD student, when surrounded by loving people.
Maxime and Alec, thanks for taking some work off my hands, making it possible to write the thesis text. Although explicit credit throughout the text is missing, a lot a implicit credit is due.
Whenever you get too frustrated, kicking a football and/or an opponent is still the best way to blow off steam. To my friends from *MLF* and *The Betonnen Muur*, thanks for those moments!
Mom, Dad, your support and love goes far beyond this PhD, it helped me to get where I am now. Thank you for always being there for me and for allowing me to always pursue my dreams, never doubting my abilities to make it work. Oma, Opa, Marainne en Bompa, ik hoop dat jullie tros zijn op Thibautje.
To Paula, you deserve most credit. Certainly towards the end, the PhD absorbed me as a person. You understood that that's 'part of the journey'. You kept feeding me, kept me company and listed to my countless rages on the world. On top of that, you were also my star reviewer.
For everyone taking the time and effort to read this *beast*, buckle up, sit tight and enjoy the ride... and thank you for your vote of confidence.

Dutch summary

Een schip dient veilig afgemeerd te zijn teneinde de lading te kunnen overslaan aan de terminal. Een afmeeranalyse betreft de studie van de veiligheid van het afgemeerde schip, tijdens het verblijf aan de kade, onder externe verstoringen. Voorbeelden van dergelijke verstoringen zijn het effect van wind, golven en passerende schepen. In de meeste gevallen wordt een wiskundig model gebruikt om de respons van het afgemeerde schip te begroten. Hierbij dient men over een accuraat model te beschikken. Het genereren van input (uitwendige krachten, afmeerconfiguratie), alsook het analyseren van de output (troskrachten, scheepsbewegingen,...), vormen echter bijkomende cruciale stappen bij het uitvoeren van een afmeeranalyse.

Schepen reizen tussen ligplaatsen in verschillende havens over heel de wereld. Elke terminal heeft daarbij te maken met een specifieke set aan externe verstoringen. In deze thesis wordt de nadruk gelegd op *Sheltered (nl. Afgeschermde)* terminals, waar de effecten van wind en passerende schepen de meest prominente externe factoren zijn. De ligplaats kan een kaaimuur omvatten, wat een waterondoorlaatbare wand is, alsook een jetty, waar water aan beide zijden van het afgemeerde schip kan stromen.
Binnen de thesis worden alle componenten van de afmeeranalyse besproken, waarbij enkele onderdelen in detail worden geanalyseerd. De keuze voor deze topics volgt uit het commerciële werk, waar deze onderwerpen een dominante rol vertolkten binnen de projecten. Het volledige werk wordt opgebouwd rond het mathematisch model *Vlugmoor* (VLaamse overheid Universiteit Gent MOORing), ontwikkeld binnen de onderzoeksgroep Maritieme Techniek van de Universiteit Gent, waarmee de respons van het afgemeerde schip onder invloed van diverse externe krachten kan worden begroot.

De afmeerconfiguratie, die bestaat uit trossen en fenders, biedt weer-

stand tegen de externe krachten en leidt deze af naar de kaai uitrusting. Het geheel van trossen en fenders zorgt ervoor dat het schip haar positie aan de ligplaats kan behouden. Zonder de aanwezigheid van deze elementen zou het schip immers afdrijven. Internationale eisen, standaarden, alsook richtlijnen, zorgen voor een goede afmeerconfiguratie van de schepen. Deze standaarden zijn vooral ontwikkeld voor de olie-en gasindustrie en kunnen dan ook niet steeds algemeen worden toegepast. Binnen deze thesis werd om deze reden een nieuwe methode voorgesteld om de kwaliteit van de afmeerconfiguratie te evalueren, met behulp van vier zogenaamde efficiëntie parameters. Deze methode kan algemeen worden toegepast voor alle terminal- en scheepstypes.

Een accurate voorstelling van de troskarakteristieken is benodigd als input voor de afmeeranalyse. De autheur heeft in samenwerking met de trosfabrikant Bexco drie trostypes onderworpen aan cyclische belastingen. Op basis van deze resultaten werd inzicht verworven in het elastisch gedrag van de trossen, alsook de wijziging van de stijfheid in de tijd. De hysteresis energie werd berekend, dewelke kan worden gebruikt in het wiskundig model om de accuraatheid van de respons bij een typische cyclische belasting (bijvoorbeeld golfwerking) te vergroten. Deze vorm van demping tijdens elke cyclus zal immers het gedrag over een groot aantal cycli (=verblijf schip aan ligplaats) beïnvloeden.

Alle schepen hebben te maken met windbelasting, zowel tijdens het varen als wanneer ze afgemeerd zijn. Door de schaalvergroting bij containerschepen, zijn deze potentieel onderhevig aan een grote krachtswerking. Binnen een afmeeranalyse wordt de windkracht begroot op basis van windsnelheid, windoppervlak en aerodynamische coëfficiënten. Deze laatste zijn bepaald voor een specifiek schip (ladingsconditie) en windveld, wat maakt dat de algemene toepasbaarheid kan worden in vraag gesteld. Een literatuurstudie bracht aan het licht dat, zeker voor schrikken en gieren, bepaalde dekladingsconfiguraties aanleiding kunnen geven tot grotere krachtswerking in vergelijking met een volledig geladen containerschip.
Het effect van het windprofiel werd onderzocht met behulp van een analytische methode en gevalideerd door middel van CFD berekeningen. Hierbij werd vastgesteld dat de keuze van referentie windsnelheid afhangt van de vorm van het windprofiel op de project lo-

catie, of meer precies het verschil tussen het windveld op de project locatie en het windveld gebruikt om de coëfficiënten te bepalen.
Tot slot werd *Vlugmoor* uitgebreid, teneinde vlagerigheid te kunnen modelleren, aan de hand van de definitie van het Von Karman windspectrum.

Het effect van passerende schepen wordt gezien als de invloed van het primair golfsysteem. Wanneer het vaargebied beperkt is, zullen de passeerafstanden potentieel klein zijn, waardoor grote interactiekrachten kunnen ontstaan. Een accurate voorstelling van dergelijke krachtswerking, voor beperkte vaarwegen, is hierbij noodzakelijk. Om dit doel te bereiken, heeft de auteur schaalmodelproeven uitgevoerd in de Sleeptank voor Manoeuvres in Beperkt Water (Waterbouwkundig Laboratorium (Antwerpen), in samenwerking met Universiteit Gent). Hierbij werden interacties tussen zeegaande schepen, alsook tussen binnenschepen, bestudeerd. In deze thesis worden 1699 unieke parametercombinaties voorgesteld.
In een eerste oefening, werd een regressietechniek gebruikt om de invloed van passeerafstand, kanaalbreedte en kielspeling op de krachtswerking te parametriseren en deze resultaten te toetsen met de literatuur. Aan de hand van deze inzichten werd een model op basis van het Gewijzigd Tuck Getal voorgesteld. Dit model is in staat alle krachtswerking in het horizontale vlak accuraat te voorspellen wanneer het schip afgemeerd is aan de steiger. In geval van het afmeren aan een kaaimuur, kan dergelijke uitmuntende kwaliteit enkel voor het schrikken worden gehaald. Aanvullende termen in functie van kielspeling en kanaalbreedte kunnen worden toegevoegd om het model verder te verbeteren, ten koste van een toename in complexiteit.
Bij het uitvoeren van een afmeeranalyse zorgen beperkingen in budget en doorlooptijd ervoor dat het uitvoeren van schaalmodelproeven meestal niet haalbaar is. Het numeriek model RoPES (potentiaalstroom) wordt dan gebruikt om de krachtswerking vanwege het passerende schip te begroten. In de literatuur wordt een correctiefactor voor grote passeersnelheid in beperkt water voorgesteld. Deze factor is verder gevalideerd op basis van het proevenprogramma. Er werd opgemerkt dat voor zeer beperkt water, de resultaten verder moeten worden genuanceerd, aangezien de vorm van het krachtenverloop in de tijd wijzigt van vorm, voornamelijk wat betreft de

relatieve grootte van de verschillende pieken binnen eenzelfde vrijheidsgraad.

Onder de aanname dat de externe krachtswerking, alsook de afmeerconfiguratie, accuraat werden gemodelleerd, dient het wiskundig model dat wordt gebruikt om de respons van het afgemeerde schip te begroten, eenzelfde hoge kwaliteit te bieden. Doordat trossen en fenders niet-lineair vervormen en de belastingen voorbijgaand (Eng. transient) van aard kunnen zijn, dient een berekening in het tijdsdomain te worden uitgevoerd. Hierbij wordt in *Vlugmoor* Newton's tweede wet uitgewerkt voor alle zes vrijheidsgraden, waarbij ook de hydrodynamische respons van het schip (demping en toegevoegde massa), dient te worden in rekening gebracht.
Wanneer een quasi-statische respons wordt aangenomen, waarbij het schip op elke tijdstap een evenwichtspositie bereikt, kan het wiskundig model sterk vereenvoudigd worden, waardoor de simulatietijd kan worden beperkt. Desondanks de bewezen sterkte van dit model, kunnen geheugeneffecten van de vloeistof, waarbij een ogenblikkelijke beweging van het schip ook de respons in volgende tijdsstappen beïnvloedt, niet worden meegenomen. Impulsantwoorden (ENG. Impulse Response Functions (IRF)) kunnen worden toegevoegd aan het model om deze invloed wiskundig voor te stellen. Gezien de aard van deze functies en de nood om elke tijdstap een convolutieintegraal te begroten, neemt de simulatietijd sterk toe. Het beperken van de bewegingshistorie die wordt in acht genomen bij de berekening, alsook een vereenvoudigde voorstelling van de IRF functies op basis van toestandsvariabelen, werden onderzocht teneinde de berekeningstijd aanvaardbaar te houden.

Onder specifieke aannames kan het systeem worden gelineariseerd, waardoor eigenperiodes kunnen worden bepaald voor de verschillende vrijheidsgraden. Het afgemeerde schip zal een grotere respons vertonen ten aanzien van belastingen met een periode dicht bij de eigenperiodes van het schip. Dit geldt zowel voor voorbijgaande als voor cyclische belastingen. Onder cyclische belastingen zal de resonantie zich echter sterker doorzetten. Vooral in de horizontale vrijheidsgraden (schrikken, verzetten en gieren) wordt de eigenperiode sterk beïnvloed door de positie en de eigenschappen van de afmeeruitrusting.

Een laatste aspect binnen de afmeeranalyse betreft de studie van de scheepsbewegingen, alsook tros- en fenderkrachten.
Wanneer de uitwendige belasting voorbijgaand van aard is (scheepspassage), is de respons ook beperkt in de tijd tot enkele pieken (kracht, beweging), dewelke kunnen worden getoetst aan criteria. Wanneer de belasting cyclisch (continu) van aard is (golfwerking), is een probabilistische analyse meer op zijn plaats, waarbij onder andere een significante waarde van de respons kan worden berekend.
Een tweede onderscheid wordt gemaakt tussen krachten (tros en fender) en scheepsbewegingen. Krachten worden begrensd door de sterkte van de trossen en fenders, alsook de algemene uitrusting van schip (winch, kluis) en kaai (bolder). Het opstellen van criteria voor bewegingen is meer complex, aangezien dit samenhangt met het scheepstype en de uitrusting kopping (ENG. manifold) geconnecteerd met een laadarm op de kade. Bij het overslaan van lading op een containerschip, moet de kraan echter de container halen op een bepaalde positie op het dek.
Daarenboven zijn er voor sommige scheepstypes verschillen in de uitrusting voor laden en lossen. Bulk carriers bijvoorbeeld worden geladen in export terminals, waar in vele gevallen een lopende band kan worden gebruikt om de bulk te laden. In een import terminal moet een grijper in het ruim binnentreden om de lading te grijpen. In dit tweede geval zijn de consequenties van scheepsbewegingen groter, aangezien de grijper contact kan maken met schip (en in sommige gevallen arbeiders die in het vrachtruim aanwezig zijn), waardoor striktere criteria nodig zijn.

English summary

Ships travel the world, delivering cargo to ports around the globe. In order to be able to load and unload this cargo in port, the ship needs to be safely moored. This can be established by conducting a mooring analysis, which assesses the safety of the moored ship and the cargo operation, during her stay at the berth, under certain external disturbances. These disturbances can include wind, waves and the effect of other ships passing by. In most cases, a mathematical model is used in the mooring analysis to calculate the response of the moored ship to these disturbances. The UGent in-house mathematical model *Vlugmoor* (VLaamse overheid Universiteit Gent MOORing) is an example of such model. Generating accurate input (forces, mooring arrangement), as well as analysing the output (motions, forces), form important aspects of the mooring analysis.

This thesis reviews all of the aspects related to a mooring analysis, with specific parts addressed in detail. The discussed topics are mainly driven by commercial project work conducted by the candidate, where different parts of the mooring analysis played a prominent role in the project.

Every port or terminal that a ship calls at will be different, and will come with a specific set of dominant external disturbances. This thesis focusses specifically on a *sheltered terminal*, which mainly suffers from wind and passing ship effects. The berth at this type of terminal can be formed by a (closed) quay wall as well as an (open) jetty construction, the latter allowing water flow on both sides of the moored ship.

All ships are affected by wind forces; the size increase of container ships, as well as a stacking of cargo on deck, makes them partic-

ularly susceptible to wind. Wind forces are commonly calculated based on the input of wind speed, wind surface and a set of aerodynamic coefficients. The effect of container stacking on the wind coefficients is significant. Particularly for the surge force and yaw moment, the magnitude can be higher for a random stacking compared to a fully stacked ship. As the wind speed increases with height above the surface, following a logarithmic velocity profile, the choice of reference wind speed should be made considering the shape of the profile, as well as the height of the ship's structures and cargo stacks. As the wind speed and direction varies on a short time scale, mathematically represented by a turbulent wind spectrum, this is considered in the definition of wind effects in *Vlugmoor*.

A passing ship affects a moored ship through her primary (long) and secondary (short) wave system. As the moored ship has significant inertia, the response to the secondary wave system is insignificant in most cases, certainly when considering large sea-going vessels. In confined areas, where passing distances are low, the effect of the primary wave system can be significant however. Most numerical and empirical tools fall short to predict the influence of this confinement on the interaction forces. In order to fill this knowledge gap, an extensive physical scale model test program has been executed at the Towing Tank for Manoeuvres in Confined Water at Flanders Hydraulics Research (in co-operation with Ghent University).
The 1699 unique interaction tests were used to build an empirical model which includes the effect of confinement on the interaction forces. This effect is represented by adding the Modified Tuck Number to common formulations. The test database is also utilised to validate the potential double body package RoPES, the numerical tool which is often used to generate input for *Vlugmoor*. This validation work confirms statements made in literature that a correction factor is needed to include the effect of confinement (at high speeds) on the interaction forces. It also highlights that an asymmetry between bow and stern wave system which is present in the physical scale model tests, due to viscous and free surface effects, is not captured by the RoPES software.

Mooring lines and fenders form the mooring configuration of the ship, serving as the restraint for the moored ship in the horizontal plane. The mooring configuration determines how the ship will react to a

given external disturbance. Results of full scale tensile tests on three different mooring ropes (synthetic lines) are presented, showing how the response of the line changes under cyclic loading. The spatial arrangement of the lines needs to chosen to optimise the response, leading to acceptable line forces and ship motions. In order to judge the quality of the mooring arrangement, four efficiency parameters are determined. These can also be used to predict the effect of changes to the mooring arrangement, on the response of the moored ship.

The mooring arrangement, as well as the external disturbances, are non-linear in nature. A time domain simulation is thus necessary to calculate the behaviour of the moored ship. As time domain calculations are slow compared to their frequency domain counterparts, well-chosen simplifications should be made. When the excitation is transient and/or has a long period, a quasi-static response can be substantiated, where the system reaches a dynamic equilibrium at every time step. When the disturbance is more complex (e.g. combination of long and short period effects), the memory effects of the flow should be taken into account. Impulse Response Functions are a proven technique to represent these effects. The need to take account of the motion history of the system however greatly increases the calculation cost.
Despite not being able to adequately calculate the moored ship's response, frequency domain techniques can still be applied to get insight into the dynamic system. An estimation of eigenperiods for different Degrees Of Freedom (DOF) can be compared with (dominant) periods of external loads, as a system will respond more to loads which are close the respective eigenperiods. This method can be applied to predict the susceptibility of the system to a certain load, prior to the execution of the time domain simulation.

The result of a time-domain simulation, time histories of forces and motions, needs to be evaluated as final part of the mooring analysis. When the load is transient, such as a passing ship effect, a peak force and motion needs to be compared with a set criterion. When the load is cyclic in nature, a statistical interpretation needs to be made.
Fender forces are limited by the capacity in compression of the system. Mooring line loads need to be kept significantly lower than their

breaking load, to avoid fast degrading of the line strength over time. The ship motion analysis is more complex, as it is a function of the ship type, (terminal) loading equipment, as well as the required loading rate. For oil and gas carriers, the ship's manifold, located around midship, is connected to a loading arm on shore. The motions at midship need to checked. For other cargo types (bulk, container, RoRo), the motions at the local cargo hold/ramp should be considered. In these cases, local translations are a function of 6DOF motions at the origin (midship, water plane).

This thesis work shows the complexity of the mooring analysis, consisting of many different components, with the time domain calculation at the heart of it. Advanced knowledge of mathematics and usage of state-of-the-art calculation software, needs to be supplemented with experience on all parts of the mooring analysis. This concerns defining representative external disturbances, creating a typical mooring arrangement, as well as making a critical review of the results. In order to successfully complete this process, the terminal, ship operator, captain, port authority and pilots should be consulted, as they need to agree with the methods and implement the conclusions.

List of Acronyms

A

ASCII	American Standard Code for Information Interchange

B

BV	Bureau Veritas

C

CEMT	Conférence Européenne des Ministres de Transport
CFD	Computational Fluid Dynamics
CoG	Centre Of Gravity

D

DNV	Det Norske Veritas
DOF	Degree Of Freedom
DTC	Duisburg Test Case

E

EN	Equipment Number
ESDU	Engineering Sciences Data Unit

F

FFT	Fast Fourier Transform
FHR	Flanders Hydraulics Research
FPSO	Floating Production Storage and Offloading
FS	Full Scale

G

GPS	Global Positioning System

H

HMPE	High Modular PolyEthylene

I

IACS	International Association of Classification Societies
IMO	International Maritime Organisation
IRF	Impulse Response Function
ISO	International Standardisation Organisation

J

JIP	Joint Industry Project

K

Blank

L

LC	Load Cell
LES	Large Eddy Simulation
LIDAR	LIght Detection And Ranging
LNG	Liquified Natural Gas
LR	Lloyd's Register of Shipping

M

MARIN	Maritime Research Institute Netherlands
MASHCON	Conference on ship MAnoeuvring in SHallow and CONfined water
MBL	Minimum Breaking Load
MEG4	Mooring Equipment Guidelines 4
MLA	Marine Loading Arm
MS	Model Scale
MTD	Maritime Technology Division

O

OCIMF	Oil Companies International Maritime Forum

P

P	Potentiometer
PESCA	Passing Effects in Shallow and Confined Areas
PIANC	World Association for Waterborne Transport Infrastructure

Q

QRH	Quick Release Hooks

R

RANS	Reynolds Averaged Navier Stokes
RAS	Replenishment At Sea
RINA	Royal Institute of Naval Architects
RoPES	Research on Passing Effects on Ships
RoRo	Roll On Roll Off
RWS	RijksWaterStaat

S

SIGTTO	Society of International Gas Tanker and Terminal Operators
STS	Ship-To-Ship
SV	State Variable

T

TDS	Time Domain Solver
TEU	Twenty feet Equivalent Unit

U

UKC	Under Keel Clearance
ULCS	Ultra Large Container Ship
UN	United Nations

V

Vlugmoor	Vlaamse Overheid Universiteit Gent MOORing

W

WG	Wave Gauge
WMO	World Meteorological Organisation

X

Blank

Y

Blank

Z

Blank

Symbol list

Latin symbols

Remark 1 - In case the unit depends on the degree of freedom (6DOF = surge, sway, heave, roll, pitch, yaw), this is indicated by the expression ”f(DOF)”.

Remark 2 - The following abbreviations are used; diff. = differential; eq. = equation; (moor.) conf. = (mooring) configuration; (moor.) equip. = (mooring) equipment; prob. = probabilistic.

A	multiplication coefficient solution diff. eq.	(-)
A_0	lateral wind area definition EN calculation	(m²)
A_1	lateral wind area definition IACS calculation	(m²)
A_{channel}	wetted area channel section	(m²)
A_{f}	frontal wind surface	(m²)
A_{l}	lateral wind surface	(m²)
A_{M}	area of midship section	(m²)
A_{ref}	reference wind area	(m²)
A_{w}	area of water plane section	(m²)
A_{s}	projected area ship in wind tunnel	(m²)
A_{t}	cross section wind tunnel	(m²)
a_{ij}	hydrodynamic added mass, ij = DOF	f(DOF)
b_{ij}	hydrodynamic damping coefficient, ij = DOF	f(DOF)
b_{l}	damping coefficient mooring line	(kg/s)
b_{moor}	damping coefficient moor. equip.	(kg/s)
B	phase angle solution diff. eq.	(-)
B	ship beam	(m)
C_{B}	block coefficient	(-)
C_{F}	generic wind coefficient	(-)

C_K	wind coefficient roll	(-)
C_{M}	midship coefficient	(-)
C_N	wind coefficient yaw	(-)
C_X	wind coefficient surge	(-)
C_Y	wind coefficient sway	(-)
c_{w0}	critical wave celerity in shallow water	(m/s)
c_{w}	critical wave celerity in restricted water	(m/s)
c_{wd}	velocity divergent Kelvin waves	(m/s)
c_{wt}	velocity transverse Kelvin waves	(m/s)
c_1, c_2	multiplication constant diff. eq.	(-)
D	discriminant diff. eq.	(-)
D	depth of the ship	(m)
d	passing distance side-to-side	(m)
d_0	uncompressed width of fender	(m)
E_{hys}	hysteresis energy per unit line length	(Nm/m)
EN	equipment number	(-)
e_X	efficiency parameter moor. conf. surge	(-)
e'_X	efficiency parameter moor. conf. surge for the combination of main line and tail	(-)
e_Y	efficiency parameter moor. conf. sway	(-)
e'_Y	efficiency parameter moor. conf. sway for the combination of main line and tail	(-)
F_{c}	RoPES correction factor	(-)
F_{G}	generic force	f(DOF)
F_{X}	mooring line force surge direction	f(DOF)
Fr	length based Froude number	(-)
Fr_h	Froude depth number	(-)
Fr_{crit}	critical Froude depth number (Schijf)	(-)
f_{ND}	non-dimensionalisation coefficient	f(DOF)
f_u	Monin similarity constant	(-)
F_{wi}	generic wind force	f(DOF)
f_{wd}	frequency divergent Kelvin waves	(Hz)
f_{wt}	frequency transverse kelvin waves	(Hz)
g	gravitational acceleration	(m/s²)
$\overline{GM_{\mathrm{L}}}$	longitudinal metacentric height	(m)
$\overline{GM_{\mathrm{T}}}$	transverse metacentric height	(m)
H	distance top superstructure to waterline	(m)
$\overline{H}$	mean height ship above waterline	(m)
h	water depth	(m)

I_{xx}	moment of inertia around x-axis	(kgm²)
I_{yy}	moment of inertia around y-axis	(kgm²)
I_{zz}	moment of inertia around z-axis	(kgm²)
K	roll moment	(Nm)
$K(t)$	memory function	f(DOF)
k_{e}	wave number eddy (wind)	(1/m)
k_{f}	elasticity constant fender	(N/m)
k_{l}	elasticity constant mooring line	(N/m)
k_q	Blendermann coefficient q_{ref}	(-)
k_{x+}, k_{x-}	restoring coeff. moor. conf. surge	(N/m)
k_{y+}, k_{y-}	restoring coeff. moor. conf. sway	(N/m)
$k_{\psi+}$, $k_{\psi-}$	restoring coeff. moor. conf. yaw	(Nm/m)
L_{b}	basin length	(m)
L_{OA}	ship length overall	(m)
L_{PP}	ship length between perpendiculars	(m)
L_u^x	turbulence length	(m)
l_0	untensioned length mooring line	(m)
M	pitch moment	(Nm)
m	mass	(kg)
$m_{0,\mathrm{R}}$	0^{th} order response moment	f(DOF)
m_{f}	total number of fenders	(-)
m_{p}	section blockage passing ship	(-)
m_{pm}	section blockage passing and moored ship	(-)
m_{wi}	section blockage wind tunnel	(-)
N	yaw moment	(Nm)
n	wind frequency	(Hz)
$\overrightarrow{n}_{\mathrm{m}}$	normal vector on body m	(-)
$\mathrm{n}_{\mathrm{H+ST}}$	number of head + stern lines	(-)
n_{SP}	number of spring lines	(-)
n_{l}	(total) number of lines	(-)
p	roll velocity	(rad/s)
p	water pressure	(N/m²)
$\dot{p}$	roll acceleration	(rad/s²)
q	wind pressure	(N/m²)
q	pitch velocity	(rad/s)
$\dot{q}$	pitch acceleration	(rad/s²)
q_{ref}	reference wind pressure	(N/m²)
Re	Reynolds number	(-)
R	rotational matrix	(-)

R^2	coefficient of determination regression analysis	(-)
R_{M}	maximum value prob. study	f(DOF)
R_{MM}	most probable maximum value prob. study	f(DOF)
R_{S}	significant value prob. study	f(DOF)
r	yaw velocity	(rad/s)
$\dot{r}$	yaw acceleration	(rad/s²)
r_{inv},r_{exp}	residual error regression	f(DOF)
r_1, r_2	roots of the diff. eq.	(-)
$\overrightarrow{S}_{\mathrm{m}}$	wetted surface body m	(m²)
$S_\zeta(\omega, \theta_{\mathrm{w}})$	wave energy spectrum	(m²/Hz)
$S_R(\omega, \theta_{\mathrm{w}})$	response spectrum	f(DOF)
S_u	wind energy spectrum	(m²/s)
T_{M}	ship draft at midships	(m)
s	passing distance centre-to-centre	(m)
T_{n}	eigenperiods ship $T_{\mathrm{n}x}$, $T_{\mathrm{n}y}$, $T_{\mathrm{n}z}$, $T_{\mathrm{n}\phi}$, $T_{\mathrm{n}\theta}$, $T_{\mathrm{n}\psi}$	(s)
T_{nb}	eigenperiod basin	(s)
Tu	Tuck number	(-)
Tu_{m}	modified Tuck number	(-)
t	time	(s)
U	wind speed (longitudinal)	(m/s)
U_{ref}	reference wind speed	(m/s)
UKC	distance between keel and bottom, % T_{M}	(%)
u	surge velocity	(m/s)
$\dot{u}$	surge acceleration	(m/s²)
$u*$	friction velocity	(m/s)
V	forward speed ship	(m/s)
v	sway velocity	(m/s)
$\dot{v}$	sway acceleration	(m/s²)
W	channel width	(m)
w	heave velocity	(m/s)
$\dot{w}$	heave acceleration	(m/s²)
X	surge force	(N)
x	surge motion	(m)
x_{G}	longitudinal position CoG relative to midships	(m)
Y	sway force	(N)
Y_{f}	lateral force fore perpendicular	(N)
Y_{a}	lateral force aft perpendicular	(N)
y	sway motion	(m)
$Y^2_{R\zeta}$	response amplitude operator (RAO)	f(DOF)

Z	heave force	(N)
z	heave motion	(m)
z	vertical position above surface (wind profile)	(m)
z_0	roughness length	(m)
z_h	arbitrary height above surface	(m)

Greek and other symbols

α	regression multiplication coefficient	(-)
α_{l}	mooring line angle in the xy-plane	(°)
β	regression coefficient passing distance	(-)
β_{l}	mooring line angle in the yz-plane	(°)
γ	regression coefficient under keel clearance	(-)
γ_{l}	mooring line vector angle at fairlead	(°)
Δ	ship mass displacement	(N)
δ	regression coefficient channel width	(-)
δ_{f}	fender angle in the xy-plane (lever arm vector)	(°)
δ_{l}	mooring line angle in the xy-plane (lever arm vector)	(°)
δ_{BLI}	boundary layer influence thickness	(m)
ϵ_{l}	mooring line strain	(-)
ϵ_{f}	fender strain	(-)
η	generic regression coefficient	(-)
θ	pitch angle	(rad)
θ_{w}	angle Kelvin waves	(°)
κ	Von Karman constant	(-)
λ	scale factor	(-)
λ_{wd}	wave length divergent Kelvin waves	(m)
λ_{t}	wave length transverse kelvin waves	(m)
μ	average value	f(DOF)
μ_{f}	friction coefficient	(-)
ν	kinematic viscosity	(m^2/s)
ξ	non-dimensional position passing ship	(-)
ρ	mass density	(kg/m^3)
σ	standard deviation	f(DOF)
σ_u	root of variance wind spectrum	(m/s)
τ	time parameter IRF function	(s)
Φ	velocity potential	(m^2/s)
ϕ	roll angle	(rad)
χ	wind direction with respect to stern	(°)
ψ	yaw angle	(rad)
ω	wave frequency	(Hz)
ω_{n}	eigenfrequency	(Hz)
∇	ship volume displacement	(m^3)
∇	gradient	(-)

Subscripts

I	moored ship 1, berth (double banking)
II	moored ship 2, alongside (double banking)
a	air
b	coordinate mooring point berth
ext	external disturbance
hydro	hydrodynamic response ship
iner	inertia
m	moored ship (general)
m1	moored ship 1 (specific)
m2	moored ship 2 (specific)
meas	measured
moor	mooring equipment
ND	non-dimensional
p	passing ship
reg	parameter result of regression model
s	coordinate ship (fairlead)
w	water
wi	wind

Table of Contents

1 Introduction

1.1 Background and definitions

1.1.1 A moored ship

A ship creates value by moving cargo from one location to another. During her voyage, the ship will mostly be cruising through open water (ocean), at both ends of the voyage however, the ship needs to berth. The approach and berthing manoeuvre itself is complex, where the captain is often assisted by local pilots.

Once the ship is berthed, mooring crews, on board of the ship and assisting from water and quay side, will start attaching mooring lines to fixed points on the berth. The hull of the ship touches the berth through fenders, which are cushion like elements. Once all lines are connected, the ship will stop her main engine; she is now moored. Figure 1.1 shows the general moored ship, as well as details regarding mooring arrangement at fore and aft ship, for the case of a moored container ship. The ship remains moored during the cargo transfer, after which the main engine is restarted and lines are slackened and hauled back on board.

This thesis solely focusses on the period where the ship is moored, i.e. where the ship can be considered as a floating object without her

own controls, kept in position by mooring lines and fenders, under various external disturbances. An external disturbance is any action on the moored ship which is not caused by her own movement, e.g. wind, waves, passing ships,...

A ship is considered to be moored safely if the following conditions are met:

- The motions are acceptable to allow cargo (un)loading and crew/passenger transfer.
- The forces in mooring equipment on board and ashore are acceptable.

1.1.2 Mooring locations

Each port, terminal and berth is unique in its design and local challenges for the moored ships. For the purpose of this thesis, a subdivision is made into three terminal locations (figure 1.2), based on the major external disturbances which are present at the location.

The definition of an **Open Terminal** (letter A in figure 1.2, yellow) is based on [Bak15], who define an *open port* as a port located in naturally deep waters. This definition is used in the present work for an individual terminal. An Open Terminal has little protection from waves, wind and current; the large navigational area limits ship-to-ship interaction. This is summarised in table 1.1. Figure 1.3 (a) shows the terminal discussed in [Bak15].

A **Coastal Terminal** (letter B,C in figure 1.2) is located behind breakwaters, limiting the wave and current action. Wind effects may still be high. Passing ship effects might become considerable in some cases, for example when a ship is coming from the lock and heading to open sea, passing berth C . The outer port of Zeebrugge (figure 1.3 (b)) is an example which fits this definition. For some particular cases of long wave action, breakwaters will only provide limited effect on the wave action. An example is discussed in [Gou19] (see also section 2.1.3).

A **Sheltered Terminal** is located either behind locks, or connected to the sea by an estuary. In both cases, wind effects are usually

(a) Moored container ships, courtesy of Marc Vantorre.

(b) Detail fore ship, courtesy of Ralf Bartholomä.

(c) Detail aft ship, courtesy of Antwerp Port Authority.

Figure 1.1: *Moored container ship - three views, four different ships.*

lower due to a more sheltered environment; when the terminal is located behind locks, no tidal current effect is present. A river discharge might still be present. Depending on the size of the basin, passing ship effects may become critical. In figure 1.2, ships may pass terminal D at considerable speed. The passing ship effect on the ships from terminal E will be limited to (low speed) manoeuvring ships. Figure 1.3 (C) gives an example of sheltered terminals in the Port of Antwerp.

1.1.3 Mooring incidents

Plenty of reports and studies discussing mooring incidents have been published, indicating the frequent occurrence, as well as important consequences of a mooring incident. Three incident types are defined here, based on the consequences rather than the actions which caused it.

- **Excessive motions** : Motions are always undesirable as they will often cause delays in the loading operations. Large motions however can also lead to structural and/or personal injury. A large motion of a moored container ship can cause a collision between the spreader, the grabbing element from the crane, and the container stack, or even worse the bridge of the ship. An oil tanker is typically connected to shore via a mechanical arm (MLA - Marine Loading Arm), which can be severely damaged if not decoupled fast enough under a large motion. Structural damage can then be secondary to the environmental damages cause by spilled oil. Reports on these types of damage are scarce. International standards on maximum ship motions are discussed in [Mar95], soon to be succeeded by [Marb], in which the author is active. This topic is also discussed in detail in chapter 2 of this thesis.

Table 1.1: *Presence of external disturbances per terminal type.*

terminal	wind	waves	current	passing ship
Open	high	high	high	low
Coastal	high	moderate	moderate	low to moderate
Sheltered	moderate	low	not present	moderate to high

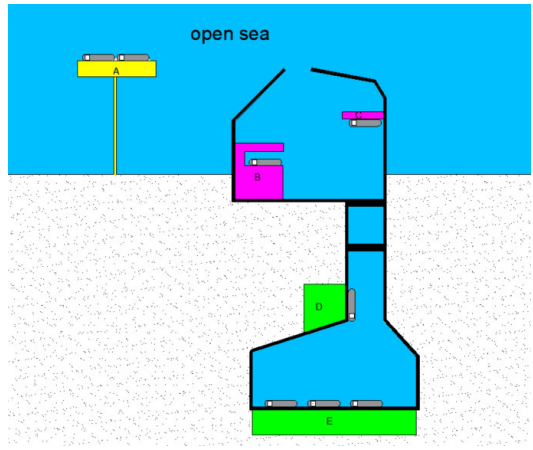

Figure 1.2: *Fictitious port, indication of terminal types, Open Terminal (A; yellow), Coastal Terminal (B,C; purple), Sheltered terminal (D,E; green).*

- **Parting of lines** : When the force in the lines becomes excessive, the line will break, releasing a huge amount of energy, in the form of a deadly whipping rope or wire. Depending on the point of breaking, backlash could cause fatality amongst crew members. [Ste09] reports two cases of line parting, one of them inflicting heavy injury to a crew member; In the second case, one linesman on shore was seriously injured and a second one was fatally injured.

- **Breakaway** : When mooring lines part, a cascade effect can cause the whole mooring system to fail. As the main engine is usually turned off in port, the ship's response will be delayed. From the moment the ship starts drifting, a large mass with plenty of energy can cause damage to port infrastructure or other (moored) ships. Even the (in)famous Titanic caused a breakaway in 1912, when she passed the liner New York [Pin09]. A collision was avoided due to the quick response of both captains. Another example involved the breakaway of the moored APL Mexico City in Port of Antwerp on December 9^{th} 2019, under the effect of wind, causing the ship to drift into and destroying a gantry crane at the other side of the dock [1].

[1] $https://www.gva.be/cnt/dmf20191209\_04758227$, visited 2021/10/08

(a) Open Terminal, image taken from [Bak15].

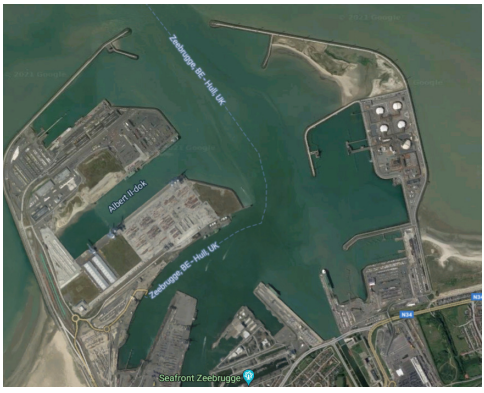

(b) Coastal Terminal, *Google Earth*.

(c) Sheltered Terminal, *Google Earth*.

Figure 1.3: *Example of Open, Coastal and Sheltered terminal.*

Next to the obvious need for a quality mooring arrangement, which is discussed extensively in this thesis, mooring operations and (a lack of) line maintenance on board also lead to many incidents, for example when the pretension force in the lines is not maintained. [Mar15] discloses that from the twelve mooring line failures noted in one port, four were the result of poor mooring line condition and eight were the result of incorrect or uneven line tensions. [UK 09] gives some examples of bad mooring practice. They also estimate that incidents involving mooring equipment have cost UK P&I club 34 million US dollars over the last twenty years.

1.1.4 Mooring analysis

The mooring analysis is the assessment of the safety of the moored ship for a given berth under a specific set of external disturbances. In most cases, this analysis is performed by modelling the response of the moored ship, using a mathematical model. As will become clear throughout this thesis, a moored ship is a highly non-linear system, meaning that a Time Domain Simulation (TDS) is required as the core of the mooring analysis.

Figure 1.4 shows the general structure of a mooring analysis. At its heart is the calculation of the ship response, which is done by solving equations of motion. As will become apparent in this work, the generation and quality of the input, as well as the assessment of the output, form important parts of the mooring analysis.

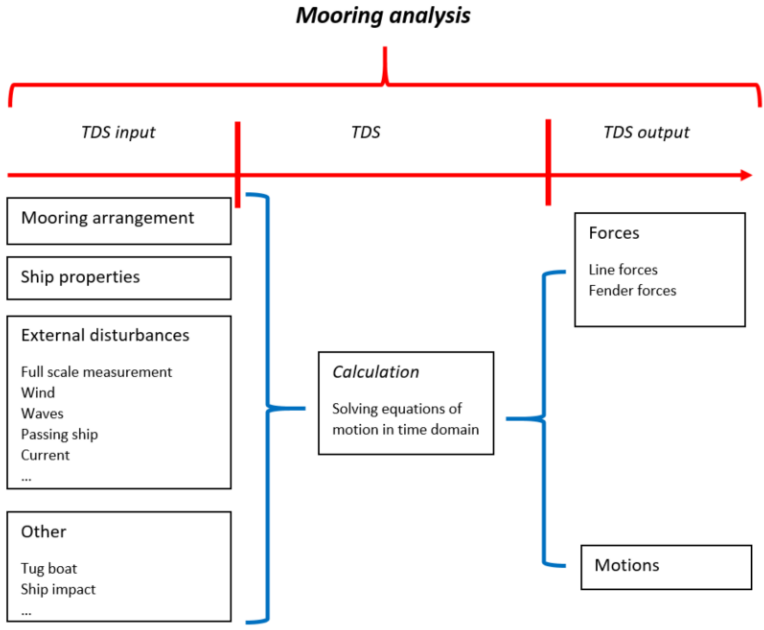

Figure 1.4: *General overview components of a mooring analysis.*

1.2 Challenges

1.2.1 Global design - local challenges

Ships are typical global units of transportation, which travel around the world visiting terminals as part of trading routes. They are essentially designed with the focus on this global, long distance trade. The International Maritime Organisation (IMO), part of the United Nations (UN), sets international standards for safety, security and environmental performance. Classification Societies develop and apply technical standards, following the ship from the drawing table to her final trip.

When it comes to the mooring equipment on board a ship, standardisation is lacking. In 2005, IMO and IACS published a set of standards for mooring lines, updated in 2020 [IAC20]. The latter requirements are based on safe mooring under a maximum current speed of 1.0 m/s (1.9 knots) and a wind speed of 25 m/s (48.5 knots).

For oil and gas tankers, OCIMF - Oil Companies International Marine Forum and SIGTTO - Society of International Gas Tanker and Terminal Operators, set their own specific standards. For mooring, the MEG4 [OCI18] forms the reference work. They stipulate that the mooring equipment on the ship should be designed to allow safe mooring in a 60 knot wind, in combination with a 3 knot current (stern/head) or 2 knot (10° from stern) or 0.75 knot (beam), whichever is more critical.

PIANC (World Association for Waterborne Transport Infrastructure) is another body discussing 'good practices', based on international working group efforts. One very relevant example here is WG186 -*Safe mooring of large ships at quay walls*.

Despite the great benchmark put forward by OCIMF (standards for tankers) and PIANC (good practice), a mooring analysis will often be required for a specific location to ensure safe mooring conditions.

1.2.2 Variety in ship and terminal types

The local challenges are not only to be viewed in function of external disturbances, but also the concept of the terminal, in combination

with the specific deck layout of some ship types, which together requires a specific mooring arrangement for that terminal.

Figure 1.5 (a) shows a mooring arrangement of an oil tanker moored at a jetty, an open piled platform with mooring points on individual piles (dolphins). The location of these points is chosen to optimise the mooring arrangement of the design ship(s). On board the ship, the cargo is stored in the tanks, with only piping on the deck. The mooring equipment can thus be positioned pretty much along the whole deck of the ship.

Figure 1.5 (b) shows the other side of the spectrum: A container ship moored at a quay wall, with gantry cranes on rails moving along the ship to (un)load the cargo. The need for the crane to travel along these rails limits the position of the mooring points to the surface at the waterside of the rail. As the position of the container ship along the berth is not fixed, a continuous line of mooring points is present (indicated by figure 1.5 (b)). On deck, most space is taken by the container cargo. The space for mooring equipment is limited to the fore and aft deck, which reduces the flexibility of the configuration.

(a) Oil tanker moored at jetty, *Google Earth*.

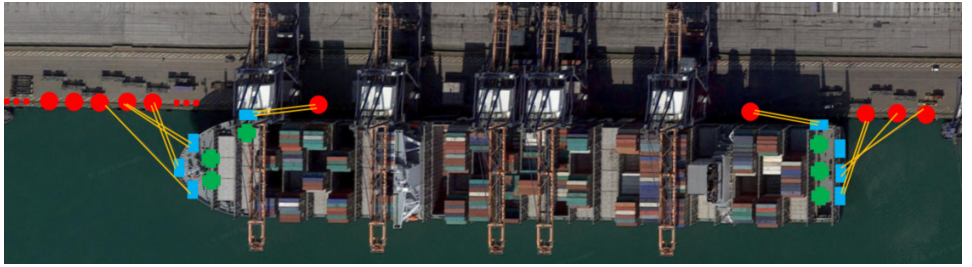

(b) Container ship moored at a quay, *Google Earth*.

Figure 1.5: *Top view moored ships.*
Orange lines = mooring lines, Red circle = line connection point on berth, rectangle = Line entering point ship, green circle = line connection point ship

1.2.3 Mooring analysis complexity

1.2.3.1 Stakeholders

When a ship is moored at a terminal, the terminal operator oversees the (un)loading process and in some circumstances imposes requirements with respect to the mooring configuration. For oil and gas terminals, terminal guidelines are usually produced and handed over to the ship prior to her arrival.

The captain of the ship is always responsible for the safety of the ship and will decide on the mooring configuration which is attained at the berth. If the captain does not deem that his/her ship can be moored safely, under certain conditions, the decision can be made not to berth (or to leave the berth). When a pilot is on board to assist with the harbour navigation, this person will often also share his/her expertise on local conditions (e.g. current, passing traffic) to assist the captain.

The function of the Port Authority differs between ports, but in essence they are landlords who rent out land to terminals and ask a fee to ships for visiting the port. The terminal can in essence operate mostly independently; however, the port does not want any irregularities to occur within the port area. A ship breaking loose from a terminal could for example block (a part of) the port for days. Therefore, the port and terminals are partners in attaining safe mooring, certainly as the port often builds the mooring infrastructure (quay, bollards,...) as well as maintains the channels and regulates the traffic. Ports can for example put minimal requirements in place for the number of mooring lines used in function of ship size. A mooring analysis is made in agreement with captains, pilots, linesmen, port authority and terminal operator.

Another tension field arises from the fact that civil engineers design port infrastructures with lifetimes of 50 to 100 years; ships are designed by naval architects, who design for a lifetime of around 30 years. The connection of the mooring line to the mooring point, as well as the support of the hull by fenders, forms the interaction plane between the two disciplines. The shorter time scale of a ship's lifetime compared to infrastructure allows ship dimensions and equipment to change more quickly, generating possible conflicts. A container quay built in the 90s was designed when the biggest ships had

around 6000 TEU on board. The same quay is now used to moor 24000 TEU container ships, with more and stronger mooring lines on board, challenging the quay equipment. A mooring analysis with the new design ship could then be deemed necessary and might in some cases lead to suggested quay renovations.

1.2.3.2 Extensive list of technical parameters

A mooring analysis is usually performed to support terminals and/or port authorities in their design and/or operational policy. This question is then typically *'Can our design ship, an oil tanker with a length of 250 m, be safely moored at our terminal?'* or *'Can the ship Y, which is larger than the design ship X, be moored safely considering the existing infrastructure?'* These questions are straightforward in one way, the answer can be *yes or no*, often complemented by a list of requirements e.g. concerning (minimum) demands for the mooring arrangement. The analysis structure however looks like figure 1.4. Below is an example of the typical actions which are needed before and after the TDS itself is performed, with the assistance of the stakeholders mentioned in section 1.2.3.1.

- Based on the main dimensions of the moored ship, a hull shape representation needs to be made. The mooring equipment on board the ship needs to be assessed based on input data from the terminal and/or available publications.
- The mooring equipment of the ship includes mooring winches, which are used be the crew to handle and store the lines. In some cases, extra shore-based equipment can be present. Examples here are line tension control systems (e.g. ShoreTension) and vacuum based pad systems (e.g. Cavotec, Trelleborg).
- If the berth is located close to a fairway, passing ship effects might be relevant. The design passing ship, as well as speed and trajectory, need to be determined.
- The design wind conditions for safe mooring in extreme conditions as well as during loading operations need to be determined.
- The response of the moored ship (line forces, fender forces and ship motions) needs to be compared to relevant criteria.

1.3 Objective

The thesis focusses on improving the mooring analysis, using the UGent in-house tool *Vlugmoor*, which allows a TDS to be performed. The emphasis is on modelling the response of ships moored at a a Sheltered Terminal according to the definition from section 1.1.2.

At Sheltered Terminals, the effect of wind and passing ships is prominent. In the mooring study examples listed in appendix A, it is seen that the passing ship effect acts as the main disturbance on the moored ship. Wind effects however reduce the capacity of the mooring configuration to deal with passing ship effects, hence the importance of improving the wind modelling.

As a mooring analysis is composed of many different parts however, a diversity of the topics need to be addressed in this thesis. Figure 1.6 shows the appearance of the mooring analysis for a Sheltered Terminal, as a specific application of the general mooring analysis structure from figure 1.4. For each block, the corresponding thesis chapter where it is discussed is indicated.

1.3.1 Input TDS

The mooring arrangement, transferring the loads from ship to berth, needs to be assessed prior to the TDS. For oil and gas tankers moored at jetties, clear standards are present and applied. In this thesis, a novel method to assess the quality of any mooring configuration is sought.

Many different mooring line types exist, either synthetic 'ropes' or steel wires. Within the synthetic rope categories, many different materials, blends and rope structures exist, which influence the way the rope responds. The response of the rope also changes over the lifetime, as creep is induced, as well as during loading cycles, manifesting in hysteresis. These aspects are investigated by looking at international standards, but also by performing full scale mooring rope tests at Bexco, a Belgian rope manufacturer.

The effect of wind is calculated through aerodynamic shape parameters, which are only openly available for a limited number of ships and loading conditions. A critical review of these parameters as

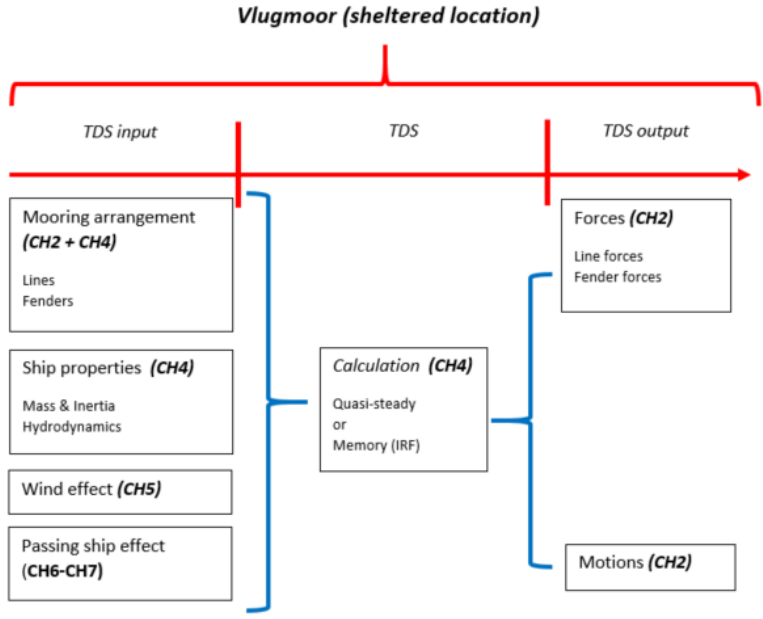

Figure 1.6: *Mooring analysis structure applied for a sheltered location, indication of thesis chapter (CH2-7).*

well as the formulas used to calculate wind forces is undertaken. A steady wind field is often applied as an external force in design studies. An expansion of the analysis to include wind gusting, via spectral representations, is presented.

The passing ship effect can be modelled using various tools (empirical, numerical, model scale,...) (see section 2.4 for definitions). For the specific purpose of passing ship events in restricted (horizontal and vertical) channels, a new, comprehensive and systematic model test series has been performed. These tests are used to generate an empirical model, as well as validate an existing numerical model.

1.3.2 TDS

In the time domain simulation, the response of the moored ship under external disturbances is calculated, by solving motion equations. A frequency domain analysis, where input and output are linked by a (linear) transfer function cannot be used, due to various sources being non-linear. Mooring lines and fenders for example are denoted by a non-linear response. Transient external disturbances (passing ship effects) are another source of non-linearities.

In *Vlugmoor*, a quasi-static approach is used by default, where the dynamic response of the ship is linked to the motions (velocity, acceleration) of the ship at, and only at, the given time step of the simulation. This model has its merits; a quick calculation time and good performance in many applications.

A more accurate representation of the fluid response includes so-called memory effects. When the fluid is excited by a body at a certain time step, it will affect the body on future time steps. The response of the body then becomes a function of its motion history, hence the 'memory' of the fluid. IRF - Impulse Response Functions - are included in the model to represent this memory effect.

At some berths, two ships are moored adjacent to each other, with possible transfer of cargo between them. This mooring type is referred to as double banking. The response of such a multi-body system is complex. A simplified, elegant model is introduced to calculate the responses of both ships in double banking.

1.3.3 Output TDS

The power of the mooring analysis lies partly in the assessment of the output of the TDS. Line and fender forces are most straightforward to assess, bound by their respective breaking loads. For lines, more complexity is added as they should not be loaded close to their theoretical breaking point, as line breaking leads often leads to damage, personal injuries and possibly a breakaway of the ship.

Ship motions need to be assessed on different levels. Any motion will affect the loading process, causing noticeable delays above certain motion magnitudes. Large motions can cause safety issues, which vary with the ship (cargo) type. A methodology is presented in this thesis to derive safety limits for surge motions of moored container ships, as these are the most critical.

1.4 Chapter per chapter

Chapter 1 is the introduction to the thesis work

Chapter 2 describes all the components of a mooring analysis, subdivided into external disturbances, mooring equipment and ship response. A description of how *Vlugmoor* is usually applied within project based questions is given.

Chapter 3 discusses mooring line properties. First, international standards and guidelines are presented and compared with two case study examples, an Aframax tanker ($T0Y$) and an Ultra Large Container Ship ($ULCS$). In the second part of the chapter, the tensile tests for three mooring ropes, performed at Bexco, are discussed.

Chapter 4 describes the mathematical form of the motion equations which are solved in the TDS. Single banking (one ship moored at a berth) as well as double banking (two ships moored to each other) are presented. The eigenperiods of the moored ship are estimated analytically and compared with periods of external loads. The quality of the mooring arrangement is assessed by defining four parameters, based on line material, length and orientation. TDS simulations are used to compare with predictions based on these parameters for the $ULCS$ case. The chapter ends with the complete derivation of the motion equations for the quasi-static model, as well as the expansion of the model to include memory effects (by using IRF functions).

Chapter 5 discusses the analysis of wind effects on moored ships, focussing on the container terminal environment. The use of wind coefficients, as well as wind force formulas are discussed, including a case study for the $ULCS$, based on literature as well as CFD. The representation of turbulent wind fields is discussed, as well as the implementation of wind spectra in *Vlugmoor*.

Chapter 6 presents the scale model test program for passing effects in confined water, called $PESCA$ - Passing Effects in Shallow and Confined Areas, performed at the Towing Tank for Manoeuvres in Confined Water (Flanders Hydraulics Research). The effect of passing distance, under keel clearance and channel width are assessed by a regression analysis. These insights are used to define an em-

pirical model for the peaks in passing ship forces in the horizontal plane.

Chapter 7 discusses the validation of the numerical model RoPES, a potential flow solver, intended to model the effect (forces) of passing ships on moored ships. It starts from a description of the software, as well as a discussion of how the scale model test environment is modelled in RoPES. The time series in 6DOF are compared. For the forces in the horizontal plane, an existing RoPES correction factor proposed by literature is examined.

Appendix A lists the publications in the topic of mooring from the author, followed by a description of a selection of ten commercial mooring studies.

Appendix B gives the axis system and conventions used in this thesis.

Appendix C extends the discussion on wind profiles and wind spectra.

Appendix D gives details on the $PESCA$ model scale test program, as an extension of the content of chapter 6.

Appendix E shows RoPES validation figures as an extension to chapter 7.

Appendix F summarizes two case study examples : moored $T0Y$ (Aframax Tanker) and moored $ULCS$, which are discussed throughout the thesis.

1.5 Work done by PhD author

The thesis work of four years included performing roughly half time commercial mooring studies, which followed three years of executing commercial mooring studies as a research associate at Ghent University. As the projects often included challenging questions, they also helped in developing the mooring analysis and have had a great influence in the topics which were investigated and are now presented in this thesis work.

Most projects were done in the Antwerp port area, either commissioned by the port or by terminal operators. Other projects were situated in Belgium (Zeebrugge), Egypt and Algeria. Figure 1.7 indicates at which locations mooring studies have been performed within the Antwerp port area. Appendix A highlights a selection of these studies, as well as their impact on the development of the mooring analysis. In most study examples, the passing ship effect is the most prominent external disturbance. This appendix also contains a list of the scientific papers published by the author.

The work done by the author largely coincides with the answer to the objectives listed in section 1.3, yet it is good to highlight here which part of the work has been done by the candidate, as a version of the quasi-static *Vlugmoor* motion solver already existed, written by Em. Prof. Dr. Marc Vantorre.

- The *Vlugmoor* code which was available in Microsoft QuickBasic structure has been rewritten in object-oriented MATLAB environment, including a user interface to set up and analyse systematic calculations.
- *Vlugmoor* has been expanded to model non-linear mooring line and fender responses.
- A simplified model of double banking, defined later as 'moving quay wall', has been implemented in *Vlugmoor*.
- The memory effect option which represents ship dynamics more accurately than the quasi-static model has been implemented in *Vlugmoor*, including two representations of the memory functions.
- The analysis of output is further refined, including in-depth analysis of the motion criteria for container ships.

- The mooring configuration is analysed analytically, by estimating eigenperiods. Also, four characteristic parameters are defined to evaluate the performance of the mooring arrangement.
- The wind analysis is broadened to include an operational analysis for a container terminal. The choice of wind coefficients is commented on, as well as the usage of said coefficients in wind force calculations. The analytical assessment is done by the author, Dr. Wim van Hoydonck (FHR) performed CFD simulations as validation.
- A scale model test program has been written, executed, analysed and post-processed by the candidate, under the guidance of Prof. Dr. Guillaume Delefortrie, who performed the first data processing step.
- The scale model test output was used to derive an empirical relationship to calculate passing ship effects, in the form of peak forces, in shallow and restricted water.
- The scale model test output was used to validate the potential flow package RoPES, as well as to check the correction factor proposed in literature for forces in shallow and restricted water.

The author is also involved in two PIANC working groups: Working Group 186 'Mooring of Large Ships at Quays' [Mara] and Working Group 212 'Criteria for Acceptable Movement of Ships at Berths (Update of MarCom WG24)' [Marb].

Within the scope of one of the commercial projects, a novel mooring method to restrict the motions of moored ships at the berth has been developed. As the project is still ongoing, the candidate will not further discuss this study in the thesis. It did lead to an extension of the *Vlugmoor* package, which is also not further discussed.

Figure 1.7: *Project locations Port of Antwerp 2014-2020 (A-P), Google Earth*

Bibliography

[Bak15] B A Bakermans. “Open ports for container vessels”. In: (2015).

[Gou19] Tim P. Gourlay. “A Coupled Ship and Harbour model for Dynamic Mooring Analysis in Geraldton Harbour”. In: *Australasian Coasts and Ports 2019 Conference*. Hobart, Australia, 2019.

[IAC20] IACS. *Anchoring , Mooring , and Towing Equipment (revision 2020)*. Tech. rep. 2020, p. 20.

[Mara] MarCom Working Group 186. *Mooring of Large Ships at Quay Walls*. -to be published -.

[Marb] MarCom Working Group 212. *Update of WG24 - Criteria for acceptable movement of ships at berths*. Tech. rep. - to be published -.

[Mar15] Maritime Safety Awareness. “Shaping Shipping for People : Thinking - mooring safety”. In: 2 (2015).

[Mar95] MarCom Working Group 24. *Criteria for Movements of Moored Ships in Harbours - a Practical Guide*. 1995.

[OCI18] OCIMF. *Mooring Equipment Guidelines - MEG4*. Witherbys, 2018, p. 312.

[Pin09] J. A. Pinkster. “Suction, Seiche and Wash Effects of Passing Ships in Ports”. In: *Transactions - Society of Naval Architects and Marine Engineers* 117 (2009), pp. 99–124.

[Ste09] Steamship Mutual. “Safe Mooring Practice”. In: RA08, December (2009).

[UK 09] UK P&I Club. “Understanding mooring incidents”. In: *LP News* (2009).

2
Mooring analysis

A mooring analysis is defined in this thesis as the study of the behaviour of the moored ship at a berth during her stay. When the ship is moored, many potential external disturbances will act on the ship (section 2.1). The mooring equipment (mooring lines and fenders in most applications) transfer these loads to the berth (section 2.2). In doing so, lines will stretch and fenders will be compressed under the motion of the moored ship. These loads and motions need to be evaluated (section 2.3).

The response of the moored ship system can be assessed using a variety of modelling tools (section 2.4); in most applications, a combination of tools will be used to perform the mooring analysis. Section 2.5 describes the structure of the UGent in-house tool *Vlugmoor*, and states for which study applications this tool is used.

The external disturbances, as well as the ship's response, are defined in the axis system shown in figure 2.1. This axis-system is right handed, with the origin at midships, water plane (see appendix B for further background). Following this definition, three translation modes (surge, sway, heave) and three rotational modes (roll, pitch, yaw) are defined.

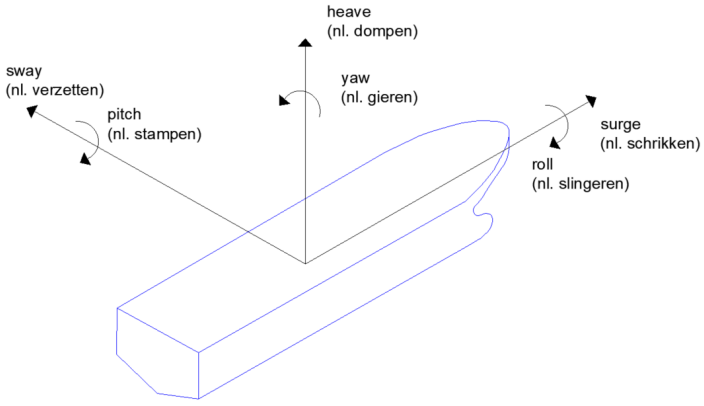

Figure 2.1: *Definition 6DOF in English and Nederlands (nl.).*

2.1 External disturbances

External disturbances are defined as any action not caused by the ship herself, which exerts forces on the (moored) ship.

2.1.1 Wind

Wind, or air flow, is present at all ship berths, caused by pressure differences in the atmosphere, on small and/or large scale. When this air flow interacts with a structure, it will cause a pressure difference between windward and leeward side, resulting in a net force acting on the structure. The structure, or in general obstacle, will also change the local wind field. As the atmosphere is a dynamic body, the wind speed will also change over time. On a short time scale, seconds to minutes, this is called gusting, which is the most relevant period for affecting a moored ship dynamically. On a larger time scale, an average (steady) wind field is present.

The nature of a port environment, consisting of open water surface, cranes, buildings, container stacks and of course (moving) ships creates a very complex situation when it comes to assessing wind effects. CFD simulations, as for example LES (Large Eddy Simulation), could be used to assess the local wind field complexity.

Performing CFD computations is however expensive, both concerning time and money. As a wind force calculation is only one aspect of a mooring analysis, a simplified approach is sought. Existing sets of wind coefficients, calculated by performing wind tunnel tests or CFD, offer a way of calculating the total wind force acting on the moored ship. These coefficients represent the aerodynamic properties of the ship. When the wind speed is varied based on a spectral wind representation, gusting wind effects can also be represented using this approach.

Chapter 5 elaborates on how to approach wind modelling for moored container ships. A similar discussion is also held within the MARIN JIP *Windlass*, in which UGent is a project partner.

2.1.2 Current

A water current is a flow of water, which can have different origins. The two most common current sources are tidal and river currents. Tidal currents change directions (ebb and flood current), whereas a river will always flow from source to mouth. River mouths connected to sea will often face interactions between tidal flows and river discharges.

The physical interaction between current and ship hull is very similar in nature to the one between wind and hull. Mathematical representations of wind and current effect are thus similar in nature. The density of the medium (air versus (salt) water) however differs greatly. [OCI18] published a list current coefficients for oil and gas carriers, along with a calculation example.

Currents are contained by the horizontal and vertical boundaries of the waterway and will thus be more predictable then wind. The interaction between ship and current however will vary depending on the vertical and horizontal clearance between ship and bank/bottom. [OCI18] gives coefficients for 2%, 5%, 10% and 200 % UKC, defined by eq. 2.1 (figure 2.2). This definition is used consistently in this thesis, as it is able to relate draft and water depth in one term. The inverse proportional relationship between UKC and squat [Bri+09] and bank effects [Lat14] is an example of the significance of this parameter.

$$UKC = \frac{h - T_{\mathrm{M}}}{T_{\mathrm{M}}} \tag{2.1}$$

The current effect on moored ships is not further elaborated on in this thesis, as most applications studied by the author are either situated behind locks (Sheltered Terminal) or are denoted by a current along the quay wall, which means the flow surface is much smaller compared to jetty applications where a transversal current is present, as discussed by [OCI18]. As far as the passing ship effect goes (section 2.1.4), the speed through the water (incl. current) should be considered as passing speed [HJ14].

2.1.3 Wind generated waves

Waves can be defined as water surface disturbances, caused by a variety of sources. A tidal surge for example is a long period wave

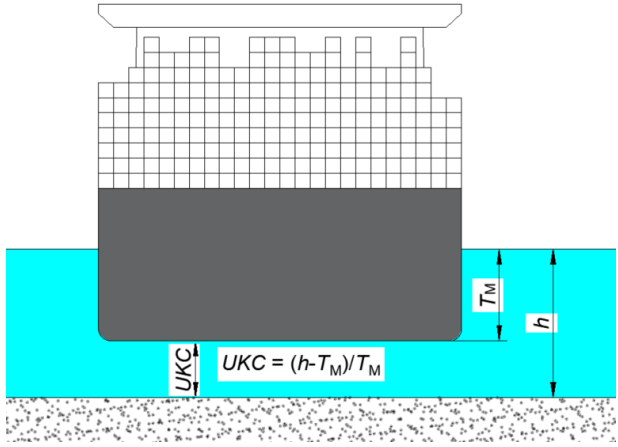

Figure 2.2: *Illustration of the UKC definition, h = water depth, T_{M} = draft ship (midships).*

system caused by the attraction of the Sun and the Moon. A tsunami is a wave system caused by a (subsea) earthquake. Within this thesis, the waves which are discussed are generated by wind excitation of the water surface. Within this definition, several subcategories can be defined. The discussion is this section is based on figure 2.3 [Hol07], which can be traced back as far as [Mun50]. The figure shows an arbitrary energy definition on the vertical axis as a function of the wave frequency, indicating different wave types allocated to frequency bands. For the purpose of this thesis, some types of infra-gravity waves are included in the definition of wind-generated waves, as will be explained further down this section.

Wind blowing over a large distance, called fetch, adds energy to the water body and will cause water surface disturbances. The period and wave height of the system depend on the wind speed and fetch length (in shallow water the bathymetry also influences these parameters). The characteristic of this system depends on fetch length and wind speed, and is composed of waves of shorter periods (10 seconds and less).

The wave system can travel beyond the storm region, forming a swell wave system, denoted by long crested waves with periods between 10s and 30s. [Mol+03] modelled the response of a moored LNG

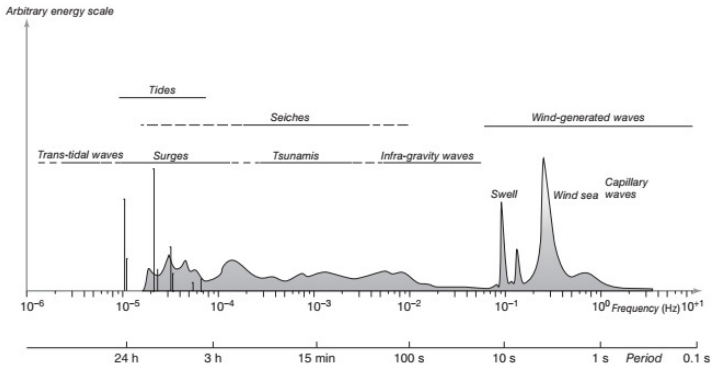

Figure 1. Frequency and period of ocean waves. (Reproduced from Holthuijsen, 2007. © Cambridge University Press, 2007.)

Figure 2.3: *Arbitrary energy content in function of frequency for ocean waves, from [Hol07].*

carrier to swell with peak periods between 14s and 18s, showing that the ship motion energy was present in the same frequency region. [Van+15] discusses how the harbour layout (breakwater and entrance channel) can be adjusted to reduce influence of swell on moored ships.

Long waves, having periods roughly between 30s and 300s [MMD06], can originate from a travelling wave system due to, amongst others, shoaling and diffraction. They can be formed when two adjacent frequencies with sufficient energy interact, generating a wave with frequency ($\frac{rad}{s}$) $\omega_1 + \omega_2$ and $\omega_1 - \omega_2$, the latter leading to long period waves. This wave system can penetrate beyond breakwaters and has relatively small amplitudes (range of cm to dm), which make them easy to overlook. Long waves however come with significant total energy content, as well as periods in the range of the eigenperiods of the ship. The hydrodynamic damping at these long periods is also negligible.

Related to the (travelling) long waves, certain basin shapes can also lead to standing wave formation. Standing waves appear in all disciplines of science (and beyond, take for example guitar strings). Eq. 2.2 show how the natural periods of a rectangular basin can be calculated (from [HJ14]). In this publication, they measured standing waves after a ship passage, albeit limited to a few periods, as

the excitation force (passing ship) is no longer present. In [MMD06], they could indeed observe that the long wave energy coming into the harbour manifested into wave energy following the three first eigenperiods of the basin.

A further discussion on the calculation of the response of a moored ship to wave forces is not present in this thesis. Section 4.5 however does link the eigenperiod of the moored ship to the energy spread of a wave system over the frequency domain (figure 2.3).

$$T_{\mathrm{nb}} = \frac{2L_{\mathrm{b}}}{n\sqrt{gh}}, n = 1, 2, 3, ...3x \quad Closed\ basin \tag{2.2a}$$

$$T_{\mathrm{nb}} = \frac{4L_{\mathrm{b}}}{(2n+1)\sqrt{gh}}, n = 0, 1, 2...3x \quad Open\ basin \tag{2.2b}$$

2.1.4 Passing ships

The effect of passing ships on moored ships is a particular case of the general ship-ship interaction problem, where one of the ships has zero forward speed. A good discussion on ship interactions was held during the 2nd MASHCON conference in Trondheim, Norway (18-20 May 2011).[VVL02] studied such interaction events, for which some discussed a zero forward speed for one of the ships involved. [VKV03] succeeded this work, focussing only on the case where one of the ships had zero forward speed.

In the scope of this work, the discussion is limited to the moored-passing ship interaction, where the moored ship has zero forward speed, which simplifies the general problem. Providing a good estimation of the passing ship effect is however cumbersome, as the list of parameters influencing the magnitude is large (table 2.1). Chapter 6 further elaborates on the effect of a selection of these parameters.

2.1.4.1 Primary and secondary wave system

Despite the nuances in how the passing ship effect manifests, the wave system generated by the passing ship always consists of two parts, defined as primary and secondary wave system, schematically represented in figure 2.4. The primary wave system consists of a large depression along the sides of the ship and a water elevation

Table 2.1: *List of parameters influencing the passing ship effect.*

f(ship)	f(passage)	f(location)
L_{OA}	distance	UKC (passing)
L_{PP}	speed	UKC (moored)
B	direction	blockage
T_{M}	drift angle	basin shape
C_{b}		

near the bow and stern region, caused by the forward motion of the ship and its corresponding return flow. The secondary wave system, called the Kelvin wave system, is a surface wave system, which is very recognisable when ships are photographed from above, where the pattern consists of high frequency waves. Due to this difference in periodicity, these waves will have a different impact on the moored ship, depending on size and mooring system of the moored ship. Note that in fact several sources will create high frequency waves, forming the Kelvin wave pattern. Figure 2.5 shows the four primary sources for Kelvin waves, superimposed on the primary wave system. In this example, the period of Kelvin waves compared to the primary wave system is significant, much larger than observed in the $PESCA$ model tests (see figure 2.4 (b)).

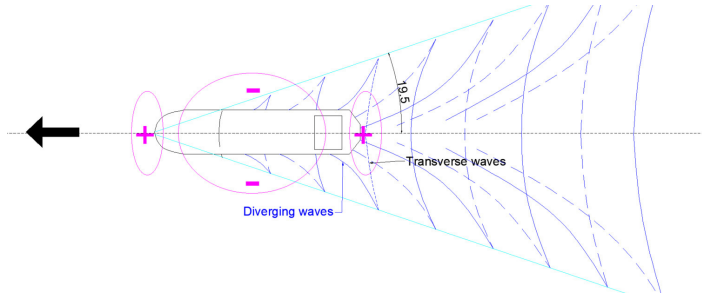

(a) Illustration wave systems

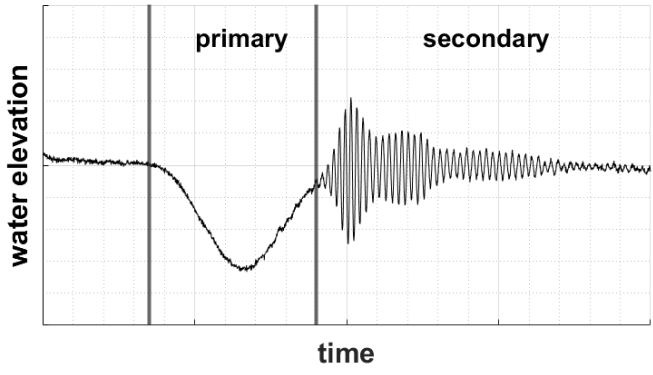

(b) Measured wave systems $PESCA$ model test program

Figure 2.4: *Primary and secondary wave pattern passing ship.*

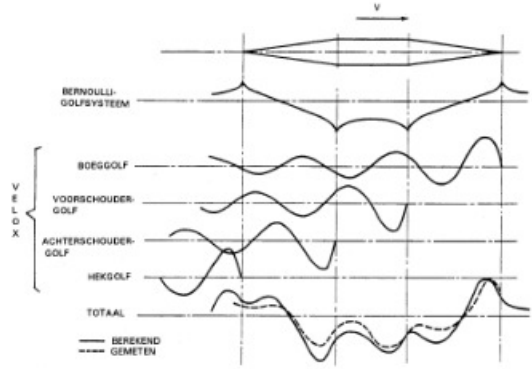

Figure 2.5: *Primary and secondary wave system simplified wedge geometry, travelling from left to right; figure taken from [SNA88], fig. 15.*

2.1.4.2 Effect primary wave system on moored ship

The primary wave system, a combination of a large water level depression and two zones with water level rise (figure 2.4 (a, purple)), causes a distinct force pattern on the moored ship. The discussion here focusses on the forces in the horizontal plane (surge, sway, yaw) (see chapter 4 for justification). Figure 2.6 shows how the magnitude of surge, sway and yaw changes during the passage. The relative position of the passing ship with respect to the moored ship (x-direction) is expressed to the parameter ξ (eq. 2.3). ξ gives the non-dimensional position of the midship of the passing ship, in the axis system of the moored ship (O_{xyz} in figure 2.6). As an example, $\xi = -1$ in figure 2.6, means that the bow of the passing ship is aligned (x) with the stern of the moored ship.

$$\xi = \frac{x_{\mathrm{p}}}{\frac{L_{\mathrm{PP,m}}+L_{\mathrm{PP,p}}}{2}} \tag{2.3}$$

Figure 2.7 shows that in fact surge, sway and yaw show 2, 3 and 4 peaks respectively. The period and exact location (and of course magnitude) of the force peaks depends on the list of parameters which was given in table 2.1. Figure 2.7 shows measured forces on a moored ship as part of $PESCA$ (chapter 6), confirming the presence of the peaks and showing how the signal varies between the peaks. For a passing ship event with a given period, say T_{p}, the period of the surge, sway and yaw motion will be approximately T_{p}, $\frac{2}{3}T_{\mathrm{p}}$ and $\frac{1}{2}T_{\mathrm{p}}$ respectively (see figure 2.7), which is relevant when comparing with the eigenperiods of the ship.

When dealing with passing ship effects, there are two main scenarios which occur; the berth is either a water impenetrable wall (called quay) or the ship is moored at a platform on slender piles (called jetty). These two concepts have also been modelled in the $PESCA$ tests as shown in figure 2.8. The presence of the solid boundary (quay) next to the moored ship will alter the flow of water around the ship, as the flow is partly obstructed. Figure 2.7 shows how the forces are affected, with a strong increase in surge and a decrease in sway and yaw. [Pin04] explains the difference between quay and jetty mooring as the effect of the flow restriction in the presence of the quay wall, causing an increase in longitudinal flow and a reduction of the transversal flow.

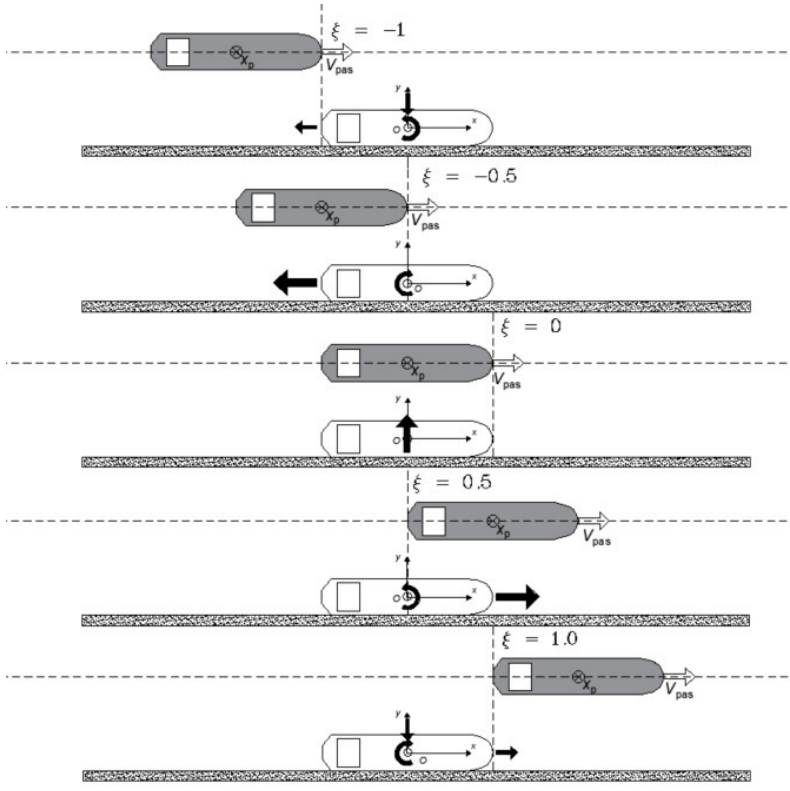

Figure 2.6: *General effect of the primary wave system of the passing ship (grey) on the moored ship for five positions ξ of the passing ship.*

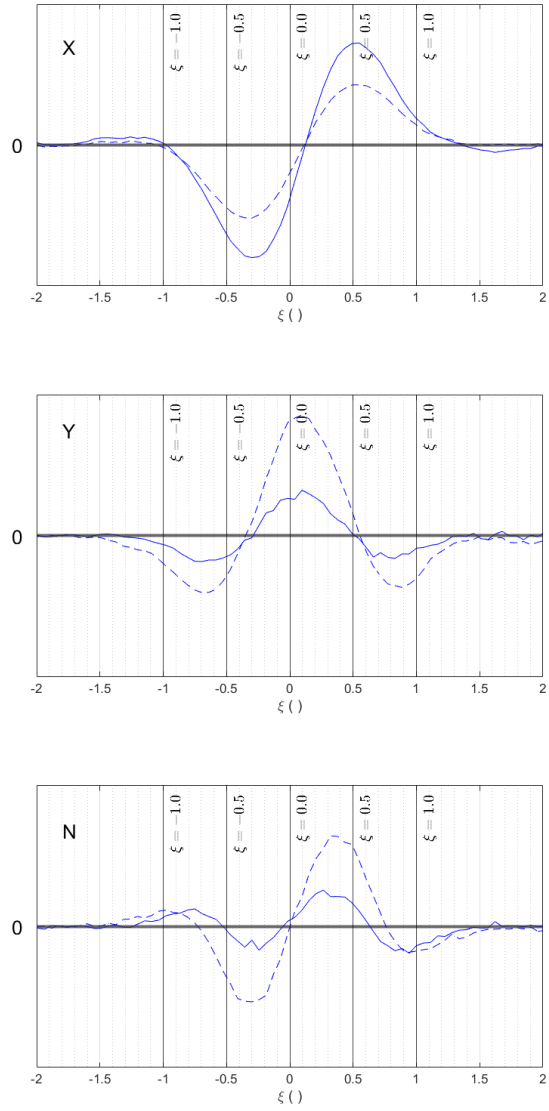

Figure 2.7: *Forces acting on moored ship, quay (full) and jetty (dashed), for the same passing event; measured signal from PESCA model tests; X = surge force (top), Y = sway force (middle), N = yaw moment (bottom)*

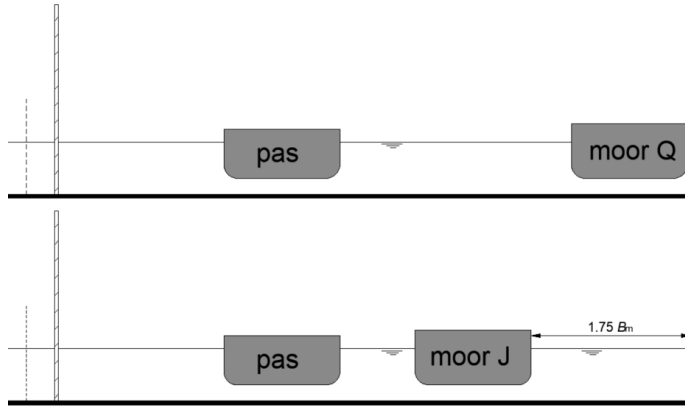

Figure 2.8: *Quay (top) and jetty (bottom) mooring position from PESCA model test.*

2.1.4.3 Effect secondary wave system on moored ship

The secondary wave system, also known as Kelvin wave pattern, consists of divergent and transverse waves (figure 2.4). This system can travel over significant distance with only limited energy loss; Fast craft passing at larger distances are then potentially dangerous for moored ships [LY19]. The period of such waves is small, which will usually not excite mooring systems of large ships. In section 6.2 the appearance of these kelvin waves is studied by a Fourier transform of wave gauge measurements alongside the moored ships.

2.1.5 Other disturbances

Waves, wind, current and passing ships form the majority of the external disturbances which need to be studied in a mooring analysis. There are however other possible loads which will affect the moored ship. Some examples are listed here:

- **Bore** A bore, also known as soliton, is a sort of wave, where a mass of water travels through a confined section, comparable in physics to a fluid pushed through a cylinder by a piston. An example is when a tidal wave travels upstream through an estuary. Figure 2.9 shows a ship travelling through a confined section, a canal, with a large blockage (ratio midship to canal section). The return flow will be restricted to a point where not all water can be evacuated. The water will then be pushed in front of the ship, generating a bore. This water mass can subsequently enter a side branch of the canal, where possibly (inland) ships are moored [Pin09].
- **Collision** A collision of two ships can lead to large damages to the ships, but also possibly causing fairway obstructions. Figure 2.10 illustrates a moored ship breaking loose from her moorings, in heavy wind conditions. The ship will start drifting as the main engine will usually not be running when the ship is at the berth. [EVM09] simulates the impact of such a drifting ship on the moored ship (hull) as well as the influence on the mooring lines of the moored ship.

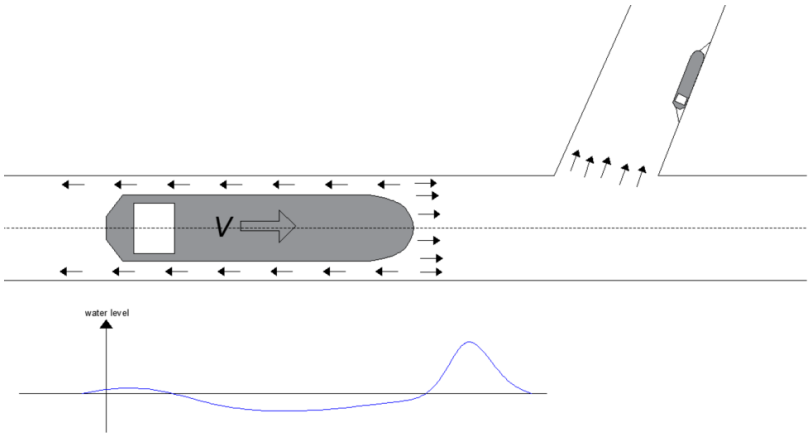

Figure 2.9: *Illustration bore wave generated by ship sailing through a canal, affecting moored ship in side branch.*

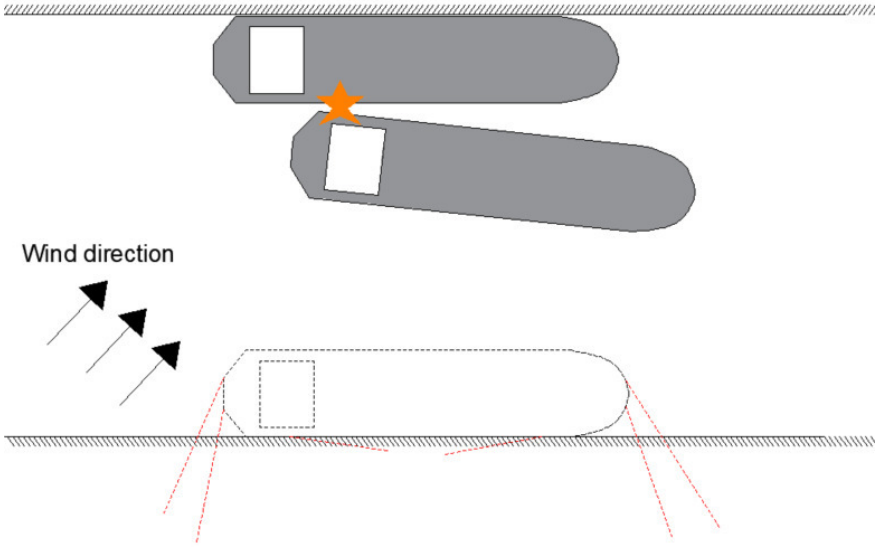

Figure 2.10: *Illustration moored tanker breaking loose from its moorings, drifting and colliding with moored ship on opposite size of channel, under the influence of wind.*

2.2 Mooring equipment

Mooring equipment is the collective name for all the hardware which is used to moor a ship at the berth. The discussion mainly focusses on the traditional mooring, where the ship uses its own mooring lines, which are connected to landside bollards. Figure 2.11 and 2.12 show the mooring equipment, illustrated for a container berth. The same components can be found at other berth types. The numbers on the figures coincide with following equipment:

1. **Bollard** is the fixed mooring point on the berth, which is used to connect the eye of the mooring line. For oil and gas terminals, Quick Release Hooks (QRH) are often used.

2. **Fender** is the cushion element which protects ship and berth under the impact velocity during berthing and when the ship is moored.

3. **Mooring line** is the steel wire or synthetic rope which runs from the ship to the shore, transferring loads from the ship to the berth.

4. **(roller) Fairlead** or **Chock** is the opening in the ship's hull / bulwark through which the mooring line runs from deck to shore.

5. **Mooring winch** is the connection of the mooring line on the ship side. The mooring winch can control the tension in the lines in various operating modes.

6. **Roller guide** is the element on the mooring deck which is used to change the direction in which the mooring line runs.

7. **Bitt** is a fixed mooring point on deck, similar to the bollard on shore, to which mooring lines are connected.

2.2.1 Ship Equipment

2.2.1.1 Mooring lines

Mooring lines are slender wires or ropes which can transfer large loads from ship to berth. Their elastic properties will play a major role in the response of the moored ship; Chapter 3 is entirely dedicated to the study of mooring line properties.

Figure 2.11: *Overview mooring equipment (I), (1) bollard, (2) fender, (3) mooring line, (4) (roller)fairlead; image courtesy of Antwerp Port Authority*

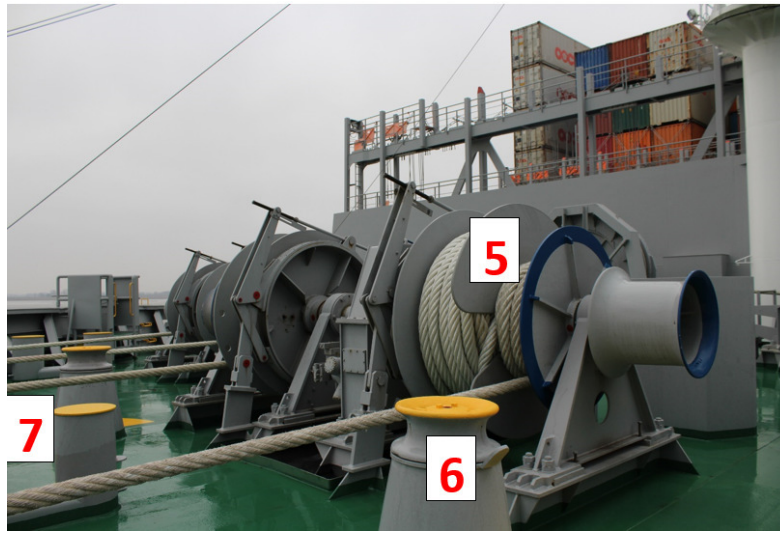

Figure 2.12: *Overview mooring equipment (II), (5) winch, (6) roller guide, (7) bitt.*

Figure 2.13 shows a generic mooring line response, which is non-linear. ϵ_l is the strain in the line, positive when the line is elongated. For positive ϵ_l values, the slope of the curve is not constant, meaning that the response is non-linear, i.e. the slope is a function of the strain. This slope is defined as k_l, a common notation for a spring constant. If the untensioned line length is larger than the distance between the two connection points, no response force is generated, denoted as 'slack'. This is mathematically represented as a zero force for negative strain in figure 2.13. Eq. 2.4 represents how the strain and force are related, the strain is defined as the ratio between elongation and untensioned length (eq. 2.5). The break load of the line which is guaranteed by the manufacturer is denoted by MBL - Minimum Breaking Load.

$$\begin{cases} F = k_l(\epsilon_l) \cdot \epsilon_l l_0 & \epsilon_l > 0 \\ F = 0 & \epsilon_l \leq 0 \end{cases} \tag{2.4}$$

$$\epsilon_l = \frac{\Delta l}{l_0} \tag{2.5}$$

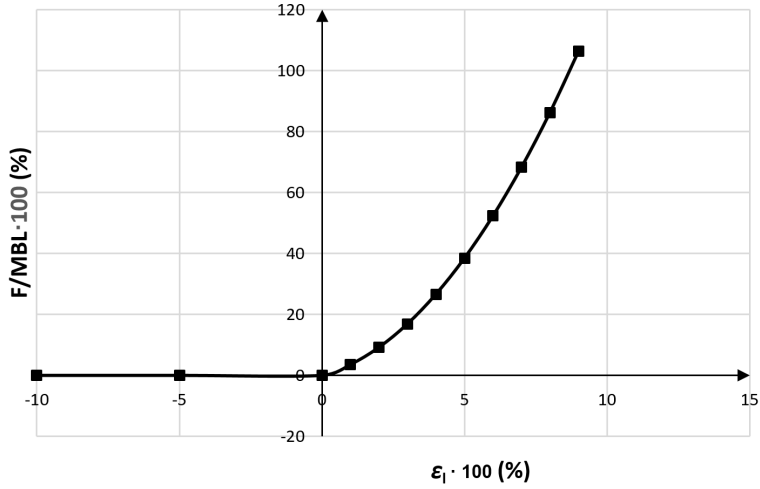

Figure 2.13: *Generic mooring line response curve.*

2.2.1.2 Mooring Winches

Mooring winches are used to control the tension in the lines and protect the lines from breaking. Their strength properties are de-

signed based on the mooring line MBL [IAC20]. For the purposes of a mooring analysis however, the working modes of the winch system are most relevant. The first parameter is the active pull force, denoted as drum load, which is the pull capacity of the winch at nominal speed. The second one is the brake load or holding load of the winch.

Requirements for both parameters are written a ISO norm [ISO12], visualised in figure 2.14. The active pull mode is used to tension the lines, which is done upon arrival (pretension). Pretension levels vary, but 10% MBL is commonly accepted as an appropriate value. After applying pretension, the engine is disengaged and a manual (hydraulic) brake is engaged, with min. 80% MBL capacity. Figure 2.14 also includes values for use of auto-tension winches, which keep the tension level constant. This is generally only allowed in good weather conditions, as the capacity is much lower than the manual brake capacity. In tidal ports, Port of Antwerp for example, the use of auto tension is not allowed, as it would cause the ship to 'walk along the quay' due to current influences, as illustrated in figure 2.15. Here, the ship moved from her original position (dashed) to a new position. A constant current force (green arrow) will cause the winch controlling line 'B' to lengthen the line if the tension becomes too high; The winch controlling line 'A' will haul in the line to keep it in tension. The result is a change of ship position with the tide, which is unacceptable.

The ISO guideline, which aims at designing a standard winch, does however not specify practical brake settings. 80% MBL is a load which will at least induce fatigue in the line, but could also induce line break, as line capacity deteriorates over time (see section 5.4.1 from [OCI18]). In line with this concern, the same source advises to limit brake load to 60% MBL in practice. As OCIMF is strictly written for oil/gas tankers, the question remains whether other ship types follow this recommendation. In PIANC WG186 discussions, port authorities mention that setting 80% brake is not uncommon for container ships. Adding to this uncertainty are winch wear and tear, as well as brake performance in dry versus wet conditions.

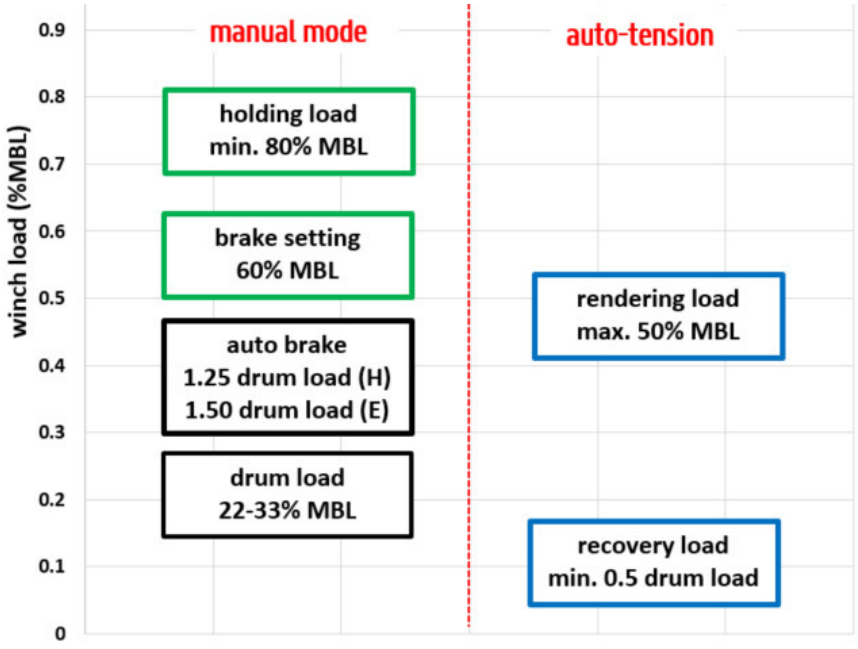

Figure 2.14: *Winch design and operation parameters, based on [OCI18]and [ISO12]*

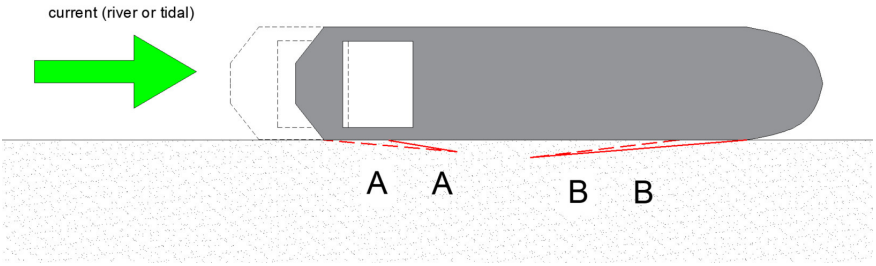

Figure 2.15: *Illustration of ship walking along the quay under the influence of current, spring lines A and B, dashed line = starting position, full line = ending position.*

2.2.1.3 Rollers, bitts and fairleads

Rollers, bitts and fairleads are static parts of the mooring equipment. They are designed based on lines' MBL (min. 1.25 times MBL, [IAC20]). Fairleads are used to lead the line through the bulwark of the ship. There are two main types, roller fairleads and panama chocks (figure 2.16). A roller makes it possible to change direction in the horizontal plane on board the ship, increasing the number of leads which can be reached by one winch (see example figure 2.17). Bitts are fixed mooring points on board. They are used for connecting tow lines (where the winch is actually on the tugboat itself). Adding extra mooring lines on bitts is also done in some cases to increase mooring capacity. As these lines cannot be pre-tensioned, their performance is however considered unreliable.

2.2.2 Terminal equipment

2.2.2.1 Bollards and QRH

The mooring lines leaving the ship's fairleads are attached to mooring points on the terminal side. A subdivision can be made into bollards and QRH - Quick Release Hook(s). A bollard is a solid steel element, anchored in the quay wall (figure 2.18 (a)). A QRH is composed of one anchor point with 2 to 4 individual hooks attached to it which can each house one mooring rope (figure 2.18 (b)). The advantage of this - more expensive - solution is that the ship can be safety released easily, which is often a demand for oil and gas terminals. At more secluded berths however, it might be unsafe to release the ship in this way, as it can collide with ships at neighbouring terminals. QRHs do offer the possibility of easily including force measuring pins. The tension in all lines can be monitored from one central control room and used to instruct the mooring crew on board.

2.2.2.2 Fenders

Fenders are large cushion elements, which protect berth and ship from damage during approach to the berth as well as during its stay. The list of fenders types is endless, with manufacturers offering their own specific systems. For most mooring applications however, two main types are used, buckling type and pneumatic type. Buckling fenders react much stiffer than their pneumatic counterparts

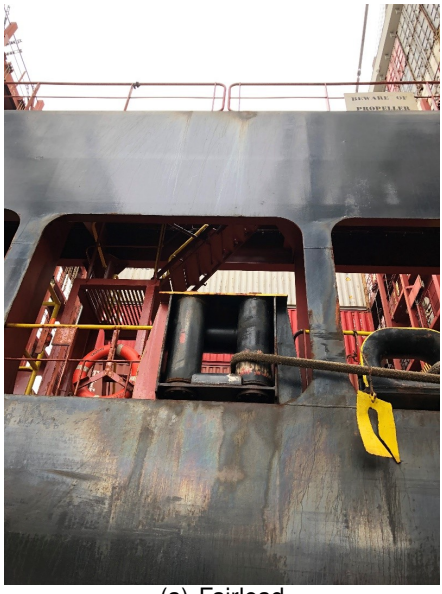

(a) Fairlead

(b) Panama Chock

Figure 2.16: *Equipment on board of ship, images courtesy of Rotterdam Port Authority (a) and Hamburg Port Authority (b).*

Figure 2.17: *Mooring line direction change on deck using rollers, figure courtesy of Hamburg Port Authority.*

(a) Bollard

(b) QRH

Figure 2.18: *Equipment on the berth image (a) courtesy of Antwerp Port Authority, image (b) taken from [Tre21]*

(2.19), affecting the mooring response. [Mar02] (to be superseded by WG211 in the near future [Mara]) offers an in-depth discussion on fender design. For ship-to-ship mooring, which is dealt with from a modelling perspective in chapter 4, pneumatic fenders are mostly used, as these fenders need to float in the absence of a quay to connect them with.

As fenders only respond in compression, a similar non-linear behaviour as for lines is present. In figure 2.19 [Tre20a][Tre20b], a positive fender strain ϵ_{f} corresponds to a compression, which delivers a non-zero reaction force. Eq. 2.6 represents the fender response, with strain defined as the compression Δd divided by the uncompressed width d_0 of the fender. k_{f} represents the stiffness of the fender.

$$\begin{cases} F = k_{\mathrm{f}}(\epsilon_{\mathrm{f}}) \cdot \epsilon_{\mathrm{f}} d_0 & \epsilon_{\mathrm{f}} > 0 \\ F = 0 & \epsilon_{\mathrm{f}} \leq 0 \end{cases} \tag{2.6}$$

$$\epsilon_{\mathrm{f}} = \frac{\Delta d}{d_0} \tag{2.7}$$

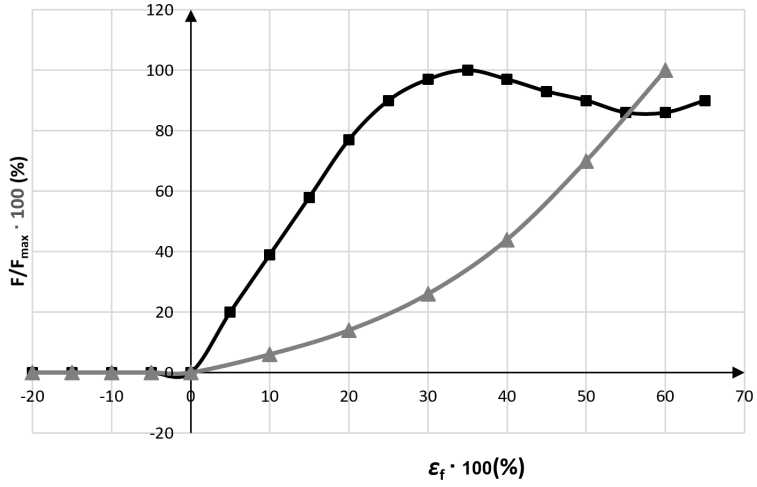

Figure 2.19: *Generic comparison buckling (black) and pneumatic (grey) fender, based on [Tre20a] and [Tre20b].*

2.2.3 Mooring configuration

The mooring configuration, also called mooring arrangement, is the spatial distribution of the mooring lines, which make the connection between a point on the berth (bollard, QRH) and a point on the ship (fairlead). The mooring lines are used to hold the ship in position at the berth and transfer loads between winch and bollard. Their biggest contribution is made to balancing the external forces in the horizontal plane (surge,sway and yaw). In the vertical plane (heave, pitch and roll) the mass of the ship cannot be sustained by the lines (i.e. mooring lines will not lift the ship out of the water when the tide drops). In this case however, a hydrostatic restoring force is present (see chapter 4 for further elaboration).

An appropriate mooring configuration is defined as a symmetric arrangement, where the lines provide efficient resistance to horizontal force components. [OCI18] has defined base rules which can be followed to attain such configuration. These are given in table 2.2. The definition of α_1 (horizontal angle) and β_1 (vertical angle) are illustrated in figure B.3 (appendix B).

Three line types are defined: head/stern, breast and spring lines. They mention that breast and spring lines are most desirable, head and stern can be added for certain configurations. Spring lines and breast lines provide optimal restraint in the longitudinal (surge) and transversal (sway,yaw) direction respectively. For all lines, the vertical angle (in ballast draft) needs to be limited to 25° from horizontal.

Figure 2.20 shows a mooring configuration which is in line with OCIMF standards for the moored $T0Y$, an Aframax type tanker (see chapter 6 and appendix F for details on $T0Y$). Lines 1, 2 are head lines; Lines 3-6 and 11-14 are breast lines; Lines 7-10 are spring lines; Lines 15,16 are stern lines. The berth type where this configuration is found is usually a jetty type berth, where the mooring points are individual dolphins and the berth design is made for a specific design ship. The configuration from figure 2.20 also shows symmetry in the mooring configuration at fore and aft ship.

As mentioned before, OCIMF standards are applied to oil/gas and not necessarily in general. In this case however, there is another reason not to apply them for general berths. Figure 2.21 shows the same moored ship, at a quay-type berth. Here, the berth is designed

as 'multi-purpose' berth, meaning that the infrastructure might be used for a different terminal in the future. To allow construction and use of crane rails (bulk or container berth), the bollards need to be positioned close to the quay waterside face. When applying the criteria from table 2.2, lines 3-6 and 11-14 show vertical angles above 25° in ballast condition. Lines 7-10 are still optimal spring lines, but only line 12 can be considered a breast line. In order to give the reader some way of evaluating and comparing configurations, a novel method using mooring configuration efficiency parameters is given in section 4.3.4.

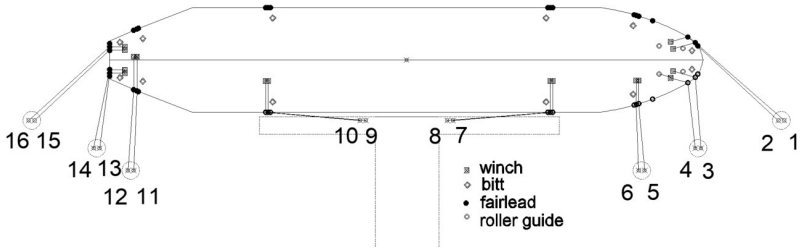

Figure 2.20: *Mooring configuration $T0Y$ at jetty berth conform [OCI18].*

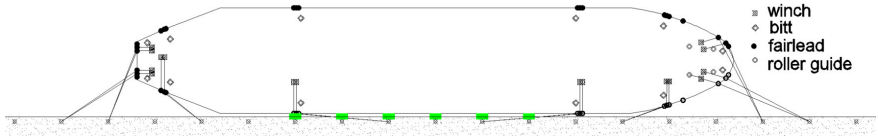

Figure 2.21: *Mooring configuration $T0Y$ at multi-purpose berth.*

Table 2.2: *Mooring line definition and angle range according to [OCI18].* α_1 *= angle in horizontal plane;* β_1 *= angle in the vertical plane; (see figure B.3 (appendix B) for visualisation)*

line type	α_1 range	β_1 range
head and stern lines	45°±15°	$< 25°$
spring lines	5°-10°	$< 25°$
breast lines	90°±15°	$< 25°$

2.2.4 Special mooring systems

Special mooring systems are for the purpose of this work defined as ways of mooring a ship at a berth by using means other than the mooring lines of the ship itself. These mooring systems can be divided into complementary and supplementary systems, the former adding to the mooring lines of the ship, the latter making the mooring lines of the ship obsolete. Table 2.3 gives a (non-exhaustive) overview of mooring systems which have been developed since the 1950s.

When it comes to commercial application, there are at this moment in time two systems which are used globally. The first one is called ShoreTension, shown in figure 2.22. A hydraulic cylinder is pressurized upon installation and provides control for mooring line tension (lower and upper limit) as well as damping (defined as 'swell chamber' in their patent). The mooring line is a stiff Dyneema line (see chapter 3) running from shore to a bitt on board of the ship, which needs to have sufficient capacity to endure the tension in the line.

Cavotec MoorMaster uses vacuum pads to connect to the ship's hull and a hydraulic system to absorb the external forces by allowing limited motions. This system replaces the need for mooring equipment on board the ship. It does come with a high installation and maintenance cost, as well as a complex risk-analysis. Once the system can no longer hold the ship, it will detach and drift away, which is highly undesirable.

Within the scope of commercial mooring studies, a selection of these modern mooring solutions was examined in more detail. Some of these systems were implemented in the *Vlugmoor* software and used to advise clients on the effect of these systems for their specific mooring situation. In another project, which is in execution at the time of writing this thesis, a novel mooring method to restrict the motions of moored ships at the berth has been developed. This method has been implemented in *Vlugmoor*. By studying various case study examples from existing mooring situations, the potential, as well as the robustness of the system was demonstrated.

Table 2.3: *Special mooring systems, C = complementary to the mooring lines of the ship, R = replaces the need for the mooring lines of the ship.*

C/R	name	patent/source	ex. application
C	ShoreTension	W02010-110666	Port Of Antwerp
R	MoorMaster	W02009-054379	St.Lawrence Seaway
R	Mampaey	W02014-05120	Woolwich Ferry
C	Moorex	SE1150850	North Sydney
R	Cottrel et al.	US2001-0029879	*N.A.*
C	Cunningham et al.	US3886887	*N.A.*

Figure 2.22: *Application of ShoreTension at a berth, from ShoreTension website.*

Figure 2.23: *Application of Cavotec MoorMaster at a berth, from Cavotec website.*

2.3 Response of the moored ship

The external disturbances (section 2.1) are balanced by the response of the mooring system (section 2.2) of the moored ship. Mooring lines and fenders need to be elongated and compressed respectively to generate a reaction force, meaning that certain motions will always be present. These forces and motions, whether they are obtained through a time domain simulation or from model scale / full scale testing, need to be analysed properly in order to draw meaningful conclusions, based on set criteria.

2.3.1 Force and motion signal analysis

Motions are defined in the 6DOF which were shown in 2.1. Line and fender forces work in the direction of the line/fender and are thus a vectorial representation of a combination of motion DOF.

Analysing line and fender forces can be considered easier than dealing with motion, as the magnitude will always have a known sign. The line will build tension if it elongates, the fender will respond in compression. For motions, positive and negative motions can be present, as shown in figure 2.24. The peak-to-peak motion is then defined as the difference (in absolute value) of the negative and positive motion. The amplitude is the largest excursion in either positive or negative direction. Both definitions are used in practice, yet the author highly favours the representation as amplitude for two reasons. The zero-level before is usually known (e.g. position gantry crane for container loading, position manifold for tankers). Therefore it makes most sense to express motions relative to this known starting position. Secondly, the peak-to-peak motion definition is ambiguous, as shown on figure 2.24, where both signals have the same peak-to-peak value (PP1-PP2) despite the difference in amplitude (A1-A2)

The definition of the zero-level is in fact not always straightforward, certainly when multiple external forces with different periodicities excite the ship. Figure 2.25 shows the measured surge motion of a moored container ship at a tidal terminal where passing ship excitation is present. Over a period of hours, the ship will move gradually along the quay due to tidal variations. The cranes can easily adjust their position over this long time scale, meaning that the zero-level

definition will change (red dashed line). Over the plotted time, the ship also moves constantly, albeit with very small amplitude, which is caused by wind fluctuations, but also GPS induced noise. A few distinct excursions can be observed, which is a typical response to a passing ship event. For these events, motion amplitudes can be derived relative to the local zero level. Bear in mind that if this plot was taken for a moored tanker, connected to a manifold, the zero level is in fact defined by the initial manifold coupling, meaning that long period as well as short period motions need to be summed to compare with motion limits (see section 2.3.3).

One last aspect which needs to be dealt with is the response to a continuous, oscillatory, loading, which is then typically waves and gusting winds.These disturbances can be either represented as theoretical energy spectra (superposition of harmonic components), as well as measured signals (non-linear or linearised). The response of the system however is always non-linear (as will be elaborated on in chapter 4). For some output parameters, some degree of linearisation is possible.
In [Mar12] for example, they define a surge response spectrum (linear) which is representative for the general surge response of a container ship at a berth. This spectrum is used as basis to come up with criteria based on significant motions. This analysis could be extended through long-term statistics, to come up with most-probable maximum motions (e.g. through a Rayleigh distribution).
In a general analysis, where for example maximum mooring line forces are sought, such linearised analysis might not deliver satisfactory results, as a mooring line response is highly non-linear. Alternative methods exist to cope with such cases. For example, 5 to 10 one-hour simulations could be run in order to derive a representative maximum [Gou19]. When such a maximum is derived, assumptions regarding the long term distribution of such maximum can be made, as is suggested in [Mol+03]. Such techniques have not been used by the author, as the focus of his research and the thesis is the response to the transient passing ship force.

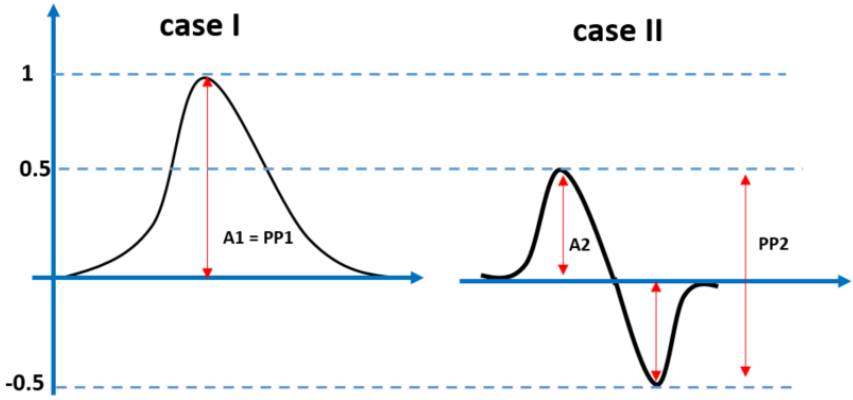

Figure 2.24: *Illustration ship motion response, comparison motion amplitude (A) and peak-to-peak (PP) motion for two exemplary motions: case I and case II*

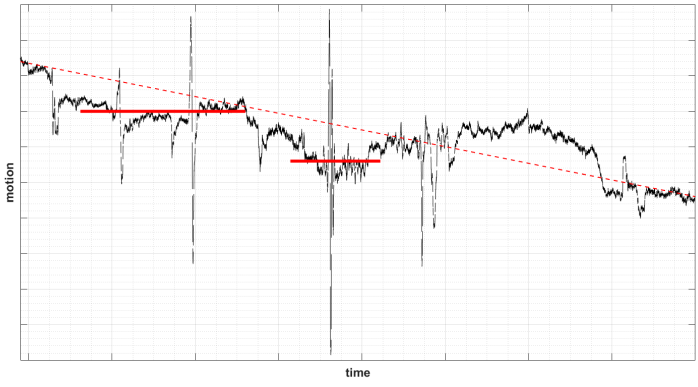

Figure 2.25: *3.5 h GPS measurement surge motion container ship at tidal terminal Port of Antwerp, courtesy of Antwerp Port Authority as the owner of the data.*

2.3.2 Force criteria

2.3.2.1 Mooring line forces

The repercussions for lines breaking are snap-back events, where a huge amount of energy is released and a large potential for injuries and fatalities exists [UK 09]. As mentioned in section 2.2.1.1, the MBL is the characteristic number when it comes to mooring line capacity. The line force should never exceed this value. Applying this limit only makes sense in preliminary assessment. In practice, the winch should always protect the line from reaching this force, by applying the winch brake at 60% to 80% MBL. In case lines are connected to bitts, this safety net disappears and the 100% MBL limit would make sense. Mooring lines however show significant degradation after a number of cycles. The higher the tensions over these load cycles, the faster the fatigue kicks in. [OCI18] therefore demands that line load should remain below 55% MBL for steel lines and 50% MBL for all other lines. In design conditions for terminals, these limits could be applied.

When assessing mooring line forces in 'daily operation', the line forces should in fact be kept to even lower values, to avoid fast deterioration of the line strength. A definition of 'daily operation' is however hard to set unambiguously. It represents conditions which are encountered all year at a berth and which induce many load cycles in the mooring lines. [OCI18] discusses testing line failure for mooring lines at tension ranging from 20 % MBL to 100 % MBL. The 20 % value could be interpreted as a target value for daily operation, which represents many load cycles. A formal statement and/or definition for a 'daily operation limit' has however not been found.

2.3.2.2 Fender forces

Fender loading is different in nature as are the consequences of failure. Fenders are compressed, meaning that worst case the unit completely deforms and is destroyed, in which case maintenance (and costs) are required, yet risks of personal injuries are lower compared to snapping of mooring lines. Another big difference is present in fender design, where it is often done based on absorbing energy during the approach manoeuvre rather than dealing with mooring energy [Mar02], as berthing velocities are usually significantly higher than mooring velocities. Another possible design event

includes fender response as a result of ship collision (section 2.1.5), where a large amount of energy needs to be transferred to the quay/-jetty through the fender system.

Based on this discussion, a limit of 90% of its rated maximum load is proposed as a limit for mooring applications. In most mooring projects where fenders have been designed appropriately, fenders loads are never critical. For cases where fender loads become critical, it is advised to get in touch with the quay designer and/or fender manufacturer to get feedback on the results.

2.3.2.3 Bollard and QRH forces

Mooring line loads need to be transferred to bollards or QRH on the berth. Historically, this was done through tabular values for Service Working Load in function of ship displacement. For oil tankers, this definition makes sense, as the capacity of the mooring equipment increases with increasing displacement. For container ships and gas carriers, these established relationships do not hold, as their wind surface is much higher compared to oil tankers, for a given displacement.

[Bro+18] offers a method which links required bollard capacity to mooring line MBL, which is a very direct relationship. They also look at the winch operation (section 2.2.1.2), where a winch in manual mode will limit the line tension to 60% to 80% MBL, depending on whether you consider the OCIMF operational recommendation for winch brake setting (60% MBL) or the ISO norm of winch brake design (80% MBL)

The difference in design lifetime between berths, typically designed for 100 years, and ships, having a lifetime of around 30 years, makes bollard and QRH design even more challenging. For container shipping, state-of-the-art terminals were built in the 90s for Panamax ships. Designers could not have foreseen such exponential growth in ship dimensions, meaning that if a 20000+ TEU ship visits such a berth, one should check the available bollard capacity. Some measures which can be taken is to limit the number of lines attached to one bollard and/or to set the brake at an acceptable setting not to overload bollards. Setting the winch brake to a predefined value

is however not common practice, as brake levels are often not indicated on the winch.

Another valid exercise is to test existing bollards and to investigate bollard design (safety factors) to gain more insight into how much the existing bollards can be loaded, but also to learn lessons for future bollard design.

2.3.3 Motion criteria

Motion criteria are difficult to set, as they depend on multiple factors, as expressed by eq. 2.8. [Mar95] gives guidelines on motion limits for several ship types and terminal equipment, for 'safe working conditions'. These guidelines are currently being reworked by [Marb], with the author as member. Refining the definitions of the motion criteria is part of the scope of the working group.

The discussion in the present section aims to explain the complexity of deriving motion limits. Subsequently, a surge motion limit for container operations is derived, which can be applied when assessing the response of the moored ship to passing ship effects.

The definition of motions is in accordance with the discussion in section 2.3.1, defining motion limits as amplitude criteria.

$$\begin{aligned} mot.\ crit. = f(&ship\ type,\ terminal\ equipment,\\ &operational\ conditions\ \&\ considerations) \end{aligned} \tag{2.8}$$

2.3.3.1 Ship type

Each ship type usually comes with a specific allocation of cargo spacing and access points for shore based equipment to (un)load the ship.

Figure 2.26 shows a top view of cargo spacing and access points on two ships. The oil tanker has one of multiple cargo holds, containing oil (derivates). Piping infrastructure makes it possible to access the holds through the central manifold installation (often this will actually be slightly off-centre). This means that when it comes to the cargo operation, motion limits should be defined at the manifold connection

point. As this is close to midships / centre of gravity (CoG), the 6DOF motions from [Mar95] should be applied.

Figure 2.26 (b) shows a bulk carrier with several cargo holds over the length of the ship. The (un)loading equipment needs to move along the length of the ship to access all holds. As the equipment is positioned far away from midships, the motion limits should be defined in the most extreme positions, as given by $O'_{x'y'z'}$. These local translations are then a function of the translation of the CoG, in combination with a the rotation about CoG, which is multiplied by the distance from CoG to the origin of $O'_{x'y'z'}$.

Similar reasoning to that presented here for bulk carriers can also be used for container ships (most forward and aft bays), RoRos (position ramps) and cruise ships (passenger bridge).

2.3.3.2 Terminal equipment

The ship type already determines to a large extent how the terminal equipment will look like. An oil tanker for example will be connected to a Marine Loading Arm (MLA) or similar structure which connects a hose to the manifold on board. For some ship types however, differences exist in equipment, depending on cargo (sub)type and loading/unloading. Bulk terminals, which are often part of dedicated berthing infrastructure, vary considerably. Export terminals, located near sources of bulk materials (grain, iron ore, copper,...), need to load the ship, filling via the hatches. Import terminals, located near processing plants, unload the ship, which requires the ability to reach the bottom of the cargo hold.

Figure 2.27 illustrates the different terminal equipment types, without getting into excessive detailing. A grabber can be used to both load and unload the ship, whereas a conveyor belt to used to load to ship at an export terminal. The stiff elevator and hose protrude down the hold to either load or unload cargo. In general, equipment entering the hold will lead to more stringent criteria, as risks for crew and ship are higher (e.g. collision in hold and/or hatch opening). Vertical motions can lead to impact at the bottom of the hold.

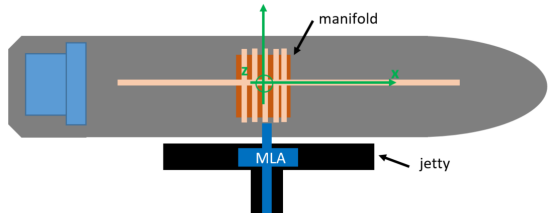

(a) Manifold position on tanker.

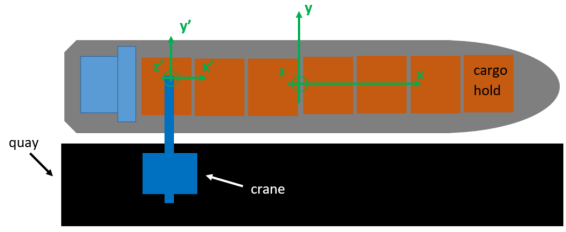

(b) Bulk cargo holds on bulk carrier.

Figure 2.26: *Top view schematic drawing cargo spacing and loading equipment on cargo ships, generic O_{xyz} axis system positioned midship, generic $O_{x'y'z'}$ axis system positioned locally in cargo hold*

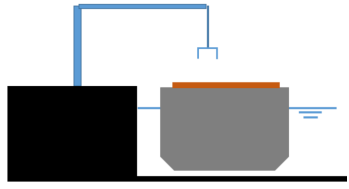

(a) Grabber

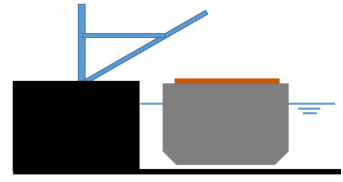

(b) Conveyor belt

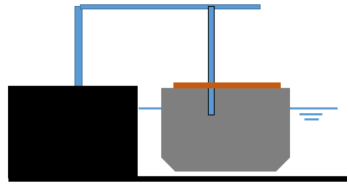

(c) Stiff elevator

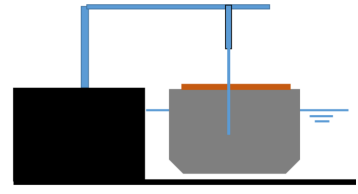

(d) Flexible hose

Figure 2.27: *Four different bulk loading and unloading equipment types.*

2.3.3.3 Operational conditions and considerations

For a given combination of ship type and terminal equipment, the motion criteria which need to be applied are a function of conditions at the specific site, as well as requirements set by the terminal.

At all terminals, a safe operation is required, meaning that motions need to limited based on the operation type. For oil and gas discharge, mechanical limitations will be present in the equipment, which serve as limiting criteria. For other ship types, risk of collisions between equipment and ship and/or dangerous situations involving crew and/or passengers need to be kept to a minimum, leading to a definition of safety criteria.

At terminals where periodic disturbances (wind gusting, wave action) are dominant, motion cycles will potentially slow down the operation, or in other words lower the efficiency of the cargo operation. The terminal needs to decide what efficiency threshold they need for their business model. As an example, a container terminal which needs to compete with many others in a small radius will most likely need to offer high container rates to attract container lines. A container port located in a remote location could lower the loading rate requirements, in order to avoid extensive capital costs e.g. building of large breakwaters.

2.3.3.4 Surge motion limit safe container loading

The study of motion criteria for moored container ships is a study field in itself. The present discussion focusses on deriving a limit for surge motion for local conditions governed by dominant passing ship effects. The discussion is introduced by giving the framework of existing standards on surge motion limits for container ships. The container operation is assumed to be done using shore based gantry cranes, as illustrated in figure 2.28.

Literature study [Mar95] provides motion limits (for 6DOF) for safe working conditions, expressed as peak-to-peak values for 100% and 50% efficiency of the operations, which is not in line with the discussion from section 2.3.1, where it was concluded that motion amplitudes form a more relevant criterion. In draft notes from [Mar95],

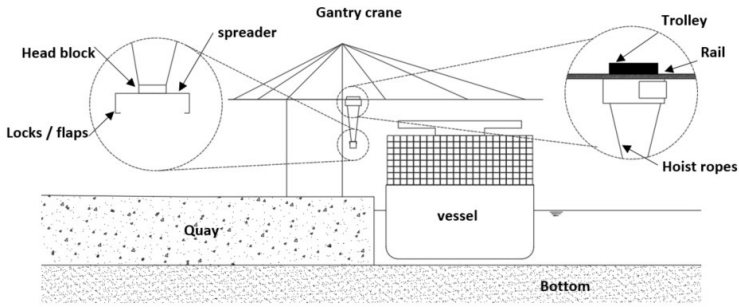

Figure 2.28: *Components of gantry crane type container cargo operation.*

which were made available to the members of PIANC WG212, amplitude limits were actually given, which were transformed by peak-to-peak criteria to be consistent with the main definition of WG24. The transformation simply multiplied the amplitude criteria by a factor of two. Table 2.4 gives the surge motion criteria as motion amplitudes, going back to the original values included in the draft notes.

In [Mar12], they specifically looked into motion criteria for container ships. They started their discussion from [Mar95], discussing that the motion criteria are deemed not strict enough considering evolved requirements set on container operations. They cite amongst others [DHo99], who states that more stringent motion limits are required. Following these signals from industry, they used a numerical approach to define motion criteria in function of efficiency requirements. As their analysis assumes the a spectral response characteristic, meaning a significant value of the response could be derived. In the work of [Mar95], the definition of the motion (amplitude, maximum, most probable maximum) was not clearly put forward. In [Mar12] they clearly state that their limit links a significant motion amplitude at which 95 % loading efficiency, is obtained.

The numerical analysis of [Mar12] already indicated that the loading efficiency depends on the motion period of the moored ship. [Sli79] in fact already observed that when the motion period matches the time needed for the operator to perform one load cycle, decent loading rates can be obtained at high motions. This will be further examined within the work of [Marb].

Table 2.4: *Surge motion amplitude limits loading of container ships, from [Mar95] [Mar12].*

source	eff* (%)	limit value (m)
PIANC24**	E100	0.50
PIANC24**	E50	1.00
PIANC115	E95	0.20/0.40

*eff = Target loading efficiency

**Peak-to-peak motion converted to amplitude

Clearance container bays - ship infrastructure The discussion in [Mar12] gives great insight on how to assess the surge motion for a moored container ship, for oscillatory motions, under efficiency considerations. When the major external disturbances are passing ship events, the frequency of their appearance will be rather low, meaning that the efficiency considerations cannot be applied. The criteria from [Mar95] seem more relevant then. They are however still linking to efficiency, as they mentioned 50 % and 100 % efficiency criteria.

In order to fill this void, a novel approach is used to define a safety limit for the surge motion of moored container ships, which can be generally applied for all operations, but serve most purpose to examine the effect of transient loads, such as passing ship effects.

The reasoning assumes that the safety risk is the highest when the gantry crane operates at the bays adjacent to bridge and/or exhaust funnel. A collision between spreader and ship structure is then defined as the unsafe situation. In line with the assessment from [Mar12], the surge motion is then the critical motion mode. A criterion is based on the analysis of the distance between container bay and ship bridge and exhaust funnel, as visualised in figure 2.29.

In order to come to a representative value for the safety margin, 73 general arrangement plans (GA) have been analysed, measuring the distance between inside of the cell guide and the bridge/funnel. Table 2.5 shows the number of GA's for four classes of TEU capacity. Figure 2.30 (a) shows the definition of the safety clearance with respect to the accommodation (C-F and B-C). Figure 2.30 (b) gives an

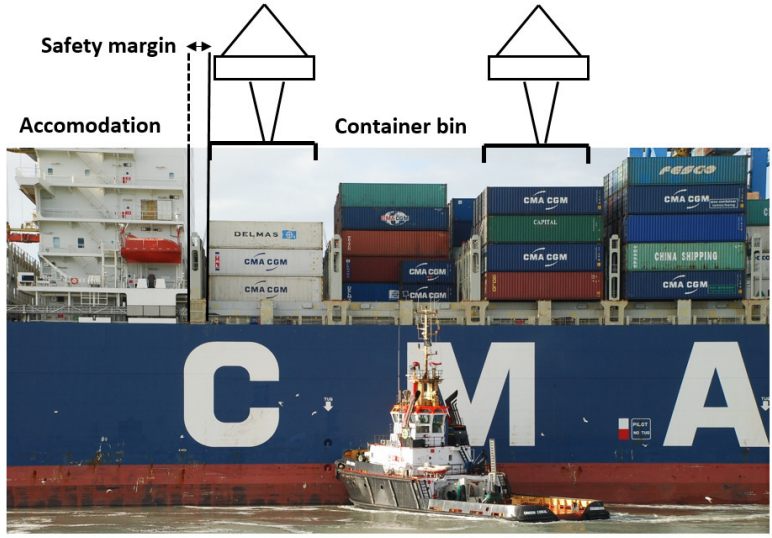

Figure 2.29: *Representation of structural clearance (safety margin) between crane (spreader) and bridge, image courtesy of Marc Vantorre.*

example of a split funnel (engine room) and bridge, which is usually the case in modern (large) container ships. Four safety distances are defined in this case (C-F, F-C, C-B and B-C).

Table 2.6 summaries the data which has been analysed. n(-) is the number of data points for each clearance definition, μ is the average clearance and σ the standard deviation. Several observations can be made. First of all, the standard deviation is quite large compared to the average, meaning that there is significant spread on

Table 2.5: *General arrangement (GA) plan database in function of ship TEU capacity (73 GA).*

TEU capacity	n° GA
TEU $<=$ 6000	24
6000 $<$ TEU $<=$ 10000	20
10000 $<$ TEU $<=$ 18000	19
18000 $<=$ TEU	10

C-F : Clearance bay - funnel

B-C : Clearance bridge – bay

UASC TABUK: 9,000TEU eco container ship

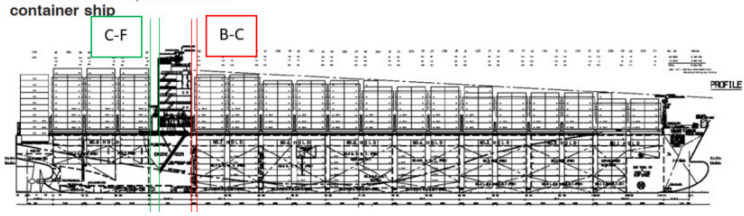

(a) Bridge and engine room not separated, images from RINA Significant Ships of 2014

C-F : Clearance bay - funnel

F-C : Clearance funnel – bay

C-B : Clearance bay – bridge

B-C : Clearance bridge – bay

CSCL GLOBE: 19,000TEU container ship from HHI

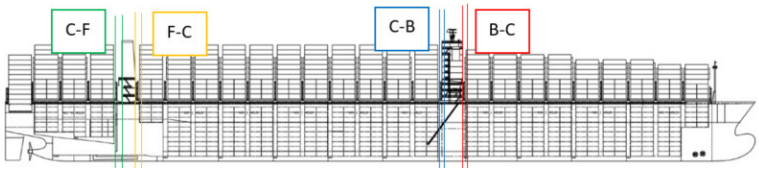

(b) Bridge and engine room separated, images from RINA Significant Ships of 2014

Figure 2.30: *Definition C-F, F-C, C-B, B-C*

the data, suggesting that there are considerable differences between container ships. An extension of the database would lead to more confidence in the average value. Note that the accuracy of this analysis will always be limited by the quality of the GA's. The clearance around the funnel is significantly larger compared to the clearance around the bridge, certainly the clearance behind the funnel (C-F) is large (3.76 m on average).

Based on the average and standard deviation, a confidence interval can be defined. Under the assumption of a normal distribution, the value of $\mu - \sigma$ means that 84.2 % of the clearance will be equal to or higher than this value. Taking the most stringent value, B-C, the criterion would be 0.97 m. This is then the surge criterion for safe mooring of a container ship under transient effects (passing ship). In the most strict sense this is valid when working on the bay adjacent to the bridge. As during the loading operation, container cranes switch between bays, this value could be used as a design value for the whole operation. When comparing to table 2.4, this value is actually close to the 50 % loading efficiency limit defined by [Mar95].

Table 2.6: *Results data analysis safety clearance for 73 GA*

def	n(-)	μ (m)	σ (m)	$\frac{\sigma}{\mu}$ (-)	$\mu - \sigma$ (m)
C-F	73	3.76	1.32	0.35	2.45
F-C	28	1.98	0.82	0.41	1.16
C-B	28	1.41	0.25	0.18	1.16
B-C	73	1.41	0.44	0.31	0.97

2.4 Analysis tools

The list of tools which can be used to assess (components) of the mooring analysis is long and diverse. For the purpose of this thesis, the following four categories of tools are specified.

1. Full scale measurement What you see is what you get, no assumptions need to be made and the result unfolds right in front of you. Inability to control conditions and no possibility of repetition make this technique hard to use. Measuring all parameters (line (pre)tension, wind field,...) will not be possible most of the time, so some assumptions will always need to be made. The most interesting conditions are usually critical conditions, e.g. a storm event. Heavy loading of the equipment as well as large risks for the personnel are to be expected. Full scale measurements can however be useful as validation material, as was done for *Vlugmoor* with GPS measurements performed at the Noordzeeterminal in Port of Antwerp [VVI18].

2. Model scale testing Working on reduced scale makes it feasible to build the model in a research facility and allows you to control the environment and repeat test conditions. All non-linear effects are captured. Disadvantages are the time and labour intensive character of the testing (need for calibration). Scaling also introduces 'scale-effects', inaccuracies in the physical scale representation as a consequence of the chosen scaling method. An example here is when Froude scaling (see section 5.3.1.4) is applied, viscous effects such as the thickness of boundary layers is not correctly represented, which causes errors when the ship sails close / into boundary layers (small clearance under keel and/or sailing close to banks). [Lat14] observed this issue with scaled boundary layers when looking at ship-bank effects, where for example the lateral force at fore perpendicular increases when approaching the bank, but then decreases again with reduced distance to the bank, even changing sign!
   Chapter 6 of this thesis elaborates on the $PESCA$ model test program, where passing ship effects are measured, which can be used as input for *Vlugmoor*.

3. Numerical models are software packages where mathematical equations which represent the water flow are solved for a given

set of boundary conditions. Within the numerical world, for the sake of the current discussion, subdivision is made into potential (inviscid) flow and turbulent flow models. Potential represents the flow by a flow potential, which is used to derive all velocities and pressures in the fluid. RoPES [PP14] is an example of a potential flow package which has been developed specifically to calculate passing ship effects. The software has been validated based on model tests executed at FHR [TB14] and Deltares [HJ14]. Chapter 7 of this thesis presents additional validation work for the ROPES package, with focus on the validity in shallow and restricted waters.
Turbulent flow models are capable of modelling - as their name suggests - turbulent flow. Within this model type, there are numerous 'subcultures', applying different equations, boundary conditions and correction models. The most prominent one in the current context is RANS - Reynolds-Averaged Navier-Stokes. In [BT11], a comparison is made between the use of potential flow (RoPES), RANS and model test results. They show that with increase in viscous effects with non-zero drift angle, potential flow could no longer accurately model the passing ship effects. The use of RANS is not further discussed in this thesis.

4. Empirical models are expressions established between influencing (independent) parameters and resulting (dependent) parameters. An example is the passing ship effect, where the magnitude of the force is a function of the parameters given in table 2.1.
Based on results from physical model tests and/or numerical models, a regression analysis can be used to obtain multiplication coefficients which define the magnitude of the force as a function of (a selection of) the parameters from table 2.1. [VV06] derived an empirical model based on a dataset, obtained through running a slender-body theory model (numerical model, potential flow). They also validated the slender-body model using scale model tests. In this thesis work, chapter 6 is devoted to checking existing empirical model predictions using PESCA validation tests. In a second part of the chapter, a new empirical model approach is proposed.

2.5 *Vlugmoor*

Vlugmoor is the UGent in-house mathematical model used to perform a mooring analysis, as introduced in sections 1.1.4 and 1.3. A mathematical model is a general definition for a system of equations built on mathematical and physical concepts. The *Vlugmoor* software package, written in a MATLAB environment, provides an input and output structure, built around the mathematical model.

The model solves motion equations, starting from Newton's second law, using input from different analysis tools which were described in section 2.4. The mathematical formulation of *Vlugmoor* is elaborated on in chapter 4.

2.5.1 Description

Vlugmoor is a time domain solver (TDS), where equations are solved at each time step and the calculation progresses until it reaches the final time step. As the system is re-evaluated at each step, non-linearities can be properly represented. A clear example is the non-linear behaviour of mooring lines (figure 2.13) and fenders (figure 2.19), which is included in the model as a set of tabular values.

The model can be run in 'quasi-static' and 'memory' modes. In the quasi-static approach (section 4.6.1), the system moves and accelerates during the simulation. At each individual time step however, an equilibrium situation is present. This is typically used for long period, transient responses of which the period is known. In the memory mode (section 4.6.2), the movement of the ship at time t will cause a wave to be generated which will still affect the ship in later time steps, hence the memory effect of the fluid. With this model, a better approximation of a general ship response can be given. This comes at the price of a more complex model (to run) and a steep increase in calculation time.

2.5.2 Structure mooring analysis sheltered berth

The general representation of *Vlugmoor* was already given by figure 1.6. All blocks shown in the figure are built as MATLAB modules, in an object-oriented environment. The modularity of the tool allows

many different types of calculations to be run, which is needed considering the questions from commercial clients are diverse (section 2.5.3 and appendix A).

Figure 2.31 gives an expanded representation of figure 1.6, including the concepts which have been introduced in the present chapter. The different tools which are available to represent the effect of wind and passing ship effects are elaborated on in the indicated chapters.

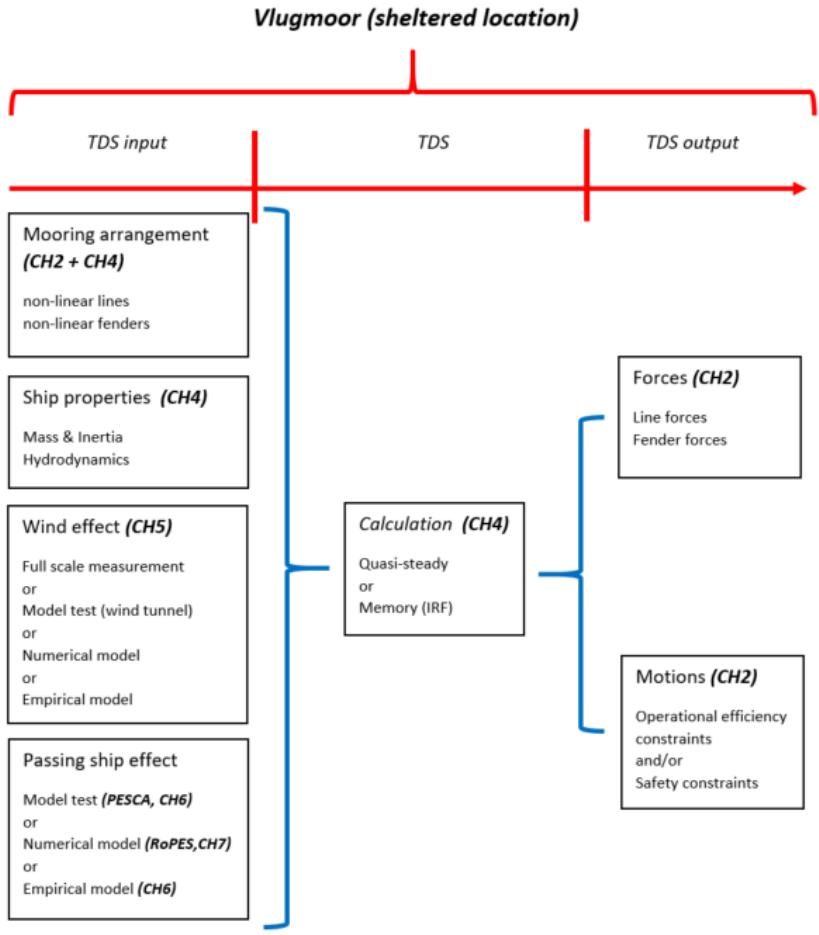

Figure 2.31: *Vlugmoor set-up for calculating and evaluating ship response under the effect of wind and waves (sheltered mooring location).*

2.5.3 *Vlugmoor* applications

Vlugmoor, in its diverse set-ups, has been used for close to forty commercial mooring studies over the seven years during which the author has been active at the department. A selection of these projects is presented in A. It is important to mention that most applications concern critical situations, both in design and operation, which need to be addressed by the mooring analysis. Critical aspects can be seen as large line forces in the vicinity of the maximum allowable loads, but also as large motions, with respect to efficiency and safety considerations.

As an example, figure 2.32 shows a simplified 1DOF motion in surge of a moored ship. The top figure is copied from figure 2.21, showing the moored $T0Y$ tanker in undisturbed condition. A good mooring arrangement should have all lines on a moderate level of tension, denoted as pretension. 10% MBL is an acceptable pretension level. In figure (b) the ship moves forward over a significant distance, which can occur under the effect of a passing ship for example. The red lines are tensioned high as they are stretched; The blue lines are slack (and thus tensionless). When the ship moves backward, the tensioned lines become slack and vice versa.

Under these conditions, the system will always be non-linear (the same line will be slack and tensioned during the simulation). As lines and fenders will both be loaded in a general motion (which will be a combined surge, sway and yaw motion), the problem is a combination of non-linear systems, which is again non-linear. In this thesis, the non-linear mooring analysis is always the default case. In case some degree of linearisation is assumed (e.g. in the analytical approximation of the eigenperiods of the system, section 4.3.3 and the assessment of the quality of the mooring arrangement, section 4.3.4), it will be mentioned explicitly.

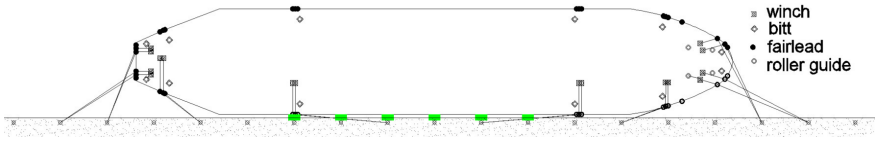

(a) Undisturbed (pretension)

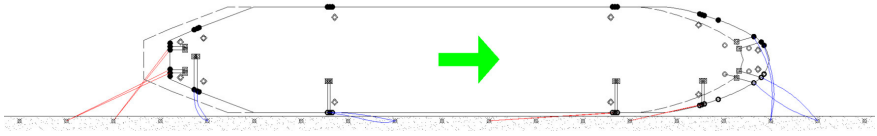

(b) External force positive surge (dashed ship = position before disturbance)

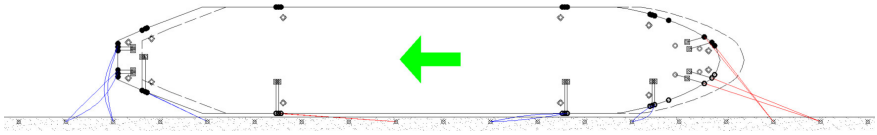

(c) External force negative surge (dashed ship = position before disturbance)

Figure 2.32: *Example surge motion of moored $T0Y$ under external disturbance; black = line at pretension; blue = slack line; red = Line under high tension*

References

[Bri+09] M.J. Briggs et al. “Prediction of Squat for Underkeel Clearance”. In: *Handbook of Coastal and Ocean Engineering: Expanded Edition*. 2009, pp. 1029–1080.

[Bro+18] E. J. Broos et al. “Bollard loads on new port infrastructure, Port of Rotterdam Authority policy”. In: *PIANC world congress*. Panama City, Panama, 2018.

[BT11] T. Bunnik and S. Toxopeus. “Viscious flow effects of passing ships in ports”. In: *Proceedings of the ASME 2011 30th International Conferenece on Ocean Offshore and Arctic Engineering (OMAE)*. Rotterdam, The Netherlands, 2011.

[DHo99] E. D’Hondt. “Port and terminal construction design rules and practical experience”. In: *11th International Harbour Congress*. Antwerp, 1999.

[EVM09] K Eloot, M Vantorre, and F Mostaert. *Haven van Zeebrugge: Uitbreiding van de LNG terminal voor QMax LNG-carriers - Simulatiestudie*. Tech. rep. 2009.

[Gou19] T. Gourlay. *Comparison of WAMIT and MoorMotions with Model Tests for a Tanker Moored at an Open Berth*. Tech. rep. 2019, p. 29.

[HJ14] A.J. van der Hout and M.P.C. de Jong. “Passing ship effects in complex geometries and currents”. In: *PIANC World Congress*. San Francisco, USA, 2014.

[Hol07] Leo H. Holthuijsen. *Waves in Oceanic and Coastal Waters*. 2007, p. 387.

[IAC20] IACS. *Anchoring , Mooring , and Towing Equipment (revision 2020)*. Tech. rep. 2020, p. 20.

[ISO12] ISO. *ISO 3730 Shipbuilding and marine structures - Mooring WinCches*. 2012.

[Lat14] E. Lataire. “Experiment Based Mathematical Modelling of Ship-Bank Interaction”. PhD thesis. Ghent University, 2014, p. 269.

[LY19] L. Li and Z. Yuan. “Transient response of a moored vessel induced by a passing ship”. In: *Proceedings of the 5th MASHCON*. Ostend, Belgium, 2019, pp. 266–272.

[Mara] MarCom Working Group 211. *Updating of WG33 - Guidelines for the design of fender systems*. Tech. rep. - to be publshed -.

[Marb] MarCom Working Group 212. *Update of WG24 - Criteria for acceptable movement of ships at berths*. Tech. rep. - to be published -.

[Mar02] MarCom Working Group 33. *Guidelines for the Design of Fenders Systems: 2002*. Tech. rep. 2002.

[Mar12] Marcom Working Group 115. *Criteria for the (Un)loading of Container Vessels*. 2012.

[Mar95] MarCom Working Group 24. *Criteria for Movements of Moored Ships in Harbours - a Practical Guide*. 1995.

[MMD06] W. van der Molen, P. Monardez, and A.P. van Dongeren. “Numerical simulation of long-period waves and ship motions in Tomakomai Port, Japan”. In: *Coastal Engineering Journal* 48.1 (2006), pp. 59–79.

[Mol+03] W. van der Molen et al. “Behavior of a Moored LNG Ship in Swell Waves”. In: *Journal of Waterway, Port, Coastal, and Ocean Engineering* 129.1 (2003), pp. 15–21.

[Mun50] W.H. Munk. “Origin and Generation of Waves”. In: *Coastal Engineering Proceedings*. 1950.

[OCI18] OCIMF. *Mooring Equipment Guidelines - MEG4*. Witherbys, 2018, p. 312.

[Pin04] J A Pinkster. “The influence of a free surface on passing ship effects”. In: *International Shipbuilding Progress* 61.4 (2004), pp. 313–338.

[Pin09] J. A. Pinkster. “Suction, Seiche and Wash Effects of Passing Ships in Ports”. In: *Transactions - Society of Naval Architects and Marine Engineers* 117 (2009), pp. 99–124.

[PP14] J.A. Pinkster and H.J.M. Pinkster. “A fast, user-friendly, 3-D potential flow program for the prediction of passing vessel forces”. In: *PIANC World Congress*. San Francisco, USA, 2014.

[Sli79] P.J.B Slinn. “Effect of ship movement on container handling rates”. In: *The Dock and Harbour Authority*. 1979, pp. 117–120.

[SNA88] SNAME. *Principles of Naval Architecture*. 1988.

[TB14] H. Talstra and A.J. Bliek. “Loads on moored ships due to passing ships in a straight harbour channel”. In: *PIANC World Congress*. San Francisco, USA, 2014, p. 19.

[Tre20a] Trelleborg Marine and Intrastructure. *Fender systems : product brochure*. 2020.

[Tre20b] Trelleborg Marine and Intrastructure. *Pneumatic Fenders*. 2020.

[UK 09] UK P&I Club. “Understanding mooring incidents”. In: *LP News* (2009).

[Van+15] A.F.J. Van Deyzen et al. “To improve the efficiency of ports exposed to swell”. In: *Australasian Coasts and Ports Conference 2015*. 2015.

[VKV03] K.S. Varyani, P. Krishnankutty, and M. Vantorre. “Prediction of load on mooring ropes of a container ship due to the forces induced by a passing bulk carrier”. In: *Proceedings of the International Conference on Marine Simulation and Ship Manoeuvrability (MARSIM)*. Kanazawa, Japan, 2003.

[VV06] K.S. Varyani and M. Vantorre. “New Generic Equation for Interaction Effects on a Moored Containership due to a Passing Tanker”. In: *Journal of Ship Research* 50.3 (2006), pp. 278–287.

[VVI18] T. Van Zwijnsvoorde, M. Vantorre, and S. Ides. “Container ships moored at the port of Antwerp : Modelling response to passing vessels”. In: *PIANC World Congress*. Panama City, Panama, 2018.

[VVL02] M. Vantorre, E. Verzhbitskaya, and E. Laforce. “Model Test Based Formulations of Ship-Ship Interaction Forces”. In: *Ship Technology Research* 49 (2002), pp. 124–141.

3
Mooring Lines

Mooring lines form the key element in how the ship will respond to external disturbances. Their capacity, Minimum Breaking Load (MBL), determines the magnitude of loads which the lines can withstand. Their elongation properties dictate how much the lines will elongate for a given reaction force. As these spring-like elements contribute significantly to the mass-spring system which is the moored ship (chapter 4), the eigenperiods of the moored ship will be a function of the elastic properties of the mooring line. The lines can be either steel lines, called wires, or made of synthetic materials (nylon, polyester,...) in which case they are denoted as ropes. This chapter discusses the relevant line properties needed as input for the mooring analysis. International standards regulating these key properties are discussed. Line testing performed at the Belgian rope manufacturers Bexco is presented, aiming to get more insight into (dynamic) stress-strain behaviour.

The chapter is ended with a suggestion of possible future work, where the elastic response of the mooring line (eq. 2.4) can be expanded with damping and time dependent terms based on the results of the Bexco model tests.

3.1 Mooring line properties

Mooring lines for seagoing ships are in all cases composed of a large quantity of individual yarns, used to make strands, which are in turn combined using different techniques (parallel lay, stranded, laid, braided,... [Bex04]) to form a mooring rope. When purchasing lines, a list of characteristic parameters is made available (see example table 3.1). For each specific line type, a table will be provided showing different rope diameters and their respective strength and weight properties (see example figure 3.1). As they are generally not required according to international standards, and as such not of interest to customers, line elongation properties are rarely found on manufacturers' websites.

Table 3.1: *Mooring line characteristic parameters (source [Bex04]).*

Material	Abrasion resistance
Construction	U.V. resistance
Colour	Temperature resistance
Specific gravity	Water absorption
Melting point	Dry/wet conditions
Range of use	Chemical resistance

BEXCOFLEX					
Dia	Circ.	Dia	Min. Break Load		Weight
mm	"	"	tf	kN	kg/100m
32	4	1 5/16	30.6	300	68.5
36	4 1/2	1 1/2	35.2	345	79.5
40	5	1 5/8	42.5	417	96.6
44	5 1/2	1 3/4	49.1	482	112
48	6	2	55.7	546	128
52	6 1/2	2 1/8	64.2	630	149
56	7	2 1/4	72.7	713	169
60	7 1/2	2 1/2	81.1	796	190
64	8	2 5/8	90,3	886	211
68	8 1/2	2 3/4	104	1025	246

Figure 3.1: *Selection of $BEXCOFLEX$ mooring rope diameters (from Bexco website), indicating the MBL corresponding to each diameter.*

3.2 International standards

3.2.1 Minimum Breaking Load (MBL)

The mooring lines on board of the ship need to meet the criteria set by the authorities, or regulating bodies. In case of a ship, a Classification Society (often called 'Class') will follow and review the construction process, which will lead to a class approval, which in turn is needed to get insurance and flag state approval. Some examples of Classification Societies are Bureau Veritas (BV), Det Norske Veritas (DNV) and Lloyd's Register of Shipping (LR). Their task is to make sure that the ship has been constructed up to the standards of today.

Each Class has their own basic set of rules. For some aspects however, they produce general standards, issued by the International Association of Classification Societies (IACS) as is the case for mooring equipment. They produced a first document on this topic in 2005 [IAC14] (most recent review 2014), where they address requirements for MBL, number of lines and line length. These three parameters are linked in tabular format to the Equipment Number (EN) (eq. 3.1) of the ship. In short, EN is a function of the displacement (Δ), the height of the superstructure (H), the beam (B) and the lateral wind area of the hull and superstructure (A_0).

The subscript 0 in the latter indicates that the lateral area is defined at design draft. The most striking aspect here is that the frontal wind area (hB) has much more weight to it than the lateral wind area (times 2 and division by 10 respectively). Note that the EN number is not specifically defined for mooring equipment, it is also used for anchoring and towing equipment, hence the importance of the frontal surface. On top of this, the lateral area of the cargo (for example container stacks) is not taken into account. This is not unsurprising, as during the times that the EN number was conceived, the largest ships were traditionally oil tankers and bulk carriers, both having modest top structures above the main deck level and no cargo on deck. In the last two decades however, container ships, gas carrier and cruise ship dimensions increased rapidly. These three ship types have a significant lateral area above the waterline, whether this is formed by passenger decks and pools, containers or gas tanks.

This trend challenges the validity of the 'MBL table' in [IAC14].

$$\mathrm{EN} = (\frac{\Delta}{1000g})^{2/3} + 2 \cdot H \cdot B + \frac{A_0}{10} \tag{3.1}$$

In 2016 (most recent review 2020 [IAC20]), IACS came up with a new set of equations for ships with EN $>$ 2000, which more or less means all seagoing cargo ships (apart from the smaller coasters). The lateral wind area A_1 is used here as the only design parameter, which is the largest lateral wind area which can be attained. For most ships, this is in ballast condition; for container ships, container stacks on deck will form the biggest wind area. The formulas to calculate MBL and required number of lines are given by eq. (3.2) and (3.3). In eq. (3.3), H,ST and SP are head, stern and spring lines respectively. [IAC20] mentions that if ships moor at quay walls, a shielding surface corresponding with a 3m quay height can be subtracted from A_1.

$$MBL = 0.1A_1 + 350(\mathrm{kN}) \tag{3.2}$$

$$\mathrm{n_{H+ST}} = 8.310^{-4}A_1 + 6 \quad \mathrm{n_{SP}} = 4 \; (EN > 5000) \tag{3.3a}$$

$$\mathrm{n_l} = \mathrm{n_{H+ST}} + \mathrm{n_{SP}} \tag{3.3b}$$

These standards are now applied to the $T0Y$ and $ULCS$ case study ships (see appendix F). The EN, MBL and number of lines are calculated according to the main dimensions given in tables F.1 and F.3. The results are shown in table 3.2. According to [IAC14], the tanker requires 8 mooring lines with MBL of 70.9 tons, the container ship needs 16 lines of 75.0 tons. [IAC20] requires 14 lines for the tanker, with an MBL of 81.0 ton and 23 lines with MBL 189.9 ton for the container ship.

In the last part of the table, representative numbers for the actual mooring equipment on board of such ships, acquired through project work, are given. The MBL standards for the tanker are similar and match the lines found on board in practice. The number of lines for the tanker (8 and 14 for 2014 and 2020 IACS standards respectively) are an under prediction of the 16 lines which are found on board. The number for the container ship shows that standardisation is not on point and that presumably individual calculations are made for each design ship at the moment. The 2014 standard heavily underpredicts the line strength (75.0 ton required), which is in

fact as expected through the theory behind the 2014 standard (EN definition). The 2020 standard however sets very high demands on strength and number of lines, which would require a significant re-assessment of the mooring decks' strength and layout, but also an assessment of the berth side mooring equipment.

Table 3.2: *Required MBL and number of lines according to [IAC14][IAC20].*

	$T0Y$	$ULCS$
[IAC14]		
EN (-)	5173	10980
A_1 (m²)	1019.9	6637.0
MBL (ton)	70.9	75.0
n_l	8	16
[IAC20]		
A_2 (m²)	5155.6	16016.0
MBL (ton)	88.2	198.9
n_l	14	23
current fleet		
MBL (ton)	81.0*	148.7**
n_l	16*	16**

* Based on data 2 ships of similar size

** Based on data 37 ships of similar size

3.2.2 Line elasticity

The previous section highlighted the difficulty to come up with one general relationship linking ship parameters to the (minimum) mooring equipment required on board. Line elasticity plays on a whole other level, as there are no particular standards on line elongation properties. Limited research in this field partly explains this void. Another aspect is formed by the difficulty to select an optimal line type for all ports visited by the ship on a yearly basis. As was explained in section 2.1, different port layouts (Open port, Coastal port, Confined port) face different dominant external disturbances. Some study work has been done in this field, which is discussed below.

Historically, lines were made of natural materials, which were then replaced by synthetic materials (nylon) as well as steel wires. Nylon lines deform significantly upon loading (length increase of 30% to 40% at full load), steel wires are very stiff (2% length increase at break). Over the last decades, more and more mixed synthetic ropes have been developed, based on polyester and polypropylene, which have moderate elasticity. Developments in synthetic lines lead to high strength, stiff lines. Dyneema is a brand name which has become almost synonymous for this category of lines. This category is also often indicated as High Modulus Polyethylene (HMPE).

The matter remains based on which considerations line types can be chosen. At most terminals, the ship motions need to be limited to allow safe and efficient cargo operation (section 2.3.3). Stiff lines are then the best choice. However, if the stiffness would be too high, let's say when only using a steel wire or HMPE line, risk of snap loading would increase. A stiff system will also have a high eigenfrequency (see section 4.3.3), which means it might resonate in waves with relatively short periods. Elastic tails prevent snap loading and unwanted resonating. In some longer wave systems (swell and seiches), mooring lines are easily overloaded as the exciting forces are large. In these cases, longer tails will allow larger motions and lower eigenfrequencies, avoiding resonance behaviour. As each port faces different external disturbances, the eventual choice will be a compromise which works well with a large variety of external loads.

A line can be composed of a stiff main line and elastic tail, which can be represented as two springs (with stiffness k_1,k_2, eq. 2.4) in series. This configuration offers a high degree of flexibility, as tails can be changed between different berths, according to the local conditions. [Wei+09] concluded that using 22 m tails would result in more desirable behaviour of the moored ship at the terminal, compared to the more traditional 11 m tail length. The paper presents the case of a moored LNG carrier, which is an example of a ship which often sails between the same ports for the duration of a contract. In this case, it is advised to consult guidance or perform a mooring analysis to select the most appropriate line type for the given ports.

The other part of the discussion concerns choosing a line representation for the design ship in a mooring study, knowing that different line types are used on board of ships of a similar size. Line types can

be obtained from mooring certificates on board of the ship, giving the brand name, the diameter and MBL. Based on the brand name, the main line material and in some cases an indication of stress-strain curve can be obtained from the manufacturer's website. In case information is incomplete, e.g. only main line material is known, [OCI18] provides four generic stress strain curves, given in figure 3.2. [Mar19], the document written by WG184 'Design Principles for Dry Bulk Marine Terminals' provides typical ranges for mooring line elasticity in their figure 8-6, showing that particularly for nylon, the spread between different nylon type lines is large.

Figure 3.3 shows a comparison between four nylon lines which has been made within a mooring study. WG184 [Mar19] gives a lower and higher limit for elasticity of used nylon lines. The MEG4 [OCI18] lies within this zone, leaning towards the stiffer side of the spectrum. As input for the mooring study, only the line type was known. The corresponding line properties were found on the website of 'manufacturer X'. This line seems to be outside of the WG184 envelope. The words *new* and *used* come into play here. When a mooring rope is produced and stretched for the first time, it will respond in a very elastic manner. During this first use, void space between the strings which make up the rope will decrease, fibres align and stiffness will increase. Over its lifetime, further (cyclic) loading will cause a further increase in stiffness, as the line will show permanent deformation, defined as creep. These two processes will cause a change in appearance of the curve, which will then fit within the WG184 envelope in figure 3.3.

The discussion in this section emphasises the need for research on (time-dependent) elastic properties. The results of such a research effort are shown in the next section.

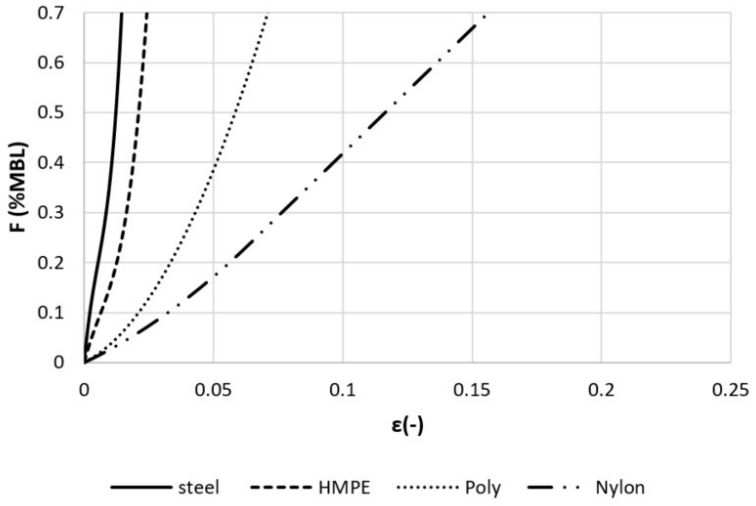

Figure 3.2: *Generic mooring line stress-strain curves according to [OCI18].*

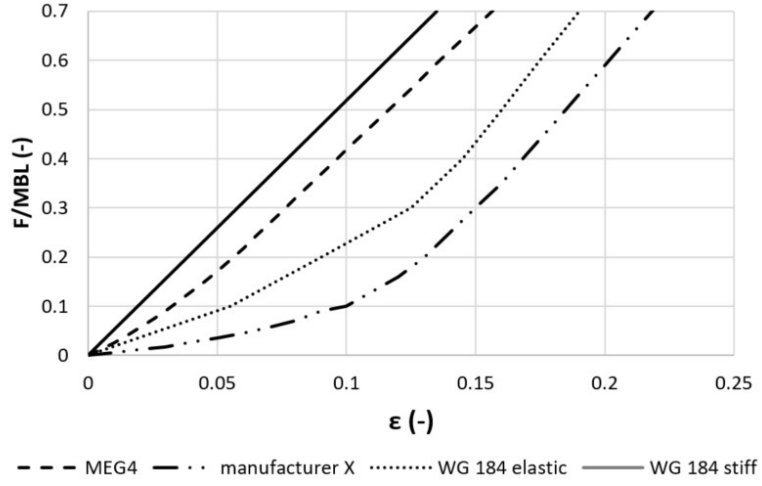

Figure 3.3: *Stress-strain behaviour for four types of nylon rope.*

3.3 Mooring rope tests

In a response to the gaps present in mooring line research, as well as in standards, the author wanted to learn more about the elastic properties of mooring lines. The Belgian rope manufacturer Bexco, with headquarters in Hamme, was willing to test a few rope samples in their tensile test set-up, based on test parameters provided by the author. This section gives a description of the tested lines, briefly discusses the test procedure and shows the results of the tensile tests.

3.3.1 Tested line types

Three types of mooring ropes have been selected based on Figure 3.2, as well as the Bexco product list. Nylon lines are interesting as they are generally the most elastic lines (figure 3.2), which also show the strongest non-linear response (figure 3.3). Their behaviour also changes strongly from first use, over later use and cyclic loading, making it an interesting test subject. Bexco produces $CAESAR$ nylon ropes. A polyester type line forms the middle segment when it comes to line stiffness, represented by the $BEXCOFLEX$ line. The 'HMPE family' is an interesting line to study, as its behaviour is close to that of steel, despite being made of fibre materials. The lines are summarized in table 3.3. An extensive list of line characteristics (construction, density, etc.) can be found on the Bexco web page.

Table 3.3: *Mooring lines tested at Bexco (HT = High Tenacity)*

Name	material	diameter (mm)	length (mm)
$CAESAR$	100% HT nylon	64	7500
$BEXCOFLEX$	FT BEX®-yarn and HT polyester	66	6730
$HMPE$	Dyneema SK78	48	9120

3.3.2 Test facility

A rope manufacturer needs to perform quality checks on their ropes in production. A destructive test for example will guarantee that the line strength is at least equal to the MBL. For these tests, samples of the total line, which is typically around 200 m for mooring applications, are taken and tested. The tensile test setup which was used is shown in figure 3.4. The tensile test can be performed by controlling line tension as well as elongation. The elongation of the rope is obtained from the movement of the pin to which the line is attached. When the test is non-destructive, e.g. cyclic loading, elongation gauges are attached to the rope, to measure the elongation directly on (a section of) the rope.

3.3.3 Test description

As mentioned in the introduction, the aim of this test program is to subject the mooring line to cyclic loading which is representative for a real-life mooring application. The variety of external loadings and mooring systems would lead to a very large test matrix. For the purpose of this test program, the cyclic loading is based on the response of a moored ship to a passing ship. The attentive reader will remark that a typical cyclic loading involves waves and wind rather than a passing ship event. A (standing) long wave system on the other hand could induce such a long period response of the mooring system, as will be further explained in chapter 4.

3.3.3.1 Preparatory numerical calculations

Numerical calculations with *Vlugmoor* in quasi-static mode (section 4.6.1) have been performed to come up with representative loading rates of mooring lines. The simulated cases as well as the observations are summarized here for future reference.

- A moored 18000 TEU container ship under the passage of a 18000 TEU container ship (4,5,6 knots) and a RoRo (6,9,12 knots). The container ship was moored using 16 lines, with MBL 140 ton and three linear line deformations (2.5, 15 and 25% strain at break)
- A moored 100000 DWT tanker at a jetty under the passage of a Suezmax tanker at 4,5,6 knots. The ship was moored with

Figure 3.4: *Tensile test set-up at Bexco*

16 lines with an MBL of 50 tons. The lines were modelled as main line + tail (2.5% and 15% strain respectively at break, both linear) and as one material (linear, 15% strain at break).

The following observations were made when analysing the *Vlugmoor* simulations :

- The loading rate of the mooring rope ($\mathrm{d}F/\mathrm{d}t$) is similar for various elasticities, at constant passing speed. The elongation rate ($\mathrm{d}l/\mathrm{d}t$) increases significantly when the elasticity of the line increases for a given passing event.

- The value of the slope ($\mathrm{d}F/\mathrm{d}t$) depends on the period (and amplitude) of the passing ship force, as well as the line length and position within the mooring line configuration. For the passage 18000 TEU - moored 18000 TEU case for example, the $\mathrm{d}F/\mathrm{d}t$ rates in the spring lines ranged from 1.5 kN/s to 13 kN/s. For the passage of the RoRo, denoted by a shorter period, this goes up to 20 kN/s for the highest passing speeds.

- The loading rates $\mathrm{d}F/\mathrm{d}t$ for the moored oil tanker are similar to the ones of the moored container ship. The most loaded line changes from spring to breast lines, due to the difference in nature of the external load (quay versus jetty mooring, see figure 2.7).

3.3.3.2 Choice test parameters

The following test sequence is chosen:

1. A newly produced line sample is installed in the test bank
2. 5 cyclic loads between 1% and 50% MBL
3. A relaxation phase of 1h to simulate recovery of non-permanent creep (1% MBL)
4. 5 cyclic loads between 1% and 50% MBL
5. Load until break (including one load cycle)

In the cyclic loading phase, the loading rate is controlled ($\mathrm{d}F/\mathrm{d}t$), taken constant at 2 kN/s ($CAESAR$ rope), 3 kN/s ($BEXCOFLEX$ rope) and 5 kN/s ($HMPE$ rope). These loading rates corresponding to interactions between 18000 TEU container ships, with passing speed in the region of 5 to 6 knots. In the final loading phase, where the line is loaded until break, the loading rate is increased with a factor 2 to 3.

For the $BEXCOFLEX$ rope, Bexco performed additional cyclic loading tests, with 50 cycles between 5 and 15 tons and 50 cycles between 20 and 40 tons, for which they also shared the data with UGent. Compared to the load rate of 3 kN/s used in the first series of cyclic loading tests, the rate was increased up to to 30 kN/s. The rate ($\mathrm{d}F/\mathrm{d}t$) is also not constant, but varies according to a sinusoidal profile. This test follows [OCI18] guidelines, regarding a test for *sheltered and exposed stiffness*.

3.3.4 *CAESAR* rope test

Figure 3.5 shows the full rope test (step 1 - 5 from section 3.3.3.2), with non-dimensional line force $\left(\frac{F}{\mathrm{MBL}}\right)$ in function of strain. A system represented by eq. 2.4 in fact only represents one unique relationship between force F and strain ϵ. From figure 3.5, it is seen that this assumption does not strictly hold, as the loading-unloading curves shift in the $F-\epsilon$ plane. This behaviour is commonly expressed as a hysteresis behaviour, where the properties of the system depend on the history of system (= previous load cycles). With each cycle, the stiffness of the line increases.

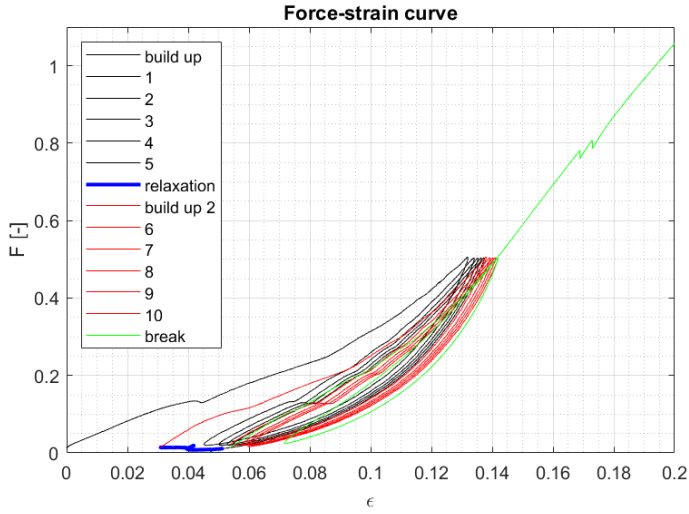

Figure 3.5: *CAESAR mooring rope test result, line force in function of strain, full rope test (initial loading, cycling loading 1, relaxation (1 hour), cyclic loading 2, load until break).*

When hysteresis occurs, the system's energy state often changes. This can be investigated by comparing the energy present in the loading and unloading curve. Figure 3.6 shows five load cycles, with the strain on the vertical axis in function of the time (=data points). If one cycle is defined as the system a-b-c (loading a-b and unloading b-c), the dissipated energy is given by eq. 3.4. The dissipated energy for each meter of rope is given, hence the unit Nm/m. The different parts of eq. 3.4 are visualised in figure 3.7.

$$E_{diss} = \int_{\mathrm{a}}^{\mathrm{b}} F(\epsilon_{\mathrm{l}})\mathrm{d}\epsilon_{\mathrm{l}} - \int_{\mathrm{b}}^{\mathrm{c}} F(\epsilon_{\mathrm{l}})\mathrm{d}\epsilon_{\mathrm{l}} \tag{3.4}$$

In between the two sets of five loading cycles, a constant tension of 1% MBL is held for one hour. In this phase, defined here as 'relaxation phase', part of the non-permanent deformation is recovered. After this relaxation phase, a second set of five loading cycles is performed, numbered cycle 6-10 for the remainder of this discussion.

After the last loading cycle, the line is loaded until break. In order

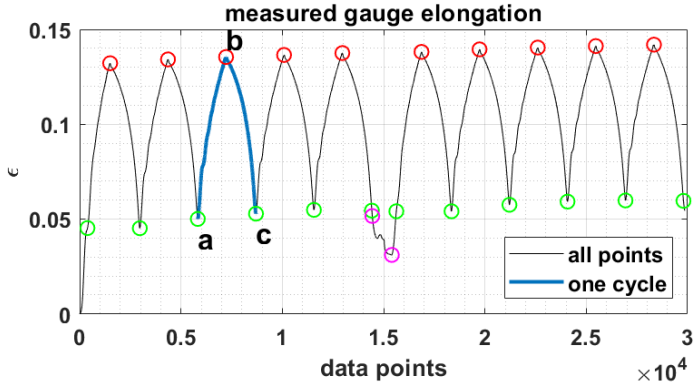

Figure 3.6: *Definition cycle (a-b-c), example time series strain CAESAR rope.*

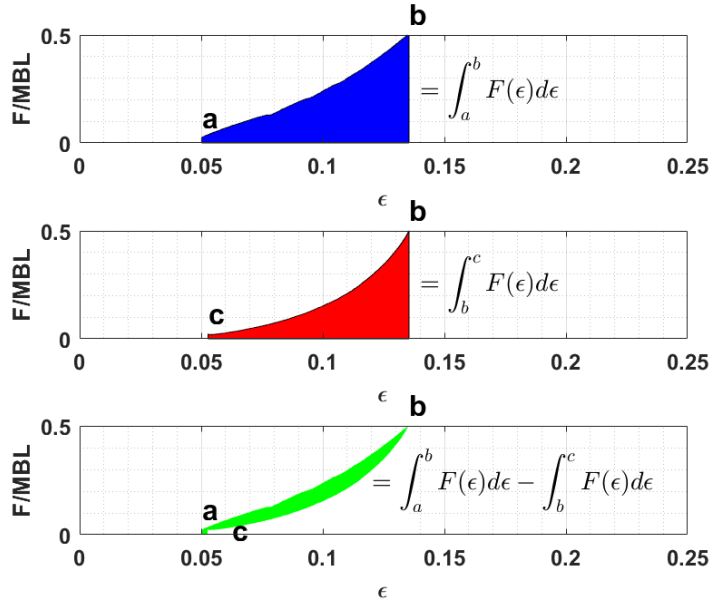

Figure 3.7: *CAESAR mooring rope energy dissipation calculation cycle 3*
Top : Work per meter rope loading curve
Middle : Work per meter rope unloading curve
Bottom : Dissipated energy per meter rope

not to damage the strain gauge, it is removed from the rope whilst at minimum tension. From this point onwards, only pin-pin readings are available.

Figure 3.8 is a reworked version of figure 3.5, highlighting three curves; The initial loading (indicated as A-B in the figure), the loading after relaxation (C-D) and the final loading until break (E-F). Between the points E-F, one more loading cycle to 0.5 MBL is present, before loading the rope until it broke. The stiffness increase in between initial loading and final load is obvious. This proves that using the initial loading *new* curve for nylon ropes as input for a mooring analysis will be an underestimation of the line stiffness.

The choice of which curve to take is however not straightforward. This plays on two levels. A first aspect concerns the storage of the line in between two moorings. The line will relax during storage, and the amount of tension on the coiled up line on the winch will determine how this process will manifest. If the winches are put on automatic mode when the ship is moored, they will control the tension in the line, meaning that the line will not show much relaxation. They will also haul in the line to keep it at the desired tension level. In theory, the curves from figure 3.8 are then translated to the origin (figure 3.9), clearly showing change of line properties over the time the ship spends at a berth.

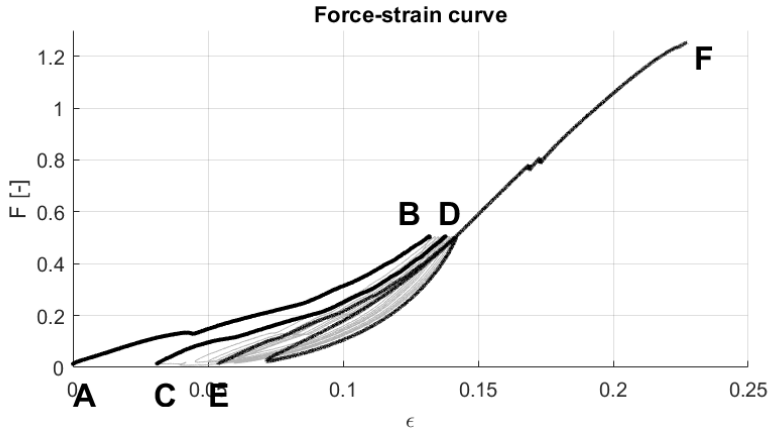

Figure 3.8: *CAESAR rope three loading stages: Initial loading (A-B), loading after relaxation (C-D), loading until break (E-F)*

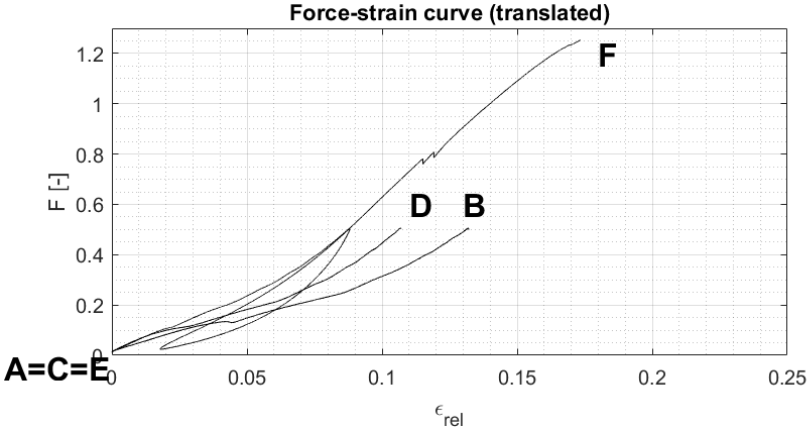

Figure 3.9: *CAESAR rope three loading stages: Initial loading (A-B), loading after relaxation (C-D), loading until break (E-F), translated to origin(0,0)*

3.3.5 Summary all ropes

For the $BEXCOFLEX$ and $HMPE$ mooring rope, a similar analysis as presented in section 3.3.4 has been performed. The results, focussing on the cyclic loading tests, are summarized in table 3.4 and 3.5. E_{diss} is the dissipated energy, ϵ_{min} and ϵ_{max} are the rope elongation at the start and end of the loading cycle respectively. The dissipated energy is also shown in non-dimensional representation, as the ratio between dissipated energy and energy under the loading curve (a-b in figure 3.6).

The following observations are made:

- The first cycle, which is the initial loading cycle, is denoted by the largest energy dissipation. In this initial loading phase, the internal strains are aligned and the voids close. Part of this deformation will be permanent and lead to a stiffer line response compared to the *new* rope. The energy dissipated in the $CAESAR$ rope is significantly higher compared to the $BEXCOFLEX$ and $HMPE$ rope, confirming the significant change in elastic properties of a nylon line, relative to the stiffer rope materials.

- When expressing the dissipated energy relative to the energy under the loading curve, the $BEXCOFLEX$ shows the highest ratio, followed by the $CAESAR$ rope. The ratio is lowest for the $HMPE$ rope. The energy ratio is between 0.4 and 0.5 for the initial cycle and lowers to between 0.2 and 0.3 in the final cycle.

- After the first load cycle, the $CAESAR$ and $BEXCOFLEX$ ropes show a similar energy dissipation number. The $HMPE$ line shows much less influence of cyclic loading on the rope properties. This means the damping of energy for a HMPE rope is limited, which is less desirable e.g. in cyclic wave conditions.Less energy dissipation however also means less heat production, which will be beneficial when it comes to degradation of the lines (short / long term). The implications for the mooring analysis should be part of future research.

Table 3.4: *Bexco model test summary : elongation parameters for $CAESAR$, $BEXCOFLEX$ and $HMPE$*

Cycle	$CAESAR$			$BEXCOFLEX$			$HMPE$		
	ϵ_{min} (%)	ϵ_{max} (%)	ϵ_{max}- ϵ_{min} (%)	ϵ_{min} (%)	ϵ_{max} (%)	ϵ_{max}- ϵ_{min} (%)	ϵ_{min} (%)	ϵ_{max} (%)	ϵ_{max}- ϵ_{min} (%)
1	4.5	13.2	8.7	4.6	9.4	4.8	2.4	3.5	1.1
2	4.5	13.4	8.9	4.6	9.8	5.2	2.4	3.6	1.2
3	5.0	13.5	8.5	5.0	10.0	5.0	2.5	3.6	1.1
4	5.3	13.7	8.4	5.3	10.1	4.9	2.5	3.6	1.1
5	5.5	13.8	8.3	5.4	10.2	4.8	2.6	3.7	1.1
6	5.4	13.8	8.4	5.3	9.9	4.6	2.6	3.6	1.1
7	5.4	13.9	8.5	5.3	10.1	4.8	2.6	3.7	1.1
8	5.8	14.0	8.3	5.5	10.2	4.7	2.6	3.7	1.1
9	5.9	14.1	8.2	5.6	10.3	4.7	2.6	3.7	1.1
10	6.0	14.2	8.2	5.7	10.3	4.6	2.6	3.7	1.1

Table 3.5: *Bexco model test summary : loading cycle parameters for $CAESAR$, $BEXCOFLEX$ and $HMPE$*

cycle	$CAESAR$		$BEXCOFLEX$		$HMPE$	
	$E_{\text{diss}}(\frac{Nm}{m})$	$\frac{E_{\text{diss}}}{E_{\text{load}}}$	$E_{\text{diss}}(\frac{Nm}{m})$	$\frac{E_{\text{diss}}}{E_{\text{load}}}$	$E_{\text{diss}}(\frac{Nm}{m})$	$\frac{E_{\text{diss}}}{E_{\text{load}}}$
1	2.5E-02	0.45	1.7E-02	0.50	4.1E-03	0.44
2	2.0E-02	0.32	1.4E-02	0.38	3.2E-03	0.31
3	1.9E-02	0.29	1.3E-02	0.34	3.1E-03	0.26
4	1.9E-02	0.28	1.3E-02	0.32	3.0E-03	0.23
5	1.8E-02	0.27	1.2E-02	0.31	3.0E-03	0.23
6	2.2E-02	0.37	1.4E-02	0.40	3.2E-03	0.31
7	1.9E-02	0.29	1.2E-02	0.32	3.0E-03	0.23
8	1.9E-02	0.27	1.2E-02	0.30	3.0E-03	0.23
9	1.8E-02	0.26	1.2E-02	0.30	2.9E-03	0.21
10	1.8E-02	0.25	1.2E-02	0.29	3.0E-03	0.20

3.3.6 Additional load cycles for $BEXCOFLEX$

For the $BEXCOFLEX$ line, extra cyclic loading sets have been performed, with 50 cycles (numbered 1 to 50) 10 ±5% MBL and 50 cycles (numbered 51-100) 30 ± 10% MBL. The results of the data analysis are shown in table 3.6.

Table 3.6: *$BEXCOFLEX$ 100 load cycles*

cycle (-)	F_{range} (% MBL)	E_{diss} ($\frac{Nm}{m}$)	ϵ_{min} (%)	ϵ_{max} (%)	ϵ_{max}- ϵ_{min} (%)
1	10 ±5	5.0E-04	5.0	6.2	1.3
10		2.7E-04	5.3	6.3	0.9
20		1.3E-04	5.5	6.3	0.8
30		1.1E-04	5.6	6.3	0.7
40		9.0E-05	5.7	6.4	0.7
50		8.8E-05	5.7	6.4	0.7
70	30 ±10	6.2E-04	8.1	9.3	1.3
80		4.8E-04	8.2	9.4	1.2
90		3.8E-04	8.3	9.5	1.2
100		3.1E-04	8.4	9.5	1.1

3.4 Conclusion

This section discussed the mooring line properties, MBL and elasticity, which are needed as input for mooring analysis. Mooring lines are subdivided into steel wire and synthetic ropes, the former having a stiff, predictable response, the latter consisting of varying line materials, with non-linear and hysteresis response.

International standards, issued by IACS, set requirements for MBL and number of lines on board. A recent update of the guidelines follows the increase in container ship, cruise and gas carrier dimensions since the early 2000s. It is observed that providing a simple criterium for all ship sizes and types is difficult. When performing a mooring analysis, the advice is given to perform a study of the fleet of interest, in order to define the mooring equipment for your design ship.

Line elasticity is not covered by IACS, despite being an important factor in determining the ship's response. Local conditions in ports make it difficult however to select one 'best' rope type of a given ship. Lines composed of a main line and a tail increase flexibility, as the tails can be swapped if necessary to allow safe mooring at a specific berth.

Research on line elongation properties, and how they change over the lifetime of the rope, are needed to understand data presented by manufacturers, primarily for nylon based ropes, where the properties change significantly over the life cycle of the rope.

Cyclic tensile tests performed at Bexco with three types of synthetic ropes, composed of nylon, polyester and HMPE fibres, confirmed that rope behaviour changes from first use over load cycles. The elongation properties of nylon change significantly after the first loading cycle, which means that the elongation curve of the new rope is not representative for usage on board of the ship. During the load cycles, a significant amount of energy was dissipated. The HMPE line's response shows limited hysteresis after the first loading cycle, giving it a response similar to steel lines.

The line elongation curves of the tested ropes, as well as the generic ropes from [OCI18], are available in the *Vlugmoor* database to use

as input for a mooring analysis. The non-linear curves are represented as a tabular format, giving line force as a function of strain for a minimum number of points which is needed to represent the curve shape accurately (around 50 points usually more than suffices). The code interpolates for intermediate strains.

3.5 Future work

In the analysis of the tensile tests on the mooring ropes, elongation properties, as well as energy dissipation were determined for the ropes when subjected to cyclic loading. The change of elongation properties (increase in stiffness over load cycles) as well as the energy dissipation, could be further quantified by expanding the stress-strain relationship from eq. 2.4.

A relationship which fully represents a result such as displayed in figure 3.5, will have the form of eq. 3.5. With respect to eq. 2.4, a damping term has been added, representing energy dissipation in the lines. Both b_1 and k_1 are a function of time. The dependency on $l_0(t)$ (eq. 3.6) is added to account for the induced creep, shifting the curve over the ϵ axis (figure 3.8).

The damping term b_1 is related to the dissipated energy. [QO14] presents an experimental setup used to derive b_1, for a sinusoidal $\frac{\mathrm{d}l}{\mathrm{d}t}$ profile. Experiments with several loading rate amplitudes would be needed to obtain b_1 as a function of $\frac{\mathrm{d}l}{\mathrm{d}t}$.

Adding damping and/or general time dependent behaviour adds considerable complexity to the analysis. The algorithm using eq. 3.5 should in fact be validated based on full scale measurements of line forces. If time series of line loads are available, these could be used as a basis to do controlled tensile tests, similar to the ones presented in this chapter.

$$\begin{cases} F(t) = k_1(l_0(t), t) \cdot \epsilon_1 l_0(t) + b_1(l_0(t), \dfrac{\mathrm{d}l}{\mathrm{d}t}) \cdot \dfrac{\mathrm{d}l}{\mathrm{d}t} & \epsilon_1 > 0\ ,\ t \leq 0 \\ F = 0 & \epsilon_1 \leq 0\ ,\ t \leq 0 \end{cases} \tag{3.5}$$

$$\epsilon_1 = \frac{l(t) - l_0(t)}{l_0(t)} \tag{3.6}$$

References

[Bex04] Bexco. *Deeprope; Polyester & Dyneema mooring ropes manual 2004*. 2004.

[IAC14] IACS. *Requirements concerning Mooring, Anchoring and Towing (revision 2014)*. Tech. rep. 2014, p. 32.

[IAC20] IACS. *Anchoring , Mooring , and Towing Equipment (revision 2020)*. Tech. rep. 2020, p. 20.

[Mar19] MarCom Working Group 184. *Design Principles for Dry Bulk Marine Terminals*. 2019, p. 290.

[OCI18] OCIMF. *Mooring Equipment Guidelines - MEG4*. Witherbys, 2018, p. 312.

[QO14] Dongsheng Qiao and Jinping Ou. “Mooring line damping estimation for a floating wind turbine”. In: *The Scientific World Journal* (2014). ISSN: 1537744X.

[Wei+09] O. Weiler et al. “Motions and mooring loads of an LNG-carrier moored at a jetty in a complex bathymetry”. In: *Proceedings of the ASME 28th International Conference on Ocean, Offshore and Arctic Engineering*. Honolulu, Hawaii, USA, 2009.

4

A moored ship as a mass-spring-damper system

A moored ship which is disturbed by external forces forms a specific engineering challenge, combining ship hydrodynamics with a spring-like constraint, formed by fenders and mooring lines. Correctly representing such a complex system is a difficult task. Fortunately, as with all engineering problems, simplifications can be made based on an assessment of the problem. The absence of forward speed as well as all velocities and accelerations being limited in case of a moored ship, creates an opportunity to reduce the number of terms which would be found in a traditional manoeuvring or seakeeping model.

This chapter elaborates on how the response of a moored ship can be represented mathematically. In essence the system is a complex mass-spring-damper system, which was already presented in figure **??**. The application of this generic system for a single moored ship at a berth is explained, including the definition of the eigenperiods of the system, which represent to a large extent the tendency of the system to react to certain external disturbances. Ship-to-ship mooring is similar in concept, but requires the modelling of two floating systems as well as two sets of mooring equipment. A simplified model approach is presented here, which is valid in a certain range

of ship-to-ship mooring applications.

Two case study examples, $T0Y$ and $ULCS$ are discussed. For the $T0Y$, the eigenperiods are approximated using an analytical approach. A novel approach to assess the quality of the arrangement is presented, applied for the moored $ULCS$, including a mooring arrangement optimisation study.

A final section deals with the main model approach, namely how to write out the mass-spring-damper equations for the application of a floating object and subsequently implement these equations in a time domain simulation.

4.1 General concept of a mass-spring-damper system

Eq. 4.1 expresses Newton's Second Law, where the external forces on the body are in dynamic equilibrium with the inertia forces, the latter depending on the body's acceleration.. For a mass-spring-damper system, this equation takes the form of eq. 4.2. If x is a translation, then m is a mass (kg), b is a damping parameter (kg/s) and c is a restoring coefficient (N/m), or spring constant in the specific application. F_{G} represents a generic force, e.g. the effect of the passing ship on the moored ship. x, $\dot{x}$ and $\ddot{x}$ is a generic motion and its first and second derivative.

$$F = m \cdot \ddot{x} \tag{4.1}$$

$$F_{\mathrm{G}} - b \cdot \dot{x} - c \cdot x = m \cdot \ddot{x} \tag{4.2}$$

The system expressed by eq. (4.2) forms a differential equation. When the external force (F_{G}) is absent, the solution can take three different forms, depending on the coefficients m, b, c. The discriminant (eq. 4.3) of the equation determines the properties of the roots. Eq. 4.4 represents (top to bottom) an under-damped system ($D < 0$), critically damped ($D = 0$) and over-damped system ($D > 0$), with specific solutions for $D < 0$ and $D = 0$. ω_{n} (for $D < 0$) is the eigenperiod (also called natural period) of the system (eq. 4.5). r_1,r_2 are the roots of the system (eq. 4.6). c_1,c_2 are constants depending on the boundary conditions. A and B are constants calculated based on c_1,c_2 (eq. 4.7). All these systems will (as they should because of damping and no external force), go to zero over time, denoted by the negative sign in the argument of the exponential terms in each solution.

$$D = b^2 - 4mc \tag{4.3}$$

$$\begin{cases} x(t) = \mathrm{c}_1 e^{-\mathrm{r}_1 t} + \mathrm{c}_2 e^{-\mathrm{r}_2 t} = e^{\frac{-bt}{2m}} \cdot \mathrm{A}\cos(\omega_{\mathrm{n}} t - \mathrm{B}) & D < 0 \\ x(t) = \mathrm{c}_1 e^{-\mathrm{r}_1 t} + \mathrm{c}_2 e^{-\mathrm{r}_2 t} = e^{\frac{-bt}{2m}} (\mathrm{c}_1 + \mathrm{c}_2 t) & D = 0 \\ x(t) = \mathrm{c}_1 e^{-\mathrm{r}_1 t} + \mathrm{c}_2 e^{-\mathrm{r}_2 t} & D > 0 \end{cases} \tag{4.4}$$

$$\omega_{\mathrm{n}} = \frac{\sqrt{4mc - b^2}}{2m} \tag{4.5}$$

$$\mathrm{r}_1 = \frac{-b + \sqrt{D}}{2m} \tag{4.6a}$$

$$\mathrm{r}_2 = \frac{-b - \sqrt{D}}{2} \tag{4.6b}$$

$$\mathrm{A} = \sqrt{{\mathrm{c}_1}^2 + {\mathrm{c}_2}^2} \tag{4.7a}$$

$$\mathrm{B} = \mathrm{atan}\left(\frac{c_2}{c_1}\right) \tag{4.7b}$$

Resonance may lead to unacceptable responses, even if the magnitude of the external load is limited. As an illustration, the simple undamped mass-spring system of eq. 4.8 is given, where the period of the external load equals the resonance period of the system. It can be shown that the particular solution of the system is of a form of eq. 4.9, where the solution will continue to increase in oscillation amplitude.

$$m\ddot{x} + cx = F_\mathrm{G} = \sin\left(\sqrt{\frac{c}{m}}t\right) \tag{4.8}$$

$$x_\mathrm{p}(t) = \frac{1}{2\sqrt{cm}} \cdot t \sin\left(\sqrt{\frac{c}{m}}t\right) \tag{4.9}$$

In what follows, the ship mooring system will be expressed according to eq. 4.2 in 6DOF. The numerous terms appearing throughout the derivation will however make it impossible to arrive at such an elegant analytical solution of the differential equations, as expressed in eq. 4.4. In order to come to a useful model, the behaviour of a floating object is examined in section 4.2. Section 4.3 elaborates on the 6DOF system representing the moored ship at the berth. Ship-to-ship mooring, where two ships are moored side-by-side is elaborated on in section 4.4. Section 4.5 analyses the 6DOF problem in the frequency domain. Section 4.6 expresses a solution in the time domain. This solution is then the description of the mathematical model *Vlugmoor*.

4.2 Equation of motion of a free floating object

A floating object will move in 6DOF, three translations (surge, sway, heave) and three rotations (roll, pitch, yaw) (figure 2.1 and appendix B for further details). These motions are not independent from each other, e.g. a yaw motion can cause a sway response force. This results in a system of six differential equations, expressing the dynamic equilibrium of the inertia forces and moments in 6DOF with external forces/moments and the hydrodynamic and hydrostatic reaction forces/moments (eq. 4.10). m, a, b and c are all 6X6 matrices, with eq. 4.11 showing the shape of the mass matrix m. As this chapter discusses 6DOF in general, the generic expression 'forces' will be used to include both forces and moments. As an example, the force vector on the right side of eq. 4.10, which consists of forces (X,Y,Z) as well as moments (K,M,N).

$$\left([m]+[a]\right)\cdot\begin{bmatrix}\dot{u}\\ \dot{v}\\ \dot{w}\\ \dot{p}\\ \dot{q}\\ \dot{r}\end{bmatrix}+[b]\cdot\begin{bmatrix}u\\ v\\ w\\ p\\ q\\ r\end{bmatrix}+[c]\cdot\begin{bmatrix}x\\ y\\ z\\ \phi\\ \theta\\ \psi\end{bmatrix}=\begin{bmatrix}X\\ Y\\ Z\\ K\\ M\\ N\end{bmatrix} \tag{4.10}$$

$$m=\begin{bmatrix}m_{11} & m_{12} & m_{13} & m_{14} & m_{15} & m_{16}\\ m_{21} & m_{22} & m_{23} & m_{24} & m_{25} & m_{26}\\ m_{31} & m_{32} & m_{33} & m_{34} & m_{35} & m_{36}\\ m_{41} & m_{42} & m_{43} & m_{44} & m_{45} & m_{46}\\ m_{51} & m_{52} & m_{53} & m_{54} & m_{55} & m_{56}\\ m_{61} & m_{62} & m_{63} & m_{64} & m_{65} & m_{66}\end{bmatrix} \tag{4.11}$$

The aim of this section is not to go over all terms in eq. 4.10, let alone explain the full background and calculation process (see [SNA88]). The physical meaning of the coefficients is elaborated on here.

Next to the inertia matrix m, an extra coefficient a is added to the inertia term in the equation. a is a representation of the integrated pressure distribution present around the body due to its acceleration. This solution, a, has the dimensions of a body mass m and is proportional to the acceleration of the body, hence the term *added mass*.

b expresses the damping contribution from the moving object. Various processes contribute to this damping term, wave radiation being the one which is discussed for the purpose of this thesis. Damping a result of viscous effects is not discussed in this work.

A last contribution $c \cdot x$ is formed by the restoring forces (=forces and moments) exerted by the surrounding water on the ship. These restoring forces are hydrostatic forces, which are caused by a disequilibrium between buoyancy force and weight, generating restoring forces and motions. These contributions are only present in the vertical plane (roll, heave, pitch), which is exactly why a mooring system is needed to restrain the ship in the horizontal plane (see section 4.3.1 for in-depth discussion).

The term at the right hand side of equation 4.10 represents the external disturbances acting on the body.

The complex underwater shape of the ship as well as its weight distribution of course makes this problem complex, certainly considering the presence of coupling terms between motion modes. b_{26} for example expresses the effect of a mode 6 radiated wave (yaw) on the damping contribution for mode 2 (sway). The magnitude of these components is not further discussed, yet the general appearance and properties are highlighted, as far as they are needed to understand their use in a mooring analysis.

Suppose the added mass (symbol a_{ij}, with ij being the motion modes) and damping (symbol b_{ij}) have been calculated based on physical model tests and/or numerical models. a and b will depend on the frequency of the motion. This makes sense as for example the radiated waves will look different at different wave lengths (=frequency). Figure 4.1 shows the diagonal coefficients of a and b matrix for the $T0Y$ ship modelled at 20% UKC with the potential panel method Hydrostar. This set of coefficients is going to be used as a basis for the discussion in the subsequence sections.

Furthermore, as could be expected based on the discussion on passing ship effects (section 2.1.4.2), horizontal and vertical restrictions of the water body will also alter the hydrodynamic response of the floating body. Certainly when a ship is moored at a closed berth, the presence of the quay wall changes the magnitude but also the

shape of the curve in function of frequency [LV94]. [Van92] describes how different sets of coefficients should be implemented within one calculation, depending on the distance of the ship to the quay, which varies due to the moored ship's motion. Including this variability could provide critical accuracy for sway and yaw dominant responses, however it is not dealt with within the scope of this thesis text. Including vertical walls and later implementing multiple sets of coefficients in *Vlugmoor* should be part of future work.

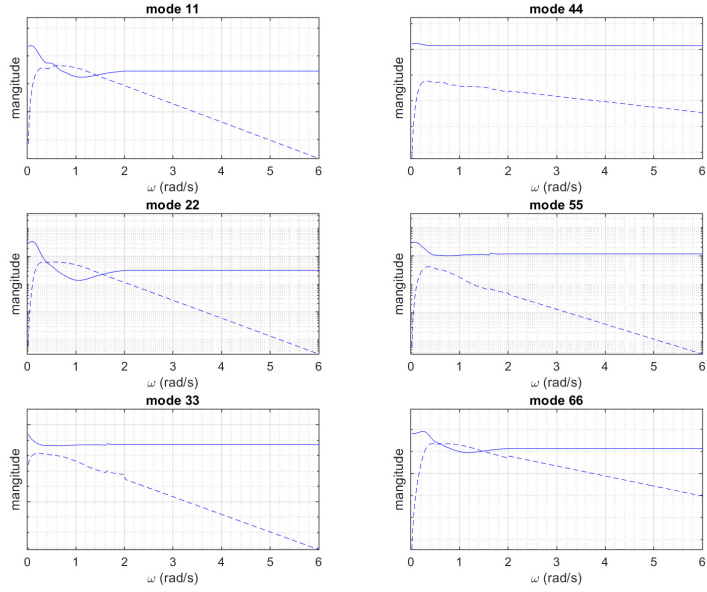

Figure 4.1: *Hydrodynamic coefficients diagonal terms a_{ii} (full line) and b_{ii} (dashed line) matrix for $T0Y$, 20% UKC, logarithmic scale on vertical axis.*

4.3 Single ship moored at berth

A moored ship is a specific case where the floating object is kept in place using mooring equipment, namely mooring lines and fenders. The form of eq. 4.10 is still applicable, albeit when terms are added to incorporate line and fender responses. Eq. 4.12 provides an extended equation, by adding b_{moor} and c_{moor} as general damping and restoring coefficients representing mooring lines and fenders.

$$[m+a]\cdot[\ddot{x}]+[b+b_{\mathrm{moor}}]\cdot[\dot{x}]+[c+c_{\mathrm{moor}}]\cdot[x]=[F] \tag{4.12}$$

As will become clear in the following sections, a moored ship is in a way less complex than a general manoeuvring ship, as the forward speed is close to zero. When the ship responds to external disturbances, all motion components are also limited in magnitude, a characteristic which will be used to simplify the time domain model (section 4.6).

Figure 4.2 shows a moored ship from three viewpoints, indicating the mooring lines and fenders.

4.3.1 Horizontal versus vertical plane

It is no longer possible to solve and analyse eq. (4.12) easily in an analytical way, as was done for eq 4.1. However, for the purpose of calculating the response of a moored ship with respect to external loads, not all terms in eq. 4.12 will carry the same weight. As presented in section 2.3, the response of a moored ship is evaluated based on line and fenders forces, as well as motions. The most relevant DOF are then the ones where mooring lines and fenders have a large influence. Examining the components of eq. 4.12 for the various DOF will lead to further insight. In order to make this analysis comprehensive, the coupling terms are not considered (assumed to be zero). On top of this, the damping due to line and fender hysteresis is neglected, as is the contribution of fender friction to the damping force ($[b_{\mathrm{moor}}]=0$).

Table 4.1 shows the general form of mass (m), damping (b) and restoring (c) contributions for the 6DOF. k_{l} and k_{f} are the generic restoring coefficients for mooring lines and fenders respectively.

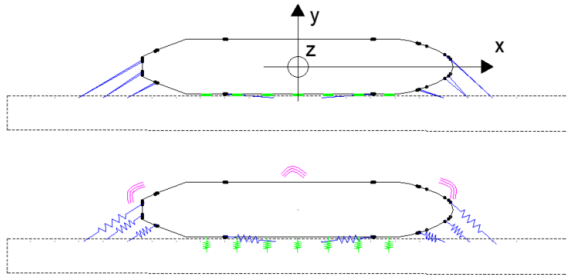

(a) Top view

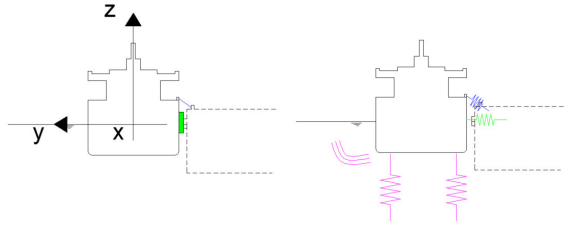

(b) Front view

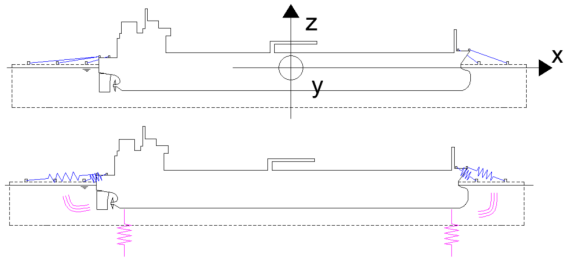

(c) Side view

Figure 4.2: *Definition axis system and components mathematical model for a generic representation of a moored ship; blue = mooring lines, green = fenders, purple = water response.*

As seen in table 4.1, the mass m and added mass a coefficients are similar in nature for all modes, as are the hydrodynamic damping terms. When it comes to the restoring coefficients however, a major difference presents itself between surge, sway and yaw on one hand and heave, roll and pitch on the other hand. For the latter, a hydrostatic force is present. For heave, this is directly related to the water plane area; For roll and pitch the coefficient is a function of the metacentre heights $\overline{GM_{\mathrm{T}}}$ and $\overline{GM_{\mathrm{L}}}$. In the horizontal plane, the restoring forces need to be generated by the mooring lines and fenders, with no hydrostatic component being available.

In heave, roll and pitch, the mooring equipment also forms a part of the restoring capacity. For heave for example, the relative contribution from mooring equipment and hydrostatic force can be compared easily, based on the example from table F.1 (appendix F). The hydrostatic restoring term (c) is 9818 ton/m, whereas the stiffness of the lines can be (conservatively) estimated at around 200 ton/m in the heave direction, or about 2% of the hydrostatic counterpart. This simple calculation shows that the potential contribution of mooring line force to the heave is insignificant. For roll and pitch, the application point of the lines, relative to the magnitude of the $\overline{GM}$ terms, needs to be taken into account. The hydrostatic contributions will however always be dominant. Bear in mind that these motions will still cause stretching of the lines and thus line forces, which will affect the equilibrium in other modes.

Table 4.1: *Mass m, damping b and restoring c terms moored ship equation (eq. 4.12), coupling of motion modes is not considered.*

	11	22	33	44	55	66
m	$\frac{\Delta}{g}$	$\frac{\Delta}{g}$	$\frac{\Delta}{g}$	I_{xx}	I_{yy}	I_{zz}
a	a_{11}	a_{22}	a_{33}	a_{44}	a_{55}	a_{66}
b	b_{11}	b_{22}	b_{33}	b_{44}	b_{55}	b_{66}
c			$\rho g A_{\mathrm{w}}$	$\Delta\overline{GM_{\mathrm{T}}}$	$\Delta\overline{GM_{\mathrm{L}}}$	
c_{moor}	k_{l}, k_{f}	k_{l}, k_{f}	k_{l}, k_{f}	k_{l}, k_{f}	k_{l}, k_{f}	k_{l}, k_{f}

4.3.2 Mooring configuration parameters

The mooring configuration consists of a number of mooring lines and fenders. The mooring lines are defined by their position, length and their elastic properties. The line force works along the vector of the line between fairlead (x_{0s},y_{0s},z_{0s}) and mooring point on the berth (x_{0b},y_{0b},z_{0b}) (figure 4.3). The total length of the line is the sum of the section between berth and fairlead (l_{bf}) and the length on deck (l_{fw}). The mooring line angle is usually represented as a horizontal angle α_{l} and a vertical angle β_{l}. γ_{l} represents the vector angle at the fairlead, with $\vec{SB}$ and $\vec{SD}$ the vectors for points ship (s)-berth (b) and ship (s)-deck(d) respectively. The point on the deck can be either a roller or a winch. The elastic properties are represented by k_{l} (eq. 2.4).

Fenders are defined in a similar way. The initial thickness of the fender d_0 in eq. 2.6 is however equal for all fenders. The most important parameter is then the x position at the berth with respect to the origin (=midships moored ship). The elasticity is expressed as k_{f} (eq. 2.6)

$$\alpha_{\mathrm{l}} = \mathrm{acos}\left(\frac{x_{\mathrm{s}} - x_{\mathrm{b}}}{\sqrt{(x_{\mathrm{s}} - x_{\mathrm{b}})^2 + (y_{\mathrm{s}} - y_{\mathrm{b}})^2}}\right) \tag{4.13a}$$

$$\beta_{\mathrm{l}} = \mathrm{atan}\left(\frac{z_{\mathrm{s}} - z_{\mathrm{b}}}{\sqrt{(x_{\mathrm{s}} - x_{\mathrm{b}})^2 + (y_{\mathrm{s}} - y_{\mathrm{b}})^2}}\right) \tag{4.13b}$$

$$\gamma_{\mathrm{l}} = \mathrm{acos}\left(\frac{\vec{SB} \cdot \vec{SD}}{|\vec{SB}||\vec{SD}|}\right) \tag{4.13c}$$

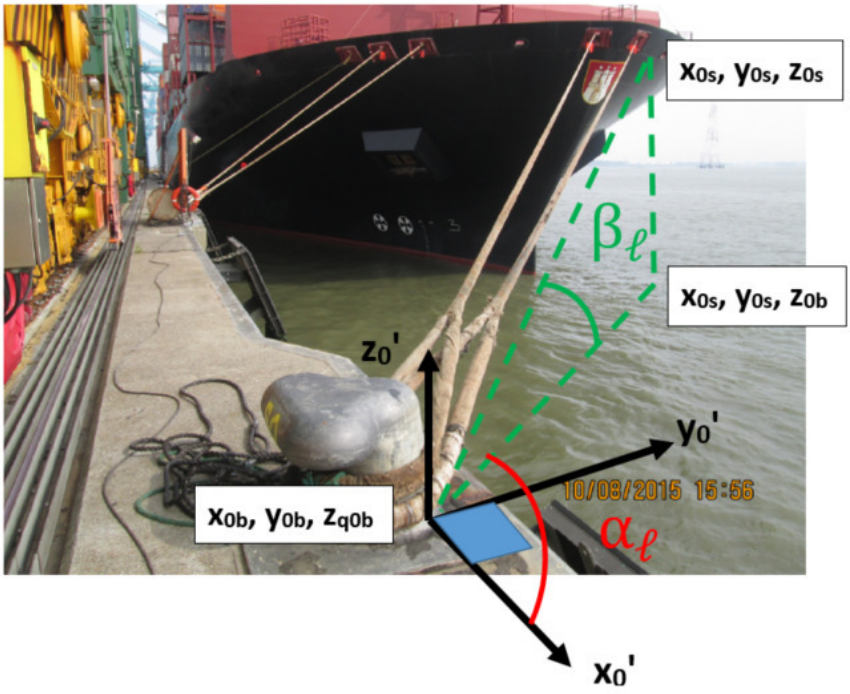

Figure 4.3: *Definition mooring line angles α_l and β_l, figure courtesy of Antwerp Port Authority*

4.3.3 Analytical approximation eigenperiod

The eigenperiod is an important characteristic parameter of the mass-spring-damper system, as was discussed in section 4.1. For a moored ship, all DOF have a corresponding eigenperiod. An analytical solution of the eigenperiod for the system as given by eq. 4.12 is not available. By making some well-chosen assumptions, an estimation of the eigenperiod can however be found for all DOF.

4.3.3.1 Assumptions

The system of equations given by eq. 4.12 is too complex to offer an analytical solution for the eigenperiods. The following assumptions are made to simplify the system, allowing to find an expression which can be solved using a pocket calculator.

1. The non-linear system, consisting of ship and mooring equipment, is partly linearised, by assuming that the slope of the line and fender deformation is constant ($k_{\mathrm{l}}(\epsilon_{\mathrm{l}})$ = cte, $k_{\mathrm{f}}(\epsilon_{\mathrm{f}})$ = cte).

2. In line with section 4.3.1, the line and fender damping is neglected, as is the fender friction.

3. The restoring terms for heave, roll and pitch are only assumed to be hydrostatic, no contribution of lines and fenders is taken into account.

4. The motions which occur in the assessment are large, as was presented in figure 2.32. A motion cycle is in other words composed of two extreme positions, where a part of the mooring equipment is loaded (heavily), whereas another part is slack (mooring line) or not compressed (fender). For surge, this assumption will usually hold. For sway and yaw, line tension might still be present when the fenders are compressed, as the lines are pre-tensioned. In other words, pretension is assumed to be minimal in the proposed calculation.

5. All coupling terms are assumed to be zero, e.g. a pure sway motion will not cause a response in yaw.

In the following sections, an expression for the eigenperiod is derived for all DOF. After this theoretical derivation, these definitions are applied to the case study example of the moored $T0Y$.

4.3.3.2 Estimation surge eigenperiod

The surge motion as given in figure 2.32 is used as a basis to derive the eigenperiod. The eigenperiod is in essence the period of the cyclic motion which is attained when the system is released after applying an initial deflection (in the surge direction). For the example of figure 2.32, assume that you move the ship forward (forced) and then release it from this position. The ship will start moving backwards under the effect of the tension in the lines with $\alpha_{\mathrm{l}} < 90^{\circ}$ (figure 4.3). When the ship moves through the equilibrium position, (spring) lines forces are zero. Once the ship moved past this position, the lines with $\alpha_{\mathrm{l}} > 90^{\circ}$ are tensioned. At the most backward position, the tension in these lines will cause the ship to move forwards again. The eigenperiod is then the sum of the periods of two half-cycle periods, which is determined by the elasticity of the two sets of lines ($\alpha_{\mathrm{l}} < 90^{\circ}$, $\alpha_{\mathrm{l}} > 90^{\circ}$).

Eq. 4.14 gives an expression for the longitudinal stiffness of these lines, which forms the restoring component of the system. As no coupling with other modes is present, the (half-cycle) eigenperiod will have the form of eq. 4.5. The damping term b is the ship damping b_{11}, the mass term m is the combination of ship's own mass $\frac{\Delta}{g}$ and added mass a_{11}. The resulting expression for the surge eigenperiod is given in eq. 4.15. $T_{\mathrm{n}x}$ is the eigenperiod (s) and $\omega_{\mathrm{n}x}$ the eigenfrequency (rad/s). For the remainder of this section, the eigenperiod will be used for the discussion.

$$k_{x+} = \sum_{\mathrm{i},\alpha<90} k_{\mathrm{l,i}} \cdot \cos(\alpha_{\mathrm{l,i}}) \cdot \cos(\beta_{\mathrm{l,i}}) \tag{4.14a}$$

$$k_{x-} = \sum_{\mathrm{i},\alpha>90} k_{\mathrm{l,i}} \cdot \cos(\alpha_{\mathrm{l,i}}) \cdot \cos(\beta_{\mathrm{l,i}}) \tag{4.14b}$$

$$T_{\mathrm{n}x} = \frac{T_{\mathrm{n}x+} + T_{\mathrm{n}x-}}{2} = \frac{\frac{2\pi}{\omega_{\mathrm{n}x+}} + \frac{2\pi}{\omega_{\mathrm{n}x-}}}{2} = \frac{2\pi \cdot (\frac{\Delta}{g} + a_{11})}{\sqrt{|b_{11}^2 - 4(\frac{\Delta}{g} + a_{11}) \cdot k_{x+}|}} + \frac{2\pi \cdot (\frac{\Delta}{g} + a_{11})}{\sqrt{|b_{11}^2 - 4(\frac{\Delta}{g} + a_{11}) \cdot k_{x-}|}} \tag{4.15}$$

4.3.3.3 Estimation sway eigenperiod

For the sway motion, a similar thought process can be followed as was done for surge, expressed in figure 4.4. When the ship moves in the positive y-direction (half cycle), the lines are tensioned and will respond. In the negative sway motion (half cycle), the fenders are loaded. Both contributions are given by eq. 4.16 and lead to the eigenperiod given by eq. 4.17.

$$k_{y+} = \sum_{\mathrm{i}} k_{\mathrm{l,i}} \cdot \sin(\alpha_{\mathrm{l,i}}) \cdot \cos(\beta_{\mathrm{l,i}}) \tag{4.16a}$$

$$k_{y-} = \sum_{\mathrm{j}} k_{\mathrm{f,j}} \tag{4.16b}$$

$$T_{\mathrm{n}y} = \frac{2\pi \cdot (\frac{\Delta}{g} + a_{22})}{\sqrt{|b_{22}^2 - 4(\frac{\Delta}{g} + a_{22}) \cdot k_{y+}|}} + \frac{2\pi \cdot (\frac{\Delta}{g} + a_{22})}{\sqrt{|b_{22}^2 - 4(\frac{\Delta}{g} + a_{22}) \cdot k_{y-}|}} \tag{4.17}$$

4.3.3.4 Estimation yaw eigenperiod

The yaw eigenperiod can be estimated based on a similar approach to the one for surge and sway. From the definition of yaw, it comprises a rotation around midships, following the axis system definition. The two half-cycles part of this rotation are then given in figure 4.6. Eq. 4.18a and eq. 4.18b give the two contributions ($k_{\psi,+}$ and $k_{\psi,-}$). In these equations, δ_{l} and δ_{f} are the angles that the line and fender vectors respectively make with the lever arm around the origin, as illustrated by figure 4.5, for a generic mooring line.

The yaw motion as given in figure 4.6 assumes a rotation around the z-axis by definition. The presence of a sway force as a result of this rotation will cause the rotation axis to shift however. A plausible axis shift is illustrated by figure 4.7, where the rotation axis shifts to the fore and aft fender during the rotation. This significant shift in rotational axis has the following consequences:

- The lever arm of the mooring equipment contribution to k_{ψ} will increase.

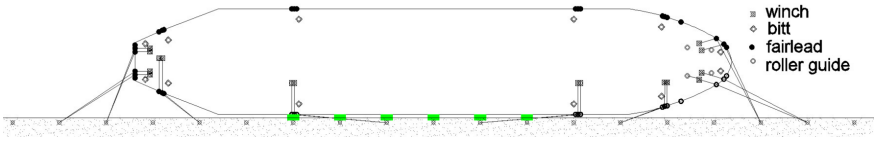

(a) Undisturbed (pretension).

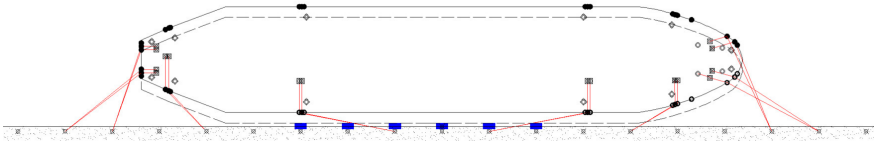

(b) Motion in positive y direction : k_{y+}, (dashed = starting position ship).

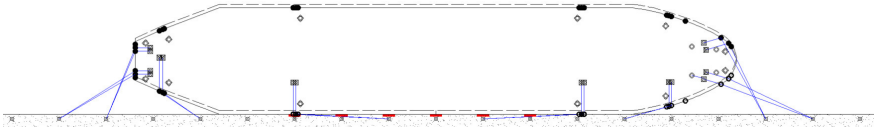

(c) motion in negative y direction : k_{y-}, (dashed = starting position ship).

Figure 4.4: *Derivation k_y moored ship, $T0Y$; black line = pre-tensioned mooring line , green = pre-compressed fender, blue = untensioned line/fender, red = high tension in line/fender*

- The moment of inertia (mass and added mass) needs to be recalculated. A term which is function of mass and the squared distance needs to be added, following Steiner's theorem.

As both actions will partly cancel each other out (nominator and denominator in eq. 4.19), the rotation centre might not actually shift as far as the fore and aft fender, substantiating the claim of the yaw rotation eigenperiod definition.

$$k_{\psi+} = \sum_{\mathrm{i},x_{\mathrm{s,i}}>0} k_{\mathrm{l,i}} \cdot \cos(\beta_{\mathrm{l,i}}) \cdot \cos(\delta_{\mathrm{l,i}}) \cdot (x_{\mathrm{s,i}}^2 + y_{\mathrm{s,i}}^2) + \sum_{\mathrm{j},x_{\mathrm{f,j}}<0} k_{\mathrm{f,j}} \cdot |\cos(\delta_{\mathrm{f,j}})| \cdot (x_{\mathrm{s,i}}^2 + y_{\mathrm{s,i}}^2) \tag{4.18a}$$

$$k_{\psi-} = \sum_{\mathrm{i},x_{\mathrm{s,i}}<0} k_{\mathrm{l,i}} \cdot \cos(\beta_{\mathrm{l,i}}) \cdot \cos(\delta_{\mathrm{l,i}}) \cdot (x_{\mathrm{s,i}}^2 + y_{\mathrm{s,i}}^2) + \sum_{\mathrm{j},x_{\mathrm{f,j}}>0} k_{\mathrm{f,j}} \cdot |\cos(\delta_{\mathrm{f,j}})| \cdot (x_{\mathrm{s,i}}^2 + y_{\mathrm{s,i}}^2) \tag{4.18b}$$

$$T_{\mathrm{n}\psi} = \frac{2\pi \cdot (I_{zz} + a_{66})}{\sqrt{|b_{66}^2 - 4(I_{zz} + a_{66}) \cdot k_{\psi+}|}} + \frac{2\pi \cdot (I_{zz} + a_{66})}{\sqrt{|b_{66}^2 - 4(I_{zz} + a_{66}) \cdot k_{\psi-}|}} \tag{4.19}$$

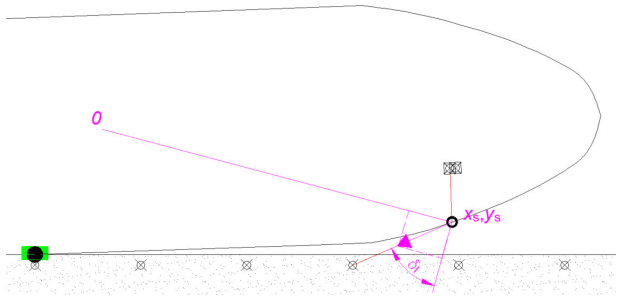

Figure 4.5: *Illustration line angle δ_{l} between mooring line vector and lever arm around rotation point.*

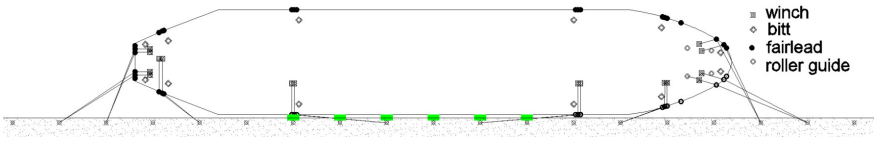

(a) Undisturbed (pretension)

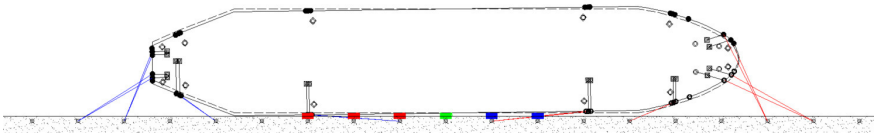

(b) Motion in positive yaw direction: $k_{\psi+}$,(dashed = starting position ship).

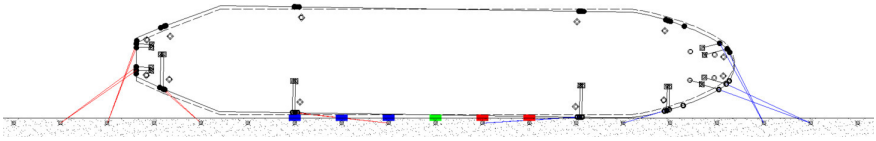

(c) Motion in negative yaw direction: $k_{\psi-}$, (dashed = starting position ship).

Figure 4.6: *Derivation k_ψ moored ship, $T0Y$; black line = pre-tensioned mooring line , green = pre-compressed fender, blue = untensioned line/fender, red = high tension in line/fender*

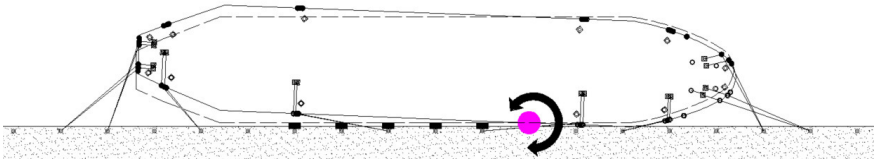

(a) Rotation around fore fender.

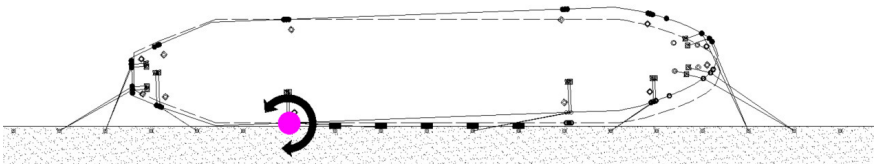

(b) Rotation around aft fender.

Figure 4.7: *Illustration possible change of rotational axis when the ship rotates in the horizontal plane.*

4.3.3.5 Estimation heave, pitch and roll eigenperiod

When neglecting the contribution of lines and fenders to the heave, pitch and roll modes, the mass, damping and restoring terms are identified easily. The expressions given by eq. 4.20, 4.21 and 4.22 are formed. For future research, it would make most sense to expand the expression for roll with the contribution from the lines and fenders, certainly in cases where the period of the external disturbances falls in the region of the roll eigenperiod.

$$T_{\mathrm{n}z} = \frac{2\pi \cdot (\frac{\Delta}{g} + a_{33})}{\sqrt{|b_{33}^2 - 4(\frac{\Delta}{g} + a_{33}) \cdot \rho g A_{\mathrm{w}}|}} \tag{4.20}$$

$$T_{\mathrm{n}\phi} = \frac{2\pi \cdot (I_{xx} + a_{44})}{\sqrt{|b_{44}^2 - 4(I_{xx} + a_{44}) \cdot \Delta \overline{GM_{\mathrm{T}}}|}} \tag{4.21}$$

$$T_{\mathrm{n}\theta} = \frac{2\pi \cdot (I_{yy} + a_{55})}{\sqrt{|b_{55}^2 - 4(I_{yy} + a_{55}) \cdot \Delta \overline{GM_{\mathrm{L}}}|}} \tag{4.22}$$

4.3.3.6 $T0Y$ case study

The $T0Y$ case study example is considered to calculate the eigenperiods according to the expressions derived in this section. The hull and mooring equipment characteristics can be found in appendix F (table F.1). The mooring configuration for quay berth mooring is considered (figure F.2 and table F.2). The calculated eigenperiods are found in table 4.2. As mooring line, the polyester type from figure 3.2 is linearised over the range of 0% to 50% MBL. As a fender, a buckling type (figure 2.19) is assumed with a maximum load of 300 tons, at which is reaches a deflection of 0.375 m.

The eigenperiod of vertical modes (heave, roll and pitch) are short compared to the ones for the horizontal modes, which is due to the relatively soft response of the mooring equipment compared to the restoring terms.

Table 4.2: *Analytical approximation of eigenperiods ($T_{\mathrm{n}}(s)$) moored $T0Y$, figure 2.21, 20% UKC.*

$T_{\mathrm{n}x}$	$T_{\mathrm{n}y}$	$T_{\mathrm{n}z}$	$T_{\mathrm{n}\phi}$	$T_{\mathrm{n}\theta}$	$T_{\mathrm{n}\psi}$
78.0	71.2	16.2	12.3	13.5	36.6

4.3.4 Assessment mooring arrangement using efficiency parameters

4.3.4.1 Need for advanced assessment method : $ULCS$ case study

In section 2.2.3, the mooring configuration for the $T0Y$ at quay and jetty was already discussed, indicating that the OCIMF requirements regarding line angles [OCI18] could not be met for quay mooring. The author developed a novel method to assess and compare the quality of a mooring arrangement, prior to performing a time domain calculation [VVI18],[Van+19]. This is done by calculating four characteristic parameters, describing the arrangement, which means each individual line does not need to be analysed, as presented by OCIMF.

[Van+19] discusses the moored $ULCS$ at a generic container terminal. The mooring arrangement is defined as 'MC0' (figure 4.8). Table 4.3 gives the line angles α_{l},β_{l} for each mooring line. Table F.4 (appendix F) gives an extended version, including the vector line angle γ_{l}, the line length of the segment between bollard and fairlead (l_{bf}) and the line length of the segment between winch and fairlead (l_{wf}).

In table 4.3, β_{l} exceeds 25° (OCIMF standard) for lines 9,11,12. Spring lines should have an angle of max. 10° with the quay, which means α_{l} needs to be in the [0 10°] or [170° 180°] interval. Only the aft springs can be be seen as 'true OCIMF springs'. Breast lines need to be inside the [75° 105°] interval. Only line 11 is a true breast line, but recall that this line is in fact too steep when applying the OCIMF definition. All other mooring lines are general head and stern line, which are in fact less efficient to moor a ship compared to spring and breast lines. This is because their cos/sin components are low compared to 'pure spring and breast lines'.

According to OCIMF, only lines 7 and 8 follow their recommendations. This arrangement seems far below standards, however considering the location of mooring points on quay and deck, it is considered as a standard arrangement for a $ULCS$. As the OCIMF does in a strict sense only apply to tankers, an alternative method to assess the mooring configuration for container ships is however still required.

4.3.4.2 Definition efficiency parameters

Efficiency parameters form a novel method to evaluate the capacity of the mooring arrangement to deal with external loading, based on simple trigonometric relationships. The thought process is explained for the surge mode.

In the x-direction (surge), the mooring line force component F_x is related to the line force F as expressed by eq. 4.23a. For a small motion dx, relative to the total line length, the corresponding line length increase is given by eq. 4.23b (figure 4.9), when only considering first order terms. Under the assumption of linear line elongation, the strain is given by eq. 4.23c.

$$F_{\mathrm{x}} = F \cdot \cos(\beta_{\mathrm{l}}) \cdot \cos(\alpha_{\mathrm{l}}) \tag{4.23a}$$

$$l_1^2 - l_0^2 = x_1^2 - x_0^2 \Rightarrow \mathrm{d}l \cong \cos(\alpha_{\mathrm{l}}) \cdot \mathrm{d}x \tag{4.23b}$$

$$\epsilon_{\mathrm{l}} = \frac{\mathrm{d}l}{l_0} \cong \cos(\alpha_{\mathrm{l}}) \cdot \frac{\mathrm{d}x}{l_0} \tag{4.23c}$$

Based on the considerations made in eq. 4.23, an expression for the efficiency parameter defined as $\mathrm{e}_{X\mathrm{i}}$ is derived as follows.

- $\mathrm{e}_{X,\mathrm{i}}$ is a function of the magnitude of the x-component of the total line force (eq. 4.23a)

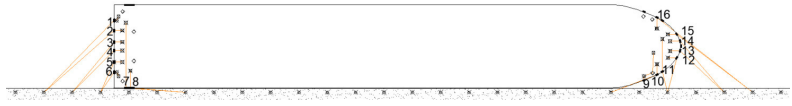

Figure 4.8: *Mooring arrangement MC0, $ULCS$.*

Table 4.3: *Mooring line angles and efficiency parameters $ULCS$, mooring arrangement MC0*

line	α_{l}	β_{l}	$\mathrm{e}_{X\mathrm{i}}$	$\mathrm{e}_{Y\mathrm{i}}$	line	α_{l}	β_{l}	$\mathrm{e}_{X\mathrm{i}}$	$\mathrm{e}_{Y\mathrm{i}}$
1	45	6	0.36	0.36	9	20	27	0.76	0.10
2	41	6	0.43	0.33	10	21	20	0.97	0.14
3	50	9	0.43	0.60	11	102	40	-0.04	0.73
4	44	9	0.57	0.55	12	74	27	0.10	1.20
5	65	17	0.30	1.38	14	131	15	-0.40	0.53
7	176	10	-0.61	0.00	15	143	11	-0.46	0.27
8	176	10	-1.05	0.01	16	142	8	-0.36	0.22

$\mathrm{e}_{X\mathrm{p}} = 4.60 \quad \mathrm{e}_{X\mathrm{n}} = 3.44 \quad \mathrm{e}_{Y\mathrm{f}} = 3.65 \quad \mathrm{e}_{Y\mathrm{a}} = 4.58$

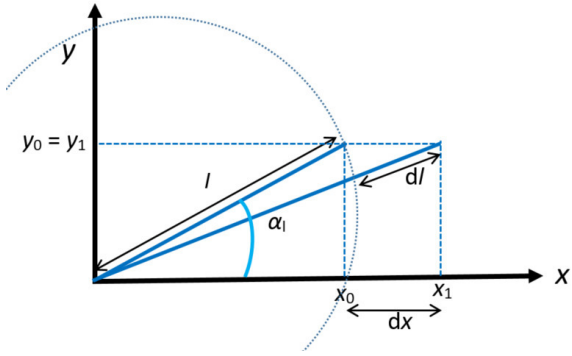

Figure 4.9: *Elongation of the mooring line dl in function of a longitudinal ship motion dx*

- A mooring line needs to elongate before it can take up loads, which is expressed by (eq. 4.23b).
- $\mathrm{e}_{X,\mathrm{i}}$ is made non-dimensional by including a reference length, l_{ref}; which is the average length of the mooring lines.

For the transversal efficiency, y-direction, a similar derivation can be made. The resulting set of efficiency parameters, for each line i, are given by eq. 4.24.

$$\mathrm{e}_{X,\mathrm{i}} = \cos^2(\beta_{\mathrm{l,i}}) \cdot \cos^2(\alpha_{\mathrm{l,i}}) \cdot \frac{l_{\mathrm{ref}}}{l_{\mathrm{i}}} \tag{4.24a}$$

$$\mathrm{e}_{Y,\mathrm{i}} = \cos^2(\beta_{\mathrm{l,i}}) \cdot \sin^2(\alpha_{\mathrm{l,i}}) \cdot \frac{l_{\mathrm{ref}}}{l_{\mathrm{i}}} \tag{4.24b}$$

$$l_{\mathrm{ref}} = \frac{1}{n_{\mathrm{l}}} \cdot \sum_{i=1}^{n_{\mathrm{l}}} l_i \tag{4.24c}$$

The values for $\mathrm{e}_{X,\mathrm{i}}$ and $\mathrm{e}_{Y,\mathrm{i}}$ can be found in table 4.3. It is obvious that the spring lines (7,8,9,10) are characterised by a large $\mathrm{e}_{X,\mathrm{i}}$. For the transversal capacity it becomes less intuitive.

Based on the contributions of the individual lines, a longitudinal and transversal efficiency of the mooring configuration as a whole can be defined (see eq. 4.25):

- $\mathrm{e}_{X\mathrm{p}}$ and $\mathrm{e}_{X\mathrm{n}}$ represent the capacity of the configuration to deal with a positive and negative surge force respectively.
- $\mathrm{e}_{Y\mathrm{f}}$ and $\mathrm{e}_{Y\mathrm{a}}$ represent the capacity of the fore and aft configuration of the ship to deal with transversal forces.

For the configuration shown in figure 4.8 and table 4.3, $\mathrm{e}_{X\mathrm{p}}$, $\mathrm{e}_{X\mathrm{n}}$, $\mathrm{e}_{Y\mathrm{f}}$, $\mathrm{e}_{Y\mathrm{a}}$ are 4.60, 3.44, 3.65 and 4.58 respectively. The positive surge capacity is higher than the negative capacity, which means that for a given impulse load, the positive surge motion will be smaller compared to applying the same load the negative direction.

The transversal capacity at the fore of the ship is smaller than the aft capacity, meaning that the ship will have a tendency to show a yaw

rotation with the fore ship moving more than the aft ship. The target should be, next to obtaining high values, to get similar values for $\mathrm{e}_{X\mathrm{p}}$ and $\mathrm{e}_{X\mathrm{n}}$, as well as for $\mathrm{e}_{Y\mathrm{f}}$ and $\mathrm{e}_{Y\mathrm{a}}$, which represents a balanced mooring configuration.

$$\begin{cases} \mathrm{e}_{X\mathrm{p}} = \sum_{i=1,\alpha_\mathrm{l}<90}^{n_{\mathrm{l,pos}}} \mathrm{e}_{X,\mathrm{i}} \\ \mathrm{e}_{X\mathrm{n}} = \sum_{i=1,\alpha_\mathrm{l}>90}^{n_{\mathrm{l,neg}}} \mathrm{e}_{X,\mathrm{i}} \\ \mathrm{e}_{Y\mathrm{f}} = \sum_{i=1}^{n_f} \mathrm{e}_{Y,\mathrm{i}} \\ \mathrm{e}_{Y\mathrm{a}} = \sum_{i=1}^{n_a} \mathrm{e}_{Y,\mathrm{i}} \end{cases} \tag{4.25}$$

4.3.4.3 Mooring arrangement optimisation

The real power of the efficiency parameters becomes visible when a given configuration is optimised to deal with a specific external force. [Van+19] presents an optimisation case for the mooring plan shown in figure 4.8, in the application of a parallel passage at a container berth in a narrow, rectangular section. The configuration MC4,MC5,MC6 and MC7 from [Van+19] are discussed here, the numbering is kept consistent with the paper numbering. All configuration discussed in the paper are given in appendix D.

- **MC0, L2+NL1** illustrates the benefits of using stiff HMPE lines (L2) in combination with elastic tails (NL1), in comparison to the use of medium elastic lines (L1).
- **MC4, L1** shows that crossing of fore and aft lines results in more efficient mooring lines (figure 4.10 (a))
- **MC5, L1** moves the winches from the (higher) forecastle deck to a lower mooring deck on the same level as the aft mooring deck (figure 4.10 (b))
- **MC6, L1** addition of winches at funnel and accommodation position in order to add two pairs of spring lines (figure 4.10 (c)-(d))

- **MC7, L1** combination of MC4,MC5,MC6, with stiff lines + tail in order to see how much improvement is theoretically possible given the proposed optimisation steps (figure 4.10 (e)-(f))

The efficiency parameters given in table 4.4 show what benefits can be expected. In eq. 4.25 however, the elasticity of the lines was not included as a factor. As such, the effect of changing the line type cannot be studied. Therefore, the impact of using stiffer lines, as was done in **MC0, L2+NL1**, cannot be assessed.

This impact can be assessed by expanding the efficiency parameter definition from eq. 4.25, with a term expressing differences in line elasticity between two configurations. Eq. 4.26 gives such an expression, here immediately applied to the case where a line L1 (linear elongation) is compared to a line composed of a main line L2 (linear elongation) and a non-linear tail (NL1). The added term expresses the ratio between the stiffness of, in this case, the medium elasticity linear line (L1) and the combination of main line (L2) and tail (NL1). The elasticity of the line composed of main line and tail is assessed by calculating the contributions from both parts, taking into account their respective lengths. As the tail is non-linear, a linearisation is needed. This is done by selecting the line strain corresponding to the force F_{ex}, which is the expected force in the line for the application. In the case of a passing ship study, as per [Van+19], 30% MBL can be taken as F_{ex}. A tail length, l_{tail} of 11 m is a reasonable assumption.

$$\mathrm{e}' = \mathrm{e} \cdot \frac{\epsilon_{\mathrm{L1}}(F_{ex})}{\frac{\epsilon_{\mathrm{L2}}(F_{ex}) \cdot (l - l_{\mathrm{tail}}) + \epsilon_{\mathrm{NL1}}(F_{\mathrm{ex}}) \cdot l_{\mathrm{tail}}}{l}} \tag{4.26}$$

Table 4.4: *Efficiency parameters $ULCS$ for different mooring configurations.*

Config	Action	line type	$\mathrm{e}_{\mathrm{X}p}$	$\mathrm{e}_{\mathrm{X}n}$	$\mathrm{e}'_{\mathrm{X}p}$	$\mathrm{e}'_{\mathrm{X}n}$
MC0	Ref config	L1	4.60	3.44	4.60	3.44
MC0	Stiff lines	L2 +NL1	4.60	3.44	10.92	8.16
MC4	Cross lines	L1	4.70	4.25	4.70	4.25
MC5	Lower deck	L1	5.64	4.6	5.64	4.6
MC6	added springs	L1	6.50	5.52	6.50	5.52
MC7	MC2+MC5+MC6	L2 +NL1	7.68	6.84	18.66	16.62

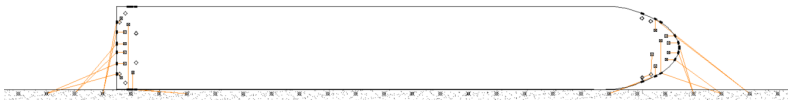

(a) $ULCS$, MC4

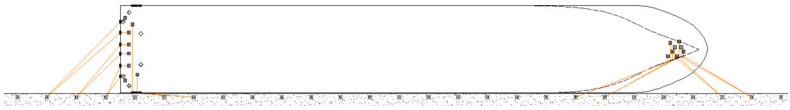

(b) $ULCS$, MC5

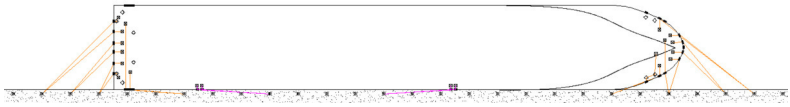

(c) $ULCS$, MC6, top view

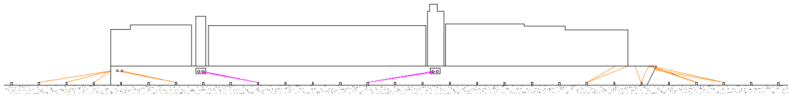

(d) $ULCS$, MC6, side view

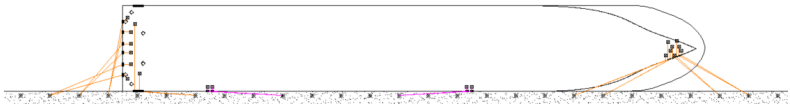

(e) $ULCS$, MC7, top view

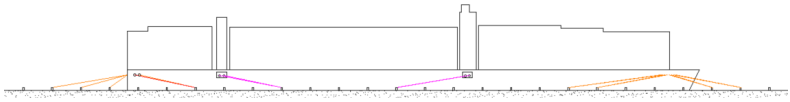

(f) $ULCS$, MC7, side view

Figure 4.10: *Mooring arrangements $ULCS$, orange lines = 16 mooring lines as present on the $ULCS$ study example, purple = addition of two sets of springs.*

In [Van+19], *Vlugmoor* simulations of a passing ship effect between a passing and moored $ULCS$ were presented and used to evaluate the performance of the efficiency parameters as given by table 4.4. One example of such simulation result is given in figure 4.11, where the moored ship's surge motion time series for MC0 and MC6 are given. As MC0 is the reference situation, the motion peaks (1.40 m and -1.28 m) are used to normalise the results for the other mooring configurations. For MC6, the peak motion ratios are then 0.66 ($\frac{0.93}{1.40}$) and 0.68 ($\frac{-0.87}{-1.28}$) for the positive and negative peak respectively. The ratio of the corresponding efficiency parameters (table 4.4) is 0.82 ($\frac{4.60}{5.64}$) and 0.74 ($\frac{3.44}{4.60}$).

Figure 4.12 summarizes the results for all considered mooring configurations. Efficiency parameters ($\mathrm{e_{X}}p$, $\mathrm{e_{X}}n$, $\mathrm{e'_{X}}p$, $\mathrm{e'_{X}}n$) and surge peaks are normalised with the values for MC0, as was shown for the example from figure 4.11. The efficiency parameters provide a decent estimate for all mooring arrangements. This technique proves to be very useful, as it can provide insight in the impact of the mooring configuration on the resulting (critical) surge motion.

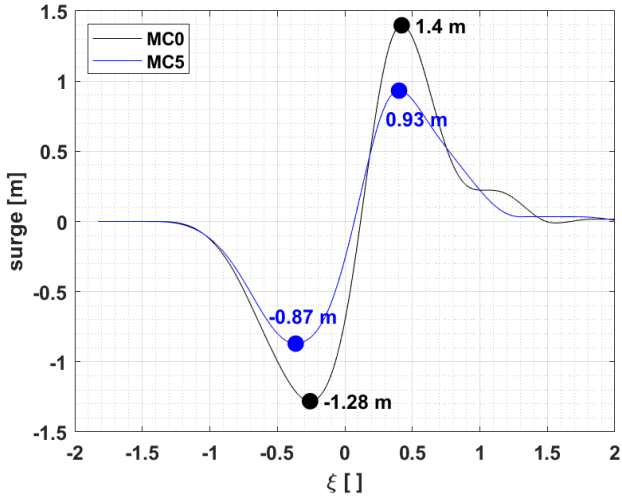

Figure 4.11: *Surge motion (x) in function of position passing ship (ξ) as result of Vlugmoor in quasi-static mode (section 4.6.1).*

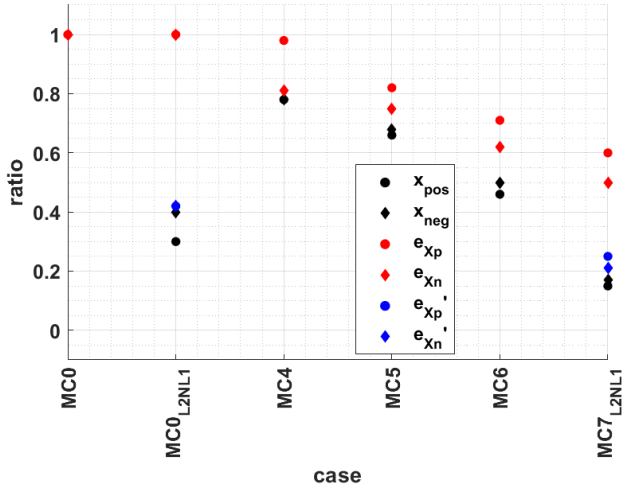

Figure 4.12: *Longitudinal ship motion calculated using Vlugmoor and efficiency parameter ratios, made non-dimensional with the values for the reference configuration (MC0).*

4.3.4.4 Method to estimate most loaded mooring line

The definition of efficiency parameters proves to be an excellent way to assess a mooring configuration, as well as compare different configurations to each other. As with all methods, it has its limitations. One example is the danger of overloading mooring lines. As explained in the introduction, line breaking can induce a cascade response leading to the breakaway of the ship. The most dangerous overloading here would be one line taking up all the load, while the other lines are loaded moderately. From the discussion up to now, one can assume that this will be a stiff short line. A high line efficiency (eq. 4.26) is also a way to express that a line will most likely be highly loaded.

Another method to assess line overload would be to look at each motion separately. When the $ULCS$ moves in positive surge direction for example, lines 1 to 6, as well as 9 and 10 will be loaded. From a ideal line loading perspective, the line loads in all lines should be equal, as expressed by eq. 4.27. Based on this definition, line 10 should break first, in the assumption that all lines have the same pre-

tension value and the same degradation. In this case, this coincides with the line having the largest $\mathrm{e}_{X\mathrm{i}}$.

$$F_{1,2,3,4,5,6,9,10} = equal \iff \frac{dl}{l_0} = \mathrm{cte} \iff \frac{\cos(\alpha_1)}{l_0} = \mathrm{cte} \quad (4.27)$$

This method can be used for example as a check when spring lines are made shorter on purpose to induce a stiffer response, to avoid them being loaded by a factor three or more higher than the other lines, which might then lead to an (unforeseen) breakaway in case a chain reaction in the lines occurs.

4.4 Ship-to-ship mooring
mass-spring-damper-mass-spring-damper

Ship-to-ship (STS) mooring covers any circumstance where two ships are connected to each other using mooring lines (and fenders). From a modelling perspective, the increase in complexity is substantial, especially as both ships may well have a forward speed during the operation. In order to exclude some of the types, an overview of STS mooring is given, indicating which types will be analysed in this thesis. A description of the components of the mathematical model covering STS is subsequently given, after which two simplified models are presented in more detail.

4.4.1 Types of ship-to-ship mooring

Figure 4.13 shows the most relevant applications of STS mooring. In some cases, STS is done at a non-zero forward speed. RAS - Replenishment At Sea - is the most extreme case, where military ships are fuelled at cruising speed. For oil tankers, lightering is often performed at low forward speed to reduce the draft of the largest tanker, for example to be able to reach a shallow berth. A mathematical model for ship lightering interaction forces is given in [Lat+12]. Similar to [OCI18], they have published guidelines specifically for STS transfer [OCI13]. Note that only one subsection of this book deals with mooring (section 6.6). For both lightering as well as RAS, a flexible hose connection is used to allow some relative motion between both ships.

Lightering can also be performed while both ships have zero forward speed. Loading bulk from large carriers to barges to reduce the draft before entering a lock or shallow berth is a common process.

In a port environment, STS mooring is commonly defined as double banking, which is the situation where two ships are moored next to each other at one berth location, as shown in figure 4.14. Double banking can be seen in the application of cargo transfer, whether it is between tankers, or when a tanker fuels another ship (called bunkering). River cruise ships are also often moored side-to-side, with passenger needing to traverse the ships to reach shore. Ships can also

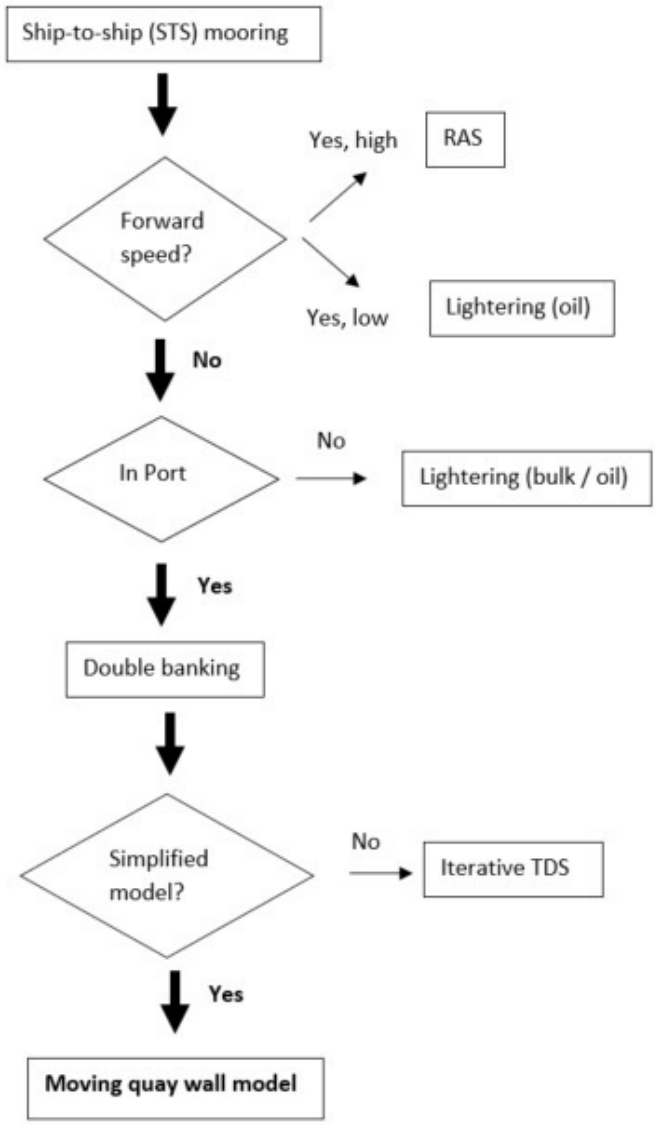

Figure 4.13: *Overview different sub-categories within ship-to-ship (STS) mooring.*

wait for a free berth in double banking. In this case, no cargo transfer will take place, nevertheless the ships should be safely moored.

Figure 4.15 gives a representation of two $T0Y$ tankers in double banking configuration. The ship moored at the quay is defined as $shipI$, the ship alongside is $shipII$. $shipII$ is deemed to not exceed the dimensions of $shipI$. $shipI$ is moored to the berth using her own mooring equipment (dark blue), on winches, as was done in single banking (figure 2.21). The ship alongside uses her equipment (light blue) to moor to $shipI$ (full lines) and in some cases also with some lines connected directly to shore (dashed lines).

When comparing the configuration of $shipII$ with the mooring configuration $shipI$ -shore, the differences are considerable. The symmetry of the latter can be easily lost, as well as the fact that short and long lines will be combined. The configuration will be limited by the position of winches, bitts and fairleads on both ships, which means that there is a large variability in double banking mooring configurations.

Having two ships which move and interact causes an increase in complexity in the mathematical representation of the problem (section 4.4.2). Section 4.4.3 presents a simplified approach which can be applied in some circumstances.

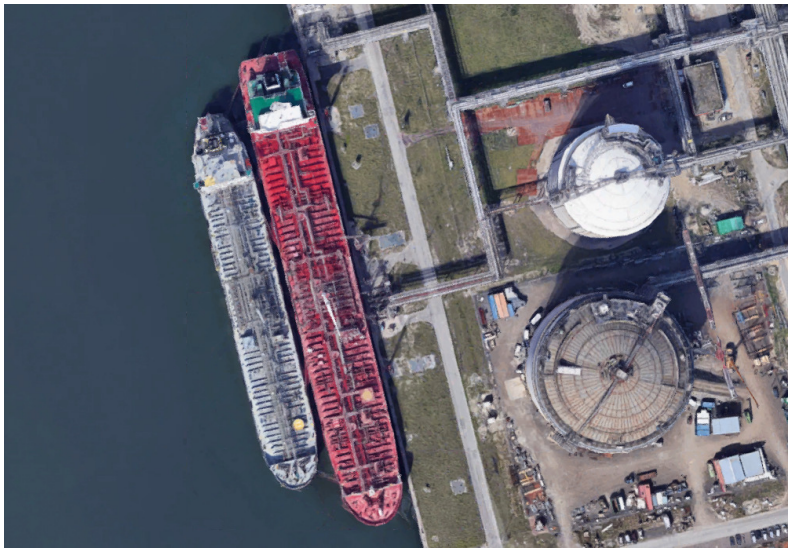

Figure 4.14: *Double banking in Antwerp port area, Google Earth.*

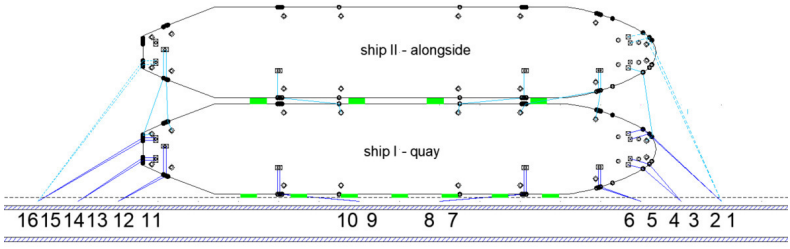

Figure 4.15: *Double banking of two $T0Y$ tankers; light blue = mooring equipment $shipII$, dark blue = mooring equipment $shipI$.*

4.4.2 Components mathematical model

The representation of the double banking system follows from the single banking model (section 4.3) and the general behaviour of a floating object (section 4.2). Both floating objects can be represented in the form of eq. 4.10. As both systems are connected, through mooring lines and fenders, interaction terms are present. A set of equations as given by eq. 4.28 is formed, with the 6DOF motion vector is represented by $\overrightarrow{x}$.

The equations for both systems are actually the same in this general expression. "$\mathrm{moor}, II \rightarrow I$" expresses the properties of the mooring system between $shipII$ and $shipI$. $\mathrm{moor,I}$ and $\mathrm{moor,II}$ represents a connection directly with the shore. For $shipII$, it is less common to connect lines directly to shore (dashed lines in figure 4.15). In this case, all "$\mathrm{moor,II}$" terms are reduced to 0.

A time domain solver with iteration can represent eq. 4.28, at the cost of large calculation times. Published research mostly focusses on the response of the water body in between the ships [HP01], or on the mooring system of the ship alongside (assuming one ship is fixed in position) [PHV07]. A publication offering validation experiments for the motion response of both ships, including their respective sets of mooring lines, has not been found. Without such validation, creating and applying such complex model cannot be justified. For projects performed thus far, a simplified approach was presented, in order to deliver results on an acceptable project timeline.

$$\begin{aligned} &m_{\mathrm{I}} \cdot \ddot{\overrightarrow{x_{\mathrm{I}}}} + (b_{\mathrm{I}} + b_{\mathrm{moor,I}}) \cdot \dot{\overrightarrow{x_{\mathrm{I}}}} + (c_{\mathrm{I}} + c_{\mathrm{moor,I}}) \cdot \overrightarrow{x_{\mathrm{I}}} \\ &\quad + b_{\mathrm{moor,II}\rightarrow\mathrm{I}} \cdot (\dot{\overrightarrow{x_{\mathrm{I}}}} - \dot{\overrightarrow{x_{\mathrm{II}}}}) + c_{\mathrm{moor,II}\rightarrow\mathrm{I}} \cdot (\overrightarrow{x_{\mathrm{I}}} - \overrightarrow{x_{\mathrm{II}}}) = \overrightarrow{F_{\mathrm{I}}} \end{aligned} \tag{4.28a}$$

$$\begin{aligned} &m_{\mathrm{II}} \cdot \ddot{\overrightarrow{x_{\mathrm{II}}}} + (b_{\mathrm{II}} + b_{\mathrm{moor,II}}) \cdot \dot{\overrightarrow{x_{\mathrm{II}}}} + (c_{\mathrm{II}} + c_{\mathrm{moor,II}}) \cdot \overrightarrow{x_{\mathrm{II}}} \\ &\quad b_{\mathrm{moor,II}\rightarrow\mathrm{I}} \cdot (\dot{\overrightarrow{x_{\mathrm{II}}}} - \dot{\overrightarrow{x_{\mathrm{I}}}}) + c_{\mathrm{moor,II}\rightarrow\mathrm{I}} \cdot (\overrightarrow{x_{\mathrm{II}}} - \overrightarrow{x_{\mathrm{I}}}) = \overrightarrow{F_{\mathrm{II}}} \end{aligned} \tag{4.28b}$$

4.4.3 Simplified model moving quay wall

Under some circumstances, the double banking mooring can be assessed using a simplified method, named here - moving quay wall. The double banking problem is split up into two separate calculations, aiming to remove the interaction terms in eq. 4.28. First,

the model is presented, after which its applicability to certain double banking configurations is discussed.

4.4.3.1 Moving quay wall model description

In this approach, two separate calculations are performed, which aim at assessing the safety of moored ship I and II respectively. The equipment of $shipI$ in double banking needs to transfer loads coming from her own mass and inertia, as well as the contribution from $shipII$. In practice this means that the captain of $shipI$ should always be consulted and asked for permission to perform double banking, as this might call for additional mooring lines between $shipI$ and the shore.

The behaviour of $shipI$ is assessed by assuming that both ships move together, as if they are welded to one another, figure 4.16. After solving the equation for $shipI$, this response $\overrightarrow{x_{\mathrm{I}}}$ is used as a boundary condition to calculate the response of $shipII$.

This system is represented by eq. 4.29, where the motion coupling is no longer present in eq. 4.29a. Eq. 4.29b can be solved after completing the simulation for $shipI$.

$$(m_{\mathrm{I}} + m_{\mathrm{II}}) \cdot \ddot{\overrightarrow{x_{\mathrm{I}}}} + (b_{\mathrm{I}} + b_{\mathrm{moor,I}}) \cdot \dot{\overrightarrow{x_{\mathrm{I}}}} + (c_{\mathrm{I}} + c_{\mathrm{moor,I}}) \cdot \overrightarrow{x_{\mathrm{I}}} = \overrightarrow{F_{\mathrm{I}}} + \overrightarrow{F_{\mathrm{II}}} \tag{4.29a}$$

$$\begin{aligned} m_{\mathrm{II}} \cdot \ddot{\overrightarrow{x_{\mathrm{II}}}} + (b_{\mathrm{II}} + b_{\mathrm{moor,II}}) \cdot \dot{\overrightarrow{x_{\mathrm{II}}}} + (c_{\mathrm{II}} + c_{\mathrm{moor,II}}) \cdot \overrightarrow{x_{\mathrm{II}}} \\ b_{\mathrm{moor,II}\to\mathrm{I}} \cdot (\dot{\overrightarrow{x_{\mathrm{II}}}} - \dot{\overrightarrow{x_{\mathrm{I}}}}) + c_{\mathrm{moor,II}\to\mathrm{I}} \cdot (\overrightarrow{x_{\mathrm{II}}} - \overrightarrow{x_{\mathrm{I}}}) = \overrightarrow{F_{\mathrm{II}}} \end{aligned} \tag{4.29b}$$

4.4.3.2 Validity moving quay wall model

The moving quay model as presented above offers a great tool for engineering purposes, however, at a cost of greatly simplifying the interaction between both ships. In case $shipII$ is much smaller than $shipI$, this assumption can be be justified easily. As $shipII$ is limited in size, her mooring equipment will be restricted, both in number of lines as well as MBL. The maximum possible interaction forces will then be low, meaning that neglecting this effect will always have limited impact. A clear example here is the double banking of an inland

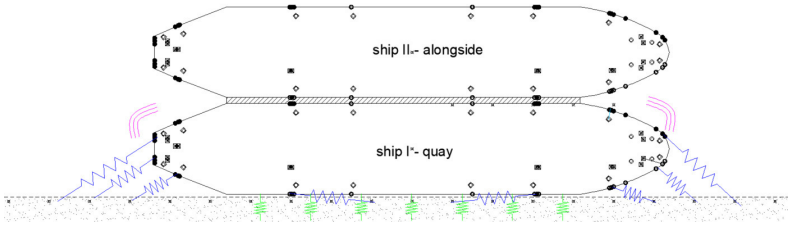

(a) Double banking model *ship I*

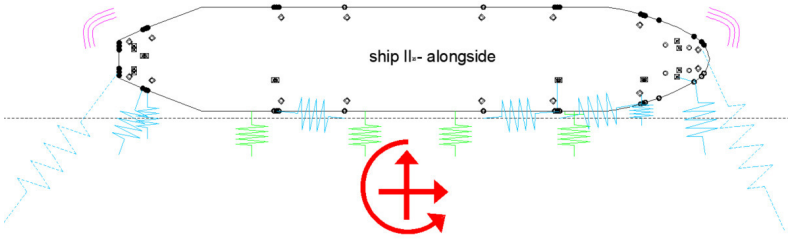

(b) Double banking model *ship II*

Figure 4.16: *Moving quay wall model as simplified model of double banking.*

tanker when supplying fuel to a seagoing ship, called bunkering (figure 4.17 (a)). The bunker tanker can take the fuel directly from a moored tanker, which is represented in figure 4.17 (b).

In the example of figure 4.15, interaction forces could be significant. In case the ships move in phase, e.g. when $shipI$ moves in positive x-direction, so does $shipII$, then this in-phase response is covered by eq. 4.29. When the ships move out of phase however, the resulting response can be higher than predicted by eq. 4.29. If the simplified model is used for these cases, a comparison of the motion vectors $\overrightarrow{x_{\mathrm{I}}}$ and $\overrightarrow{x_{\mathrm{II}}}$ is advised to check how the ships tend to move relative to each other.

(a) Bunkering of container ship, courtesy of Marc Vantorre.

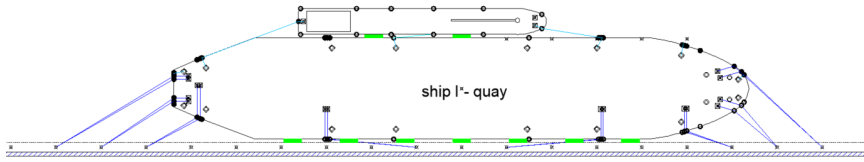

(b) Schematic representation bunker ship alongside $T0Y$.

Figure 4.17: *Bunkering as sub-category of double banking*

4.5 Frequency domain analysis

In engineering sciences, a subdivision is made into frequency and time domain simulations. In the time domain, the solution of the problem progresses over time; a frequency domain transforms variables based on (linear) transfer functions. As the moored ship system is highly non-linear, it needs to be solved in the time domain. Concepts such as eigenperiod and spectral representation of loads can however be applied prior to a TDS, to deliver insight into the characteristics of the system.

4.5.1 Theory : representation of a linear system

Frequency domain computations are generally much faster than their time domain counterpart. The possibility of simulating thousands of cases creates a data matrix which can be used for long term statistical interpretation and/or prediction.

In a frequency domain analysis, the response of a system to an external loading at a certain frequency, say ω_{F}, is calculated, through the definition of a transfer function. In the example of a ship moving in waves, the sea state will consist of multiple wave components, with their respective frequency (ω_{w}) and direction (θ_{w}). This sea state can be represented as its energy spectrum $S_\zeta(\omega, \theta_{\mathrm{w}})$. If the response of the ship to each component is known, a response spectrum can be calculated, $S_R(\omega, \theta_{\mathrm{w}})$ (eq. 4.30a). Using a similar definition as is done for wave analysis, a significant response can be calculated (R_{S}, eq. 4.30b - 4.30c). An example of such an application is the calculation module *RIVSEA*, developed by the Maritime Technology Division, to assess the risk of inland ships performing a limited sea journey [Don+18].

$$S_R(\omega, \theta_{\mathrm{w}}) = S_\zeta(\omega, \theta_{\mathrm{w}}) \cdot Y^2_{R\zeta}(\omega, \theta_{\mathrm{w}}) \tag{4.30a}$$

$$m_{0,R} = \int_0^\infty \int_0^{2\pi} S_R(\omega, \theta_{\mathrm{w}}) d\omega d\theta_{\mathrm{w}} \tag{4.30b}$$

$$R_{\mathrm{S}} = 4 \cdot \sqrt{m_{0,R}} \tag{4.30c}$$

Frequency domain models can be summarized by stating that if the amplitude of the loading doubles, the response will double as well,

according to eq. 4.30a. As was already stated previously, linearity is key when using frequency domain concepts.

4.5.2 Relevance for the non-linear mooring system

Despite not having a direct application for a mooring problem, the relationship between period of external disturbance and eigenperiods of the ship is still relevant. The moored ship system will have a tendency of responding more when the external load is close to the eigenperiod of a certain mode.

This is valid for both transient as well as cyclic (periodic) loading. The response to a passing ship event (one to two cycles, see figure 2.7) will be higher if the period of the event is close to the eigenperiods of the system. The transient nature of the load, in combination with the presence of damping in the system, means that the impact will be limited. After the passing event occurred, the external load is no longer present and the free oscillating system will, after some cycles, return to an equilibrium position.

For cyclic disturbances, where wave action is the most prominent effect, system resonance can lead to a significant, amplified, ship response if one of the eigenperiods is close to the period of the external load.

Figure 4.18 shows the energy distribution in the frequency domain for several external disturbances. Sea waves, represented by a Pierson-Moskowitz spectrum (full developed waves), are short compared to other loadings, certainly for lower wind speeds as driving force. A wind spectrum is broader and has lower frequency contributions as well, represented here by a Von Karman spectrum. For long waves and swell waves, a frequency range is indicated. The periods of X,Y and N coinciding with the passage from figure 2.7 are added to the figure, showing that the period of a ship passage is in fact similar to the effect of a general long wave system.

Figure 4.19 again plots the external disturbances, limited to the wave excitations in this case, accompanied by the eigenperiods of the moored $T0Y$ (table 4.2). The vertical modes (heave, roll and pitch) are mainly excited by shorter period disturbances (sea waves, swell).

The surge, sway and yaw mode are eigenperiods are longer, situated in the region of swell and long waves, which is why harbour resonance for example can be so problematic, even for small exciting wave amplitudes.

An analysis as presented by figures 4.18 and 4.19 can be used as a sensitivity check for the mooring configuration. Furthermore, possible mitigating measures could be proposed based on this assessment. For the modes where the mooring system is of little effect, heave, pitch and roll, the external disturbances must be targeted. A breakwater for example could limit swell energy, or change the period of the wave system, to avoid a large roll response of the system.

For the other modes, changes can be made to the mooring arrangement (line position). For dedicated berths, investigating the effect of pretension and/or mooring line type (tail type) could be interesting. Stiffer response (more lines, stiffer lines, more pretension) will cause the vertical lines to move to the right on figure 4.19, the opposite holds for more elastic lines. [MMD06] did measurements of ship response to swell and long waves, which were used for validation of their numerical mooring tool. Based on this information, they modelled different lines and pretension settings to investigate how this would influence the response.

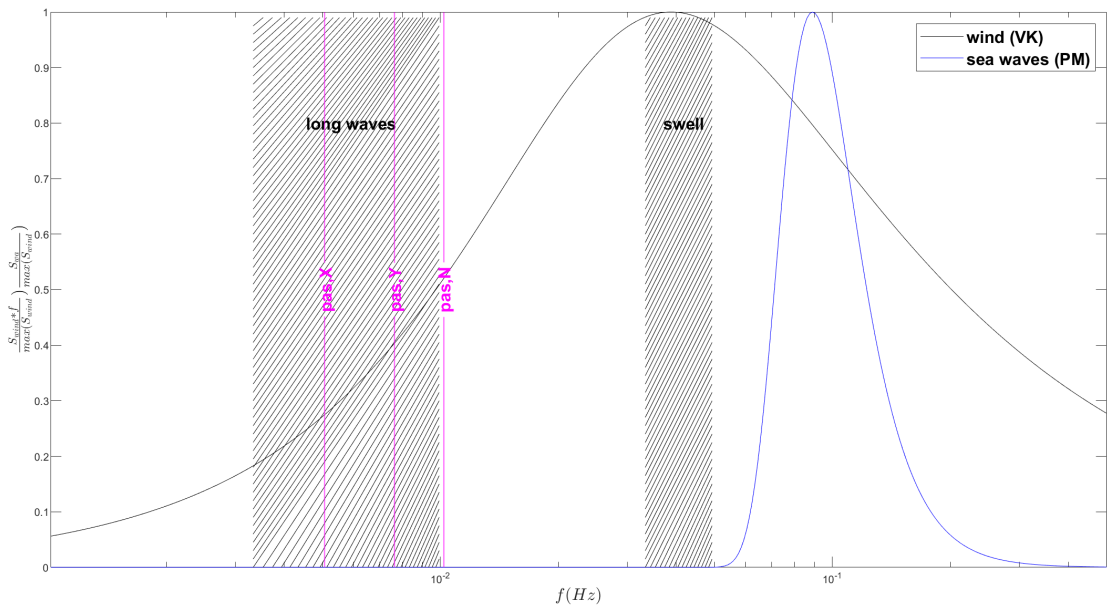

Figure 4.18: *Frequency external disturbances for moored T0Y; passing ship force periods 'pas,X pas,Y pas, N' based on figure 2.7 , sea wave spectrum Pierson-Moskowitz (15 m/s wind, 10 m height), wind Von Karman wind spectrum (40 knot wind and roughness 0.006 m). Logarithmic scale x-axis (frequency, Hz).*

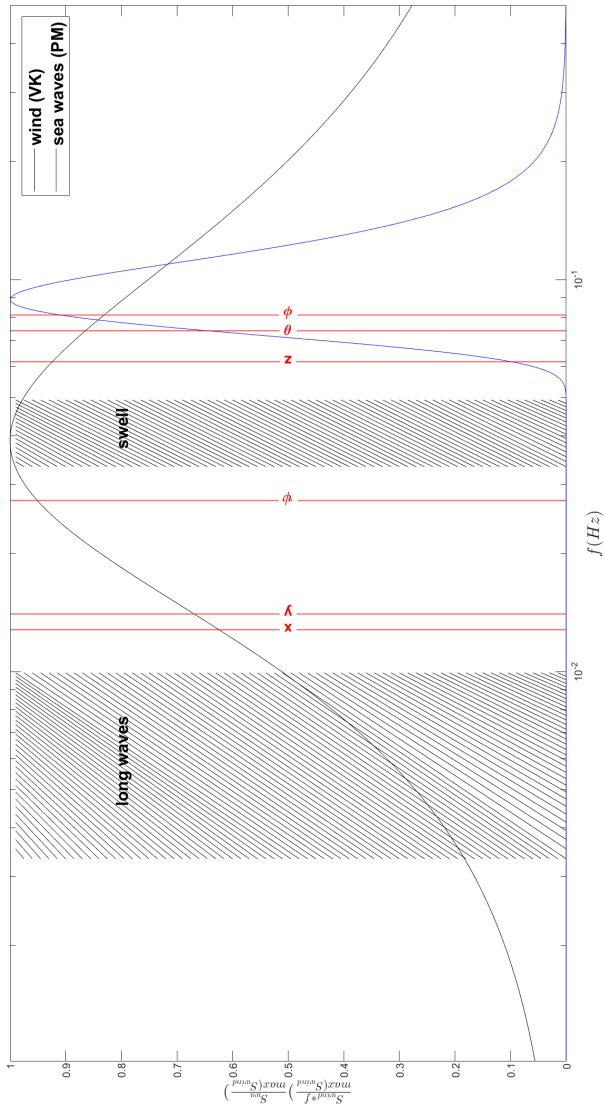

Figure 4.19: *Comparison eigenfrequencies moored T0Y (appendix F, figure F.2) with period external disturbances sea wave spectrum Pierson-Moskowitz (15 m/s wind, 10 m height), wind Von Karman wind spectrum (40 knot wind and roughness 0.006 m). Logarithmic scale x-axis (frequency, Hz).*

4.6 Time domain analysis

A time domain analysis, where equations are solved for each time step, is a method which is suitable for incorporating the response of non-linear systems. This however comes at the cost of a time demanding simulation. Solving eq. 4.10 also still presents a challenge, with simplifications being required to come to solvable equations, with acceptable calculation times.

In this section, two calculation approaches are presented, which are both included in the *Vlugmoor* tool. The first method is denoted as a *quasi-static model*, where each calculation step is seen as a disturbance of an equilibrium situation. The second method makes use of Impulse Response Functions (IRF) to take into account the motion history of the floating object, denoted here as *dynamic model*. The purpose of these sections is not to elaborate on each line of the *Vlugmoor* code, yet it should explain to the reader how the two algorithms are defined. After this discussion, the method used for moving forward in time is presented.

Both methods present a model which solves and couples equations in 4DOF (surge, sway, yaw, roll). The vertical modes (heave, pitch) are treated separately, following the reasoning from section 4.3.1, where it was shown that the contribution of the mooring lines and fenders to the total system is very limited. The vertical motions will however influence the mooring line length and thus the mooring response.

4.6.1 Quasi-static model

The quasi-static time domain model provides a simplified solution to the Newton equation as denoted in eq. 4.12. For the purpose of identifying the different terms in the equation, it is rewritten as eq. 4.31. F_{iner} are the inertia terms, or the forces present due to acceleration of the body (excluding the water surrounding it). F_{hydro} is the hydrodynamic response of the body, due to the disturbance of the water. $\sum F_{\mathrm{ext}}$ and $\sum F_{\mathrm{moor}}$ are the contributions due to external disturbances (waves, wind, passing ship,...) and the response of mooring equipment (lines, fenders,...) respectively. The appearance of these last two contributions has been discussed in chapter 2 in

general. Mooring lines (chapter 3), wind (chapter 5) and passing ship effects (chapter 6) are discussed in detail in separate chapters.

$$\begin{aligned}&[F] = [m] \cdot [\ddot{x}] + [b + b_{\text{moor}}] \cdot [\dot{x}] + [c + c_{\text{moor}}] \cdot [x] \\ &\quad \Rightarrow [F_{\text{iner}}] = [F_{\text{hydro}}] + \sum [F_{\text{ext}}] + [b_{\text{moor}}] \cdot [\dot{x}] + [c_{\text{moor}}] \cdot [x]\end{aligned} \tag{4.31}$$

4.6.1.1 Vertical plane

Heave and pitch response are calculated based on time series of external forces (Z and M respectively, eq. 4.10). The hydrostatic response is then expressed by eq. 4.32 and 4.33. The effect of these motions is restricted to a change in vertical position of ship (and thus fairleads). This however changes line angles as well as line tensions, which can potentially have a significant impact on the response of the moored ships in the other modes. This representation is similar to the one used in the moving quay wall model (section 4.4.3.1) for STS mooring.

$$z(m) = \frac{Z}{\rho g A_{\text{w}}} \tag{4.32}$$

$$\theta(^\circ) = \frac{M}{\Delta \overline{GM_{\text{L}}}} \tag{4.33}$$

In the derivation of the roll motion equation,the assumption is made that no coupling with other motion modes is present, which is similar to the surge equation. As the definition states, it is a function of the motion, in this case ϕ. The c term in this case is $\Delta \overline{GM_{\text{T}}}$, as was already stated in table 4.1.

4.6.1.2 Horizontal plane

Inertia terms Inertia forces are caused by a motion (acceleration) relative to a fixed reference (=inertial axis system) (figure 4.20). The axis system which is used in *Vlugmoor* was already defined in section 4.3. As the ship will move during the simulation, a more elaborate definition of the axis system is necessary. The inertial coordinate system is the starting position of the moored ship, defined as $O_{0x0y0z0}$. The ship fixed axis system is denoted as O_{xyz}. Both systems follow the definition of section 4.3 : The x-axis is defined

positive to the bow, the y-axis positive to port side, the z-axis positive upwards. For the horizontal motion modes, the inertia terms are expressed in eq. 4.34 in the earth-fixed (inertial) system. The relationship between earth and ship system is formed through the rotational matrix R (eq. 4.35).

Newton's laws are only valid for the centre of gravity of the body however, whereas the origin is located at midships (O_{xyz}). The detail in figure 4.20 shows how a rotation around the centre of gravity G causes a sway velocity in the ship axis system, equal to $-x_G \cdot r$. Based on the above considerations, the inertial forces are expressed by eq. 4.36 in the axis system O_{xyz}.

$$\begin{cases} X_0 = m \cdot \dot{u_0} \\ Y_0 = m \cdot \dot{v_0} \\ N_0 = I_{zz,\mathrm{G}} \cdot \dot{r} \end{cases} \tag{4.34}$$

$$R = \begin{bmatrix} \cos\psi & \sin\psi \\ -\sin\psi & \cos\psi \end{bmatrix} \tag{4.35}$$

$$\begin{cases} X_{\mathrm{iner}} = m \cdot (\dot{u} - v \cdot r - x_G \cdot r^2) \\ Y_{\mathrm{iner}} = m \cdot (\dot{v} + u \cdot r + x_G \cdot \dot{r}) \\ N_{\mathrm{iner}} = I_{zz} \cdot \dot{r} + m \cdot x_G \cdot (\dot{v} + u \cdot r) \end{cases} \tag{4.36}$$

Hydrodynamic terms As explained in section 4.2, a floating body will cause a response of the surrounding water body, in the form of added mass and damping, as a function of the velocity and acceleration of the floating body. For sway, the general response is discussed, which can then be applied in a similar way for surge and yaw. This response is a function of the form of eq. 4.37. Note that this is already a simplification of the 6DOF case, as only motions in the horizontal plane are considered. The function can be expressed as a Taylor expansion around a random condition (subscript 1). Eq. 4.38 represents a first order Taylor approximation, which already implies that all higher order components of the expansion are neglected. This equation however still contains many terms, including a expression of the function value at step 1.

This is where the quasi-static condition comes into play, where it is assumed that at condition 1, an equilibrium situation is reached,

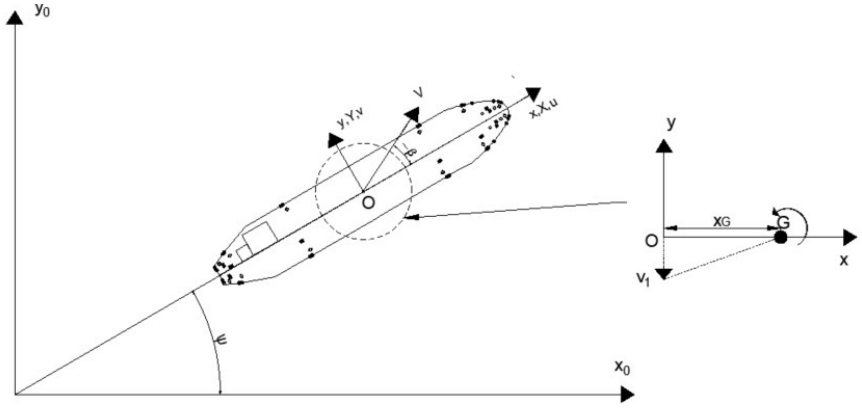

Figure 4.20: *Ship (O_{xyz}) and earth inertial ($O_{0x0y0z0}$) system as defined in Vlugmoor.*

where $u_1 = v_1 = r_1 = \dot{u}_1 = \dot{v}_1 = \dot{r} = 0$. Furthermore, the hull shape is assumed to be symmetric around the x-axis, eliminating several cross terms $\frac{\partial X}{\partial v} = \frac{\partial X}{\partial \dot{v}} = \frac{\partial X}{\partial r} = \frac{\partial X}{\partial \dot{r}} = \frac{\partial Y}{\partial u} = \frac{\partial Y}{\partial \dot{u}} = \frac{\partial N}{\partial u} = \frac{\partial N}{\partial \dot{u}} = 0$.

This leads to the set of equations given in eq. 4.39. In order to be consistent with the definitions from eq. 4.10, these equations are rewritten as eq. 4.40.

$$Y_{\text{hydro}} = f(u, \dot{u}, v, \dot{v}, r, \dot{r}) \tag{4.37}$$

$$\begin{aligned} Y_{\text{hydro}} = f(u_1, \dot{u}_1, v_1, \dot{v}_1, r_1, \dot{r}_1) \\ + (u - u_1) \cdot \frac{\partial Y}{\partial u} + (\dot{u} - \dot{u}_1) \cdot \frac{\partial Y}{\partial \dot{u}} \\ + (v - v_1) \cdot \frac{\partial Y}{\partial v} + (\dot{v} - \dot{v}_1) \cdot \frac{\partial Y}{\partial \dot{v}} \\ + (r - r_1) \cdot \frac{\partial Y}{\partial r} + (\dot{r} - \dot{r}_1) \cdot \frac{\partial Y}{\partial \dot{r}} \end{aligned} \tag{4.38}$$

$$\begin{cases} X_{\text{hydro}} = \dfrac{\partial X}{\partial u} \cdot u + \dfrac{\partial X}{\partial \dot{u}} \cdot \dot{u} \\ Y_{\text{hydro}} = \dfrac{\partial Y}{\partial v} \cdot v + \dfrac{\partial Y}{\partial \dot{v}} \cdot \dot{v} + \dfrac{\partial Y}{\partial r} \cdot r + \dfrac{\partial Y}{\partial \dot{r}} \cdot \dot{r} \\ N_{\text{hydro}} = \dfrac{\partial N}{\partial r} \cdot r + \dfrac{\partial N}{\partial \dot{r}} \cdot \dot{r} + \dfrac{\partial N}{\partial v} \cdot v + \dfrac{\partial N}{\partial \dot{v}} \cdot \dot{v} \end{cases} \tag{4.39}$$

$$\begin{cases} X_{\text{hydro}} = -b_{11} \cdot u - a_{11} \cdot \dot{u} \\ Y_{\text{hydro}} = -b_{22} \cdot v - a_{22} \cdot \dot{v} - b_{26} \cdot r - a_{26} \cdot \dot{r} \\ N_{\text{hydro}} = -b_{66} \cdot r - a_{66} \cdot \dot{r} - b_{62} \cdot v - a_{62} \cdot \dot{v} \end{cases} \tag{4.40}$$

4.6.1.3 Representation mooring line and fender forces

The mooring line and fender behaviour has already been elaborated on in chapter 2. Eq. 2.4 and eq. 2.6 give the general expressions to calculate mooring line and fender forces, to be applied for each line 'i' and fender 'j'.

In these equations, no damping terms are present, as was addressed in chapter 3. For time domain modelling of cyclic loading (wind, waves) this contribution might become significant over a large number of cycles.

The vectorial line and fender forces need to be decomposed into their contribution to the different DOF, as well as summed over the total number of lines (n) and fenders (m). The resulting restoring terms to be included in the motion equations are given by eq. 4.41 and eq. 4.42. For the fenders, a friction component is added to the equation, which will work against the local velocity direction (eq. 4.43), expressed by the sign function. In eq. 4.42, $\pi/2$ and $-\pi/2$ is included for starboard and portside mooring respectively to obtain the correct sign for X_{f} and Y_{f}.

$$\begin{cases} X_{\text{l}} = \sum_{\text{i}=1}^{\text{n}_\text{l}} X_{\text{l,i}} = -\sum_{\text{i}=1}^{\text{n}_\text{l}} F_{\text{l,i}} \cdot \cos(\psi - \alpha_{\text{l,i}}) \cdot \cos(\beta_{\text{l,i}}) \\ Y_{\text{l}} = \sum_{\text{i}=1}^{\text{n}_\text{l}} Y_{\text{l,i}} = \sum_{\text{i}=1}^{\text{n}_\text{l}} F_{\text{l,i}} \cdot \sin(\psi - \alpha_{\text{l,i}}) \cdot \cos(\beta_{\text{l,i}}) \\ N_{\text{l}} = \sum_{\text{i}=1}^{\text{n}_\text{l}} N_{\text{l,i}} = \sum_{\text{i}=1}^{\text{n}_\text{l}} Y_{\text{l,i}} \cdot x_{\text{s,i}} \\ K_{\text{l}} = \sum_{\text{i}=1}^{\text{n}_\text{l}} K_{\text{l,i}} = \sum_{\text{i}=1}^{\text{n}_\text{l}} Y_{\text{l,i}} \cdot z_{\text{s,i}} \end{cases} \tag{4.41}$$

$$\begin{cases} X_{\mathrm{f}} = \sum_{\mathrm{j}=1}^{\mathrm{m_f}} X_{\mathrm{f,j}} \\ \quad = \sum_{\mathrm{j}=1}^{\mathrm{m_f}} \left(F_{\mathrm{f,j}} \cdot \cos(\pm\frac{\pi}{2} - \psi) - \mu_{\mathrm{f}} \cdot |F_{\mathrm{f,j}} \cdot \sin(\pm\frac{\pi}{2} - \psi)| \cdot \mathrm{sng}(u_{\mathrm{f}}) \right) \\ Y_{\mathrm{f}} = \sum_{\mathrm{j}=1}^{\mathrm{m_f}} Y_{\mathrm{f,j}} \\ \quad = \sum_{\mathrm{j}=1}^{\mathrm{m_f}} \left(F_{\mathrm{f,j}} \cdot \sin(\pm\frac{\pi}{2} - \psi) - \mu_{\mathrm{f}} \cdot |F_{\mathrm{f,j}} \cdot \cos(\pm\frac{\pi}{2} - \psi)| \cdot \mathrm{sng}(v_{\mathrm{f}}) \right) \\ N_{\mathrm{f}} = \sum_{\mathrm{j}=1}^{\mathrm{m_f}} N_{\mathrm{f,j}} = \sum_{\mathrm{j}=1}^{\mathrm{m_f}} (Y_{\mathrm{f,j}} \cdot x_{\mathrm{f,j}} - X_{\mathrm{f,j}} \cdot y_{\mathrm{f,j}}) \\ K_{\mathrm{f}} = \sum_{\mathrm{j}=1}^{\mathrm{m_f}} K_{\mathrm{f,j}} = \sum_{\mathrm{j}=1}^{\mathrm{m_f}} Y_{\mathrm{f,j}} \cdot z_{\mathrm{f,j}} \end{cases} \tag{4.42}$$

$$u_{\mathrm{f}} = u - r \cdot y_f \tag{4.43a}$$

$$v_{\mathrm{f}} = v + r \cdot x_f \tag{4.43b}$$

4.6.1.4 Summary quasi-static model

The discussion for the 6 different motion modes can be summarized in one set of equations which need to be repeatably solved for each time step (section 4.6.3). They are represented in eq. 4.44 with acceleration terms on the left side and all other terms on the right, which will make sense for the time stepping algorithm. All added mass and damping terms are chosen for a given frequency (ω) or averaged over a frequency interval, yet are constant for the time domain simulation. The next section provides an expansion of this quasi-static model, by including a representation for memory effects.

$$
\begin{cases}
m\dot{u} + a_{11}\dot{u} = -b_{11}u + mvr + mx_G r^2 + \sum X_{\text{ext}} \\
\qquad\qquad - \sum_{\text{i}=1}^{\text{n}_\text{l}} F_{\text{l,i}} \cdot \cos(\psi - \alpha_{\text{l,i}}) \cdot \cos(\beta_{\text{l,i}}) \\
\quad + \sum_{\text{j}=1}^{\text{m}_\text{f}} \Big(F_{\text{f,j}} \cdot \cos(\pm\frac{\pi}{2} - \psi) - \mu_\text{f} \cdot |F_{\text{f,j}} \cdot \sin(\pm\frac{\pi}{2} - \psi)| \cdot \text{sng}(u - r \cdot y_f) \Big) \\
m\dot{v} + a_{22}\dot{v} + a_{26}\dot{r} + m\dot{r}x_G = -b_{22}v - b_{26}r - mur + \sum Y_{\text{ext}} \\
\qquad\qquad + \sum_{\text{i}=1}^{\text{n}_\text{l}} F_{\text{l,i}} \cdot \sin(\psi - \alpha_{\text{l,i}}) \cdot \cos(\beta_{\text{l,i}}) \\
\quad + \sum_{\text{j}=1}^{\text{m}_\text{f}} \Big(F_{\text{f,j}} \cdot \sin(\pm\frac{\pi}{2} - \psi) - \mu_\text{f} \cdot |F_{\text{f,j}} \cdot cos(\pm\frac{\pi}{2} - \psi)| \cdot \text{sng}(v + r \cdot x_f) \Big) \\
z = \dfrac{Z}{\rho g A_\text{w}} \\
I_{xx}\dot{p} + a_{44}\dot{p} = -b_{44}p - mg\phi\overline{GM_\text{T}} + \sum K_{\text{ext}} \\
\qquad\qquad + \sum_{\text{i}=1}^{\text{n}_\text{l}} F_{\text{l,i}} \cdot \sin(\psi - \alpha_{\text{l,i}}) \cdot \cos(\beta_{\text{l,i}}) \cdot z_{\text{s,i}} \\
\quad + \sum_{\text{j}=1}^{\text{m}_\text{f}} \Big(F_{\text{f,j}} \cdot \sin(\pm\frac{\pi}{2} - \psi) - \mu_\text{f} \cdot |F_{\text{f,j}} \cdot cos(\pm\frac{\pi}{2} - \psi)| \cdot \text{sng}(v + r \cdot x_f) \Big) \cdot z_{\text{f,j}} \\
\theta = \dfrac{M}{\Delta\overline{GM_\text{L}}} \\
I_{zz}\dot{r} + a_{66}\dot{r} + a_{62}\dot{v} + m\dot{v}x_G = -b_{66}r - b_{62}v - murx_G + \sum N_{\text{ext}} \\
\qquad\qquad + \sum_{\text{i}=1}^{\text{n}_\text{l}} F_{\text{l,i}} \cdot \sin(\psi - \alpha_{\text{l,i}}) \cdot \cos(\beta_{\text{l,i}}) \cdot x_{\text{s,i}} \\
\quad + \sum_{\text{j}=1}^{\text{m}_\text{f}} \Big(F_{\text{f,j}} \cdot \sin(\pm\frac{\pi}{2} - \psi) - \mu_\text{f} \cdot |F_{\text{f,j}} \cdot cos(\pm\frac{\pi}{2} - \psi)| \cdot \text{sng}(v + r \cdot x_f) \Big) \cdot x_{\text{f,j}} \\
\quad - \sum_{\text{j}=1}^{\text{m}_\text{f}} \Big(F_{\text{f,j}} \cdot \cos(\pm\frac{\pi}{2} - \psi) - \mu_\text{f} \cdot |F_{\text{f,j}} \cdot \sin(\pm\frac{\pi}{2} - \psi)| \cdot \text{sng}(u - r \cdot y_f) \Big) \cdot y_{\text{f,j}}
\end{cases}
\tag{4.44}
$$

4.6.2 Memory model using IRF functions

4.6.2.1 IRF concept

The usage of IRF functions to model the dynamic response of moored ships is not novel as such, as it is mentioned by several authors [Gou19], [MMD06]. Back in the 70s this technique was in fact already used by [Van79] [Rem74] to compute the dynamic response of a moored ship.

The discussion of IRF starts from the limitations of the quasi-static model. This model performs adequately when the system as well as the external disturbance are close to linear. A linear external disturbance is a sinusoidal (or near to it) load, as discussed in section 4.1. If the period of this signal is in the range of the natural period of a motion mode, the system will respond close to this period. The added mass and hydrodynamic damping, which are frequency dependent (figure 4.1), can be chosen close to the natural frequency of the system.

When eq. 4.44 is solved for a random external disturbance, the acceleration (right hand side equation) is linked to the state of the system at and only at that particular time step. This is not true in general. As explained above, a moving ship will radiate waves, causing damping effects. If this ship would suddenly stop, the generated waves are however still present. The system response is thus not only a function of the instantaneous motion state, but also of the motion history. This is commonly indicated as memory effects, which can be represented mathematically by IRF functions.

4.6.2.2 IRF model

[Cum62] has published a mathematical description of how the general motion equation can be rewritten to make it suitable for time-domain solving of non-linear systems. Without elaborating on the proof, eq. 4.45 was found, with x as a generic motion. The memory term is present in the convolution integral $\int_0^t K(t-\tau) \cdot \dot{x} d\tau$. The function $K(t-\tau)$ represents the effect of a velocity pulse at origin time $t-\tau$ at the present time t. A few years later, [Ogi64] presented a formulation of such a function, based on the damping response of

the ship in the frequency domain, expressed as eq. 4.46.

$$(m + a_\infty) \cdot \ddot{x} + \int_0^t K(t-\tau) \cdot \dot{x}(\tau) d\tau + c \cdot x = F \tag{4.45}$$

$$K(t) = \frac{2}{\pi} \cdot \int_0^\infty b(\omega) \cdot \cos(\omega t) d\omega \tag{4.46}$$

4.6.2.3 IRF implementation

When comparing eq. 4.31 and 4.45, the hydrodynamic response is expressed differently. All other terms have a similar appearance. The added mass however in the IRF model is always taken at infinite frequency. Solving the convolution integral demands large calculation times, as the $K(t)$ function contains many terms and the integral needs to be evaluated at each time step, over all previous simulation steps. Therefore, the implementation of IRF is in the current *Vlugmoor* version limited to 3DOF (surge, sway, yaw) and is not considered for the coupling terms 26 and 62 between sway and yaw. This is substantiated by the low velocities of the system, which will lead to important contributions in the cross terms.

Appearance K(t) As denoted by eq. 4.46, the form of $K(t)$ is a function of the damping representation in the frequency domain (figure 4.1). Figure 4.21 shows the $K(t)$ functions for modes 11,22 and 66, based on the b_{ij} coefficients from figure 4.1. In this particular case, $b(\omega)$ has been calculated up to a frequency of 2 $\frac{rad}{s}$ using Hydrostar. Calculations at higher frequencies gave rise to erroneous results, as the wave lengths become small and of similar length to the panels. An exponentially decreasing curve has been fitted to account for larger frequencies. The curves as shown in figure 4.21 have been generated based on damping coefficients in the interval 0 to 6 rad/s, with a frequency step of 0.02 rad/s. The $K(t)$ function then consists of 300 harmonic terms forming the function.

Calculation time The implementation of IRF functions comes at a cost of a steep increase in the computational effort needed, as the convolution integral needs to be calculated for each time step. Using a laptop (16 GB ram, 2.2 GHz i7 processor) and the *integral*

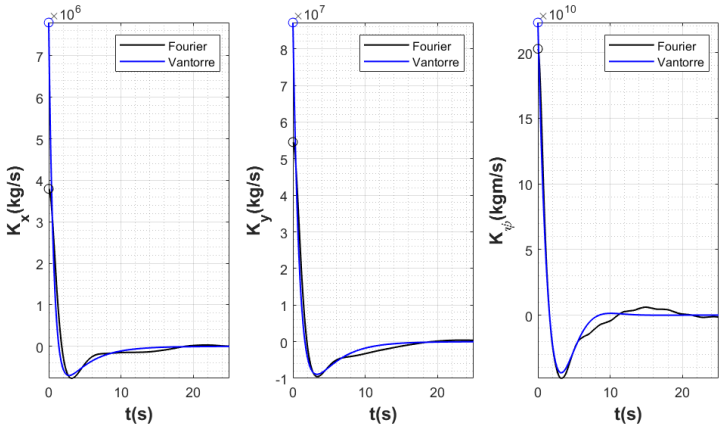

Figure 4.21: *$K(t)$ memory functions for $T0Y$ at 20% UKC, calculated based on coefficients from figure 4.1.*

function in MATLAB, the calculation time for a 1000 s real life simulation (time step ,Δt, of 0.1s) increases from one minute to hours for each IRF function which is included. Such long simulation times can be tolerated for dedicated research projects. When several ships, mooring arrangements, external loads,... need to be calculated systematically however, this IRF implementation cannot be used without multi-processor computational power. Fortunately, multiple techniques exist to limit this calculation time, which are discussed below.

4.6.2.4 IRF approximation

Several methods to reduce calculation time have been published since [Cum62] presented the IRF technique as a mathematical method to include memory effects.

Limiting memory time As mentioned before, memory effects represent the response of the ship at a time t to an impulse at time $t - \tau$. The $K(t)$ function represents this correlation. All functions shown in figure 4.21 go close to 0 within the first 20 s, meaning that these pulses will have limited contribution to the overall damping force beyond a memory time of 20 s. The general expression is then simplified as shown in eq. 4.47. Limiting this integrand in time

cuts down calculation times to around 1 hour for each IRF integral (10000 time steps).

$$\int_0^t K(t-\tau)\cdot\dot{x}(\tau)d\tau \approx \sum_{j=1}^{\frac{t_{\mathrm{mem}}}{\Delta t}} \dot{x}(t-\tau_{\mathrm{j}})\cdot\int_{\frac{\tau_{\mathrm{j}}+\tau_{\mathrm{j-1}}}{2}}^{\frac{\tau_{\mathrm{j}}+\tau_{\mathrm{j+1}}}{2}} K(\tau)d\tau \qquad (4.47)$$

State-space formulation The $K(t)$ function as expressed by eq. 4.46 contains many cosine terms, leading to such large computational effort. Expressing the $K(t)$ function using a limited amount of terms would greatly cut down calculation times. The definition of state variables (SV) allows such simplified functions to be defined, based on mathematical considerations. These functions are elegant in form, but require advanced knowledge on hydrodynamics. [Van92] provided a discussion on obtaining simplified expressions for $K(t)$. In figure 4.21, this technique is applied to represent the $K(t)$ function. There are some differences between both representations. The $K(t)$ is defined by 1 exponential and one cosine function, which is much more pleasant to work with compared to the function consisting of 300 cosine terms. Calculation times are cut significantly, from hours to minutes, making it possible to apply IRF for systematic PC-based calculations.

More research in this topic would be needed to investigate the use of SV for representing IRF functions. When a quay is present, which leads to different shapes of added mass and damping coefficients, SV representation can be used to accommodate for the distance between ship and quay, as described in [LV94]. The state-space representation according to [Van92] (figure 4.21) has been implemented in *Vlugmoor*, as an alternative to the $K(t)$ function expression by eq. 4.46.

Prony-Sheng method Similar to the state-space formulation, a "Prony-type" method can be used to calculate a $K(t)$ function with a limited number of coefficients. Gaspard de Prony was a mathematician who came up with a technique for handling big data sets, representing them by functions instead of big series of numbers. His methods are used in all kinds of disciplines, not only engineering.

[Ver+15] implemented a Prony based technique to calculate the response of a wave buoy. The function $K(t)$ is a sum of exponential functions, where the number of terms is again limited.

[SAL15] built on this work, by using a Prony based representation of $K(t)$. They state that after calculating all coefficients of the system at the first time step, the memory effect for each subsequent time step is calculated by adding one term to the result of the previous time step, assuming the time step is small enough. They prove that this works for a heaving buoy, but did not give any insight on the limitations of this method.

Prony/Sheng have not been implemented in the *Vlugmoor* code. Within the Maritime Technology Division, colleagues are working on developing and validating these methods as a basis for their software codes *Capytaine-MTD* and *MoorDyn-UGent* [Fer+21].

4.6.3 Time stepping

The motion equations, whether quasi-static or memory based, need to solved for each time step. A scheme for this time stepping is given in figure 4.22. When assessing passing ship interaction cases for seagoing ships, a time step Δt of 0.1 s is appropriate. The appearance of the motion equations is in line with this scheme. The motions $\overrightarrow{x}$ and velocities $\overrightarrow{\dot{x}}$ which are known from the calculation of the previous time step, are used to compute the right hand side of eq. 4.31, together with the external disturbances $\overrightarrow{F}_{\text{ext}}$. The mooring line and fender forces $\overrightarrow{F}_{\text{moor}}$ are also computed based on said motions and velocities. Based on this input, the accelerations on the left hand side of eq. 4.31 can be computed, which are then subsequently used to derive motions and velocities, as input for the next time step calculation. The same process is then repeated for each time step until the simulation is completed.

In order to compute the memory effects, the motion history needs to be taken into account, which is represented in figure 4.22 by the red arrows.

An important note to make here is that the motion equations are solved for the ship axis system O_{xyz}. The coordinates of the mooring

equipment on the other hand are given in the earth fixed axis system $0_0x0_y0_z0$. A transformation is needed to obtain the motions in the earth fixed axis system. On top of this, the position and rotation is taken as the average between the two last time steps, to improve the accuracy of the calculation, as was done in [LV94]. This is expressed in the ship axis system by eq. 4.48 and transformed to the earth fixed system according to eq. 4.49.

$$\begin{cases} u_2 = \left(u(t-\Delta t) + \dot{u}(t) \cdot \dfrac{\Delta t}{2}\right) \\ v_2 = \left(v(t-\Delta t) + \dot{v}(t) \cdot \dfrac{\Delta t}{2}\right) \\ p_2 = \left(p(t-\Delta t) + \dot{p}(t) \cdot \dfrac{\Delta t}{2}\right) \\ r_2 = \left(r(t-\Delta t) + \dot{r}(t) \cdot \dfrac{\Delta t}{2}\right) \end{cases} \rightarrow \begin{cases} \mathrm{d}x = \left(u_2 - \dfrac{1}{2} \cdot v_2 \cdot r_2 \Delta t\right) \Delta t \\ \mathrm{d}y = \left(v_2 + \dfrac{1}{2} \cdot u_2 \cdot r_2 \Delta t\right) \Delta t \\ \mathrm{d}\phi = p_2 \Delta t \\ \mathrm{d}\psi = r_2 \Delta t \end{cases} \tag{4.48}$$

$$\begin{cases} x_0(t) = x_0(t-\Delta t) + \mathrm{d}x \cdot cos(\mathrm{d}\psi) - \mathrm{d}y \cdot sin(d\psi) \\ y_0(t) = y_0(t-\Delta t) + \mathrm{d}x \cdot sin(\mathrm{d}\psi) + \mathrm{d}y \cdot cos(\mathrm{d}\psi) \\ \phi(t) = \phi(t-\Delta t) + \mathrm{d}\phi \\ \psi(t) = \psi(t-\Delta t) + \mathrm{d}\psi \end{cases} \tag{4.49}$$

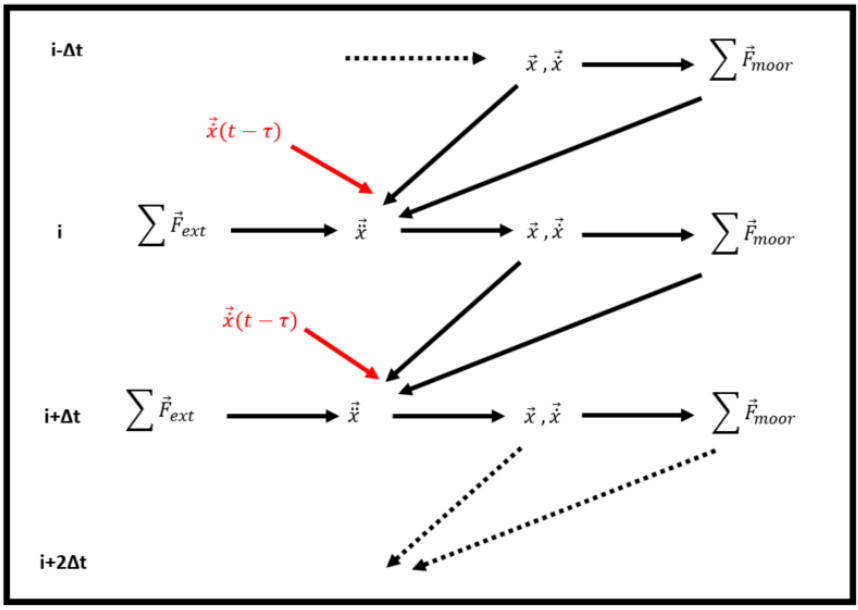

Figure 4.22: *Vlugmoor explicit time stepping scheme;*
black = quasi-static and memory, red = memory (velocity history).

References

[Cum62] W.E. Cummins. “The impulse response function and ship motions”. In: *Symposium on Ship Theory*. Hamburg, Germany, 1962.

[Don+18] L. Donatini et al. “Belgian Royal Decree for sea-going inland vessels : A review for container and bulk cargo vessels”. In: *PIANC World Congress*. Panama City, Panama, 2018.

[Fer+21] G. Fernandez et al. “Experimental validation of a state space model of a moored cuboid in waves”. In: *14th European Wave and Tidal Energy Conference*. 2021.

[Gou19] T. Gourlay. *Comparison of WAMIT and MoorMotions with Model Tests for a Tanker Moored at an Open Berth*. Tech. rep. 2019, p. 29.

[HP01] R.H.M. Huijsmans and J.A. Pinkster. “Diffraction and radiation of waves around side-by-side moored vessels”. In: *Proceedings of the 11th International Offshore And Polar Engineering Conference*. Stavanger, Norway, 2001. ISBN: 1880653516.

[Lat+12] E. Lataire et al. “Mathematical modelling of forces acting on ships during lightering operations”. In: *Ocean Engineering* 55 (2012), pp. 101–115.

[LV94] E. Laforce and M. Vantorre. “Application of Manoeuvring Simulation Techniques for Dimensioning Quaywall Fenders”. In: *28th International Navigation Congress*. Seville,Spain, 1994.

[MMD06] W. van der Molen, P. Monardez, and A.P. van Dongeren. “Numerical simulation of long-period waves and ship motions in Tomakomai Port, Japan”. In: *Coastal Engineering Journal* 48.1 (2006), pp. 59–79.

[OCI13] OCIMF. *Ship to Ship Transfer Guide for Petroleum, Chemicals and Liquefied Gases*. 2013.

[OCI18] OCIMF. *Mooring Equipment Guidelines - MEG4*. Witherbys, 2018, p. 312.

[Ogi64] T.F. Ogilvie. “Recent progress toward the understanding and prediction of ship motions”. In: *5th Symposium on Naval Hydrodynamics*. Bergen, Norway, 1964.

[PHV07] W. H. Pauw, R.H.M. Huijsmans, and A. Voogt. “Advances in the hydrodynamics of side-by-side moored vessels”. In: *Proceedings of the International Conference on Offshore Mechanics and Arctic Engineering - OMAE*. California, USA, 2007. ISBN: 0791842703. DOI: 10.1115/OMAE2007-29374.

[Rem74] G.F.M. Remery. “Mooring Forces Induced by Passing Ships”. In: *Offshore Technology Conference*. Dallas, USA, 1974.

[SAL15] W. Sheng, R. Alcorn, and A. Lewis. “A new method for radiation forces for floating platforms in waves”. In: *Ocean Engineering* 105.105 (2015), pp. 43–53.

[SNA88] SNAME. *Principles of Naval Architecture*. 1988.

[Van+19] T. Van Zwijnsvoorde et al. “A mooring arrangement optimisation study”. In: *11th International Workshop on Ship and Marine Hydrodynamics*. Hamburg, Germany, 2019.

[Van79] G. Van Oortmerssen. *The motions of a moored ship in waves*. Tech. rep. 1979.

[Van92] M. Vantorre. “Mathematical modeling of fender forces and memory effects for simulation of ship manoeuvres in confined waters”. In: *10th International Harbour Congress*. Antwerp,Belgium, 1992.

[Ver+15] T. Verbrugghe et al. “New Results on Hydrodynamic Response of Generic Point-Absorber Wave Energy Converters”. In: *Proceedings of the 11th European Wave and Tidal Energy Conference*. Nantes, France, 2015.

[VVI18] T. Van Zwijnsvoorde, M. Vantorre, and S. Ides. “Container ships moored at the port of Antwerp : Modelling response to passing vessels”. In: *PIANC World Congress*. Panama City, Panama, 2018.

5

Wind force model for moored container ships

In line with the discussion in section 2.1.1, wind forces on moored ships, as input for a mooring analysis, are calculated using eq. (5.1). F_{wi} is a wind force (surge,sway,...), C_{F} is the wind coefficient,ρ_{a} is the air density, U_{ref} is the reference wind speed and A_{ref} is the reference wind surface.

$$F_{\mathrm{wi}} = C_{\mathrm{F}} \cdot \frac{1}{2} \rho_{\mathrm{a}} \cdot U_{\mathrm{ref}}^2 \cdot A_{\mathrm{ref}} \tag{5.1}$$

Throughout this chapter, a case study example will be used to discuss how to approach wind force calculations for a moored container ship. This method is also applicable to other types of moored ships, yet container ships come with most challenges in determining wind loading. The chapter follows the thought process which is followed in a mooring project, where the client, a port authority, wants to have an operational procedure for the container terminals within the port environment. This operational procedure should allow the port to create a safe mooring situation, which might require operational measures, during the ship's stay at the berth. Within the project, time domain calculations are performed for a variety of ship sizes and the results are linked to the berth location, orientation and general wind forecast. The focus here is however solely on the calculation of the

wind force as an external disturbance.

Section 5.1 deals with appearance of the wind field at a container terminal. In section 5.2 the relation between a general wind forecast and the wind climate at the terminal is discussed. Section 5.3 forms the main part of this chapter, discussing how to calculate wind forces on a moored ship, assuming that a reference wind speed at the terminal location is known. When using the *Vlugmoor* (time domain) model as explained in chapter 4, the response to time varying wind can be modelled. Section 5.4 elaborates on how to model turbulent wind field.

For further details on (vertical) wind profiles and wind power spectra, appendix C can be consulted.

5.1 Container terminal environment

A container terminal is a major challenge when it comes to analysing wind as it consists of many obstacles which will locally affect the appearance of the wind field. Figure 5.1 illustrates an important subdivision which needs to be made. Wind coming from the water side of the terminal is characterised by a relatively uniform flow. Wind coming from the landside needs to flow across container stacks, buildings, straddle carriers and gantry cranes. The gantry cranes which are standing close to the ship will also funnel the wind in between the cranes. In many ports, container terminals are positioned in docks, meaning that actually a few hundred meters to the right of figure 5.1 (b), there might be another terminal, with moored ships and terminal equipment, affecting this wind coming into the terminal. Wind modelling in such complex environments is within the scope of the JIP Windlass (2019-2022). However, the conclusion will come too late to elaborate on in this thesis.

The difference between landside and waterside wind profiles is represented in figure 5.1 (c)-(d), where a wind profile in function of the height above the surface is visualised. The profile is a logarithmic velocity distribution (eq. 5.2). In appendix C the theory behind the logarithmic profile, as well as an alternative expression including thermal mixing effects is given. In eq. 5.2, the roughness length $z_0(m)$ is the parameter which describes the shape of the profile. A higher roughness means that the wind is decelerated more near the surface, for a given wind speed at the edge of the atmospheric boundary layer.

$$U(z) = \frac{1}{\kappa} u_* \ln \frac{z}{z_0} \tag{5.2}$$

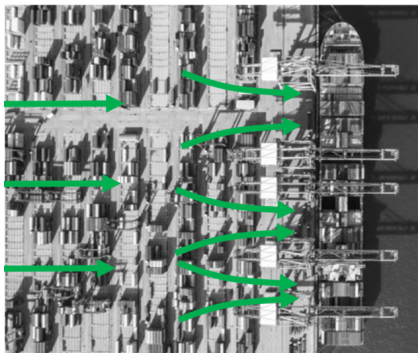

(a) Container terminal, disturbed,rough wind field, image from *Google Earth*.

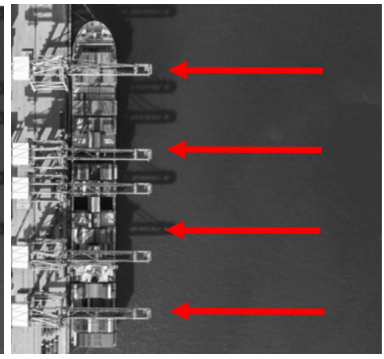

(b) Container terminal, undisturbed wind field, image from *Google Earth*.

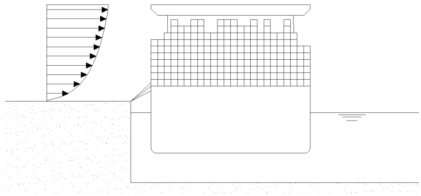

(c) High rougness wind profile

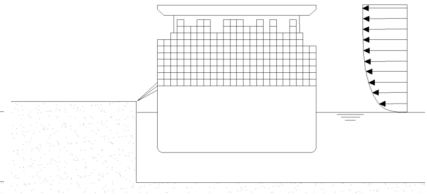

(d) Low roughness wind profile

Figure 5.1: *Top : Wind flow container terminal, difference between landside and waterside wind. Bottom : Corresponding high and low roughness wind profiles.*

5.2 Interpretation of wind forecasts

Wind flow can be simulated on many different length as well as time scales. One example where small scale models are widely used is for wind farm design and operation. When it comes to weather forecasting, often regional and/or national forecast systems will be the only source which is available to make operational decisions at port level. In order to make their forecast standardised, guidelines from the World Meteorological Organisation (WMO) are implemented. Wind speeds will be expressed at 10 m height above the surface, meaning that information regarding the vertical wind profile is not always available. Most ports will have measurement devices, anemometers, installed at various locations throughout the port to monitor the wind. These are however real-time measurements and not forecasts. They can however be used to validate the forecast model data for the port area.

If WMO guidelines are followed, the anemometer must be positioned at least 10 times the height of the closest obstruction away from said obstruction. This again makes a lot of sense from the viewpoint of standardisation. Following this definition, container terminals are certainly not suitable locations for (standardised) wind measurements. Terminals will always measure wind speeds on their gantry cranes, and compare them with thresholds for safe working of the crane.

Assume that the following information is available:

- Forecast data for the next two days in one location within the port
- Undisturbed real-time measurements (port authority)
- Disturbed real-time measurements (terminal)

On a first level, a historic comparison should be made between forecasts from some time in the past and the undisturbed measurements performed in the port. This exercise was actually performed and revealed, for the specific port which was studied, that the forecast matches the measurements throughout most of the year. Unstable weather conditions, thunderstorms, are an exception to this general observation. This however should not come as a surprise as thunderstorms are local instabilities, which cannot be covered by large scale models.

On a second level, undisturbed measurements at different locations near the container terminals were compared, revealing that the wind speed and direction was similar at these locations.

The third question is the hardest one, namely how does the disturbed wind at the terminal relate to the undisturbed wind forecast? A comparison here is hard to make, as different definitions in measured wind (average over 10 mins, maximum over 10 mins, 3s gust, 2s gust) are used, as well as different heights above the surface. A dedicated campaign using well-positioned equipment, as well as numerical tools would be needed to draw conclusions here. However, theoretical considerations could still be used to study how the undisturbed, smooth, wind and disturbed, rough, wind relate.

At the edge of the atmospheric boundary layer, the wind flows on a large scale and velocity equals the geostrophic wind (appendix C). Figure 5.2 shows two vertical wind profiles. They share the same wind speed at the edge of the boundary layer (assumed to be 400 m above the surface in this case). This geostrophic wind speed is calculated based on the forecast wind speed at 10 m height and assuming that the profile is very smooth (set to z_0 = 0.001, see section 5.3 for further discussion on z_0). Locally at the container terminal, the roughness will be higher for the same geostrophic wind speed. The local wind speed at 10 m height is then determined by going down the curve with higher roughness (set to z_0 = 1), meaning that the wind speed at the container terminal should be lower is this assumption holds. Multiple factors challenge this hypothesis, as there is local funnelling due to container cranes, dependency on wind direction,...

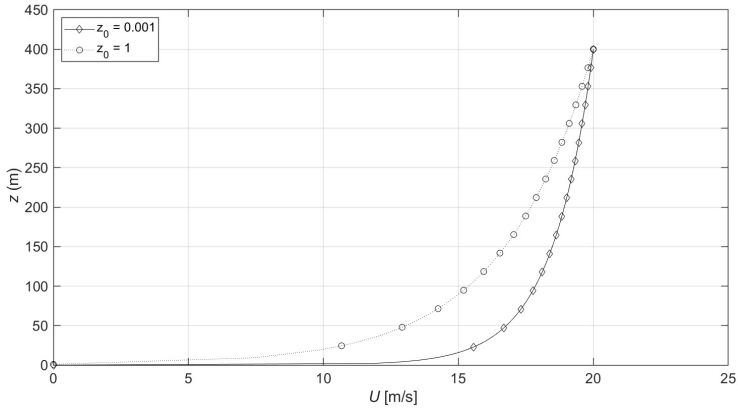

Figure 5.2: *Relation local rough wind field z_0 = 1 m and general forecasted undisturbed wind field z_0 = 0.001 m, for the same geostrophic wind condition (20 m/s, boundary layer thickness of 400 m).*

5.3 Wind force calculation

For this discussion, it is assumed that the wind speed at 10 m height above the surface has been determined locally at the terminal. The question then shifts to how eq. 5.1 should be used to calculate wind forces for a given set of wind coefficients (C_{F}). This problem actually needs to be solved on two levels, the first one regarding the theory behind wind coefficients (section 5.3.1), after which a value for the reference wind speed needs to be determined (section 5.3.2).

The $ULCS$ case study example (attachment F) is used here to illustrate the wind force calculation, which was published by the author of this thesis [Van+19]. The relevant ship parameters for the discussion in this chapter are given in table 5.1 (full parameter list in table F.3). The definitions are illustrated in figure 5.3 and figure 5.4.

Four possible wind profiles which are representative for a container terminal are used. Table 5.2 gives roughness values for a uniform profile, open sea, grass and town. Grass and town coefficients are taken from [SS96], a book on civil structure engineering, as for specific maritime terminals this coefficient is not readily available. The sea roughness will vary in function of the sea state, with a value of 0.0002 corresponding to a rough sea. Appendix C elaborates further on the calculation of roughness for sea surface wind.

Figure 5.5 shows the four profiles based on the roughness from table 5.2, denoted by a wind speed of 10 m/s at 10 m height. For an air draught of 56.1 m (table 5.1), the difference in wind speed and thus pressure over the superstructure becomes evident.

(a) A_{f} (b) A_{l}

Figure 5.3: *Definition wind surfaces $ULCS$*

Table 5.1: *Parameters $ULCS$ for wind analysis.*

Variable (unit)	value	Variable (unit)	value
H (m)	56.1	A_{f} (m²)	3146
$\bar{H}$ (m)	44.0	A_{l} (m²)	17583

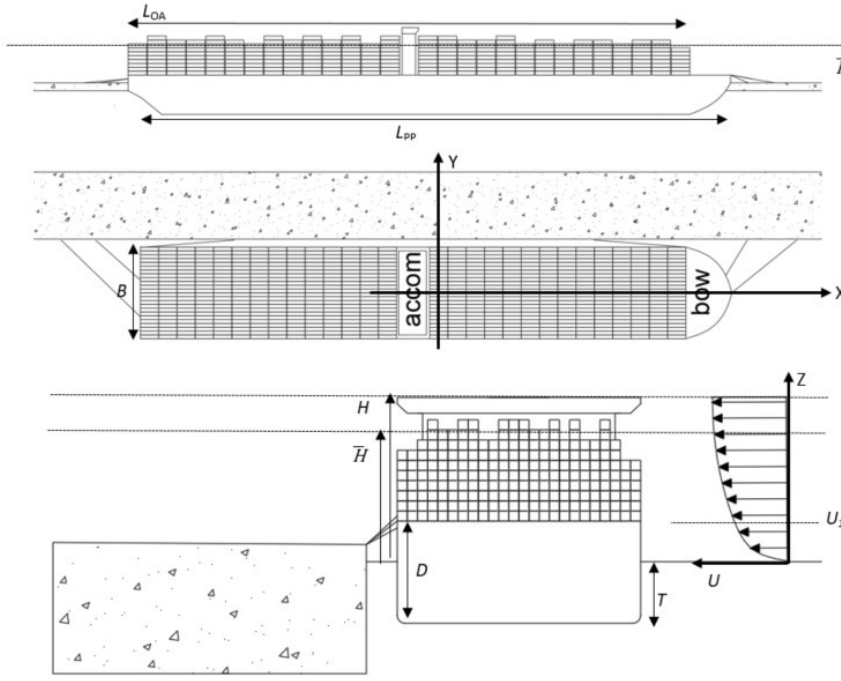

Figure 5.4: *Definition ship parameters of wind modelling.*

Table 5.2: *Terrain roughness z_0 (m) for four different terrains.*

Uniform	open sea	grass	town
0	0.0002	0.1	1.0

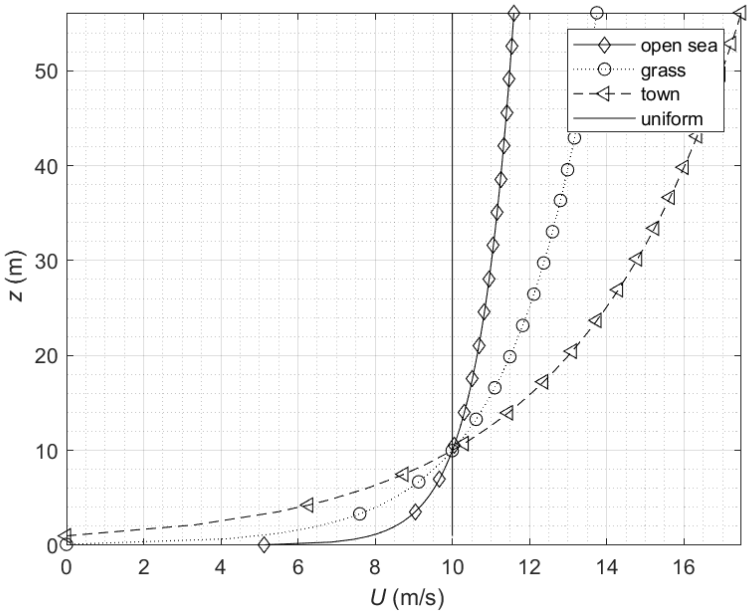

Figure 5.5: *Wind field shape $U(z)$ for four different terrain roughness (table 5.2), 10 m/s wind at 10 m height for all profiles.*

5.3.1 Wind coefficients : theory

5.3.1.1 Determination of wind coefficients

Wind coefficients as used in eq. 5.1 are in most cases defined in wind tunnel tests, although CFD is presenting itself more and more as a valuable alternative. In the wind tunnel, the total force acting on the ship form is measured. The non-dimensional wind coefficient is then calculated by reversing eq. 5.1. For the surge component, this could be represented by eq. 5.3. C_{X} thus depends on the choice of non-dimensionalisation parameters (U_{ref},A_{l}). This choice is arbitrary, as long as C_X is non-dimensional . In some cases, A_{l} is replaced by A_{f} or L_{pp}^2.

$$C_X = \frac{X_{\mathrm{wi}}}{q_{\mathrm{ref}} \cdot A_{\mathrm{l}}} \tag{5.3}$$

5.3.1.2 Literature sources wind coefficients

In literature, various sources for wind coefficients are given. More data and knowledge is certainly available globally, but is often deemed to be too confidential to share. Also, in many cases, detailed information regarding the test set-up and the procedure to come up with non-dimensional coefficients is not shared.

A good start is the research and publications of Blendermann, who is an authority in the research field of wind effects on (moored) ships. In [Ble93] an extensive list of coefficients is given, accompanied by a thorough discussion regarding the modelling and derivation of the coefficients. The disadvantage here is that it concerns ships from the 90s and earlier, which means that the largest container ships, RoRo's and cruise ships are not covered.

For oil and gas tankers, information is provided through SIGTTO [SIG07] and OCIMF [OCI18]. In the SIGTTO document, not only are the coefficients given for spherical and prismatic tanks, they also mention that the wind tunnel tests were performed in a natural boundary layer with 1/7 power law. The results were made non-dimensional using the wind speed at 10 m height (full scale).

Several authors extracted mathematical models from wind tunnel test data, using physical considerations. [FN05] provides an overview of several models, referring to [YS70], [YJK92] and [Ish72], and

compares them with his mathematical model. Fujiwara is aware of the different wind profiles used in various sources and presents all results normalised for uniform wind profiles, according to [Ble95]. The wind coefficients are composed of lift and drag components, for which coefficients were acquired using regression analysis on the available wind tunnel test data.

5.3.1.3 Wind coefficients for Ultra Large Container Ships

Container ships deserve special treatment when it comes to modelling of wind coefficients, as each deck loading configuration is unique. In an ideal world, each configuration is defined by a specific set of wind coefficients. With the increase in TEU capacity, the overall shape of the ship changes as well. As the length of the container ships is, for now, capped at 400 m, the ships have the tendency of getting wider for a given length (lower L/B ratio), as well as having a higher deck stacking (higher H/L ratio).

[And13] discloses a large series of model tests, performed at scale 1:450 on a post-panamax container ship, including a discussion on the shape of the (turbulent) wind field. Different container stacking configurations are also discussed. [JBW17] uses the published model tests in [And13] for validation of a CFD model (3D steady RANS), where good agreement is found, as long as there is sufficient detail present in the CFD model.

In general practice, if ships are tested in a wind tunnel, it is in fully loaded condition (full stacking of containers) and in a (near) ballast condition (no containers on deck). As mentioned higher, these are just two ends of the spectrum, which are in fact never reached in practice, where configurations as shown in figure 5.6 are attained.

From figure 5.6, it becomes clear that the stacking varies significantly in time for a given ship. In [FTK09] the difference between a fully- and comb-stacked ship is discussed (figure 5.7)). In comb stacking, the wind can blow 'in between' the bays (see detail in figure 5.8), meaning that wind flow becomes more complex, and there are more individual contributions which lead to the total force. These contributions are not included in the definition of A_{l},A_{f}, which is the projected wind surface, fixed for a given ship. These contributions thus need to be incorporated in the wind coefficient C_{F}.

(a) Gerd Fick, Hamburg

(b) Divemarno, Hamburg

(c) Niels Wunstorf, Hamburg

(d) Aart van Bezoojen, Rotterdam

Figure 5.6: *GMA CGM Antoine de st. Exupery, four different loading conditions, images taken from Vesselfinder, author and location included below each figure.*

If the force contribution on each bay i is given as $X_{\mathrm{wi,i}}$ and $Y_{\mathrm{wi,i}}$, then the total wind force depends on the lever arm of $X_{\mathrm{wi,i}}$ and $Y_{\mathrm{wi,i}}$, as well as the magnitude of the components. [FTK09] shows that the total longitudinal force coefficient C_X can double, with a total lateral force coefficient C_Y being quite close to the one for a fully stacked ship. Also interesting is that the yaw moment coefficient C_N changes signs for small angles of attack, which is also very interesting for modelling manoeuvring ships.

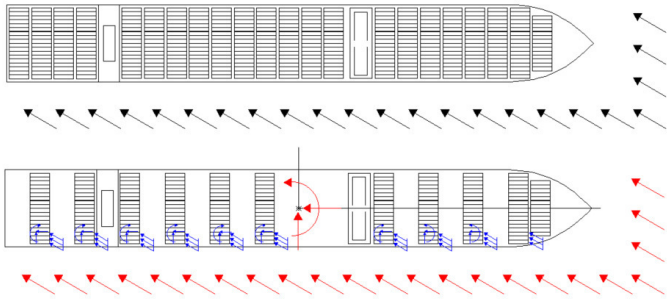

Figure 5.7: *Fully stacked (top) and comb stacked (bottom) container configuration for a* 30° *incoming wind relative to the bow.*

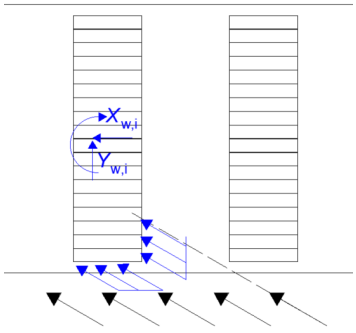

Figure 5.8: *Detail wind impact on each container row for the comb stacked configuration,* 30° *incoming wind relative to the bow.*

5.3.1.4 Wind tunnel test considerations

Scaling laws Wind tunnel tests are in all practical cases performed at scale. Given that the construction of a wind tunnel is complex and expensive, the scale factor is usually quite high, around 1:100 (and higher, 1:450 in [And13]) for large seagoing ships. This means that the full scale dynamics are scaled. As a results of this, similarity needs to be checked based on dimensional analysis. An in-depth analysis is given in [SS96], presenting 7 non-dimensional numbers, describing similarity in geometrics, inertia, viscous forces and temperature. Two of them, Froude and Reynolds numbers, are used most for practical considerations.

The Froude number represents the ratio between inertia and gravitational forces. In eq. 5.4, V $(\mathrm{m/s})$ is the velocity of the fluid, g $(\mathrm{m/s^2})$ the gravitational constant and L (m) a representative length dimension.

$$Fr = \frac{V}{\sqrt{Lg}} \tag{5.4}$$

The Reynolds number on the other hand represents the ratio between inertia and viscous forces, given as the product of velocity and length, divided by the kinematic viscosity of the fluid ν $(\mathrm{m^2/s})$ (eq. 5.5).

$$Re = \frac{VL}{\nu} \tag{5.5}$$

When scaling, all variables of Re and Fr can be scaled, commonly expressed as scale factors λ, being the ratio between the factor in model scale and prototype. Froude and Reynolds similarity are obtained when eq. 5.6 is met.

$$Fr_m = Fr_p \Leftrightarrow \frac{\lambda_V}{\sqrt{\lambda_L \lambda_g}} = 1 \tag{5.6a}$$

$$Re_m = Re_p \Leftrightarrow \frac{\lambda_V \lambda_L}{\lambda_\nu} = 1 \tag{5.6b}$$

In most conventional wind tunnels, air is used at normal gravity, meaning that λ_g and λ_ν equal 1. This means that to obtain Froude similarity, $\lambda_V = \sqrt{\lambda_L}$ and for Reynolds similarity, $\lambda_V = \frac{1}{\lambda_L}$. These two requirements cannot be met at the same time, which makes it impossible to obey both Froude and Reynolds, when using air under normal gravitational conditions.

For turbulent, viscous flows, the Reynolds similarity is deemed to be of prime importance. This means that only equation 5.6b needs to be met, requiring $\lambda_V = \frac{1}{\lambda_L}$. As discussed above, the ship's dimensions (λ_L) are often scaled down with a factor 1:100 or higher. In order to obtain Reynolds similarity, the wind speed needs to be scaled with $\frac{1}{\lambda_L}$, or 100 times higher than in the real-life application. As the capacity of wind tunnels is limited, these wind speeds are never met, which means that the Reynolds number is lower at model scale.

Flows with sufficiently high Re numbers tend to have similar characteristics (Kolmogorov's theorems, appendix C), which means that perfect similarity does not necessarily need to be achieved if it can be proven that the turbulent wind field remains nearly constant above a certain wind speed (see [SS96] for more background).

Correction for blockage Due to limited dimensions of the flow section, the ship blocks the wind flow and as such alters the flow fields. This is accounted for by implementing correction factors. Few researchers discuss this is their papers however, which means for all other sources it is not clear if this correction has been applied and if so, which formula has been used. Despite the existence of different formulas, they all contain the blockage, defined as m_{wi}, to make a distinction with the blockage of a ship is restricted water (m).

$$m_{\mathrm{wi}} = \frac{A_{\mathrm{s}}}{A_{\mathrm{t}}} \tag{5.7}$$

In this equation, A_{s} is the projected area of the ship and A_{t} the section of the wind tunnel at the position of the ship. Note that the projected wind area is the largest when the ship is positioned perpendicular to the main flow direction. Different expressions and opinions can be found in literature, where it is evident that the correction factor becomes higher for increasing blockage. [Tho03] presents a CFD simulation with and without wind tunnel walls to derive a correction factor, where it is concluded that correction factors from literature [SS96] could overestimate the correction and as a result deliver non-conservative results.

5.3.2 Wind coefficients : application

When assessing wind effects on a ship, the main interest is in the surge, sway, yaw and roll modes. Eq. 5.1 is then written as eq. 5.8. C_{X}, C_{Y}, C_{N}, C_{K} are the wind coefficients for surge, sway, yaw and roll respectively, which are a function of the incoming wind direction χ (°). A_{l} (m^2) is the lateral wind surface. q_{ref} (N/m²) is the reference wind pressure, as a function of the mass density of air ρ_{a} (kg/m³) and the relative wind velocity U_{ref} (m/s) (eq. 5.9)

$$\begin{cases} X_{\mathrm{wi}} = C_X \cdot q_{\mathrm{ref}} \cdot A_{\mathrm{l}} \\ Y_{\mathrm{wi}} = C_Y \cdot q_{\mathrm{ref}} \cdot A_{\mathrm{l}} \\ N_{\mathrm{wi}} = C_N \cdot q_{\mathrm{ref}} \cdot A_{\mathrm{l}} \cdot L_{\mathrm{PP}} \\ K_{\mathrm{wi}} = C_K \cdot q_{\mathrm{ref}} \cdot A_{\mathrm{l}} \cdot H \end{cases} \tag{5.8}$$

$$q_{\mathrm{ref}} = \frac{1}{2} \cdot \rho_{\mathrm{a}} \cdot U_{\mathrm{ref}}^2 \tag{5.9}$$

In the case that the ship shape and loading condition is satisfactorily approximated by the wind coefficients, the application at a specific terminal is illustrated in figure 5.9. If the wind field which was used to establish the wind coefficients matches the one at the project site, a correction is not needed. In the other extreme, the terrain roughness at the project location is high, whereas the wind coefficients have been established based on a uniform wind profile.

For the $ULCS$ a calculation example of a procedure which is proposed, is presented. In this example, the wind coefficients have been derived based on wind tunnel tests for a uniform wind profile. The choice of reference velocity (U_{ref}) and corresponding pressure (q_{ref}) for four different roughness profiles encountered at a project site (figure 5.5) is discussed. Two methods are presented. The first one is based on the work by Blendermann (section 5.3.2.2); A second method used CFD calculations to compare different wind profiles (section 5.3.2.3).

5.3.2.1 Wind pressure calculation

For the wind profiles shown in figure 5.5, the wind pressure can be calculated in function of the height above the surface (z) according

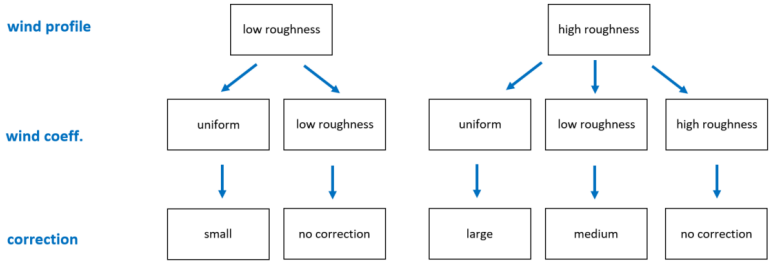

Figure 5.9: *Situational matrix wind coefficients for application to different wind fields.*

to eq. 5.10. The average pressure between z = z_0 (roughness length where by definition $U = 0$ for logarithmic profile (eq. 5.2)) and z = z_h (with z_h being an arbitrary height) is given in eq. 5.11. This is the 1D representation of the problem, disregarding changes in the width of the surface over the height.

eq. 5.12 shows the analytical solution of eq. 5.11, assuming that $U(z)$ follows a logarithmic profile. The average pressure over the mean height (see definition in figure 5.4) is obtained by replacing z_h by $\bar{H}$ in eq. 5.12. The resulting pressures are given in table 5.3, giving the wind speed and wind pressure at $\bar{H}$ and the average wind pressure over $\bar{H}$.

$$q(z) = \frac{1}{2} \cdot \rho_{\mathrm{a}} \cdot \ U(z)^2 \tag{5.10}$$

$$\overline{q(z_h)} = \frac{\int_{z_0}^{z_h} q(z)\mathrm{d}z}{z_h} \tag{5.11}$$

$$\overline{q(z_h)} = \frac{u_*^2 \cdot \rho_{\mathrm{a}}}{2 \cdot \kappa^2 \cdot z_h} \cdot \left[ln^2 \frac{z_h}{z_0} \cdot z_h - 2 \cdot z_h \cdot ln \frac{z_h}{z_0} + 2 \cdot z_h - 2 \cdot z_0 \right] \tag{5.12}$$

In table 5.3 it is observed that the wind pressure changes significantly over the height of the ship, despite the common wind speed definition of 10 m/s at 10 m height. If wind coefficients are defined for a uniform wind field, it becomes obvious from table 5.3 that the total wind pressure will be underestimated when plugging in the wind speed at 10 m as reference speed in eq. 5.8. A more appropriate definition for q_{ref} is needed.

Table 5.3: *Calculated wind speed (at $\bar{H}$) and pressures (at $\bar{H}$ and averaged over $\bar{H}$) for four wind fields, $ULCS$ case study.*

	$U_{\bar{H}}$ (m/s)	$q_{\bar{H}}$ (N/m²)	$\overline{q_{\bar{H}}}$ (N/m²)
uniform	10.00	61.3	61.3
open sea	11.37	79.2	67.4
grass	13.22	107.0	77.6
town	16.43	165.4	100.6

5.3.2.2 Definition reference pressure: Blendermann method

As was mentioned in the literature overview of wind coefficients (section 5.3.1), [Ble95] came up with a method to convert a given set of wind coefficient to be consistent with the definition of a uniform profile. This method is now used in reverse. We want to define a q_{ref} which can be used when wind coefficients defined in a uniform wind field are used in rough wind conditions.

The proposed definition of q_{ref} for the different force components is expressed in eq. 5.13. Using these definitions, the q_{ref} can be calculated for the use of the four wind profiles with wind coefficients for uniform wind profile. q_0 is defined as the wind pressure at 10 m height (10 m/s wind for all profiles). The results are shown in table 5.4. It appears that the q_{ref} should be between 1.22 and 2.70 higher compared to the one calculated based on the 10 m wind speed. This method however was designed to make small corrections in wind coefficients, so it is unfair to hold Blendermann responsible for the results shown in table 5.4. In the next section, a CFD study is used to validate eq. 5.13.

$$\begin{cases} [X] & q_{\mathrm{ref}} = q_{\bar{H}} \\ [Y, N] & q_{\mathrm{ref}} = k_q \cdot \overline{q_{\bar{H}}} + (1 - k_q) \cdot q_{\bar{H}} \\ [K] & q_{\mathrm{ref}} = q_{\bar{H}} \; or \; same \; as \; Y, N \end{cases} \tag{5.13}$$

5.3.2.3 Definition reference pressure CFD validation

A CFD analysis using FINE/Marine has been presented in [Van+19], where a simplified superstructure of the $ULCS$ has been imple-

Table 5.4: *q_{ref} calculation for four wind profiles, Blendermann method [Ble95], $ULCS$ case study.*

	Y,N,K		X,K	
	q_{ref} (N/m²)	q_{ref}/q_0 (-)	q_{ref} (N/m²)	q_{ref}/q_0 (-)
uniform	61.3	1.00	61.3	1.00
open sea	74.8	1.22	79.2	1.29
grass	95.4	1.56	107.0	1.75
town	139.6	2.28	165.4	2.70

mented (see figure 5.10). Full credit for this work goes to Wim van Hoydonck (FHR), who performed the simulations. Calculations have been performed for three wind directions (0°,90°,180°), for a uniform and a non-uniform wind profile. For the two wind profiles, the reference pressures can be calculated based on Blendermann's method, shown in tables 5.5 and 5.6.

The measured forces on the ship and the ratio of the force under uniform / non-uniform profile can be compared with the q_{ref} definition from eq. 5.13. This is shown in table 5.7. Good agreement is seen for surge. The yaw moment is overestimated by eq. 5.13. For the roll moment, there is again a good prediction, using the same factor as for Y (remember that [Ble95] left the reader with a choice with respect to the correction factor). Additional CFD calculations with more wind fields and incoming wind directions are needed however to take a more substantiated stand.

Table 5.5: *Calculated wind speed (at $\bar{H}$) and pressures (at $\bar{H}$ and averaged over $\bar{H}$) for CFD wind fields, $ULCS$ case study.*

	$U_{\bar{H}}$ (m/s)	$q_{\bar{H}}$ (N/m²)	$\overline{q_{\bar{H}}}$ (N/m²)
uniform	11.81	85.4	85.4
non-uniform	13.97	119.6	97.4

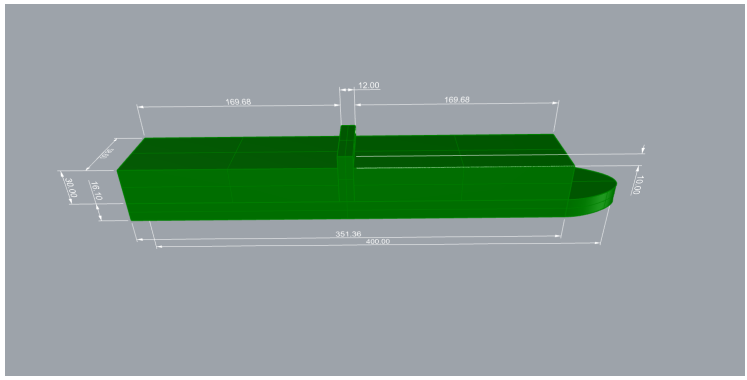

Figure 5.10: *Modelled wind surface of $ULCS$ in FINE/Marine.*

Table 5.6: *q_{ref} calculation for CFD wind profiles, Blendermann method [Ble95], $ULCS$ case study.*

	Y,N,K		X,K	
	q_{ref} (N/m²)	q_{ref}/q_0 (-)	q_{ref} (N/m²)	q_{ref}/q_0 (-)
Uniform	85.4	1.00	85.4	1.00
Non-uniform	105.1	1.23	119.6	1.40

Table 5.7: *Calculated wind forces using CFD, comparison force ratio uniform and non-uniform wind field with Blendermann's method [Ble95].*

	F CFD uniform (kN(m))	*F* CFD non-uniform (kN(m))	ratio CFD *N.A.* (-)	ratio Blendermann *N.A.* (-)
X, 0°	-214	-299	1.40	1.40
X, 180°	263	367	1.40	1.40
Y, 90°	1805	1919	1.06	1.23
k, 90°	41477	51602	1.24	1.23

5.4 Turbulent wind modelling

Vlugmoor is capable of calculating the ship's response to turbulent wind fields. The time series of wind speeds however needs to be delivered as an input. As was shown in figure 4.18, a typical wind spectrum has energy spread over a wide frequency band, meaning that the time signal will appear chaotic, as many different sine functions are superimposed.

Time varying wind is usually expressed similarly to eq. 5.1, with the addition of a wind speed function which is function of t, as given by eq. 5.14. The matter which needs to be addressed is how to define $U_{\mathrm{ref}}(t)$ for the purpose of a mooring analysis.

Wind field measurements are in fact the most direct way to represent the wind conditions at a specific site. From the discussion in sections 5.1 and 5.2 it is obvious that, certainly for a container terminal, defining the most representative measurement location will never be straightforward. This objective is part of the *Windlass* JIP which is ongoing, where 3D wind scans (LIDAR) as well as RANS and LES computations are used to study local wind fields. These results could be used to define local wind spectra, as was done in [Yan+12].

For a mooring analysis, the wind field only forms a part of the project, which means that only limited resources can in fact be allocated to it. This means that in practice, a representative wind spectrum from literature needs to be chosen as input for the time domain calculation.

$$F_{\mathrm{wi}}(t) = C_{\mathrm{F}} \cdot \frac{1}{2}\rho_{\mathrm{a}} U_{\mathrm{ref}}(t)^2 \cdot A_{\mathrm{ref}} \tag{5.14}$$

5.4.1 Time varying wind as input for TDS in *Vlugmoor*

In literature, several spectral representations can be found, based on theoretical considerations, often complemented by wind measurement analysis. A discussion on the theory behind wind spectra is given in Appendix C. The representation of turbulent wind in the manoeuvring simulator at FHR is used as a basis for the implementation in *Vlugmoor*. A Von Karman wind spectrum, following eq. 5.15, is used to represent the energy spectrum of the wind. In this equation, $S_u(z, n)$ is the spectral energy, n the frequency, L_u^x the integral scale

for turbulence and z the height above the surface. f_u is a dimensionless representation of the frequency (eq. 5.16). The variance of the spectrum, σ_u is expressed by eq. 5.17. The integral scale for turbulence is given by eq. 5.18. Alternative expressions for eq. 5.17 and eq. 5.18 exist and are discussed in Appendix C.

$$\frac{nS_u(z,n)}{\sigma_u^2} = \frac{4f_u}{(1+70.8f_u^2)^{5/6}} \tag{5.15}$$

$$f_u = \frac{nL_u^x}{U} \tag{5.16}$$

$$\begin{cases} \sigma_u = \dfrac{1.1}{ln(\frac{z}{z_0})}, \ z_0 < 0.2m \\ \sigma_u = \dfrac{-0.14 \cdot ln(z_0) + 0.775}{ln(\frac{z}{z_0})}, \ z_0 > 0.2m \end{cases} \tag{5.17}$$

$$L_u^x = 25z^{0.35}z_0^{-0.063} \tag{5.18}$$

The spectrum representation from eq. 5.15 can be converted to a time signal of wind velocities which can subsequently by used as input to calculate wind forces using eq. 5.14.

5.4.2 Future work

The structure of this chapter, including the references to international study work in this field, indicate that in almost all aspects of modelling the response of a moored ship to wind loads, room for improvement is definitely present. Four actions are identified.

1. Studying the response under time-varying wind field should definitely be a subject of future work.

2. Measurement campaigns, supplemented by numerical modelling should be used to identify which spectral representations (Appendix C, section C.4) are most appropriate to use for ship berths. A direct fit of general spectral representations using measurement data could be used.

3. The theoretical wind spectra can be compared with the measurements, to identify in which region of the spectrum each model performs best. The frequency band(s) which are of most interest are the ones close to the natural period of the moored ship (section 4.5).

4. The output time series needs to analysed, following the method described in 2.3.1, meaning that a statistical analysis is performed on the data, and used to come up with the most representative value to compare with criteria. For ship motions, this might be a significant value, linked to efficiency considerations. For line forces, a most probable maximum can be sought and compared with OCIMF and/or winch brake limits.

References

[And13] I.M.V. Andersen. “Wind loads on post-panamax container ship”. In: *Ocean Engineering* 58 (2013), pp. 115–134.

[Ble93] W. Blendermann. *Schiffsform und Windlast- Korrelations- und Regressionsanalyse von Windkanalmessungen am Modell*. 1993.

[Ble95] W. Blendermann. “Estimation of wind loads on ships in wind with a strong gradient”. In: *Proceedings of the International Conference on Offshore Mechanics and Arctic Engineering (OMAE)*. 1995.

[FN05] T. Fujiwara and T. Nimura. “New Estimation Method of Wind Forces Acting on Ships on the Basis of Mathematical Model”. In: *Proceedings of the 15th International Offshore and Polar Engineering Conference*. 2005, pp. 82–89.

[FTK09] T. Fujiwara, Y. Tsukada, and F. Kitamura. “Experimental Investigation and Estimation on Wind Forces for a Container Ship”. In: *Proceedings of the 19th International Offshore and Polar Engineering Conference* (2009), pp. 555–562.

[Ish72] R.M. Isherwood. “Wind resistance of merchant ships”. In: *R.I.N.A. transactions* 115 (1972), pp. 327–338.

[JBW17] W. D. Janssen, B. Blocken, and H. J. van Wijhe. “CFD simulations of wind loads on a container ship: Validation and impact of geometrical simplifications”. In: *Journal of Wind Engineering and Industrial Aerodynamics* 166 (2017), pp. 106–116.

[OCI18] OCIMF. *Mooring Equipment Guidelines - MEG4*. Witherbys, 2018, p. 312.

[SIG07] SIGTTO. *Prediction of Wind Loads on Large Liquefied Gas Carriers*. 2007.

[SS96] E. Simiu and R. H. Scanlan. *Wind effects on structures : Fundamentals and applications to design*. 1996.

[Tho03] C.A. Thoresen. *Port designer's handbook: Recommendations and guidelines*. Thomas Telford Books, 2003, p. 549.

[Van+19] T. Van Zwijnsvoorde et al. "Wind modeling for large container vessels: a critical review of the calculation procedure". In: *International Journal of Transport Development and Integration* 3.4 (2019), pp. 369–381.

[Yan+12] Q. Yang et al. "Statistical spectrum model of wind velocity at Beijing Meteorological Tower". In: *The s-7th International Colloqium on Bluff Body Aerodynamics and Applicatoin (BBAA7)*. Shanghai, China, 2012.

[YJK92] K. Yoneta, S. Januma, and K. Karasuno. "Analysis vessels' wind forces through the utilization of a physical-mathematical model-II". In: *Japanese Institue of Navigation Journal* 86 (1992), pp. 169–177.

[YS70] T. Yamano and Y. Saito. "An esimation method of wind forces acting on ships". In: *The Kansai Society of Naval Architects* 228 (1970), pp. 91–100.

6

Empirical model passing ship effect

Passing ship effects are transient forces, which can potentially cause unsafe mooring situations. Section 2.1.4 already discussed the general appearance of a passing ship effect, consisting of the effect of a primary (section 2.1.4.2) and secondary (section 2.1.4.3) wave system. It was also highlighted that the slower (long period) primary system has much more impact on the moored ship in general harbour manoeuvres involving large seagoing ships, because of its longer periodicity, compared to the short secondary wave system.

Important passing ship effects are to be expected in restricted areas, where flow effects become complex, with significant influence of vertical and horizontal restriction of the waterway. As these conditions are challenging to model in numerical models, a dedicated model test program has been performed at FHR. This chapter presents a large database of ship interaction scale model tests (sections 6.1 and 6.2).

Scale effects are inherent to scale model tests. The model test parameters are chosen so as to fulfil Froude similarity, which is common for towing tank experiments. Remember that for wind tunnel testing, Reynolds similarity was pursued (see section 5.3.1.4). As a consequence of Froude scaling, Reynolds numbers are significantly lower in model scale, introducing scale effects. Section 6.3 explains

how scale effects manifest in the $PESCA$ program. This discussion is later expanded in the framework of the RoPES validation (chapter 7).

The scale model test results are used to examine the effect of three parameters on the peak forces acting on the moored ship due to the passage (section 6.5), based on a least squares regression approach (section 6.4). These insights are used to propose a novel empirical model for predicting the magnitude of passing ship effects in restricted waters for several combinations of moored and passing ships (section 6.6). Non-dimensionalisation of the forces is proposed to create a model which can be used for a variety of ship types (section 6.7).

Important remark In this chapter, quantities are expressed in model test scale, as they were measured and defined in the towing tank. All variables are dimensional. In case variables are made non-dimensional, it will be explicitly written as a ratio of two parameters. An example is given here:

d = passing distance in meters model scale (m)
$\frac{d}{B_{\text{pas}}}$ = non-dimensional passing distance (-)

Two exceptions exist to this general rule.

- In the description of model tests, the full scale velocity V_{FS} in (kn) (seagoing ships) or (km/h) (inland ships) is given, as this is easier to interpret for the reader. In all calculations, the speed V is expressed in model scale, (m/s). A conversion between model test speed and full scale speed is given in table 6.1. If the unit (m/s) is used, the speed is always model scale speed.
- The under keel clearance, UKC, is expressed in % of the draft, as was given by eq. 2.1 and figure 2.2.

Table 6.1: *Conversion ship speed from model scale to full scale*

seagoing		inland	
MS(1:80) (m/s)	FS(1:1) (kn)	MS(1:25) (m/s)	FS(1:1) (km/h)
0.115	2	0.111	2
0.173	3	0.167	3
0.230	4	0.222	4
0.288	5	0.278	5
0.345	6	0.333	6
0.403	7	0.389	7
0.460	8	0.444	8
0.518	9	0.500	9
0.575	10	0.556	10
0.633	11	0.611	11
0.690	12	0.667	12
0.748	13	0.722	13
0.805	14	0.778	14
0.863	15	0.833	15
0.920	16	0.889	16
0.978	17	0.944	17

6.1 *PESCA* scale model test description

All (passing ship) model tests described in this thesis have been performed at FHR, as a cooperation between FHR and the MTD UGent. For a detailed overview of the project plan and a description of the model tests, reference is made to [Del18] and [Del+19].

6.1.1 Towing tank for Manoeuvres in Confined Water

The *Towing Tank for Manoeuvres in Confined Water*, is part of the testing facilities at FHR in Antwerp (figure 6.1). Commissioned by the Flemish Government, the facilities were built in 1992 to provide more scientific insight into the shallow water issues encountered by the increasing ship sizes calling at Belgian/Flemish ports.

The towing tank has a total length of 87.5 m, of which 68 m can be used to perform model tests (defined as useful or effective length). The width of the tank is 7.0 m, with a maximum water depth of 0.5 m. The $PESCA$ ship length vary between 2.2 m and 4.5 m.

A planar motion carriage (see figure 6.1) is used to tow a ship along a predefined trajectory in the horizontal plane, when it is operating in captive mode. In free running mode, the carriage follows the (self-propelled) ship through the tank. Other equipment includes an auxiliary carriage, making it possible to model encounters and overtakes [VVL02] , as well as a wave maker to investigate the ship's response in (irregular) seas [Van+19] [Spr+17]. [DGV16] elaborates further on the towing tank (equipment).

The passing ship, which is towed by the carriage, uses the conventional captive measuring set-up used in the towing tank. For the moored ships, a custom Rose Krieger frame (figure 6.2) has been built. Slight adjustments to this frame were then made to accommodate the different moored ships.

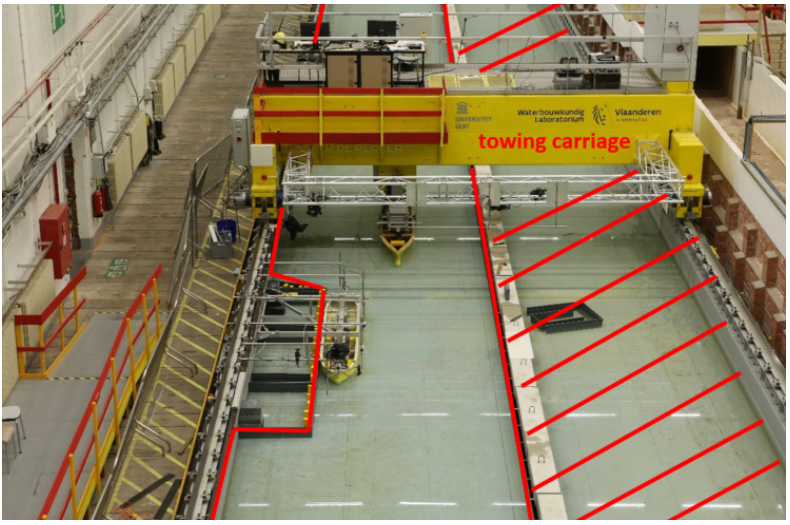

Figure 6.1: *Towing tank test setup for $PESCA$ model tests in narrow channel configuration, towing tank test with short quay element where $T0Y$ is moored (appendix D).*

Figure 6.2: *Rose Krieger measuring frame for moored ships, example moored $T0H$.*

6.1.2 Ship models

6.1.2.1 Seagoing ships

Four seagoing ship models are part of the test matrix. The choice for specific models is based on the ship-ship interactions which occur in ports with relatively narrow channels and docks. As container loading operations require minimal ship motions of the moored ship, the berths are usually constructed in sheltered environments, inherently increasing the potential of passing ship effects in these locations. This explains the choice of neo-panamax type container ships as the moored and passing ship, using the ship models $C0P$ and $C04$ respectively. These models represent full scale container ships at a chosen scale of 1:80. The $C04$ is always taken as the passing ship, meaning that the scale factor for all tests is then fixed at 1:80. The main parameters describing these models can be found in table 6.2. Further details regarding the ship models are provided in appendix D.

The largest oil and gas carriers are often not able to enter more sheltered environments, due to draft (oil tanker) and/or safety (gas carrier) restrictions, which is why the largest (full scale) oil and gas carriers are omitted. An Aframax oil tanker as been tested, the model $T0Y$, which is actually built at scale 1:75. As is mentioned above, the scale factor chosen for the test program has been based on the container ship's dimensions, being 1:80. A second tanker,$T0H$, is significantly smaller (table 6.2) than the other ships, aiming to get insight into the passing ship effect between ships with significantly different dimensions.

6.1.2.2 Inland ships

Inland ships are on average a lot fuller than seagoing ships (=higher block coefficient). As inland ship underwater shapes are very similar for different cargo types, no specific selection is made here. $E01$ is selected as the passing ship, with as moored ship the $B01$ and a modelled push barge convoy, composed of hulls $D03$ and $D04$ (indicated here as ship $D03D04$). These models represent full scale ships at a factor 1:25.

Inland ships are often subdivided into CEMT(Conférence européenne des ministres des Transports) classes. The $B01$ corresponds to a

Table 6.2: *Ship models used in $PESCA$ seagoing ship test program.*

	$C04$	$C0P$	$T0Y$	$T0H$
	MS(1:80)			
L_{OA} (m)	4.414	4.615	3.160	2.316
L_{PP} (m)	4.367	4.350	3.067	2.215
B (m)	0.611	0.610	0.560	0.295
T_{M} (m)	0.190	0.190	0.188	0.100
m (kg)	320.6	326.2	247.3	54.3
C_{B} (-)	0.632	0.636	0.766	0.830
	FS(1:1)			
L_{OA} (m)	353.1	369.2	252.8	185.3
L_{PP} (m)	349.4	348.0	245.3	177.2
B (m)	48.9	48.8	44.8	23.6
T_{M} (m)	15.2	15.2	15.0	8.0
m (ton)	164147	167014	126618	32973

CEMT-Va 'Large Rhine' ship at full scale, the convoy $D0304$ is denoted as CEMT-VIa. The ship $E01$ is also a CEMT-VIa ship. This is because the CEMT-class can be considered slightly outdated, making it more difficult to capture the (larger) inland ships, as well as the push-barge combinations. Rijkswaterstaat (RWS)[Rij20] came up with an updated classification, which is given in table 6.3. The main dimensions of the ship models are given in table 6.4 (see appendix D for further details)

Table 6.3: *Inland ship classes according to CEMT and RWS.*

ship model	CEMT class	RWS class
$B01$	CEMT-Va	M8
$E01$	CEMT-VIa	M12
$D03D04$	CEMT-VIa	BII-2b

Table 6.4: *Ship models used in $PESCA$ inland ship test program.*

	$B01$	$D03D04$	$E01$
	MS(1:25)		
L_{OA} (m)	4.398	3.076	4.377
L_{PP} (m)	4.393	3.017	4.334
B (m)	0.458	0.912	0.684
T_{M} (m)	0.140	0.140	0.140
m (kg)	249.4	365.8	342.7
C_{B} (-)	0.885	0.950	0.826
	FS(1:1)		
L_{OA} (m)	110.0	76.9	109.4
L_{PP} (m)	109.8	75.4	108.3
B (m)	11.45	22.8	17.1
T_{M} (m)	3.5	3.5	3.5
m (ton)	3897	5716	5355

6.1.3 PESCA test set-up in towing tank

Figure 6.3 shows a representation of the towing tank environment for the specific case of the $PESCA$ model test series. The figure shows the full towing tank length of 87.0 m. The parameters for the test definitions are expressed in the earth bound coordinate system $O_{0\mathrm{t}x0\mathrm{t}y0\mathrm{t}z0\mathrm{t}}$. The axis system definition is in line with the *Vlugmoor* convention (chapter 4, figure 4.20). This system differs from the default towing tank system, which is defined z-axis positive downwards. Appendix D elaborates on how the test output, which is further discussed in section 6.2, is transformed to be in line with the thesis definition (z-axis positive upwards).
The following parameters are defined in the earth bound towing tank system $O_{0\mathrm{t}x0\mathrm{t}y0\mathrm{t}z0\mathrm{t}}$.

- The narrow channel is formed by a solid, vertical wall element positioned between $x_{0\mathrm{t}}$ = 3.00 m and 63.23 m. The $y_{0\mathrm{t}}$ position varies as a function of the channel width (see section 6.1.4.2)

- The moored ships are positioned with their midship at $x_{0\mathrm{t}}$ = 23.0 m and $x_{0\mathrm{t}}$ = 43.0 m, defined as mooring location 1 and

mooring location 2 respectively. All ships are moored starboard side, 0.02 m from the theoretical tank wall (located at $y_{0\mathrm{t}}$ = -3.5 m). This gap between solid wall and ship represents the presence of fluid when a fendering system is present. In one series, the moored *T0Y* ($x_{0\mathrm{t}}$ = 43.0 m) is modelled in a jetty configuration (figure 2.7); defined by $y_{0\mathrm{t}}$ = -2.52.

Figure 6.4 shows a transversal section plane at $x_{0\mathrm{t}}$ = 23.0 m. Table 6.5 explains the test symbols introduced in figure 6.4. For the purpose of the analysis of the model tests, the subscript p and m are used to indicate if the parameter is of the passing or moored ship respectively. For example where B_{p} is the beam of the passing ship, B_{m} is the beam of the moored ship.

6.1.4 Test conditions

In order to build a proper empirical model, a substantial amount of parameter variations is needed. For bookkeeping purposes, each model test is labelled by a specific code; in case test repetitions have been performed, this is also included in the code. [Del+19] lists all model tests which have been performed within the $PESCA$ program. Not all model tests are considered in this thesis, and specifically in chapters 6 and 7; these tests are mentioned in the text and explained in appendix D, but not considered in the analysis.

6.1.4.1 Test environment

Following towing tank procedures, each test is given a unique code, linking ship, channel width (W) and under keel clearance (UKC).

Table 6.5: *Test parameters defined in figure 6.4.*

Parameter (unit)	explanation
h (m)	water depth
UKC (%)	under keel clearance, as percentage of the draft
d (m)	passing distance side-to-side
W (m)	channel width
T_{M} (m)	draft of the ship

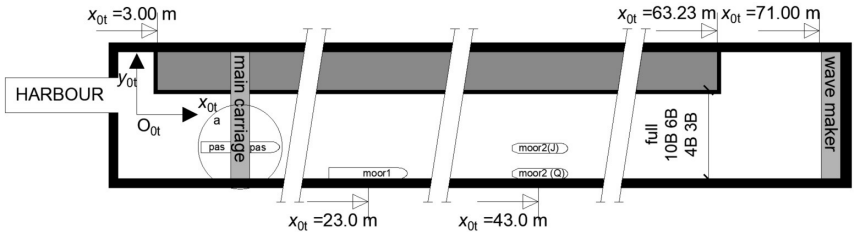

Figure 6.3: *Schematic representation towing tank environment $PESCA$ tests. Top view*

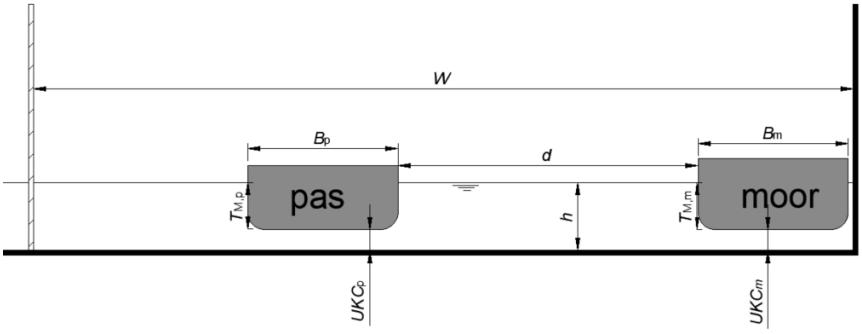

Figure 6.4: *Schematic representation (2) towing tank environment $PESCA$ tests. Cross section*

The channel width W is expressed as multiples of B_{p}. In $PESCA$, three ships are actually present during each test, one passing ship and two moored ships, hence the need to subdivide each test into the passing event for the first and second ship respectively.

In the $PESCA$ test program, the inland ship interaction was tested first, with the $B01$ positioned at $x_{0\mathrm{t}}$= 23.0 m and the $D03D04$ at $x_{0\mathrm{t}}$ = 43.0 m. The first series has been run without any channel wall built into the tank, meaning that the towing tank width (7.0 m) forms the channel, hence the $\frac{W}{B_{\mathrm{p}}}$ = 11.46. As the $D03D04$ combination is wider than the $B01$ moored ship, during some tests, $E01$ only passes the first ship and then decelerates and stops before reaching the second ship.

The passage of the moored $C0P$ and $T0Y$ at $x_{0\mathrm{t}}$= 23.0 m and $x_{0\mathrm{t}}$= 43.0 m by the $C04$ was modelled next. As these moored ships have approximately the same beam, all tests involved passing both moored ships.

When the $T0Y$ was moored in jetty configuration at $x_{0\mathrm{t}}$= 43.0 m and the $T0H$ at the tank wall ($x_{0\mathrm{t}}$ = 23.0 m), the passing $C04$ decelerated after passing $T0H$.

Table 6.6 gives an overview of the $PESCA$ test environments, giving the number of unique tests (so excluding test repetitions) for each parameter combination listed. For some tests, test repetitions have been executed (section 6.2.2). These tests are not included in the numbers from table 6.6. In total, 1699 parameter combinations are included and will be used for the regression analysis presented in this chapter. No tests are excluded, unless mentioned explicitly.

Within $PESCA$, two more test batches have been run. For the moored $C0P$ and $T0Y$, passing events with drift angles have been modelled (appendix D). These tests can be used to investigate the influence of a drift angle on the magnitude of the forces. A second set involves the moored $T0Y$ ship at $x_{0\mathrm{t}}$ = 43.0 m at a short quay element, with different lengths and angles (appendix D). As both test settings are not further discussed within this thesis, they are not included in table 6.6, nor in any other analysis described in chapter 6.

Table 6.6: *Test environment : channel width W, UKC (see figure 6.4); Number of unique tests executed within each environment (excluding test repetitions).* N.A. *= environment is not tested.*

				$UKC(\%)$				
Pas	Moor	x_{0t} (m)	W/B_p (-)	50	40	30	20	10
$C04$	$C0P$(Q)	23	10	37	N.A.	N.A.	37	36
			6	33	N.A.	N.A.	36	27
			4	21	N.A.	N.A.	20	16
$C04$	$T0Y$(Q)	43	10	37	N.A.	N.A.	37	36
			6	33	N.A.	N.A.	36	27
			4	21	N.A.	N.A.	20	16
$C04$	$T0H$(Q)	23	10	86	N.A.	N.A.	80	77
			6	65	N.A.	65	64	52
$C04$	$T0Y$(J)	43	10	47	N.A.	N.A.	45	44
			6	30	N.A.	30	29	24
$E01$	$B01$(Q)	23	11.46	36	N.A.	N.A.	33	38
			4	24	N.A.	N.A.	19	18
			3	33	22	20	20	N.A.
$E01$	$D03D04$(Q)	23	11.46	31	N.A.	N.A.	27	32
			4	13	N.A.	N.A.	11	8
			3	18	12	10	10	N.A.

6.1.4.2 Section width and UKC - blockage

The towing tank test environments are denoted by under keel clearance UKC and channel width W. A parameter which can be derived here is the blockage of the section, or the ratio between the total wetted section and the midship section of the ship. This definition implies a simplification to a 2D problem, which is then presented at midships. Generally, blockage is a way to describe the ratio between ship and water body for a sailing ship. This parameter is defined as m_{p} (eq. 6.1), expressed as the ratio between the ship's area of midship and the wetted area of the channel. When considering the effect on a moored ship, there is also a local blockage, which is defined when the passing and moored ship are present in the same channel section. This parameter is called m_{pm} (eq. 6.2).

Figure 6.5 shows the number of model tests per m_{p} (a) and m_{pm} (b) class. The bar at m_{p} 0.20 gives all tests in the interval]0.175, 0.20]. The black bar indicates the number of tests with seagoing ships, the grey bar shows the number of tests with inland ships. It is clearly visible that when m_{p} can be considered reasonable high (up to 0.3), m_{pm} goes up to 0.7. In the latter case, the flow section is reduced by 70% locally when the ships are side-to-side.

$$m_{\mathrm{p}} = \frac{A_{\mathrm{M,p}}}{A_{\mathrm{channel}}} \tag{6.1}$$

$$m_{\mathrm{pm}} = \frac{A_{\mathrm{M,p}} + A_{\mathrm{M,m}}}{A_{\mathrm{channel}}} \tag{6.2}$$

6.1.4.3 Passing distance

Figure 6.6 gives the number of tests performed at each passing distance, d (a) and non-dimensional ratio $\frac{d}{B_{\mathrm{pas}}}$ (b). Most tests are concentrated in the left side (low passing distance) of the graph, which is intentional as the effect of the primary wave system dissipates for large passing distances. At distances of $\frac{d}{B_{\mathrm{pas}}}$ = 5 and higher, the secondary wave system becomes more prominent. The concentration of tests at $\frac{d}{B_{\mathrm{pas}}}$ = 1 can be explained due to the test environment with channel widths W/B = 3 and 4 (see table 6.6), where the passing distance cannot be higher than $1.5\frac{d}{B_{\mathrm{pas}}}$.

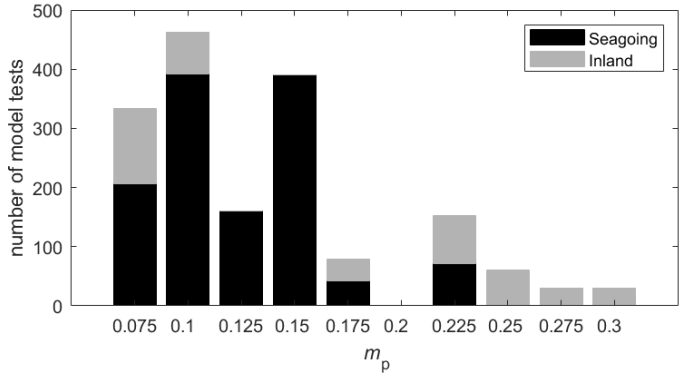

(a) Continuous blockage m_{p}

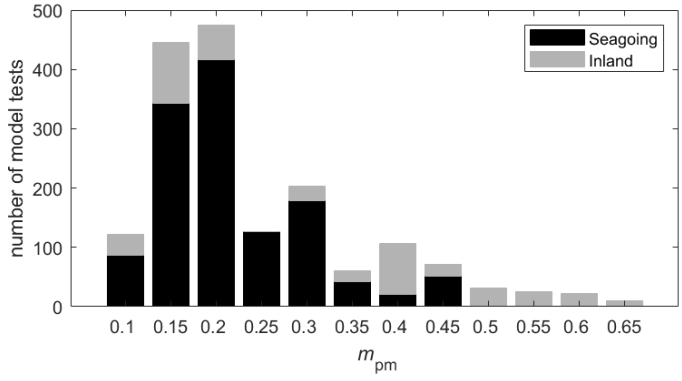

(b) Local blockage m_{pm}

Figure 6.5: *Number of model test for each blockage class*

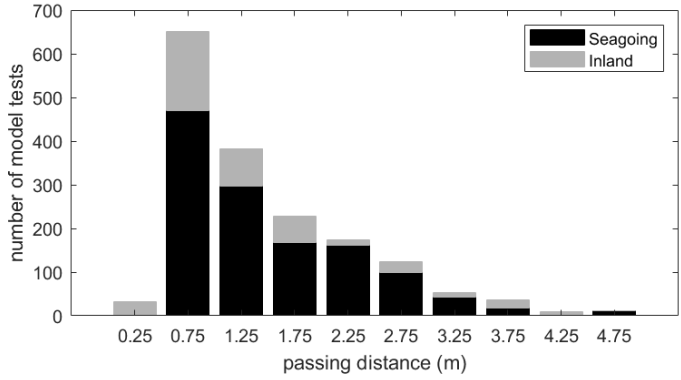

(a) Dimensional passing distance d_{pas}

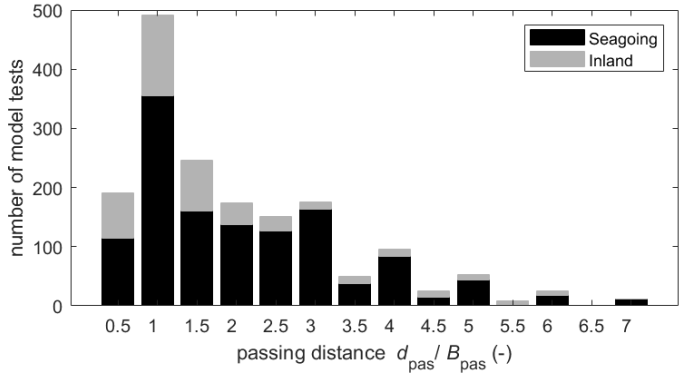

(b) Non-dimensional passing distance $\frac{d_{\mathrm{pas}}}{B_{\mathrm{p}}}$

Figure 6.6: *Number of model test for each passing distance class.*

6.1.4.4 Passing speed

Figure 6.7 shows the number of model tests performed at each ship speed, dimensional (a) and in function of Fr (b).The speed is given in model scale m/s. The full scale speed is added, which is expressed in knots for the seagoing ships (scale 1:80) and in km/h for inland ships (scale 1:25). Figure 6.8 (a) shows the number of tests in classes based on the Froude-Depth number,(Fr_{h}, eq. 6.3). In (b) and (c) Fr_{h} is divided by the critical Froude number, according to the theory of [Sch49] (eq. 6.4). In (b) the continuous blockage (m_{p}, eq. 6.1) is used to calculate the critical Froude number. In (c), the local blockage (m_{pm}, eq. 6.2) is considered. Note that using the local blockage is not according to the definition of [Sch49]. It does indicate the narrow flow section during the passage, which will lead to local effects. The meaning behind the usage of the expression by Schijf is further explained in section 6.6.1

$$Fr_{\mathrm{h}} = \frac{V}{\sqrt{g \cdot h}} \tag{6.3}$$

$$Fr_{\mathrm{crit}} = \left[2 \cdot \sin\left(\frac{\mathrm{asin}(1-m)}{3}\right)\right]^{2/3} \tag{6.4}$$

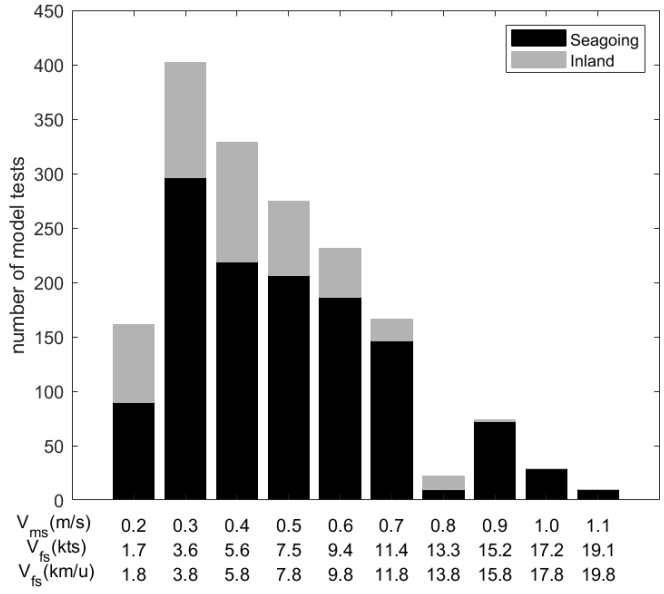

(a) Dimensionsal passing speed (m/s,kts,km/h)

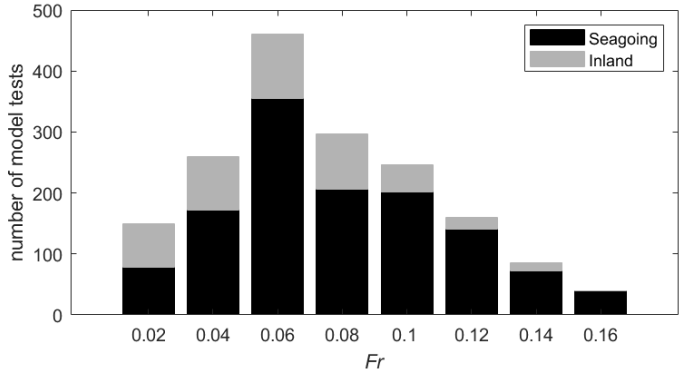

(b) Non-dimensional passing speed (Fr)

Figure 6.7: *Number of model test for each passing speed class.*

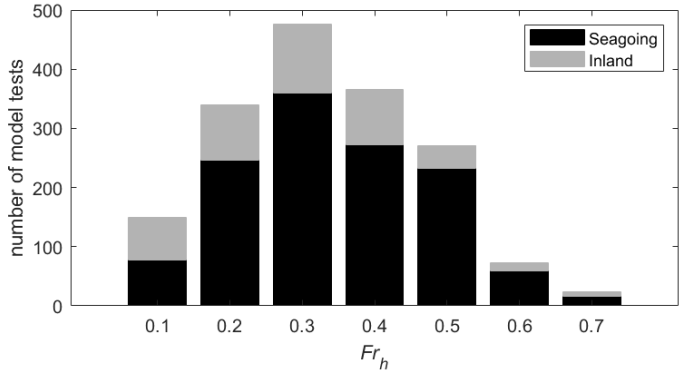

(a) Fr_{h}

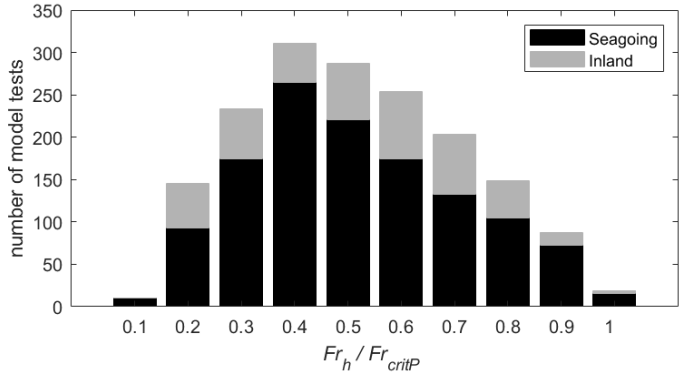

(b) $\frac{Fr_{\mathrm{h}}}{Fr_{\mathrm{crit}}}$ based on m_{p}

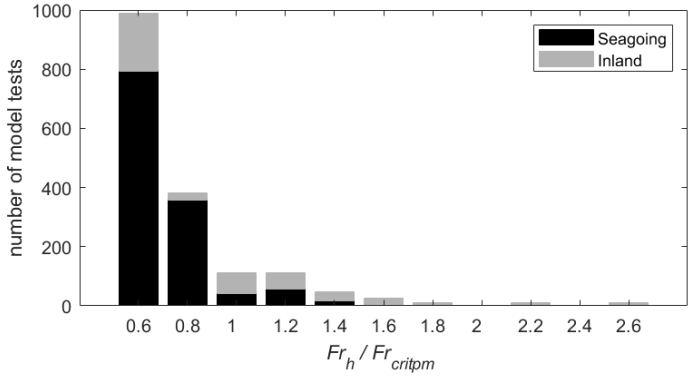

(c) $\frac{Fr_{\mathrm{h}}}{Fr_{\mathrm{crit}}}$ based on m_{pm}

Figure 6.8: *Number of model test for each Fr_{h} class.*

6.1.5 Registrations

The towing tank environment was already presented in figures 6.3 and 6.4; where the axis system $O_{0\mathrm{t}x_0\mathrm{t}y_0z_0\mathrm{t}}$ is the tank fixed system. Within each environment, three ships are present, one passing ship (with varying $x_{0\mathrm{t}}$ position) and two moored ships (at $x_{0\mathrm{t}}$ = 23m and $x_{0\mathrm{t}}$ =43 m). On each ship, forces and motions are measured, using load cells and motion gauges. For this test program, the ships are restrained in 4DOF (surge, sway, yaw, roll), being free to heave and pitch. The measured ship data is supplemented with water level recordings, using 13 wave probes.

6.1.5.1 Passing ship

The passing ship is attached to the towing carriage, meaning that the carriage moves the ship through the towing tank, commonly defined as a captive model test. In a captive model test, the ship is restrained in 4DOF (surge, sway, yaw, roll), being free to heave and pitch. Figure 6.9 shows the position of load cells (LC) and motion gauges (P, potentiometer) for the $C04$. Table 6.7 gives the values of $|x_1|$, $|x_2|$, $|x_3|$ and $|y_1|$, expressed in the ship fixed axis system $0_{x\mathrm{p}y\mathrm{p}z\mathrm{p}}$. Note that as the ship is in fact restrained in 4DOF, 2 motion gauges would be sufficient to measure the heave and pitch. The four gauges are however part of the standard captive setup, leading to redundant measurements. The position of the measurement equipment on $E01$ is given in appendix D

6.1.5.2 Moored ship

The moored ships are connected to the towing tank wall using a Rose-Krieger frame (figure 6.2). Load cells (LC) and motion gauges

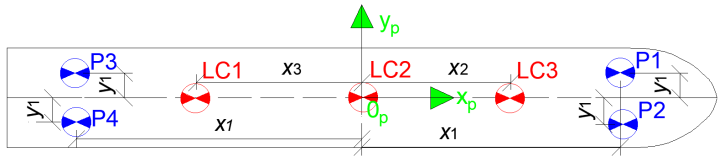

Figure 6.9: *Position load cell (LC) and motion gauge (P) for $C04$.*

Table 6.7: *Position LC and P for $C04$ and $C0P$ in(m) (figure 6.9 and figure 6.10).*

	$C0P$	$C04$
$\|x_1\|$	1.140	1.137
$\|x_2\|$	0.700	1.004
$\|x_3\|$	0.050	0.998
$\|x_4\|$	1.000	N.A.
$\|y_1\|$	0.295	0.295

(P) are added to come to a similar configuration as for the passing ship attached to the towing carriage, albeit with only two motion gauges. For the moored $C0P$, figure 6.10 gives the positions of the measuring equipment, expressed in the axis system 0_{xmymzm}, with the numerical values given in table 6.7. For all moored ships, the positions of the equipment is given in appendix D.

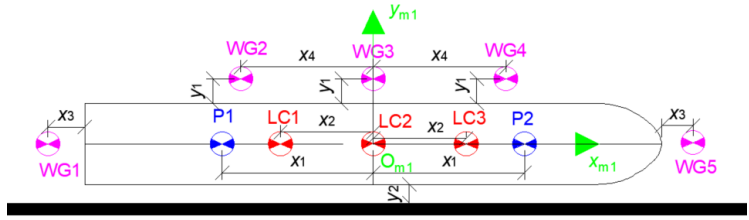

Figure 6.10: *Position load cell (LC) and motion gauge (P) for $C0P$. Indication position five wave gauges (WG) around moored ship.*

6.1.5.3 Wave Gauges

In figure 6.10, wave gauges - notation WG - are indicated for the moored $C0P$. For each environment, wave gauges are named 1 to 13. Each moored ship is surrounded by five gauges (WG 1-5 for location 1 (x_{0t} = 23 m) and WG 6-10 for location 2 (x_{0t} = 43 m). Wave gauges 11-13 are positioned along the built-in bank, at positions x_{0t} = 8.0, 33.0 and 58.0 m respectively. They are positioned at 0.05 m from the wall, except when the width of the section is limited to three and four times the passing ship's beam, where they are positioned at 0.01 m from the bank, allowing all passing trajectories to be executed.

6.2 Processing and quality assessment measured signals

6.2.1 Processing of measured signal

The outputs of each model test are registrations of forces, motions and water level, as described in section 2.1.4.2. These signals are stored with up to 100 Hz sampling frequency. When ships move slowly, the logging frequency is adjusted, to limit the size of the data files. These results are stored in what is called *DOC* files (named after the extension of the file type). At FHR, a dedicated software tool *Zeeman* has been developed, which allows the measured test signals to be processed, in order to increase the workability of the tests for specific (post-) processing purposes. The following actions are performed (for a full description, see [Del+19]).

- Before the start of each test, an average of a 10 second registration of all the signals is made, to monitor any initial offsets in the registered values. If an offset is present, it is subtracted from the measurement series, in order to have an (averaged) zero value at the start of each test.
- The measured signals of the passing ship under the carriage are transformed into $6DOF$ forces and motions.
- The high frequency, up to 100 Hz, signals are averaged to one data point every 21 cm model scale, which suffices to model the (primary) wave system of the passing ship event.

These processed results are stored as *DPT* files (again named after the file extension). A few further actions are performed on this file, using MATLAB routines. Appendix D elaborates on this processing.

- For the moored ship, the conversion of load cell and potentiometer readings to $6DOF$ forces and motions needs to be performed.
- All formats provided by *Zeeman* follow the towing tank axis convention (z-axis positive downward, y-axis positive to starboard). This is converted to the default axis system used in this thesis (z-axis positive upwards, y-axis positive to port). Appendix D elaborates on this transformation.

All data analysed for the remainder of this thesis follows the processing approach outlined above. Most steps involve mere transformation of the data (e.g. axis system, force definition). When the high frequency signals are averaged however, this changes the data series.

Averaging the data removes high frequency signal noise as well as condensing the data sets, making them easier to work with. This comes at the cost however that information is inevitable filtered out. For a passing event, the high frequency Kelvin wave (secondary wave system) for example will be distorted by this processing step. As the main interest is in the effect of the primary wave system, the consequences are limited. However, it is good to compare a raw *DOC* and averaged *DPT* data signal to understand how the signal is affected. Apart from this example, all the analysis in chapters 6 and 7 is done based on the *DPT* file. The *DOC* output files would need to be consulted to analyse the secondary wave system.

This is illustrated using the following model test ; Passing ship : $C04$, Moored ship : $C0P$, passing speed : 12 knots, passing distance : $3.9B_p$, 50% UKC, $\frac{W}{B_p}$ = 10. This is a fast test at larger passing distance, in order to have a significant contribution of the Kelvin wave system to the total measured signal. The measurement is logged at a frequency of 66.7 Hz.

Figure 6.11 compares the measured (*.DOC*) and processed (*.DPT*) test signal for the water level registration at wave gauge 3 (midship side of moored ship 1, figure 6.10). The right hand axis shows the forward speed of the passing ship during the test. Five lines are indicated (a-b1-b2-c1-c2).

- **a** Is the start of the acceleration phase of the passing ship. The first registration at WG3, at round t = 15 s, is that of the acceleration wave.
- **b1** The end of the acceleration or start of the regime phase of the test.
- **b2** The start of the deceleration or end of the regime phase of the test.
- **c1** Start of the effect of the primary wave system at the moored ship

- **c2** Start of the effect of the secondary wave system at the moored ship

Figures 6.12 and 6.13 show the time and frequency domain representations of the measured and processed signal. For this comparison, the measured signal has been corrected, so that it reads '0' at the start of the test, (which was not the case in the representation of figure 6.11). The high frequency components are partly filtered out in the processed signal, distorting the physical effect (right side figures). This is even more clear in the frequency domain (left side figures). It is seen that the measured 66.7 Hz signal shows energy in the 2 to 3 Hz region, which is not present in the 3.3 Hz averaged signal.

This energy is in the region of the kelvin wave energy. For the example test, the Kelvin wave pattern is denoted by a frequency of 2.26 Hz (f_{t} in figure 6.12) for the transverse waves and 2.40 Hz (f_{d}) for the diverging waves, calculated using eq. 6.5. In this eq., V is the ship's forward speed and θ_{w} is the angle of the secondary wave system (see figure 2.4). θ_{w} is calculated for shallow water, equalling 19.47 deg for this case. The frequency domain representation is done using FFT- fast Fourier Transform, meaning that the highest frequency which can be captured is 33.3 Hz and 1.65 Hz for the raw and processed signal respectively (half of the time trace step).

$$f_{\mathrm{wt}} = \frac{c_{\mathrm{wt}}}{\lambda_{\mathrm{wt}}} = \frac{V}{\frac{2 \cdot \pi \cdot V^2}{g}} \tag{6.5a}$$

$$f_{\mathrm{wd}} = \frac{c_{\mathrm{wd}}}{\lambda_{\mathrm{wd}}} = \frac{V \cdot \cos\theta_{\mathrm{w}}}{\frac{2 \cdot \pi \cdot V^2 \cdot \cos^2\theta_{\mathrm{w}}}{g}} \tag{6.5b}$$

When looking at the the hull forces (X, Y, N, figure 6.13), the presence of the acceleration wave, as well as the low and high frequency contributions of the ship passage are visible. The surge force is showing the least presence of high frequency components, even at this higher speed and larger passing distance. For sway and yaw, the effect of secondary waves can clearly be observed, directly in the 2 to 3 Hz region, but also the presence of reflections in the region between 0.5 and 2 Hz. The primary passing ship wave has a

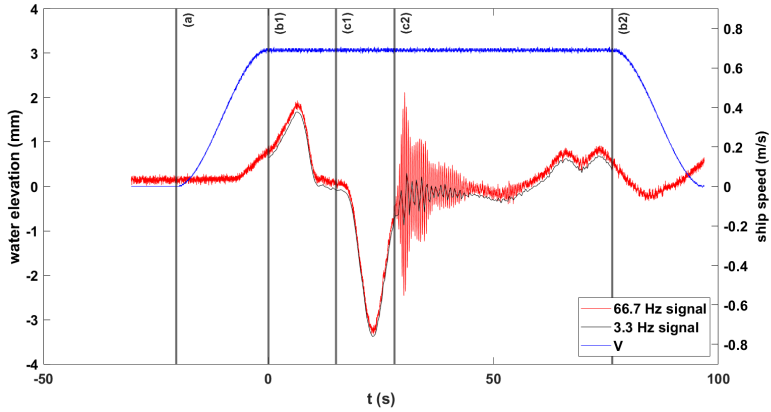

Figure 6.11: *Left axis : Measured (66.7 Hz) and processed (3.3 Hz) signal water elevation (WG3); Right axis : Passing ship speed (m/s). Passing $C04$, moored $C0P$, $\frac{W}{B_{\mathrm{p}}}$ = 10, UKC_{p} = 50%, $\frac{d}{B_{\mathrm{p}}}$ = 3.9, V_{FS} = 12 knots.*

period of around 20s or 0.05 Hz. The energy content in the low frequency range is compared in figure 6.14, which is a zoom plot of the surge force from figure 6.13.

The above discussions show that for higher passing speeds, the Kelvin waves are clearly observed by the wave gauges and also affect the forces, mostly Y, N. This relative contribution will increase for higher passing speeds and passing distance; For lower speed passage at lower passing distance, the secondary wave contribution becomes negligible. When considering that the moored ship will mostly react to longer period motions, this high frequency part of the measured signal is not studied in this thesis.

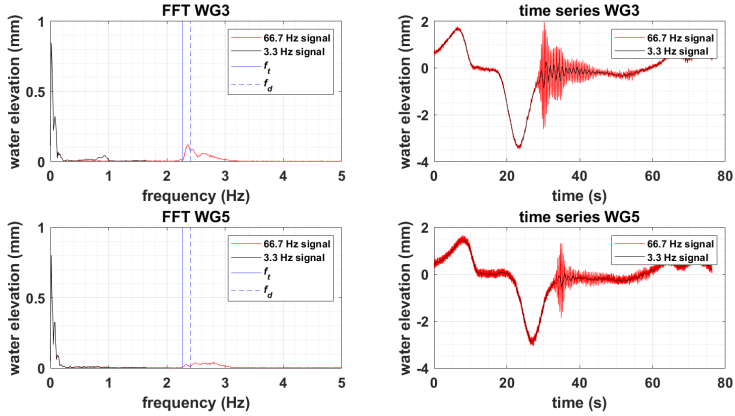

Figure 6.12: *Measured (66.7 Hz) and processed (3.3 Hz) signal WG3 and WG5; frequency (left) and time domain (right) representation. Passing $C04$, moored $C0P$, $\frac{W}{B_\mathrm{p}}$ = 10, UKC_p = 50%, $\frac{d}{B_\mathrm{p}}$ = 3.9, V_FS = 12 knots.*

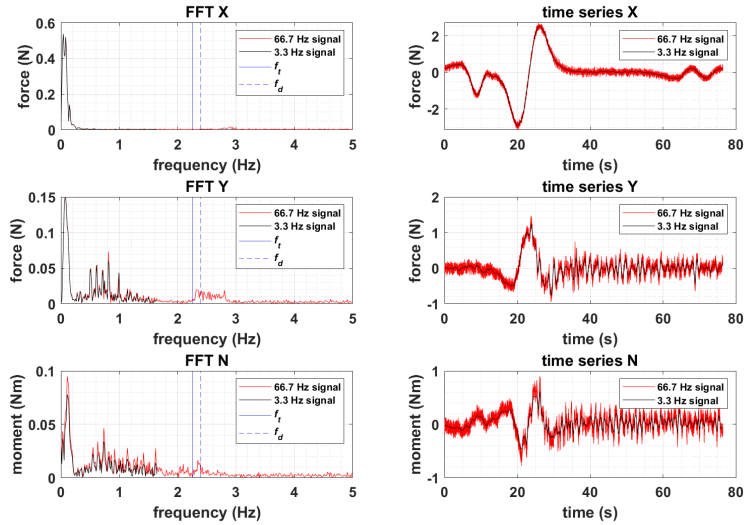

Figure 6.13: *Measured (66.7 Hz) and processed (3.3 Hz) signal X, Y, N; frequency (left) and time domain (right) representation. Passing $C04$, moored $C0P$, $\frac{W}{B_\mathrm{p}}$ = 10, UKC_p = 50%, $\frac{d}{B_\mathrm{p}}$ = 3.9, V_FS = 12 knots.*

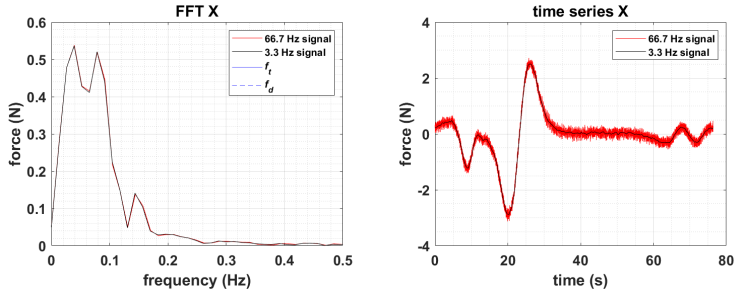

Figure 6.14: *Measured (66.7 Hz) and processed (3.3 Hz) signal X; frequency (left, zoom of figure 6.13) and time domain (right) representation. Passing $C04$, moored $C0P$, $\frac{W}{B_{\mathrm{p}}}$ = 10, UKC_{p} = 50%, $\frac{d}{B_{\mathrm{p}}}$ = 3.9, V_{FS} = 12 knots.*

6.2.2 Repeatability of model tests

The quality of the model test data can be assessed using a wide array of uncertainty analysis techniques, [ITT14b]. In this section, the repeatability of the model tests is checked by analysing 18 different model tests, which have been repeated between 10 and 13 times.

6.2.2.1 Repeatability of peak values

A first assessment considers the repeatability of the peaks in forces and wave gauge readings, expressed as the ratio between standard deviation σ (eq. 6.7) and mean value μ (eq. 6.6). This ratio is considered more relevant for quality analysis compared to the dimensional standard deviation. This can be illustrated by a fictional example. Say test set A averages 10000, with a standard deviation of 50. Test set B averages 10, with a standard deviation of 5. Both sets contain the same number of tests. The standard deviation of set A is much higher than for set B. When assuming a normal distribution of the tests around the mean, 68% of the data will be inside the interval [10050;9950] and [5;15] for set A and B respectively. The first interval gives us much more confidence when assessing a random point, compared to the second interval. Therefore, the ratio $\frac{\sigma}{\mu}$ is considered, being 0.5% and 50% for set A and B respectively, indicating the better result for set A.

As the calibration setting of the measurement equipment is the same for the whole test series, it makes sense that the measurement of smaller force magnitude (small μ) will be less accurate, despite similar σ, expressed as the ratio $\frac{\sigma}{\mu}$. This is confirmed when looking at the time series (section 6.2.2.2).

$$\mu_F = \sum_{i=1}^{n} F_{\mathrm{i}}, F = max/min\ of\ variable \tag{6.6}$$

$$\sigma_F = \sqrt{\frac{\sum_{i=1}^{n}(F_{\mathrm{i}} - \mu_F)^2}{n-1}}, n = number\ of\ tests \tag{6.7}$$

The results for the 18 model test set-ups are given in tables 6.8, D.11 (appendix D) and D.12 (appendix D), for moored ship 1, moored ship 2 and the wave gauge readings respectively. The first column gives

the number of test repetitions, the second column gives the name of the moored ship. In the remaining columns, the ratio $\frac{\sigma}{\mu}$ for the different measured forces (positive and negative peak) are given.

Table 6.8 : The confidence in the value for the peak surge force is high, as the standard deviation is always smaller than 5%. For the moored $C0P$, sway, yaw and roll are also denoted by small standard deviations. It is to be expected that these are higher than surge, as the magnitude is smaller. For the $T0H$, the roll moment was not measured; Sway and yaw show a high standard deviation on the measured peak forces. For the moored $B01$, this significant spread on measured sway and yaw is also observed. This is most noticeable for the test performed at 10% UKC.

Table D.11 (appendix D) : For the second moored ship, surge, but also sway and yaw peaks are repeated well. In the roll moment measurements, there is a larger deviation in the peak values. Note that some numbers are missing, which coincide with tests where the passing ship only passed the first moored ship, decelerating after the passage.

Table D.12 (appendix D) shows that the wave gauge readings of the water level depression are repeatable between different tests. In the third test series, WG4 data storage was corrupted, hence the *N.A.* notation.

6.2.2.2 Repeatability of time series

A second assessment considers not only the repeatability of the force and water level depression peaks, but in fact that of the entire signal. This is calculated for each value of the time series according to eq. 6.8 and 6.9. Figure 6.15 give three examples of such analysis, for the tests indicated with a * in table 6.8, D.11 and D.12.

The range of the right hand axis in figure 6.15, σ, is intentionally kept constant, to be able to compare the value between the three examples. The surge measurement shows smaller σ compared to the sway measurement. The σ in (b) is actually smaller compared to (c), the smaller force magnitude measured however leads to a larger ratio $\frac{\sigma}{\mu}$ of the peak force (27.4 % and 8.6 % for $Y+$, (b) and (c) respectively), confirming that the larger $\frac{\sigma}{\mu}$ is partly caused by the

smaller force magnitude of the measured force.

$$\mu(f_{\mathrm{j}}) = \sum_{i=1}^{n}(f_{\mathrm{j}})_{\mathrm{i}}, f_{\mathrm{j}} = value\ of\ variable\ at\ \mathrm{j}_{th}\ time\ step \tag{6.8}$$

$$\sigma(f_{\mathrm{j}}) = \sqrt{\frac{\sum_{i=1}^{n}((f_{\mathrm{j}})_{\mathrm{i}} - \mu(f_{\mathrm{j}}))^2}{n-1}} \tag{6.9}$$

Table 6.8: *Test repeatability analysis for moored ship at position $x_{0\mathrm{t}}$ = 23 m, ratio standard deviation over the average for peaks in X,Y,N and K.*

		$\sigma/\mu(\%)$							
n	ship	$X-$	$X+$	$Y-$	$Y+$	$N-$	$N+$	$K-$	$K+$
11	$C0P$	0.5*	1.1*	1.9	2.8	2.0	2.7	3.0	4.5
12	$C0P$	0.7	1.2	1.7	1.5	1.6	2.9	3.2	4.4
12	$C0P$	1.0	1.0	5.7	4.4	9.4	13.0	5.2	3.6
11	$C0P$	0.7	0.3	2.0	2.8	2.0	2.4	2.9	5.6
13	$T0H$	0.5	0.4	2.9	2.1	6.7	5.5	7.3	7.8
13	$T0H$	1.1	1.3	4.1	8.8	6.0	18.9	*N.A.*	*N.A.*
12	$T0H$	1.0	2.3	3.5	7.9	6.1	13.2	*N.A.*	*N.A.*
13	$T0H$	2.2	3.1	12.1**	27.4**	17.3	34.3	*N.A.*	*N.A.*
13	$T0H$	3.5	2.9	11.3	11.0	9.3	23.2	*N.A.*	*N.A.*
13	$T0H$	1.6	2.7	8.1	13.1	7.3	20.7	*N.A.*	*N.A.*
11	$T0H$	2.1	3.1	10.3	16.9	14.8	17.6	*N.A.*	*N.A.*
11	$T0H$	2.7	2.7	14.8	21.2	6.5	8.7	*N.A.*	*N.A.*
10	$B01$	3.3	3.9	16.3	22.9	21.4	18.7	15.5	22.2
13	$B01$	1.2	0.6	3.1	2.1	7.7	17.2	9.6	6.0
15	$B01$	1.8	1.9	5.7	8.8	9.3	10.0	21.7	23.3
12	$B01$	2.5	3.1	12.1	18.6	19.5	28.9	13.5	20.1
12	$B01$	0.5	0.9	4.8	3.1	7.9	18.5	31.5	5.4
13	$B01$	0.5	0.4	2.9	2.1	6.7	5.5	7.3	7.8

* *Time series repetition tests shown in figure 6.15*
** *Time series repetition tests shown in figure 6.15*

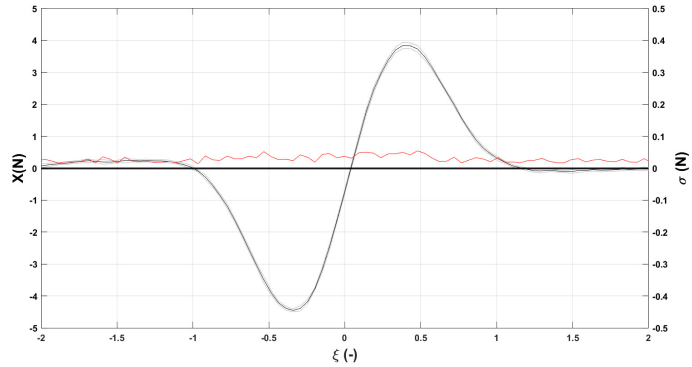

(a) Example 1 (* in table 6.8).

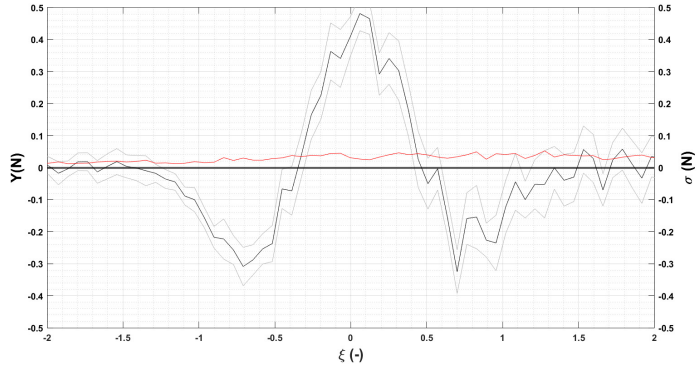

(b) Example 2 (** in table 6.8).

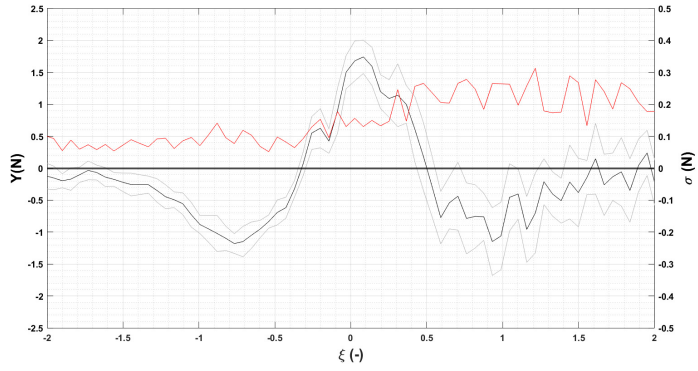

(c) Example 3 (*** in table D.11).

Figure 6.15: *Left axis : Average value measurement, confidence band of 2* $\sigma(f_j)$*; right axis : standard deviation.*

6.3 Scale effects in $PESCA$

6.3.1 Impact of viscosity on passing ship effect

In section 2.1.4, the passing ship effect was already introduced. A distinction was made between primary and secondary wave systems and a discussion was held on return flow in correlation with the formation of a bore wave. The characteristics of these disturbances depend on a number of parameters: the ship's speed, the section blockage and UKC. The path of the passing ship, as well as position of the moored ship relative to flow boundaries (bottom and channel) also impact the flow interaction.

In an ideal fluid, no shear stresses are present, which implies that only pressures normal to the surfaces of the ship and the banks are of importance. Moreover, boundary conditions on these surfaces allow tangential flow components. In real (=viscous) fluids however, shear stresses do appear. As a consequence, normal and tangential relative flow components on impermeable surfaces need to be zero to avoid infinite shear stresses. A boundary layer will thus be formed along these surfaces (figure 6.16).

6.3.2 Boundary layers

Two effects related to the presence of boundary layers are discussed here. For a non-zero forward speed of the ship, the boundary layer starts developing at the fore and increases in thickness along the length of the ship. The particles in this thicker layer have also lost part of their kinetic energy. Both effects increase the likelihood of flow separation. Secondly, the presence of a boundary layer reduces the available flow section (as shown by figure 6.16). In large sections, this effect is of minor importance. However when the clearance between ship and bottom and/or wall becomes small, the impact of the boundary layer on the flow becomes significant. With regard to UKC, the effect is amplified by the squat phenomenon, which further reduces the available space with increasing speed.

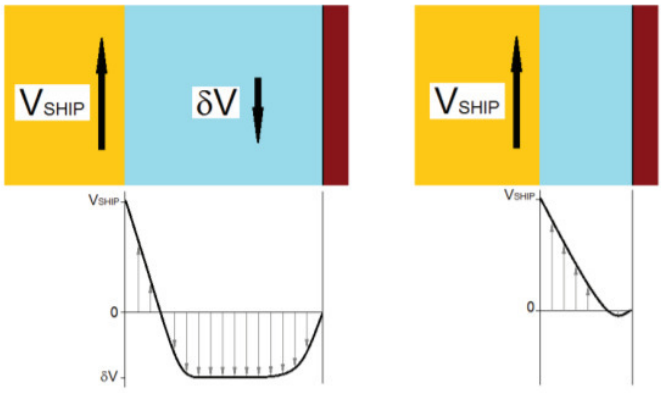

Figure 6.16: *Velocity profile in between ship (yellow, forward speed V_{ship}) and wall (brown, zero speed), with (δV) the return flow.*
Left : Development of return flow, presence boundary layer.
Right : Flow obstruction because of presence boundary layer.
Figure taken from [Lat14] (fig6.11)

6.3.3 Scaled boundary layers

The effects described in the section above are real flow effects, occurring in viscous flows. The question which needs to be answered now is how the scaling affects the appearance of this boundary layer. Scale effects were already discussed in section 5.3.1.4 concerning wind tunnel tests at scale, where Reynolds similarity was pursued. When assessing ship hydrodynamics, Froude similarity is generally sought, as was done for the $PESCA$ test program. According to eq. 5.6a, this requires that $\lambda_V = \sqrt{\lambda_L}$. This definition has an important consequence for the Reynolds number (eq. 5.6b), which becomes much lower at model scale compared to full scale, when Froude similarity is applied.

At lower Reynolds numbers, the boundary layers will be relatively thicker compared to the full scale equivalent. This means that the flow section will be more reduced in model scale compared to full scale. [Lat14] derived an formulation which expresses the distance to the bank below which the lateral force at the aft perpendicular of the sailing ship is affected by the presence of the boundary layer. This is shown in 6.17, defined as the *boundary layer influence thickness,* δ_{BLI}.

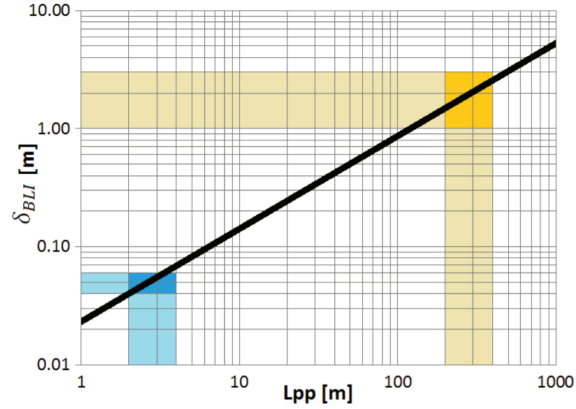

Figure 6.17: *Boundary layer influence thickness δ_{BLI} in function of ship length. Figure taken from [Lat14] (fig 6.13)*

6.3.4 Scale effects affecting the moored ship

Figure 6.17 is used as the basis for this discussion. For a ship model of around 4 m in length, δ_{BLI} is around 0.07 m. For the full scale ship, with length 320 m (scale 1:80), δ_{BLI} is around 2 m.

As the moored ship has zero forward speed, only the return flow caused by the passing ship will cause flow boundaries to exist around the moored ship. Scale effects might however impact the flow around the passing ship, which in turn impacts the moored ship. The following possible effects are identified:

- **Effect on the pressure field caused by the passing ship (primary wave).** It can be expected that the pressure field around the fore part of the passing ship is hardly affected by viscous effects, due to the limited boundary layer thickness. In the aft part of the ship, boundary layers are relatively thicker at model scale compared to full scale, and flow separation (caused by instability of the boundary layer in decelerated flow) is more likely to take place, which might result in a weaker pressure field. For the moored ship, it may be expected that the first part of the interaction phenomenon will not be affected by viscous effects, while such effects cannot be excluded during the second part.

- **Effect on the return flow.** Due to the relatively thicker boundary layer, the sectional area available for the return flow is relatively smaller during model tests. This will lead to an increased average return flow velocity in the more open zones of the available cross section, where the return flow will be concentrated. As a moored ship will always be located in a relatively open zone of the cross section, it can be expected that average return flow experienced by the moored ship could be (slightly) greater at model scale. This is especially the case when the passing ship sails with a small UKC and/or at a close distance to the opposite bank, concentrating the flow in the section where the moored ship is located.
  When passing distances would be around 0.07 m in model scale, the boundary layer influence would be present. At full scale ($0.07\ m \cdot 80 = 5.6\ m$), the ship will not feel the effect of the boundary layer. As minimum passing distances modelled in $PESCA$ are $0.5B_{\mathrm{p}}$ (around 0.3 m model scale), major scale effects are not expected here.

- **Effect of quay/jetty mooring.**

  – In case of a jetty, the distance between the bank and the side of the ship will be sufficient to avoid boundary layer effects that may obstruct the return flow caused by the passing ship, in both model as well as full scale.

  – In case of a quay wall, the distance between quay and ship's side is within boundary layer influence thickness for both the model and full scale ship, meaning that the flow is severely obstructed (figure 6.16, right) in both cases. For this reason, only minor differences between full and model scale are expected.

6.4 Regression analysis approach

In the following sections, the dataset of *PESCA* model tests is used as a basis to investigate the influence of test parameters (passing distance, UKC,...) on the passing ship effect, as well as to build and validate an empirical model for prediction of passing ship effects.

The time series of passing ship forces in the horizontal plane are reduced to two data points for each variable, as indicated by the red circles in figure 6.18. The choice is made to only consider the largest positive and negative value of the time series, denoted as 'force peaks' for the remainder of this thesis.

The time series of yaw N in fact shows four distinct peaks during the passage, whereas we only consider the two largest amplitudes (one positive and one negative). A motivation for this choice is given by rewriting the sway force and yaw moment as two lateral forces, at the fore (Y_{f}) and aft (Y_{a}) perpendicular respectively, eq. 6.10. This convention is illustrated in figure 6.19. The blue (Y_{f}) and purple (Y_{a}) time series in figure 6.18 show that the yaw moment causes a shift, in time and magnitude, of the lateral forces, yet the impact is limited. The sway force is dominant over the yaw moment, hence only the consideration of two of the four yaw peaks.

$$\begin{cases} Y_{\mathrm{f}} = \dfrac{Y}{2} + \dfrac{N}{L_{\mathrm{PP}}} \\ Y_{\mathrm{a}} = \dfrac{Y}{2} - \dfrac{N}{L_{\mathrm{PP}}} \end{cases} \tag{6.10}$$

Appendix D, section D.4 shows an example of a passage where the Kelvin wave amplitude is higher than the amplitude of the primary wave system. For these tests, the peaks used in the analysis will be questionable, as they originate from the secondary wave system. As these cases are limited in quantity, the effect on the regression analysis will be limited. It is recommended however for future work to consider the primary and secondary wave system separately, to further increase the quality of the regression.

In chapter 7, where $PESCA$ is used to validate the numerical model RoPES, a distinction will be made between the first and second negative peak in sway, which is not done in the present chapter.

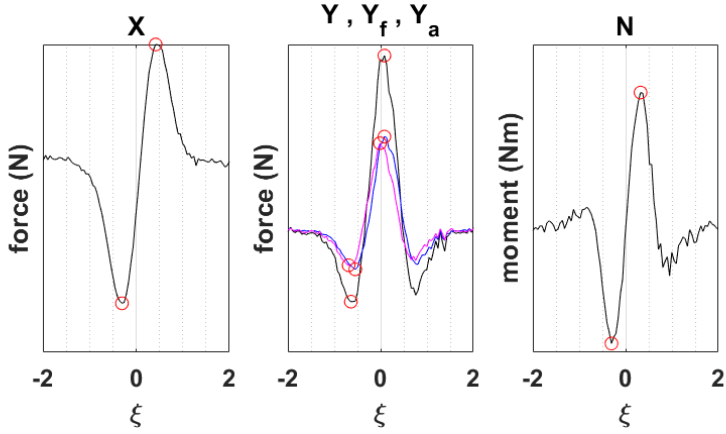

Figure 6.18: *Selection positive and negative peak value from model test signal Passing $C04$, moored $T0Y(J)$, UKC_{p} = 50%, $\frac{d}{B_{\mathrm{p}}}$ = 2.0, $\frac{W}{B_{\mathrm{p}}}$ = 10, V_{FS} = 8 knots. Black, blue and purple give Y, Y_{f} and Y_{a} respectively*

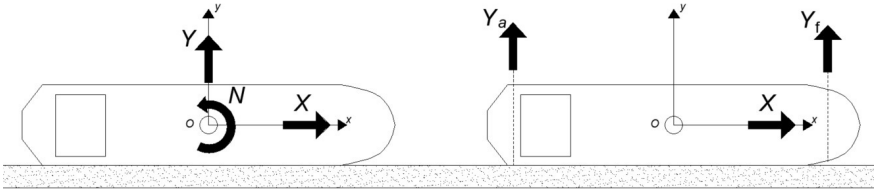

Figure 6.19: *Force representation horizontal plane.*
Left : X, Y, N, right : $X, Y_{\mathrm{f}}, Y_{\mathrm{a}}$.

Reconstructing the time series from a peak value can be done based on known considerations on the general shape of the signal, as presented by [VVL02]. This is out of the scope of this thesis. In line with the discussion regarding moored ship response in the horizontal and vertical plane (section 4.3.1), only the forces in the horizontal plane are studied : surge, sway and yaw.

A regression analysis technique is used to assess the quality of the relationship between one or more independent variables and one dependent variable. The least-squares fitting technique is used in this thesis, as part of the MATLAB *fit toolbox*.

Within this regression approach, an estimation of the dependent variable y is made based on a modelled function $\hat{y}$ of the independent variables x_1,...,x_i,...,x_n (eq. 6.11a). In the least-squares method, the summed square of the residuals is minimized, as given by eq. 6.11b. A common way to evaluate and compare different regression result is by the R^2 value (eq. 6.11c), which is also calculated by MATLAB. The larger R^2 ($R^2 < 1$), the better the model represents the measured variable, or to be more precise the more the variability is explained by the regression model. A high R^2 by itself does not guarantee the most satisfactory regression result. One aspect that it does not cover is possible bias, as the model uses the squared residual. In many regression plots in this thesis, this residual itself ($y_\mathrm{j} - \hat{y}_\mathrm{j}$) is also plotted to deliver additional insight. For the model to be unbiased, the residual should ideally be spread randomly around 0 over all the data points.

$$\hat{y} = f(x_1, ..., x_\mathrm{i}, ..., x_\mathrm{n}) \tag{6.11a}$$

$$S = \sum_{\mathrm{j}=1}^{\mathrm{n}} r_\mathrm{j}^2 = \sum_{\mathrm{j}=1}^{\mathrm{n}} \left(y_\mathrm{j} - \hat{y}_\mathrm{j}\right)^2 \tag{6.11b}$$

$$R^2 = 1 - \frac{\sum_{\mathrm{j}=1}^{\mathrm{n}} \left(y_\mathrm{j} - \hat{y}_\mathrm{j}\right)^2}{\sum_{\mathrm{j}=1}^{\mathrm{n}} \left(y_\mathrm{j} - \mu_y\right)^2} \tag{6.11c}$$

In section 6.5, several functions of type eq. 6.11a are considered, using different regression parameters $\alpha, \beta, ...$, to find the best relationship between forces (dependent variable) and passing distance, UKC, channel width respectively (independent variables). In section 6.6, an empirical model representing the passing ship effects in shallow and confined water is validated by evaluating R^2.

6.5 Effect of passing distance, UKC and channel width on peak forces

The relationship between the individual model test parameters and the measured forces is investigated in this section, using a regression based approach. The function eq. 6.11a can be a very complex formulation. In this thesis, a compromise between high correlation (R^2), but also model simplicity (convenience of use in practice) is sought. As a way to limit complexity of the model, *cross term correlations* are not modelled. An example of this is given in eq. 6.12, where the force (F) is a function of passing distance d, which is in turn a function of UKC (ζ).

$$F = \alpha \cdot d^{(\eta \cdot UKC)} \tag{6.12}$$

The effect of three parameters on the magnitude of the peak passing ship forces is studied:

- The passing distance d (section 6.5.1)
- The effect of UKC (section 6.5.2)
- The channel width W (section 6.5.3)

All sections have the same structure, with a literature review to start followed by the analysis of the PESCA tests and some conclusions to finish.

6.5.1 Passing distance

From literature, but also from general physical insight, the passing ship forces increase when the passing distance decreases. A sign change in the passing ship force, as was seen by [Lat14] when sailing close to banks, is not present. This can be explained due to the limited length of the moored ship, which is an irregular bank shape in a way, but also the fact that the passing distance is limited to $0.4B_{\mathrm{p}}$ as the closest distance, with reduced speed to be a realistic condition.

6.5.1.1 Literature

Table 6.9 shows and compares five literature sources. Two definitions for the passing distance are used, where d is the passing distance side-to-side, s is the distance between the midships. Both are shown on figure 6.20. The second definition, s, partly includes the effect of the beam of the ships. From the viewpoint of application in regression formula, d goes to 0 in the limit, s reaches $B_{\mathrm{m}}/2 + B_{\mathrm{p}}/2$.

The effect of passing distance on passing ship forces seems to be best represented by a power law or an exponential law. Some authors use dimensional representation, others represent the passing distance as a non-dimensional numbers, by dividing the passing distance by the length of the moored ship (in [Kri05] the length of passing and moored ship are equal).

6.5.1.2 PESCA analysis

The PESCA model tests have been performed for a wide range of passing distances (as shown in chapter 6, figure 6.6). For the generation of the model test matrix, the passing distance has been defined as the ratio $\frac{d}{B_{\mathrm{p}}}$. This choice is arbitrary in a way. As explained earlier, the variables are used in dimensional form in the regression analysis. Based on literature, two relationships are presented, a power law eq. 6.13a and an exponential law eq. 6.13b with α a general multiplication factor and β as the regression coefficient for the passing distance.

Table 6.9: *Literature review dependency passing ship forces on passing distance; passing distance represented by d and s (see figure 6.20).*

Source	X	Y	N
[WP08]	d^{-1}	d^{-1}	d^{-1}
[TB14]	d^{-1}	d^{-1}	d^{-2}
[Swi11]	$e^{-0.011s}$	$e^{-0.0115s}$	$e^{-0.0154s}$
[Kri05]	$e^{-1.55\frac{s}{L}}$	$e^{-1.2\frac{s}{L}}$	$e^{-3.4\frac{s}{L}}$
[VV06]	$\left(\frac{s}{L_{\mathrm{m}}}\right)^{-1.3}$	$\left(\frac{s}{L_{\mathrm{m}}}\right)^{-1.3}$	$\left(\frac{s}{L_{\mathrm{m}}}\right)^{-1.3}$

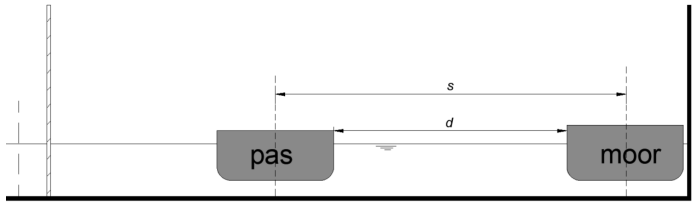

Figure 6.20: *Comparison passing distance side-to-side (d) and midship-to-midship (s).*

Figure 6.21 compares the general shape of both functions, normalised at (1,1). The exponential function is finite when in general x, in this case d, goes to zero, the inverse function moves to infinity for passing distances approaching zero. In this context, it is also important for which interval the expression is used. The inverse relationship cannot be used for zero passing distance, however this distance will never be reached in practice, and thus does not need to be part of the regression model. At passing distance zero, other forces would become more prominent...

$$F = \alpha \cdot (d)^{-\beta} \tag{6.13a}$$

$$F = \alpha \cdot e^{-\beta \cdot d} \tag{6.13b}$$

The effect of passing distance on passing ship force can now be investigated for different moored ships, blockage, force components,... Figure 6.22 shows a result for the negative surge peak ($X-$); Moored $C0P$, $\frac{W}{B_{\mathrm{p}}} = 10$, UKC_{p} = 10%, V_{FS} = 8 kn. All these parameters need to be fixed, in order to study the effect of the passing distance, as dimensional force representations are used. The left hand axis shows measured forces (y_{j}, eq. 6.11b, discrete data points) and modelled regression functions ($\hat{y}$, eq. 6.11a). The residuals (r_{j}, eq. 6.11b) are given on the right hand axis.

Only five points are available here to draw the regression line. It is self-evident that making a model using only four points is not advised, however it gives valuable insight into the preferred regression function. Both inverse and exponential functions perform well here, with R^2 of 0.966 (exponential) and 0.999 (inverse). For low passing

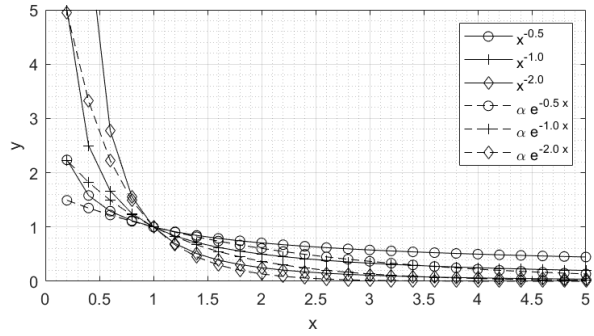

Figure 6.21: *Comparison exponential and inverse function ($y = \mathrm{f}(x)$); all functions are normalised to go through (1,1).*

distances, the inverse curve overestimates the passing ship force. The plot of the residuals (right axis) shows positive as well as negative data points, which means there is no obvious bias present.

Figure 6.23 shows a regression result for the positive sway peak ($Y+$); Moored $T0Y$ for 10% UKC_{p} . Both curves are satisfactory in use, with the inverse model outperforming the exponential model (R^2 of 0.962 and 0.930 respectively), based on six points. One data point (d around 2 m) is not following the general tendency. The closest passage (1 m) shows a large increase in force, favouring the inverse relationship in this case.

For the narrow sections, at low UKC, other effects become prominent, next to the effect of the passing distance. One important aspect here is the behaviour of the passing ship, which sails close to the opposite bank when the passing distance becomes larger. Figure 6.24 shows the regression result for such a case. On the left axis, it is clearly visible that the magnitude of the positive surge peak ($X+$) is hardly affected by the passing distance. The R^2 for power and exponential law is 0.724 and 0.563 respectively. The β values are 0.0432 and 0.0608, which means that there is only a weak correlation present.

Figure 6.25 shows the β values for the different force components and the two regression relationships. In total, 232 regressions were performed for each component and relationship, over all environ-

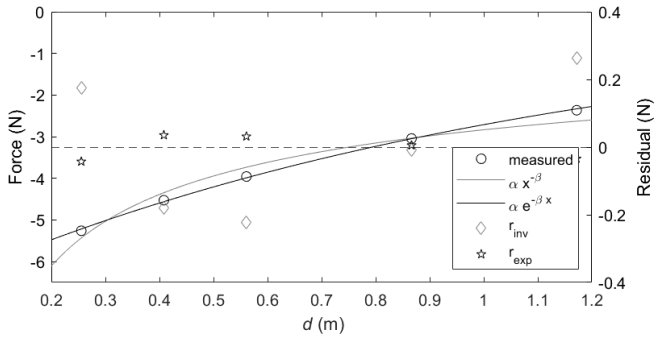

Figure 6.22: *Regression model passing distance for negative surge force ($X-$); passing $C04$, moored $C0P$, $\frac{W}{B_{\mathrm{p}}} = 10$, UKC_{p} = 50%, V_{FS} = 8 kn; left axis : Measured (y_{j}) and modelled ($\hat{y}$) force right axis : residual r_{j}*

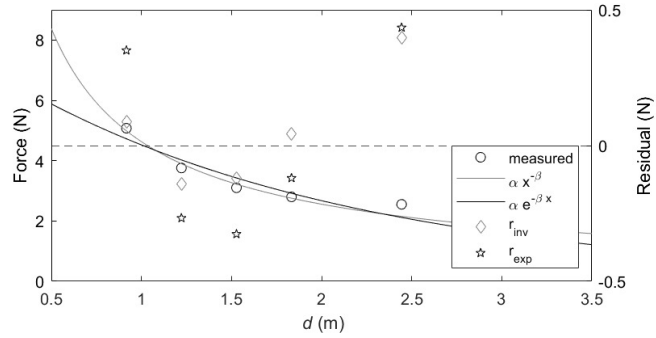

Figure 6.23: *Regression model passing distance for positive sway force ($Y+$); passing $C04$, moored $T0Y(Q)$, $\frac{W}{B_{\mathrm{p}}} = 10$, UKC_{p} = 10%, V_{FS} = 10 kn. left axis : Measured (y_{j}) and modelled ($\hat{y}$) force right axis : residual r_{j}*

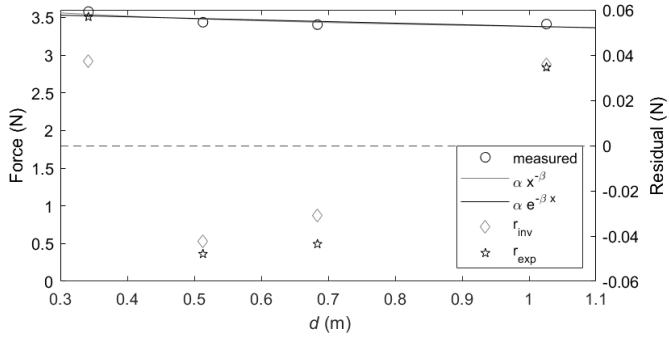

Figure 6.24: *Regression model passing distance for positive surge force ($X+$); passing $E01$, moored $B01(Q)$, $\frac{W}{B_{\mathrm{p}}} = 4$, UKC_{p} = 10%, V_{FS} = 6 km/h.*
left axis : Measured (y_{j}) and modelled ($\hat{y}$) force
right axis : residual r_{j}

ments (Table 6.6). A minimum of four data points is required, except for the $D03D04$ case in the small channel widths, where 3 passing distances are acceptable to perform the regression. For each variable and regression relationship, a box is displayed which represents the interval in which 50% of the results are situated. The red line is the median, the top and bottom edges of the box are the 75% and 25% percentile respectively. This representation is similar to a 'boxplot'. However, the values which are traditionally seen as 'outliers' (blue circles), are in this case all correct regression results. Figure 6.24 gave an example and explanation of such result where a weak correlation (small β and R^2) between passing distance and measured force is present.

The following observations are made (figure 6.25 and figure 6.26).

- The surge and yaw force can be better predicted than the yaw moment
- In most cases, the spread on the β value is smaller for the exponential model compared to the inverse model, making it more suitable for use in a general regression formula.
- The behaviour of the negative and positive force peak is similar, meaning that one β value suffices to predict both peaks

- In literature (table 6.9), most authors agree that the sway and yaw forces increase faster as the passing distance decreases compared to the surge force. Figure 6.25 indeed shows a similar trend (larger β on average for yaw compared to surge and sway), but the distinction is not as clear as made in literature.

Figure 6.26 gives the R^2 value for the regression analysis. The surge and sway perform consistently better than the yaw, which could already be predicted based on the spread in β values in figure 6.25. The exponential and inverse model both attain high correlation coefficients in most cases.

6.5.1.3 Conclusion

The regression analysis on the dimensional passing ship forces confirms the general trends which were observed in literature. The exponential model performs better than the inverse relationship on average, yet it is shown that for low UKC, the inverse relationship could better predict the increase in passing ship forces with reduced passing distance. The yaw moment is most influenced by the passing distance, however the difference is not as pronounced as observed in literature.

In the analysis, all passing distances were expressed side-to-side in dimensional form. Further investigation can include a model based on midship-midship passing distance. Using a non-dimensional passing distance (e.g. $\frac{d}{B_\mathrm{p}}$) would affect the relationships defined in eq. 6.13 as given by eq. 6.14. In the inverse relationship, the multiplication constant (α) is affected; In the exponential function, the coefficient β is affected.

$$F = \alpha \cdot (\frac{d}{B_\mathrm{p}})^{-\beta} = \alpha \cdot (\frac{1}{B_\mathrm{p}})^{-\beta} \cdot (d)^{-\beta} = \alpha' \cdot (d)^{-\beta} \tag{6.14a}$$

$$F = \alpha \cdot e^{-\beta \cdot \frac{d}{B_\mathrm{p}}} = \alpha \cdot e^{-d \cdot \frac{\beta}{B_\mathrm{p}}} = \alpha \cdot e^{-\beta' \cdot d} \tag{6.14b}$$

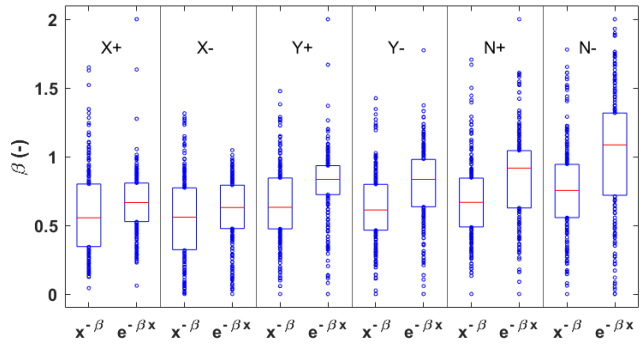

Figure 6.25: *Visualisation β for six force peaks ($X+$,$X-$,$Y+$,$Y-$,$N+$,$N-$); inverse ($x^{-\beta}$) and exponential ($e^{-\beta x}$) relationship. Box indicates 75%, 50% and 25% data percentile. 12 times 232 regressions*

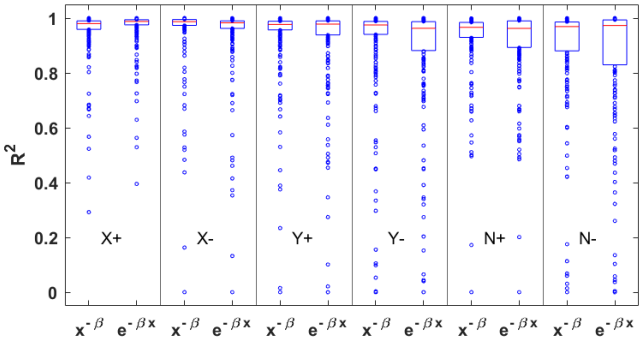

Figure 6.26: *Visualisation R^2 (d regression) for six force peaks ($X+$,$X-$,$Y+$,$Y-$,$N+$,$N-$), inverse ($x^{-\beta}$) and exponential ($e^{-\beta x}$) relationship. Box indicates 75%, 50% and 25% data percentile. 12 times 232 regressions*

6.5.2 UKC

The effect of a smaller under keel clearance on passing ship behaviour, as well as interaction forces is also generally known : a smaller UKC means a reduction in the available cross section, resulting in higher return flows and thus large forces. How these forces, on the moored ship, vary in function of the water depth is discussed in this section.

6.5.2.1 Literature

In most applications, the term shallow water is used when the ratio h/T_{M} drops below 4 [ITT14a]. In the $PESCA$ test program, this ratio ranges from 1.5 to 1.1, indicating very shallow water and the expectancy of large effects on the magnitude of passing ship forces. In the specific case of passing ship interaction, the shallow water effect manifests in three ways, which all contribute to the resulting passing ship force.

1. The change in flow field around the moving ship. This causes change in squat and resistance amongst others.
2. The change in the moving pressure system which eventually causes forces on the moored ship.
3. The change in flow field around the moored ship, which impacts the pressure distribution around the ship and thus the forces caused by the moving ship.

Table 6.10 gives an overview of the proposed relationships between h, T_{M} and passing ship forces in literature, which need to be compared to the definition of UKC used in this thesis, as $\frac{h/T_{\mathrm{M}}}{T_{\mathrm{M}}}$. $\frac{T_{\mathrm{M}}}{h}$ and $\frac{h-T_{\mathrm{M}}}{T_{\mathrm{M}}}$ are used as terms in the empirical relationships found in literature. The last expression corresponds to the UKC definition used in this thesis. Furthermore, exponential and inverse relationships are defined, as was the case for passing distance (table 6.9).

The literature also indicates that there is a distinction between surge force on the one hand, and sway and yaw on the other hand. The sway force and yaw moment increase considerably more with decreasing under keel clearance, compared to the surge force. This

is also observed by other authors [Den+15b]. Most sources agree that the draft of the moored ship has the biggest impact on the passing ship forces. [Cap12] shows that, certainly for the transversal forces, the UKC of the moored ship indeed has the biggest impact on the passing ship forces. He also observed that for h/T = 1.05, the passing ship forces seem to decrease again. This is in line with the observations made by [Lat14], that trend (and even sign) changes can occur in extremely shallow water conditions. These extremely shallow water conditions are not studied here.

6.5.2.2 PESCA analysis

Two elements need to be looked into: the expression for the relative clearance under the keel, as well as the type of relationship. Three relationships are proposed in eq. 6.15. The expressions are written so that a positive γ indicates an increase in force with decreasing UKC, which is what we expect based on the effect of the reduced flow section. Figure 6.27 visualises these expressions, their value for deep and shallow water is given in table 6.11. Considering that for infinite water depth, the effect should tend to zero, $\frac{T_{\mathrm{M}}}{h-T_{\mathrm{M}}}$ is a good candidate. The linear relationship $\frac{T_{\mathrm{M}}}{h}$ represents a more limited increase in force.

In the analysis, the draft of the passing ship is used to define the clearance underneath the keel. For most ship interactions, the draft of the moored and passing ship is equal (or close to equal for $T0Y$ and $C04$.) For the moored $T0H$, an expansion of this research could include comparing the regression for both drafts.

$$F = \alpha \cdot \left(\frac{T_{\mathrm{M,p}}}{h} \right)^{\gamma} \tag{6.15a}$$

$$F = \alpha \cdot e^{\gamma \frac{T_{\mathrm{M,p}}}{h}} \tag{6.15b}$$

$$F = \alpha \cdot \left(\frac{T_{\mathrm{M,p}}}{h - T_{\mathrm{M,p}}} \right)^{\gamma} = \alpha \cdot (UKC_{\mathrm{p}})^{-\gamma} \tag{6.15c}$$

A comparison of the behaviour of the three proposed models (eq. 6.15) is given in figures 6.28 (γ) and 6.29 (R^2). The regression quality is best for the sway force (largest R^2). The prediction of the yaw

Table 6.10: *Literature review dependency passing ship forces on UKC*

Source	X	Y	N
[Flo02][1]	$e^{0.0955-0.6367\frac{h-T_{\mathrm{M}}}{T_{\mathrm{M}}}}$	$e^{0.5157-0.3438\frac{h-T_{\mathrm{M}}}{T_{\mathrm{M}}}}$	$e^{0.343-2.288\frac{h-T_{\mathrm{M}}}{T_{\mathrm{M}}}}$
[Swi11][2]	$\left(\frac{h}{T_{\mathrm{M}}}\right)^{-1.5}$	$\left(\frac{h}{T_{\mathrm{M}}}\right)^{-3.1}$	$\left(\frac{h}{T_{\mathrm{M}}}\right)^{-2.3}$
[Kri05][3]	$e^{2.6\frac{T_{\mathrm{M}}}{h}}$	$e^{3.6\frac{T_{\mathrm{M}}}{h}}$	$e^{3.2\frac{T_{\mathrm{M}}}{h}}$
[VV06][3]	$(\frac{h}{T_{\mathrm{M}}})^{-1}$	$(\frac{h}{T_{\mathrm{M}}})^{-1}$	$(\frac{h}{T_{\mathrm{M}}})^{-1}$

[1] *mentions that T_{M} can be either draft of moored or passing ship, whichever is greatest* [2] *used a velocity dependency of power 2.32, which is more than the quadratic dependency (Bernoulli), which in a way already takes into account a reduced flow section, whether it is due to shallowness or confinement.* [3] *T_{M} is the draft of the moored ship*

Table 6.11: *Three different non-dimensional representations of UKC and their behaviour for limit $h \to +\infty$ and $h \to T_{\mathrm{M}}$*

formulation	$\lim_{h\to+\infty}$	$\lim_{h\to T_{\mathrm{M}}}$
$\frac{T_{\mathrm{M}}}{h}$	0	1
$\frac{T_{\mathrm{M}}}{h-T_{\mathrm{M}}}$	0	$+\infty$
$\frac{h}{h-T_{\mathrm{M}}}$	1	$+\infty$

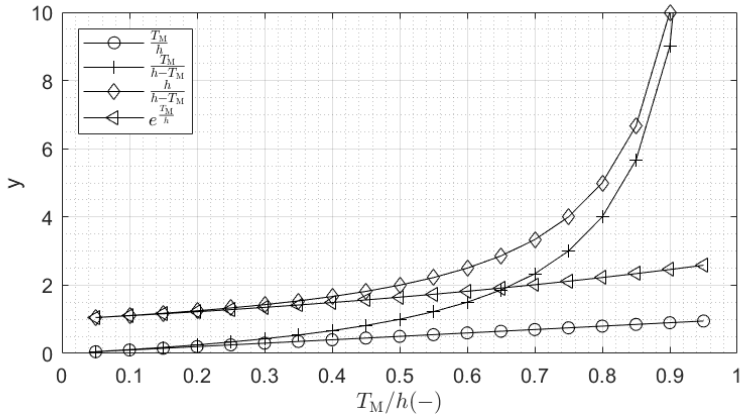

Figure 6.27: *Comparison non-dimensional representations of clearance underneath the keel.*

moment is less good. Overall, the third model gives the highest R^2 for sway and yaw. For the surge force, models 1 and 2 are slightly favoured. When looking at the spread on γ, the first two models show high γ factors (up to 5 within 75 % percentile), with a significant spread. This confirms the higher-order dependency of forces on UKC, especially sway and yaw.

6.5.2.3 Conclusion

The effect of UKC on passing ship forces is significant, as was already observed in literature. Using $\frac{T_{\mathrm{M,p}}}{h-T_{\mathrm{M,p}}}$ (=UKC_{p}^{-1}), in combination with a power law (eq. 6.15c) gives the best regression result (high R^2 combined with narrow range of γ), with a stronger dependency of sway and yaw on UKC. When comparing with literature, the proposed relationship would be a combination of [Flo02] definition of UKC and [Swi11] power law.

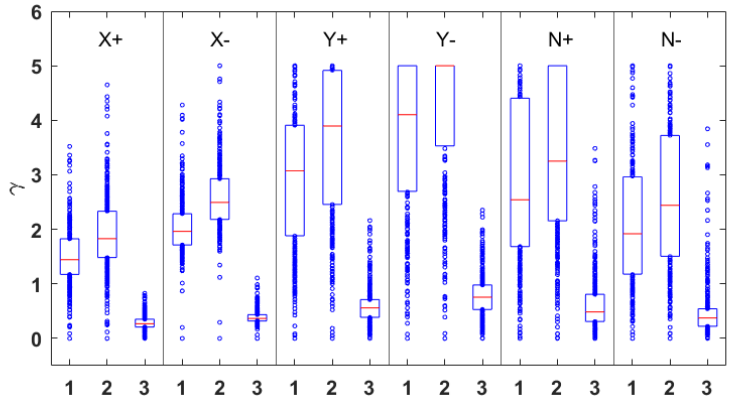

Figure 6.28: *Visualisation γ for six force peaks ($X+$,$X-$,$Y+$,$Y-$,$N+$,$N-$),*
(1) $\left(\frac{T_{\mathrm{M,p}}}{h}\right)^{\gamma}$ (2) $e^{\gamma\frac{T_{\mathrm{M,p}}}{h}}$ (3) $\left(\frac{T_{\mathrm{M,p}}}{h-T_{\mathrm{M,p}}}\right)^{\gamma}$
Box indicates 75%, 50% and 25% data percentile.
18 times 318 regressions

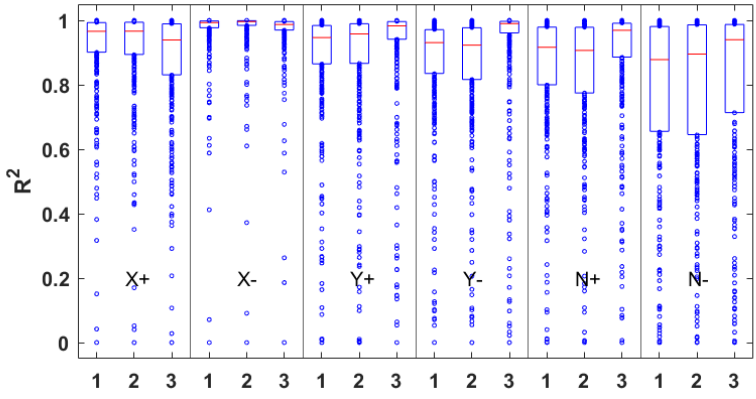

Figure 6.29: *Visualisation R^2 (UKC regression) for six force peaks ($X+$,$X-$,$Y+$,$Y-$,$N+$,$N-$) (1) $\left(\frac{T_{\mathrm{M,p}}}{h}\right)^{\gamma}$ (2) $e^{\gamma\frac{T_{\mathrm{M,p}}}{h}}$ (3) $\left(\frac{T_{\mathrm{M,p}}}{h-T_{\mathrm{M,p}}}\right)^{\gamma}$*
Box indicates 75%, 50% and 25% data percentile.
18 times 318 regressions

6.5.3 Channel width

The effect of the channel width is commented on by several authors. Most research efforts only include two different channel widths, which does not allow a regression relationship to be drawn up. The channel width effect on the passing ship forces is present for both jetty as well as quay mooring, hence why both mooring types were also addressed within $PESCA$ for the moored $T0Y$.

Next to the total channel width, the distance between moored ship in jetty configuration (figure 2.8) and nearest channel wall is also given whenever it is made available in literature.

6.5.3.1 Literature

The magnitude of the passing effect is different for quay and jetty mooring, given all other parameters are equal, as was already shown in figure 2.7. This distinction is well known from literature ([Swi11], scale model tests; [Pin04] [Mol+11], numerical models). The current discussion focusses on the effect of channel width on quay mooring and the effect of channel width on jetty mooring.

Tables of the form of table 6.9 and 6.10 cannot be produced, as regression relationships are not available from literature. Many authors however have shared insights on the effect of channel width on passing ship forces, which are summarized below. In order to be able to compare the results with $PESCA$, the channel width is expressed as multiples of the beam of the passing ship.

[TB14] state that no significant influence of the channel width on the passing ship forces could be distinguished. The cross sections studied have a width of 11.11, 9.34 and 7.94 B_{p}.

[Cap12] has examined the same model tests as [TB14] and does see up to a 25 % increase between 11.11 B_{p} and 7.94 B_{p} channel width. The author does state that in general however, the effect is small for the tested cases, which is a similar conclusion to [TB14].

[Swi11] is the only reference which presents relationships between different channel configurations, for the three force components. One test series was performed in jetty condition, with $12.5B_{\mathrm{p}}$ distance between moored ship and closest wall. In quay mooring, three channel

widths were modelled, 6,9 and 12 times B_{m} (or 4.8, 7.2 and 9.6 B_{p}). The force ratios are given in table 6.12. The author does not make a distinction between 7.2 and 9.6 B_{p} when it comes to passing ship forces. When the channel width is decreased, the surge force increases significantly (1.37). Yaw also increases (1.23), sway on the other hand slightly decreases (0.91). [Mol+11] analysed a subset of these tests and concluded that the surge increases with decreasing channel width, whereas the impact on sway and yaw is limited.

[Den+15b] did experiments with a wide channel (jetty mooring) and a narrow channel (quay mooring). It is observed that the surge forces increase significantly, whereas sway and yaw decrease. Of course, both observations include combination of quay to jetty and change of channel width might thus disguise the effect of channel width on its own.

6.5.3.2 PESCA analysis

The values identified by [Swi11] (table 6.12) can be used to compare with PESCA observations. Based on PESCA tests, table 6.13 is generated. The ratios of the force peak (positive and negative) are shown for several channel configurations. J10 and J6 are the jetty configurations (figure 2.8, bottom) with channel width ten and six times the beam of the passing ship. Q10, Q6, Q4, Q3 are the quay mooring configurations (figure 2.8, top) with channel width ten, six, four and three times the beam of the passing ship. As an example, the first line of the table, Q10/J10, expresses the ratio of the peak forces between the quay (Q) configuration and jetty (J) configuration, each for channel width ten times the beam of the passing ship.

Note that the widest inland section is in fact 11.46 B_{p}, which is the full width of the tank (7.0 m). [Swi11] and [Cap12] however already observed that the influence of channel width on passing ship forces is limited for larger sections. Therefore, these tests are also defined as Q10 for the analysis given in table 2.8. Each ratio expressed in table 6.13 is discussed below.

The distinction between positive and negative peak force is limited for most cases. However, for surge and yaw, the negative force peak is influenced more by the change in channel width compared to the positive peak. In the $PESCA$ tests, the negative peak for surge is

Table 6.12: *Effect of channel width on passing ship forces (from [Swi11], table 3-3)*

case	X	Y	N
jetty $\rightarrow$ quay (7.2-9.6 B_{p})*	1.92	0.34	0.43
open water $\rightarrow$ quay (4.8 B_{p})	2.63	0.31	0.33
quay (7.2-9.6 B_{p}) $\rightarrow$ quay (4.8 B_{p})**	1.37	0.91	1.23

**The table actually says "Transform quay walls, 12B and 9B channels to open water", which would then be the opposite of what it should be (surge will always increase from jetty to quay mooring). As the thesis text refers to [Pin04] and says it confirms their findings, the assumption is made that the table description is either wrong or there is a linguistic issue*
***These numbers were based on the first two rows of the table and were not directly given by the author*

the first peak, the positive peak is the second peak (figure 6.18). The difference is largest for Q3/Q10, which is the most extreme case, with only 21 data points in total to obtain the general force ratio. This distinction between positive and negative force peak is further addressed in section 7.4. For the current discussion, the positive and negative peaks are averaged, leading to the second part of the table.

The Q10/J10 ratio from table 6.13 can be compared with the first line of table 6.12. The sway and yaw factors are in good agreement, the increase in surge in the PESCA tests is lower (on average) compared to the tests by [Swi11] (1.52 and 1.92 respectively). In the test program of [Swi11], the water body next to the moored ship in the open water condition was larger than in PESCA tests however, which can explain this difference to a certain extent.

The Q10/Q4 ratio from table 6.13 can be compared with the third line of table 6.12. The PESCA tests predict a lower increase in surge force due to the reduction in channel width. The sway and yaw increase significantly in the $PESCA$ analysis, which was not observed by [Swi11], who even observed a decrease in sway force.

Comparison between Q10/Q6 and J10/J6 in table 6.13 shows that the effect of confinement on the passing ship forces are on average similar for quay and jetty configuration, which was not observed in

the literature.

Q3/Q10 ratios are high, up to 2.43 for the surge force. This shows that in very narrow channels, which are then rivers and canals for inland ships, the effect of horizontal confinement on passing ship forces is, on average, more than a factor of two.

In the absence of any empirical formula to account for the influence of channel width on passing ship force, a first effort is made here. In PESCA, the number of channel widths tested for each moored ship are limited to three, meaning that the results of a regression effort should be treated with great modesty. From the analysis in table 6.13 it is clear that the forces increase considerably for narrow channels. For wider channels, the influence of a change in channel width is limited. The exponential and inverse relationships, both of which are capable of representing the above qualitative description of the model, are presented as regression formulas (eq. 6.16).

$$F = \alpha \cdot W^{-\delta} \tag{6.16a}$$

$$F = \alpha \cdot e^{-\delta \cdot W} \tag{6.16b}$$

The data analysis for regression parameter δ and R^2 are given in figures 6.30 and 6.31. The regression parameters differ for the force components (X, Y, N), which was already visible in table 6.13. The spread on δ for the inverse relationship is higher compared to the exponential relationship. For both regression functions, significant outliers are observed, even with a sign change for Y and N, which would indicate that an increase in channel width would lead to larger forces. Figure 6.32 shows an example where the surge force peak is higher for a channel width of 10 B_{p}, compared to 6 B_{p}. The measured forces however are small, meaning that the identified trend is uncertain.

6.5.3.3 Conclusion

As the effect of channel width on passing ship forces has not been investigated systematically in literature, no regression relationships had been established. A comparison of peak forces between two channel widths however is available and compared with $PESCA$ observations. The difference between quay and jetty mooring was confirmed, as was done in literature already. The significant increase in surge force with decreasing channel width was confirmed,

Table 6.13: *Effect of channel width on passing ship forces based on analysis PESCA model tests.*

case	n_{test}	X+	X-	Y+	Y-	N+	N-
Q10/J10	105	1.54	1.51	0.49	0.37	0.40	0.43
Q6/Q10	326	1.20	1.25	1.22	1.13	1.15	1.32
Q4/Q10	168	1.62	1.80	1.51	1.46	1.21	1.77
Q3/Q10	21	2.21	2.64	1.85	1.71	1.27	1.72
J6/J10	73	1.26	1.29	1.23	1.28	1.20	1.22

case	n_{test}	X	Y	N
Q10/J10	105	1.52	0.42	0.41
Q6/Q10	326	1.23	1.17	1.24
Q4/Q10	168	1.71	1.49	1.49
Q3/Q10	21	2.43	1.78	1.49
J6/J10	73	1.28	1.26	1.21

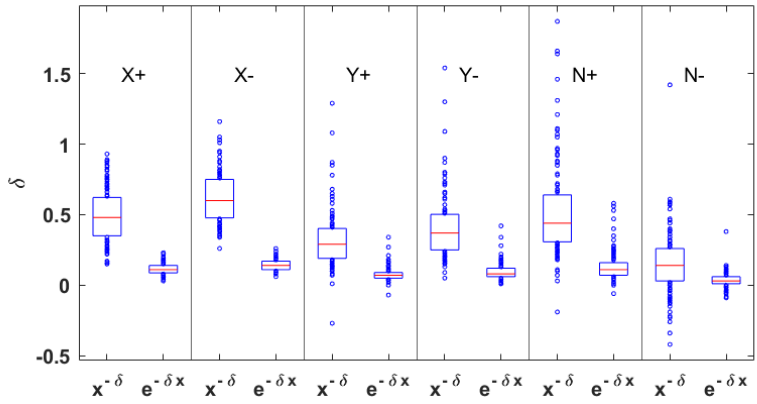

Figure 6.30: *Visualisation δ for six force peaks ($X+, X-, Y+, Y-, N+, N-$), inverse ($x^{-\delta}$) and exponential ($e^{-\delta x}$) relationship. Box indicates 75%, 50% and 25% data percentile. 12 times 113 regressions*

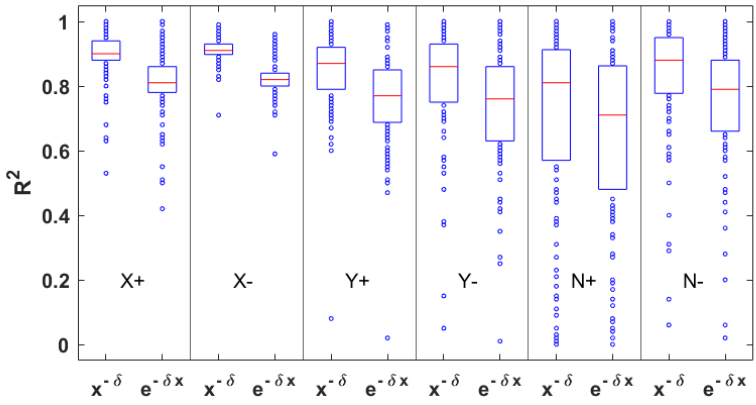

Figure 6.31: *Visualisation R^2 (W regression) for six force peaks ($X+$,$X-$,$Y+$,$Y-$,$N+$,$N-$), inverse ($x^{-\delta}$) and exponential ($e^{-\delta x}$) relationship.*
Box indicates 75%, 50% and 25% data percentile.
12 times 113 regressions

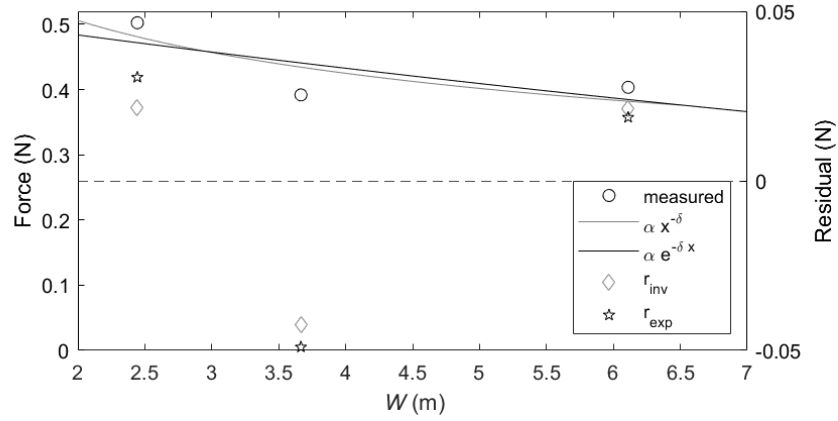

Figure 6.32: *Regression model channel width for positive surge force ($X+$) passing $C04$, moored $C0P$, UKC_{p} = 10%, $\frac{d}{B_{\mathrm{p}}} = 0.67$, V_{FS} = 2 km/h.*
left axis : Measured (y_{j}) and modelled ($\hat{y}$) force
right axis : residual r_{j}

with slightly smaller increase compared to literature. For sway and yaw, literature predicted a status-quo with decreasing channel width. $PESCA$ analysis shows that for these forces and small channel widths, there is also a significant increase in forces, albeit smaller than for surge.

An attempt at defining a regression relationship for channel width influence proves to have limited success, certainly compared to the results obtained for passing distance and UKC.

6.5.4 Overall conclusion regression analysis

The limitation of the relationships developed above, certainly for UKC and channel width, is that they are based on a limited amount of data points for each regression variable. At most, four UKC and three channel width variations have been tested for a given ship-ship interaction. Regression results could be enhanced by using different regression models and/or limiting the values of variables to certain intervals. Adding weight functions could also lead to a model which is most representative in the area of interest. e.g. a model which works best in the range of $1.5B_{\mathrm{p}}$ to $3.5B_{\mathrm{p}}$ passing distance. These methods have not been further explored within this thesis work.

Non-dimensionalisation of the variables could assist to get more points to base the regression on, however it adds complexity and makes it harder to assess the value of the model. This is in line with literature, where either they mention that the number of tests are limited, or they did not formulate any empirical relationships (e.g. channel width).

The size and form of the $PESCA$ dataset however gives a unique opportunity to assess the combined effect of UKC and channel width, expressed as section blockage. In the next section an empirical model representation of such a relationship is presented.

6.6 Empirical model modified Tuck number

The modelling approach presented here is based on the work performed in [Lat14], where a mathematical model was built to assess the effect of the presence of banks on hull forces, for a ship with a non-zero forward speed. In the current thesis work, the forces on the moored ship are in fact of interest, however, the general intent is similar : assessing the effect of a confinement of the waterway on the generated pressure field and its effect on the moored ship.

6.6.1 Definition and background modified Tuck number

The Tuck number was introduced in [Tuc66]. It is a relationship based on the Froude Depth Number (eq. 6.3), which has an asymptotic behaviour for Fr_h = 1. The Tuck Number , Tu, is given by eq. 6.17. This relationship is visualised in figure 6.33 (a). This function looks promising as a representation of the influence of speed and water depth on the forces, similar to the inverse UKC relationship developed in section 6.5.2.

[Lat14] recognised the usefulness of Tu to express the effect of reduced flow section on forces. This however only comprised the effect of the vertical flow section (water depth). In order to add the effect of a horizontal confinement, the Tuck Number was modified, as given by eq. 6.18 (figure 6.33 (b)), where the asymptote becomes (Fr_{crit}). In the analysis, the blockage used in the formulation of Fr_{crit} (Eq. 6.4) is the one of the continuous section, so only taking into account the section of the passing ship. This blockage is more representative for the general pressure distribution around the passing ship, which affects the moored ship, rather than the temporary change due to presence of the moored ship.

The use of Tu_{m} in the regression analysis means that the relationship between passing ship force and speed, water depth and blockage is accounted for, without the need to define regression parameters. The model test measurements are then used to validate the proposed relationship. The advantage of having a predefined relationship however also leads to its biggest disadvantage : It does not allow individual relationships for UKC and channel width to be formulated, as was presented above. On the contrary, it fixes how water

depth, speed and blockage interact in the empirical relationship.

$$Tu(Fr_h) = \frac{{Fr_h}^2}{\sqrt{|1 - {Fr_h}^2|}} \tag{6.17}$$

$$Tu_m(Fr_h, Fr_{\text{crit}}) = \frac{\left(\frac{Fr_h}{Fr_{\text{crit}}}\right)^2}{\sqrt{|1 - \left(\frac{Fr_h}{Fr_{\text{crit}}}\right)^2|}} \tag{6.18}$$

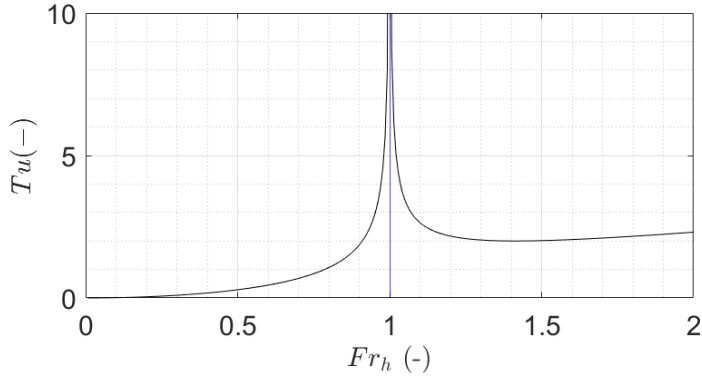

(a) Tu in function of Fr_h.

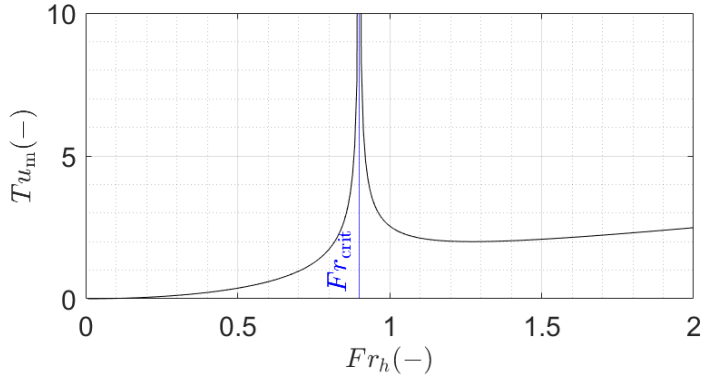

(b) Tu_{m} in function of Fr_h.

Figure 6.33: *Visual representation of* Tu *and* Tu_{m}.

6.6.2 Validation Modified Tuck model

As explained above, the Modified Tuck Model is an established relationship on its own, which now needs to be validated using the $PESCA$ measurements. One aspect which is not covered by Tu_{m} is the effect of the passing distance. The exponential relationship from eq. 6.13b is used to model this effect. The corresponding relationship is shown in eq. 6.19

$$F = \alpha \cdot e^{-\beta \cdot d} \cdot Tu_{\mathrm{m}} \tag{6.19}$$

The quality of this relationship can be assessed by calculating the regression coefficients for the different moored and passing ship interactions, using the least-squares regression model from eq. 6.11. The resulting R^2 values for $X+, X-, Y+, Y-, N+, N-$ are given in table 6.14. The results in the table can be subdivided into three regions.

1. For $X+, X-$, the R^2 values are in the interval [0.90, 0.98], indicating that Tu_{m} can predict the effect of speed and blockage on the forces. Figure 6.34 (a) shows a good regression for $X+, C0P$, $R^2 = 0.96$. The left plot shows the absolute value of the measured ($|F_{meas}|$) versus the modelled ($|F_{reg}|$) force. A line with slope 1:1 is added, where $|F_{meas}| = |F_{reg}|$. The right side of the figures shows the residual ($|F_{meas}| - |F_{reg}|$), for all the model tests in the regression (263 in this case, see also table 6.14).

2. For the $T0Y$ moored in jetty configuration, the Tuck model is satisfactory in predicting all force peaks. Figure 6.34 (b) shows the regression analysis for $Y+$. The point cloud for larger forces seems to deviate slightly from the ideal 1:1 slope.

3. For all other ships moored at a quay, $Y+, Y-, N+, N-$ predictions are not good. Figure 6.34 (c) gives the result for $Y+$ for the $T0Y$ quay mooring, which can be compared directly to figure 6.34 (b). This is investigated in more detail in the next section.
   Especially for the moored $B01$, the regression result is poor. This ship was part of the first test program which was executed as part of $PESCA$, where it was noticed that the load cells (LC, figure D.10) showed some slack after consecutive days of running tests. This mainly impacts the transversal force

measurement (Y, N). For the subsequent batch series, quality checks were executed to avoid this unwanted response of the load cells.

Table 6.14: *R^2 for Tu_{m} model (eq. 6.19) for six force peaks $(X+, X-, Y+, Y-, N+, N-)$.*

case	n_{test}	X+	X-	Y+	Y-	N+	N-
$C0P$ (Q)	263	0.96	0.97	0.75	0.54	0.69	0.63
$T0H$ (Q)	489	0.89	0.90	0.55	0.55	0.75	0.58
$T0Y$ (Q)	263	0.93	0.97	0.69	0.62	0.65	0.63
$B01$ (Q)	263	0.95	0.95	0.24	0.25	0.23	0.22
$D03D04$ (Q)	172	0.93	0.94	0.57	0.63	0.66	0.71
$T0Y$ (J)	249	0.96	0.98	0.91	0.89	0.96	0.93

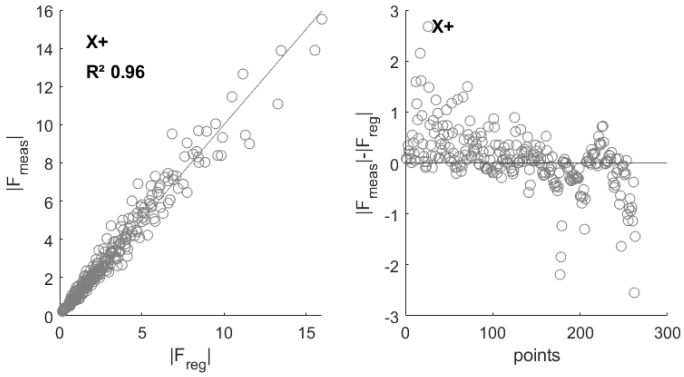

(a) $X+$, passing $C04$, moored $C0P$(Q), 263 tests.

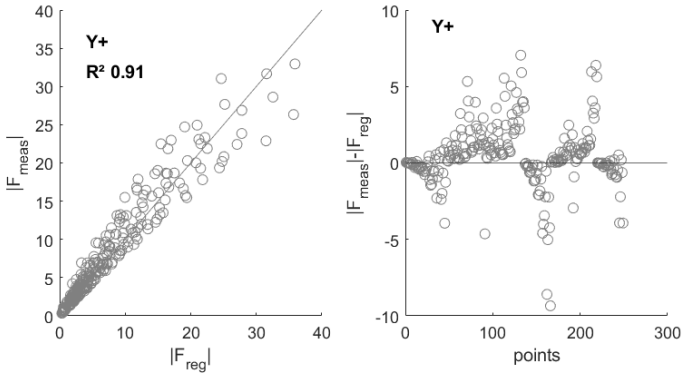

(b) $Y+$, passing $C04$, moored $T0Y$(J), 249 tests.

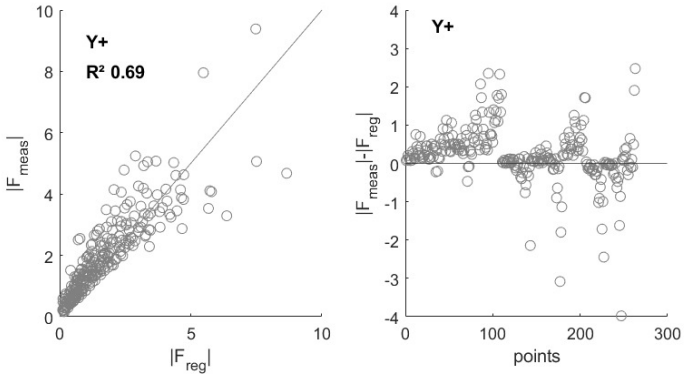

(c) $Y+$, passing $C04$, moored $T0Y$(Q), 263 tests.

Figure 6.34: *Regression analysis Tu_{m} (eq. 6.19)*
Left : Comparison measured (F_{meas}) and modelled (F_{reg}) force
Right : Plot of residuals (F_{meas}-F_{reg})

6.6.3 Modified Tuck for modelling sway and yaw forces

The shortcoming in the Modified Tuck model can be addressed by analysing the residuals from figure 6.34 (b) (right side) in more detail. Figure 6.35 shows the same residuals, divided by the measured value F_{meas}. The vertical lines indicate different environments (W,UKC). The red lines show the average of the residuals within each environment. The blue lines show the average per individual channel width (10, 6 and 4 B_{p}).

The red lines show that the Tu_{m} model cannot fully represent the effect of UKC for $Y+$. This is in line with the observations in section 6.5.2, showing the higher order (γ) dependency on UKC (figure 6.28) for sway (and yaw) compared to surge.

The blue lines show that in fact the effect of channel width is overpredicted by Tu_{m} (level of blue line decreases with decreasing channel width). Section 6.5.3 already predicted this effect, as it was stated that the effect of channel width on sway and yaw is smaller compared to surge.

These observations can be taken into account by expanding the Tu_{m} model with factors to model the effect of UKC (eq. 6.15c) and channel width W (eq. 6.16a), forming eq. 6.20. The result of this regression analysis is given in table 6.15. The table given the values for all regression parameters (α, β, γ, δ), as well as the resulting R^2 values for each force component.

$$F = \alpha \cdot e^{-\beta \cdot d} \cdot UKC^{-\gamma} \cdot W^{-\delta} \cdot Tu_{\mathrm{m}} \tag{6.20}$$

When looking at the R^2 values, which can be compared with the ones from table 6.14 (row $T0Y$(Q)), all results improve. For surge, the Tu_{m} model already provides a really good fit, the results further improve from 0.93 and 0.97 to 0.97 and 0.99 for $X+$ and $X-$ respectively. For sway and yaw, the increase in R^2 is significant, with an increase from 0.69 to 0.86 for $Y+$.

The γ parameters are positive for sway and yaw, meaning that the effect of UKC was indeed underpredicted and could use an extra regression parameter. For surge, the values are negative, meaning that Tu_{m} actually slightly overestimates the effect of UKC on surge. The values of the coefficients for surge however are low, which means that the correction is not that significant.

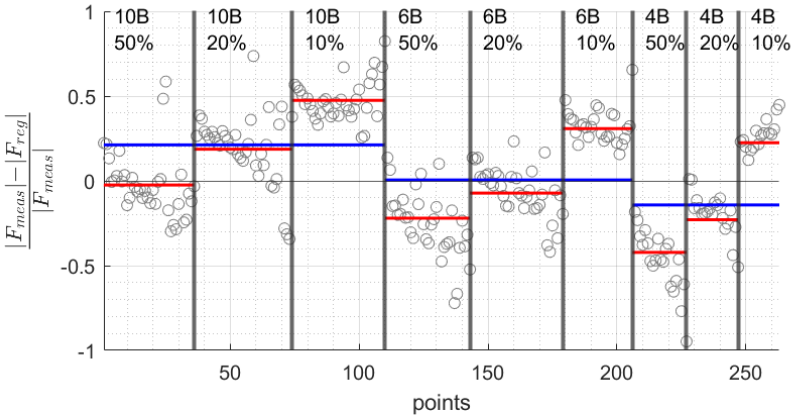

Figure 6.35: *Plot of non-dimensional residuals $T0Y,Q,Y+$ ($R^2 = 0.69$) with indication environment W,UKC, 263 model tests.*

δ is actually significant for all parameters. For surge, this could be expected from section 6.5.3 as the effect of horizontal confinement is large on the surge force. For sway and yaw, in combination with the UKC correction, the δ value is also positive.

Figure 6.36 shows the performance of the model eq. 6.20, which can be directly compared to figure 6.34.

Table 6.15: *Regression result (α,β,γ,δ,R^2) for Tu_{m} model, with additional terms for UKC and W (eq. 6.20), moored $T0Y$ in quay configuration (263 tests).*

parameter	X+	X-	Y+	Y-	N+	N-
α	14.82	-18.35	5.29	-3.41	3.28	-1.32
β	0.71	0.69	1.13	0.94	0.87	0.80
γ	-0.13	-0.01	0.28	0.60	0.33	0.15
δ	0.38	0.25	0.53	0.19	0.18	0.61
R^2	0.97	0.99	0.86	0.87	0.74	0.75

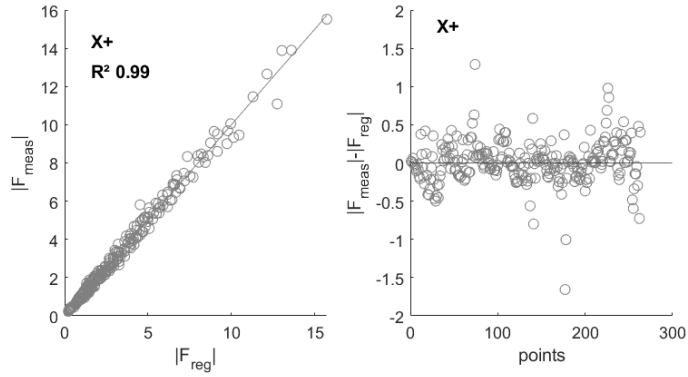

(a) $X+$, passing $C04$, moored $C0P$(Q), 263 tests.

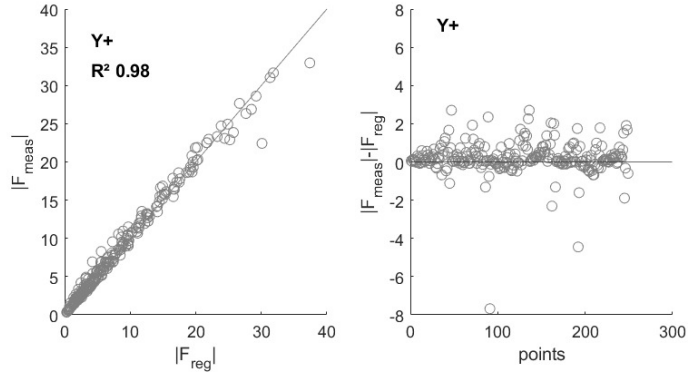

(b) $Y+$, passing $C04$, moored $T0Y$(J), 249 tests.

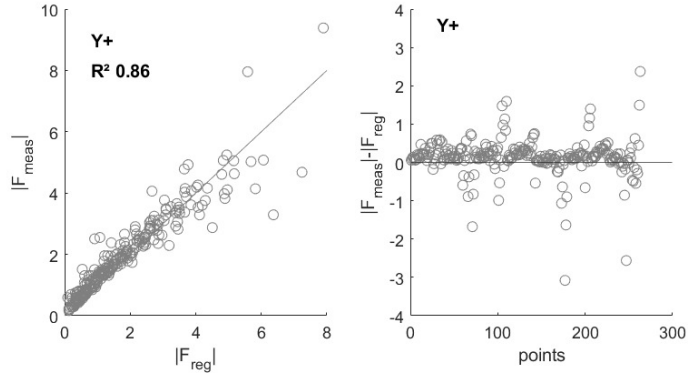

(c) $Y+$, passing $C04$, moored $T0Y$(Q), 263 tests.

Figure 6.36: *Regression analysis Tu_{m} (eq. 6.19)*
Left : Comparison measured (F_{meas}) and modelled (F_{reg}) force
Right : Plot of residuals (F_{meas}-F_{reg})

6.6.4 Conclusion validation Modified Tuck model

The Modified Tuck model can predict the effect of confinement, horizontal and vertical, on passing ship forces. This forms a very elegant relationship, only needing two parameters (α,β). The prediction of sway and yaw when the ship is moored at a quay is less optimal. An expansion of the model with factors modelling the effect of UKC (γ) and channel with W (δ) leads to much more satisfactory results, at the cost of a more complex model (number of parameters goes from two to four). For surge, this expanded model also delivers slightly higher regression quality, but considering the large increase in model complexity, the simpler model only depending on Tu_{m} can be used.

6.7 Non-dimensional empirical model

The discussion in sections 6.5 and 6.6 focusses on describing the the effect of passing distance, UKC and channel width on the passing ship forces. Regression coefficients ($\alpha, \beta, \gamma, \delta$) were calculated to model these effects. For the Modified Tuck model, (α, β) and ($\alpha, \beta, \gamma, \delta$) coefficients were derived.

The limitations of these models have already been addressed in the respective sections. The UKC regression coefficients according to eq. (6.15) for example have been derived for fixed combinations of speed, passing distance and channel width, as shown in figure 6.28. The Tu_{m} model can be applied for all combinations of passing speeds, distance and blockage which have been tested in $PESCA$, however only for the specific combination of passing and moored ship.

Up to this point, all variables included in the regression model were dimensional. Non-dimensionalisation of the measured force is a tool which is often used to represent measurements (eq. 6.21). The measured force F_{meas} can be made non-dimensional (by the number $\mathrm{f_{ND}}$). Mathematically, this has the same value as including $\mathrm{f_{ND}}$ in the regression model, however it is common to visualise the non-dimensional form of the forces.

In this section, literature is consulted to come up with a well-chosen $\mathrm{f_{ND}}$, targeting the applicability of the Tu_{m} model for various types of moored and passing ships. These suggested coefficients are then used to perform a Tu_{m} regression for all model tests which were performed.

$$F_{\mathrm{meas,ND}} = \frac{F_{\mathrm{meas}}}{\mathrm{f_{ND}}} \Leftrightarrow F_{\mathrm{reg}} = f(\alpha, \mathrm{f_{ND}}, \beta, ...) \tag{6.21}$$

6.7.1 General considerations

Many of the literature sources referenced in sections 6.5 and 6.6 apply some kind of non-dimensionalisation of the passing ship forces. The insights brought to the table by these sources can be used as a basis for an analysis of the Tu_{m} model. The proposals made are in fact in line with the general theory behind the appearance of the primary wave system.

The magnitude of the passing ship effects are a function of the passing speed squared (Bernoulli) and increase with increasing displacement of the ship. The latter induces a bit of complexity, as the displacement of both passing and moored ship will influence the magnitude of the passing ship effect. An overview of the non-dimensionalisation definitions from literature is given in table 6.16.

As most authors only tested a limited amount of moored ship and passing ship combinations, their choice of non-dimensionalisation could in fact have been arbitrary in some cases. Bear in mind that despite the large test matrix studied in $PESCA$, the number of ships is still limited and for each ship, only one draft has been examined.

The following observations are made when studying table 6.16:

- The speed squared factor is present in all formulas (in VI, VII it is included via the term Fr_h^2).
- I and III explicitly use the dimensions of the moored ship. In II, the moored and passing ship are the same, which is why no subscript m or p is added.
- IV,V and VII introduce a ratio of moored and passing ship dimensions
- VI and VII use Fr_h, meaning that the effect of shallow water is included in the factor

Table 6.16: *Non-dimensionalisation coefficient* $\mathrm{f_{ND}}$ *for each force component* (X, Y, N) *used in literature.*

ID	X	Y	N	source
I[1]	$V^2 L_\mathrm{m}^2 1.510^{-5}$	$(= X)$	$X \cdot L_\mathrm{m}$	[Flo02]
IIa[2]	$\frac{1}{2}\rho_\mathrm{w} V^2 B T_\mathrm{M}$	$\frac{1}{2}\rho_\mathrm{w} V^2 B L$	$X \cdot L$	[WZ16]
IIb[2]	$\frac{1}{2}\rho_\mathrm{w} V^2 \nabla^{\frac{2}{3}}$	$(= X)$	$\frac{1}{2}\rho_\mathrm{w} V^2 \nabla$	[WZ16]
III	$\rho_\mathrm{w} \frac{S_\mathrm{m}}{L_\mathrm{m}}^2$	$(= X)$	$X \cdot L_\mathrm{m}$	[VKV03]
IV[3]	$\frac{1}{2}\rho_\mathrm{w} V^2 T_\mathrm{M,m} L_\mathrm{m} \frac{\Delta_\mathrm{p}}{\Delta_\mathrm{m}}$	$(= X)$	$X \cdot L_\mathrm{m}$	[Kri05]
V[4]	$\frac{1}{2}\rho_\mathrm{w} V^2 T_\mathrm{M,m} B_\mathrm{m} \frac{L_\mathrm{m}}{L_\mathrm{p}}^{-4.1}$	$(= X)$	$X \cdot L_\mathrm{m}$	[VV06]
VI	$\rho_\mathrm{w} g \nabla_\mathrm{m} Fr_h^2$	$(= X)$	$X \cdot L_\mathrm{m}$	[Mol+11]
VII[5]	$\rho_\mathrm{w} g \frac{\nabla_\mathrm{m} + \nabla_\mathrm{p}}{2} Fr_h^2$	$(= X)$	$X \cdot \frac{Lm + L_\mathrm{p}}{2}$	[Den+15a]

[1] *The displacement ratio between passing and moored ship were included in regression formulas.*
[2] *Moored and passing ship were the same ship type. Paper is not clear on why two different non-dimensionalisation formulae are proposed. The differentiation between* X *and* Y *is also not clear.*
[3] $\frac{\Delta_\mathrm{p}}{\Delta_\mathrm{m}}$ *ratio of 0.52 and 1.10 in model tests*
[4] $\frac{L_\mathrm{m}}{L_\mathrm{p}}$ *ratio of 0.8,0.9,1.0,1.1 and 1.2 in slender body calculation*
[5] *Length and displacement are defined as averaged over passing and moored ship, however the presented tests are performed with the same ship type passing and moored, at same draft*

6.7.2 Application to Modified Tuck model

The work done by previous authors (table 6.16) can now serve as a basis for the non-dimensionalisation of the forces in the Modified Tuck Model. For this analysis, the surge force peaks ($X+$ and $X-$) are investigated, following the Tu_{m} model expressed by eq. 6.19 (so without terms for UKC and W).

When the regression model according to eq. 6.19 is applied for all ship interactions mentioned in table 6.6, excluding the jetty mooring, as this would require a different coefficient α, R^2 is 0.53 and 0.50 for $X+$ and $X-$ respectively. This low quality correlation is to be expected as in eq. 6.19 a factor which represents the different ships which are modelled is not included.

Based on literature, three different non-dimensional representations of the measured forces and moments are included, given by eq. 6.22. A speed term is not included in the left-hand side denominator, as the effect of speed is already included in Tu_{m} (through Fr_h). The R^2 values which are obtained are given in table 6.17.

$$F_{\mathrm{ND}} = \frac{F}{\rho g B_{\mathrm{m}} T_{\mathrm{M,m}} L_{\mathrm{m}}} = \alpha \cdot e^{-\beta \cdot d} \cdot Tu_{\mathrm{m}} \tag{6.22a}$$

$$F_{\mathrm{ND}} = \frac{F}{\Delta_{\mathrm{m}}} = \alpha \cdot e^{-\beta \cdot d} \cdot Tu_{\mathrm{m}} \tag{6.22b}$$

$$F_{\mathrm{ND}} = \frac{F}{\frac{\Delta_{\mathrm{m}}+\Delta_{\mathrm{p}}}{2}} = \alpha \cdot e^{-\beta \cdot d} \cdot Tu_{\mathrm{m}} \tag{6.22c}$$

Table 6.17 indeed shows that the chosen non-dimensional representation allows the effect of different combinations of moored and passing ships to be represented. The best regression result, following eq. 6.22c, gives a R^2 value of 0.70 and 0.66 for $X+$ and $X-$ respectively. This result indicates that a general model for all possible interactions between a moored and a passing ship is hard to obtain. A more extensive test matrix including many different ships and loading conditions would offer much more data to map the effect of these parameters. Changing ship and/or loading condition is however a time demanding process in the towing tank.

Another way to look at this problem is to start from the Tu_{m} regression analysis, where for each ship a multiplication coefficient α was

Table 6.17: *Regression results all model tests with moored ship at quay wall (1450 tests), $X+$, $X-$ for three non-dimensionalisation coefficients (ND, eq. 6.22).*

ND	$X+$	$X-$
N.A.	0.53	0.50
eq. 6.22a	0.58	0.62
eq. 6.22b	0.57	0.61
eq. 6.22c	0.70	0.66

determined through the regression model (table 6.14). Table 6.18 shows these coefficients. It seems that the ships $C0P$, $T0Y$ and $D03D04$ have similar multiplication coefficients, despite the shorter length of $T0Y$ and $D03D04$ compared to $C0P$ (tables 6.2 and 6.4), as well as the different passing ship ($C04$ for moored $C0P$ and $T0Y$ and $E01$ for $D03D04$). This indicates that the beam B and draft T have a larger influence on the interaction forces compared to the length of the ship. A more extensive parameter variation would be needed to calculate regression coefficients for the contribution of L_{pp} on one hand and $T \cdot B$ on the other hand.

In section 7.6 another approach is presented, where the coefficient α is determined by the numerical model RoPES and combined with the Tu_{m} model to represent the effect of the confined section.

Table 6.18: *Regression multiplication coefficient α for the moored ships at quay, according to the Tu_{m} regression model from eq. 6.19.*

ship	n_{test}	$X+$	$X-$
$C0P$	263	20.81	-26.51
$T0H$	489	8.33	-9.69
$T0Y$	263	20.92	-26.09
$B01$	263	8.23	-10.99
$D03D04$	172	19.40	-36.28

6.8 Summary

A scale model test series, $PESCA$, was set up and executed in the towing tank at FHR, to investigate the effect of confinement on passing ship effects. A seagoing and inland ship interaction program was performed, with high blockages occurring frequently in the latter.

Passing distance and speed were varied for up to three channel widths and up to five water depths. The moored ships were connected to a measurement frame, allowing the ship to heave and pitch, with all other DOF fixed. Forces and water level elevations, in the channel and around the moored ships, were measured at different positions.

The high frequency measurements (up to 100 Hz) have been averaged following common towing tank procedure, focussing on the effect of the low frequency primary wave system. As a consequence, the high frequent Kelvin wave recording is partly distorted. A selection of tests has been repeated between ten and thirteen times, showing the excellent repeatability of the tests.

The effect of passing distance, channel width and UKC on passing ship forces has been investigated by performing a regression analysis and comparing the results with observations made by other authors in literature.

Based on these insights, a empirical model based on Tu_{m} is presented and validated, to model the effect of speed and confinement on passing ship forces. When the ship is moored in jetty configuration, this model represents these effects well. When the ship is moored at a quay, the best result is obtained for surge. For sway and yaw, additional terms representing the effect of channel width and UKC are added to improve the quality of the regression.

A well chosen non-dimensional representation of the measurements can be used to apply the same model coefficients to multiple combinations of passing and moored ships. The common representations suggested by literature seem to fall short in representing the effect of varying ship sizes and shapes. A first analysis indicates that the effect of beam and draft is more important compared to the length of the ships. A larger matrix of moored and passing ship combinations, with different drafts, would be needed to derive a new relationship.

References

[Cap12] J. Cappelle. “Invloed van passerend scheepvaartverkeer op afgemeerde schepen”. PhD thesis. Ghent University, 2012.

[Del+19] G. Delefortrie et al. *Gedrag van afgemeerde schepen in beperkt vaarwater: Deelrapport 1 - Verloop van het proevenprogramma. Versie 2.0. WL Rapporten, 18_087_1.* Tech. rep. Waterbouwkundig Laboratorium: Antwerpen, 2019.

[Del18] G. Delefortrie. *Gedrag van afgemeerde schepen in beperkt vaarwater : projectplan, WL108P18_087_1*. Tech. rep. Waterbouwkundig Laboratorium : Antwerpen, 2018.

[Den+15a] S.P. Denehy et al. “Channel width effects on berthed ship - passing ship interaction from experiments and CFD predictions”. In: *International Conference On Ship Manoeuvrability And Maritime Simulation (MARSIM)*. Newcastle, UK, 2015.

[Den+15b] S.P. Denehy et al. “Restricted water effects on berthed ship – passing ship interaction”. In: *Australasian Coasts & Ports Conference*. Auckland, New Zealand, 2015.

[DGV16] G. Delefortrie, S. Geerts, and M. Vantorre. “The towing tank for manoeuvres in shallow water”. In: *Proceedings of the 4th MASHCON*. Hamburg, Germany, 2016, pp. 226–235.

[Flo02] J.F. Flory. “The effect of passing ships on moored ships (revised)”. In: *Prevention First 2002 Symposium*. Long Beach, USA, 2002.

[ITT14a] ITTC. *Recommended Procedures and Guidelines - Captive Model Test Procedure (7.5-02-06-02)*. Tech. rep. 2014, p. 20.

[ITT14b] ITTC. *Recommended Procedures: General Guideline for Uncertainty Analysis in Resistance Tests (7.5-02-02-02)*. Tech. rep. 2014.

[Kri05] D. Kriebel. *Mooring loads due to parallel passing ships*. Tech. rep. 2005.

[Lat14] E. Lataire. “Experiment Based Mathematical Modelling of Ship-Bank Interaction”. PhD thesis. Ghent University, 2014, p. 269.

[Mol+11] W. van der Molen et al. “Calculation of forces on moored ships due to passing ships”. In: *2nd MASHCON, ship to ship interaction*. Trondheim, Norway, 2011.

[Pin04] J A Pinkster. “The influence of a free surface on passing ship effects”. In: *International Shipbuilding Progress* 61.4 (2004), pp. 313–338.

[Rij20] Rijkswaterstaat. *Richtlijnen Vaarwegen 2020*. 2020.

[Sch49] J.B. Schijf. “Protection of embankments and ed in inland and maritime waters, and in overflows or weirs”. In: *XVII International Navigation Congress*. Lisbon,Portugal, 1949, pp. 61–78.

[Spr+17] F. Sprenger et al. “Experimental Studies on Seakeeping and Maneuverability of Ships in Adverse Weather Conditions”. In: *Journal of Ship Research* 61.3 (2017), pp. 131–152.

[Swi11] P.B. Swiegers. “Calculation of the forces on a moored ship due to a passing container ship”. Msc. thesis. Stellenbosch University, 2011.

[TB14] H. Talstra and A.J. Bliek. “Loads on moored ships due to passing ships in a straight harbour channel”. In: *PIANC World Congress*. San Francisco, USA, 2014, p. 19.

[Tuc66] E.O. Tuck. “Shallow-water flows past slender bodies”. In: *Journal of Fluid Mechanics* 26 (1966), pp. 81–95.

[Van+19] T. Van Zwijnsvoorde et al. “Sailing in Shallow Water Waves With the DTC Container Carrier: Open Model Test Data for Validation Purposes”. In: *Proceedings of 5th MASHCON*. 2019.

[VKV03] K.S. Varyani, P. Krishnankutty, and M. Vantorre. “Prediction of load on mooring ropes of a container ship due to the forces induced by a passing bulk carrier”. In: *Proceedings of the International Conference on Marine Simulation and Ship Manoeuvrability (MARSIM)*. Kanazawa, Japan, 2003.

[VV06] K.S. Varyani and M. Vantorre. “New Generic Equation for Interaction Effects on a Moored Containership due to a Passing Tanker”. In: *Journal of Ship Research* 50.3 (2006), pp. 278–287.

[VVL02] M. Vantorre, E. Verzhbitskaya, and E. Laforce. “Model Test Based Formulations of Ship-Ship Interaction Forces”. In: *Ship Technology Research* 49 (2002), pp. 124–141.

[WP08] H.J. van Wijhe and J.A. Pinkster. “The effects of ships passing moored container vessels in the Yangtzehaven, Port of Rotterdam”. In: *International Conference on Safety and Operations in Canals and Waterways*. 2008, pp. 117–130.

[WZ16] H. Wang and Z. Zou. “Numerical Prediction of Hydrodynamic Forces on A Berthed Ship Induced by A Passing Ship in Different Waterway Geometries”. In: *China Ocean Engineering* 30.2 (2016), pp. 205–216.

7

RoPES validation with $PESCA$ tests

The potential, double body numerical flow model RoPES, has been developed with the specific purpose of modelling the interaction between passing and moored ships. The mathematical description of the interaction effect in RoPES allows fast calculation times, at the price of making assumptions regarding the appearance of the flow (section 7.1). Scale model testing has been used to validate the numerical results showing good agreement, but also that for confined sections, the forces on the moored ship are underestimated. The $PESCA$ test program is dedicated to shallow and restricted water interaction, forming the ideal validation matrix for the numerical tool. In line with the discussion so far in this thesis, the forces in the horizontal plane (surge, sway, yaw) are the main focus.

7.1 Description of RoPES

RoPES has been developed as a product within the JIP - Joint Industry Project - RoPES, under the lead of MARIN - Maritiem Research Instituut Nederland. Pinkster Marine Hydrodynamics developed the RoPES software [PP14] back then and are up to today continuing to improve the modelling of passing ship interaction effects. UGent was a participant in the JIP, which entitles them to use the software package which was released to the JIP members as an end product of the project. It is this product which is discussed and validated in this chapter. This section serves the purpose of informing the reader how the problem is represented and solved mathematically in RoPES, as well as what this representation means for modelling the interaction in confined water.

7.1.1 Double body potential flow

The definition of *double body potential flow* is composed of two parts, the potential flow assumption and the double body assumption. An in-depth description of the flow problem can be found in [Pin04].

In potential flow, a velocity potential (Φ) represents the properties of the flow. The flow velocity for example is then calculated as the gradient of the flow ($\nabla\Phi$). The potential flow problem, assuming a inviscid, incompressible and irrotational flow, can be represented by the continuity (Laplace) condition (eq. 7.1)

$$\nabla^2\Phi = 0 \tag{7.1}$$

The assumption of double body flow greatly simplifies the solution of eq. 7.1, as it is a method to have a fixed water surface. In case the water surface would move, the problem of memory effects, similar to what was presented in section 4.6.2.1, is encountered, i.e. the ship will move the surface and influence the equilibrium at other time steps. As an example, when the surface is fixed, the solution is only a function of the instantaneous ship speed.

A fixed water surface, and fixed bottom, are expressed by eq. 7.2, demanding a zero normal velocity at bottom and surface. This is mathematically represented by mirroring sources an infinite amount

around the water surface and bottom; This technique is called a double body method.

$$\frac{\partial \Phi}{\partial z} = 0 \quad at\ z = 0 \tag{7.2a}$$

$$\frac{\partial \Phi}{\partial z} = 0 \quad at\ z = -h \tag{7.2b}$$

The bodies, ships, introduced in the model, are flow boundaries, as the flow cannot go through the body. This condition is expressed by eq. 7.3, with V_{m} the velocity vector of body m and n_{m} the normal vector of the wetted surface of body m.

$$\frac{\partial \Phi}{\partial n_{\mathrm{m}}} = \overrightarrow{V}_{\mathrm{m}} \cdot \overrightarrow{n}_{\mathrm{m}} \tag{7.3}$$

Each panel then represents a source, which is the basis to represent the velocity potential Φ in $\overrightarrow{X}$, a vector representing a (random) point in the earth-fixed coordinate system. Eq. 7.4 gives the expression of the velocity potential. $\sigma(\overrightarrow{A}_{\mathrm{m}})$ is the strength of a source, located in $(\overrightarrow{A}_{\mathrm{m}})$. $G(\overrightarrow{A}_{\mathrm{m}}, \overrightarrow{X})$ is the Green function of a source in $(\overrightarrow{A}_{\mathrm{m}})$. S_{m} is the wetted surface of a body m.

$$\Phi(\overrightarrow{X}) = \sum_{m=1}^{M} \frac{1}{4\pi} \int\int_{S_{\mathrm{m}}} \sigma(\overrightarrow{A}_{\mathrm{m}}) G(\overrightarrow{A}_{\mathrm{m}}, \overrightarrow{X}) dS_{\mathrm{m}} \tag{7.4}$$

Once the velocity potential is calculated using 7.4, obeying boundary conditions expressed by eq. 7.2a, 7.2b and 7.3, the resulting pressures on the body (m) can be calculated based on Bernoulli's equation (eq. 7.5). Integrating these pressures over the surface of the body delivers the forces (eq. 7.6), which are then given to the user as output.

$$p = -\rho \frac{\partial \Phi}{\partial t} - \frac{1}{2}\rho \left(|\nabla \Phi|^2 - |\overrightarrow{V}^2_{\mathrm{m}}| \right) \tag{7.5}$$

$$\overrightarrow{F}_{\mathrm{m}} = -\int\int_{S_{\mathrm{m}}} p \overrightarrow{n}_{\mathrm{m}} dS_{\mathrm{m}} \tag{7.6}$$

7.1.2 RoPES software

The RoPES software solves the double body potential flow theory internally and provides the user with a Graphical User Interface to

generate the simulation environment as well as visualise the output. The forces (eq. 7.6) are the only results which are made available to the user. For the simulations performed in this chapter, RoPES version 1.1.0.27090 is used. [PP14] gives an overview of the software package, including a description of the in- and output.

The results (forces) are given in the axis system of the moored ship. The convention of this axis system is identical to the one used in $Vlugmoor$, with x-axis positive to bow, y-axis positive to port and z-axis positive upward. The origin is located midships on the calm water plane.

7.1.3 RoPES validation in literature

The typical structure of a JIP is a mix of the development of a particular software and research within the topic. For this JIP, performing towing tank tests formed the backbone of the RoPES validation.

7.1.3.1 Horizontal plane

At FHR, an extensive model test program has been executed within the JIP [TB14]. This test matrix was later expanded in the scope of work for Antwerp Port Authority [Del+12], where meetings of passing ships were modelled. In both test series, interactions between moored and passing ships in straight channels are studied.

In [TB14], they show that for passing events at moderate passing speed (5 knots, 25% UKC) the RoPES and model test results match very well (surge, sway, yaw). At a higher passing speed (14 knots, 25% UKC), RoPES underestimates the passing ship effect. They concluded that for jetty mooring, this holds for (at least) 5DOF. As the roll moment was not measured in the test program, no statement was made regarding roll. In quay mooring, only surge is underpredicted significantly.

The authors discuss the higher order dependency on the passing speed for high Froude depth numbers, compared to the velocity squared relationship which follows from potential flow theory. They propose a correction factor based on one dimensional flow. From the analysis of $PESCA$ tests in chapter 6, this higher order dependency on speed for confined water was confirmed already. In section

7.5.2 this factor is further discussed and validated based on the high blockage $PESCA$ model tests.

[HJ14] analyses model tests performed at Deltares, where next to tests with parallel passage in a straight channel, more complex geometries with docks adjacent to the channel were analysed. For the straight channel, the results align with the work of [TB14]. When the moored ship is positioned in a dock next to the main channel, a standing wave is produced, as a function of the geometry of the dock (section 2.1.4). The double body, fixed water surface, model used in RoPES does not allow to model a travelling long wave as water surface disturbance. [Pin04] shows how a free surface model potential flow model can accurately predict these standing waves as well.

7.1.3.2 Vertical plane

The above discussion focusses on the forces in the horizontal plane (surge, sway, yaw), which are indeed the most relevant passing ship forces when studying the behaviour of the moored ship (section 4.3.1). In [TB14] they show that the heave and pitch (roll was not measured in model tests) can be reproduced well by RoPES for moderate passing speeds (up to 7 knots). For higher passing speeds, they observe an underestimation of the forces in RoPES, similar to what was observed for the forces in the horizontal plane.

7.2 RoPES model of *PESCA* tests

When comparing scale model test results with numerical results, the numerical and scale model environment should be identical. The word identical does however need to be interpreted within the context of numerical modelling, where both hull as well as channel geometry are composed of panels with finite size. The smaller the panel size and the more detailed the towing tank itself is modelled in RoPES, the longer the calculation time. As the author wants to examine a substantial test matrix, calculation times for each individual simulation needed to be limited. This section discusses some sensitivity work which has been performed before moving to systematic simulations.

7.2.1 Hull forms RoPES ships

RoPES requires a specific panel size representation (.dat extension, ASCII), which is in fact similar to the one required by Hydrostar (.hst extension). The lines of the ships used in the towing tank tests are all stored in a centralised location in .3dm format, in the dimensions of the actual towing tank ship model. The calculation algorithm and representation of numbers (memory usage - bit precision) used in RoPES requires to include the ship hull in full scale dimensions. A full scale panellised representation of the model tests ships is needed. As this process takes up a significant amount of time, a selection of three is made to do the numerical validation. The $C04$ is taken as the passing ship, with the $T0Y$ and $C0P$ as moored ships. This allows to compare quay and jetty mooring ($T0Y$).

Wim Van Hoydonck (FHR) was kind enough to share Hydrostar (.hst) representations at full scale of the three ships. The author then used ConvertHullForm (version February 2021), a tool developed by Serge Toxopeus (MARIN). Required actions included scaling ($T0Y$ at scale 80 compared to model scale), as well as changing the origin of the axis system (from aft perpendicular to midships).The panellised model was cut at the modelled drafts for $PESCA$. Wim delivered three panel sizes for each model. The sensitivity of RoPES with respect to panel size is presented in section 7.2.3.2.

7.2.2 Sensitivity towing tank representation in RoPES

The model tests were performed in a restricted channel built into the towing tank as was visualised in figure 6.3. The most accurate RoPES model then would incorporate this geometry as a panellised environment. Bear in mind that even when doing so, the RoPES calculation uses a fixed surface and a combination of mirror planes and impenetrable panel walls, whereas acceleration and standing waves can travel through the actual towing tank, with the harbour and wave maker ends having dampening packs.

A sensitivity analysis was performed by comparing two configurations. In the first geometry, the full towing tank, upscaled by a factor of 80, is modelled using panels, with a size of 10 m. The wall where the ships are moored can be represented using a mirror wall, which uses the same technique as for water surface and bottom. All other walls are formed by panels. This geometry is shown in figure 7.1. The moored ships are arbitrary container ships and tanker with the same dimensions (and blockage), as these simulations were run prior to generating the $PESCA$ hulls. A comparison in fact shows that for modelling passing ship forces, the exact geometry only causes limited differences in the magnitude of the forces.

This simulation is compared with two separate RoPES simulations, where only one moored ship at a time is modelled. The channel is represented by two parallel boundaries, one formed by a mirror wall and one formed by a panel wall (10 m panel size). The simulation for the moored ship at position 1 is shown in figure 7.2.

The time series generated by RoPES are visualised in figure 7.3, showing that the differences are limited, with slightly larger deviations for ship 1. The full towing tank representation is still not fully compliant with the model test set-up. Of foremost importance is keeping the calculation time acceptable, even with finer ship meshes (see section 7.2.3), therefore only the channel is modelled in RoPES. This channel is composed of a mirror plane as quay wall (or in general starboard side wall) and a panel wall as port side channel wall.

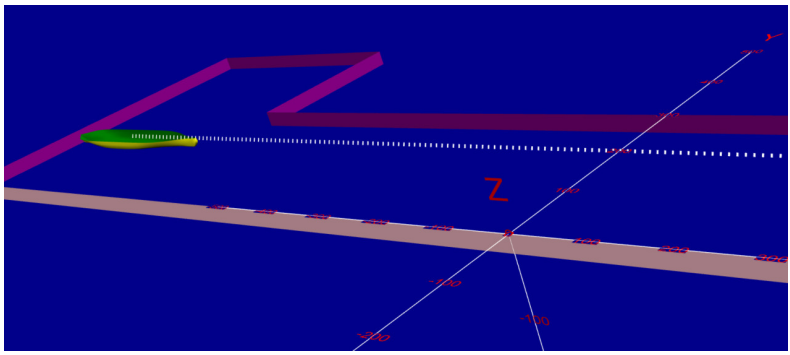

(a) view 1

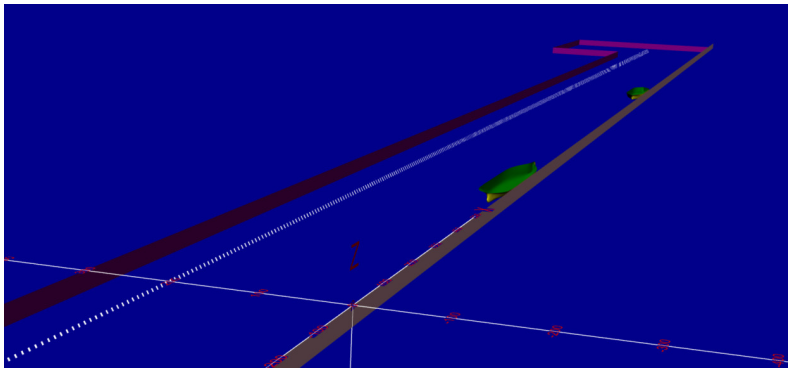

(b) view 2

Figure 7.1: *Panellised representation of the towing tank in RoPES.*

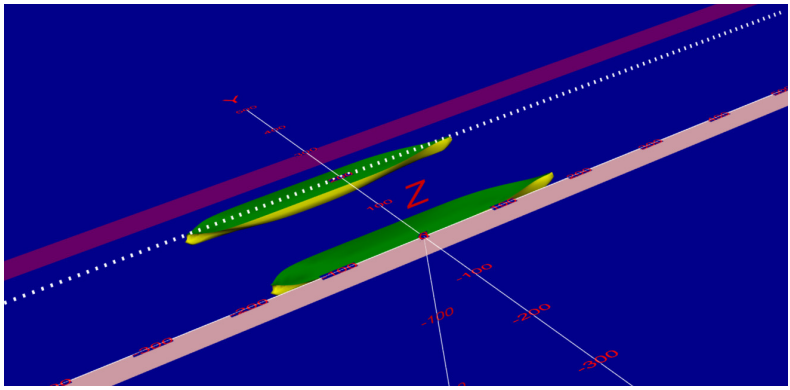

Figure 7.2: *Panellised representation of one moored ship and channel in RoPES.*

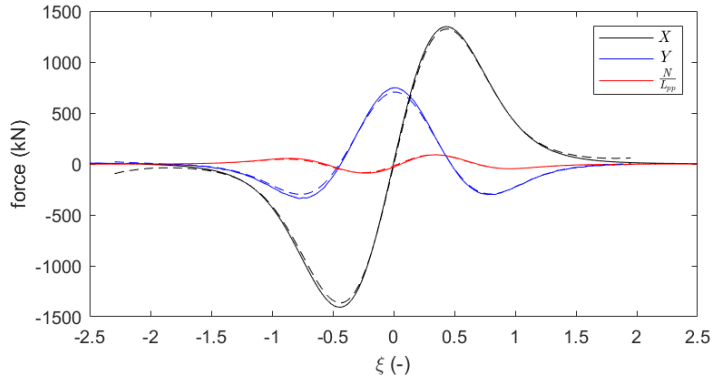

(a) ship 1 $x_{0,\mathrm{t}}$ = 23 m

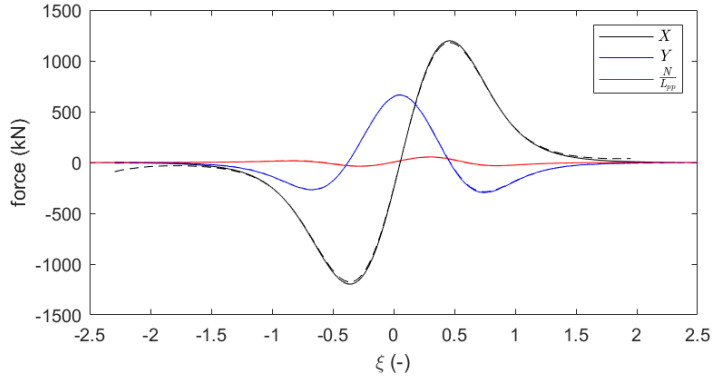

(b) ship 1 $x_{0,\mathrm{t}}$ = 43 m

Figure 7.3: *RoPES simulation result moored ship 1 (top) – moored ship 2 (bottom);*
simulation with panellised towing tank (full lines);
simulation with separate moored ships in channel (dashed lines).

7.2.3 Sensitivity study panel size

In RoPES, part of the geometry is constructed using panel walls, complemented with mirror planes. The ship hull needs enough panels to accurately represent the geometry. The panel size of the ship and wall geometry should be similar to obtain good results. As a general rule of thumb, the panel size of the wall element should match the ship's panel size.

7.2.3.1 Channel wall panel size

Default, 10 m X 10 m rectangular panels are proposed in the user manual [Pin14]. A Panamax container ship is then composed of 794 panels. This panel size was also used in figure 7.1 to build the towing tank geometry. Figure 7.4 shows that the results are identical for 5 m X 5 m panels and 10 m X 10 m panels. A similar event was also modelled, where the passing ship sailed close to the panellised bank opposite to the moored ship. Here, the maximum deviation in the force time series was 0.1 %.

7.2.3.2 Ship hull panel size

The determination of appropriate ship hull panel sizes is known under the term grid convergence study. In such a study, the panel size is reduced in steps until the change in panel size has no significant effect on the results of the simulation. The nature of RoPES, a potential flow solver, but also the main interest in the effect of the long period primary wave system, allows larger panel sizes compared to most other numerical applications. The RoPES hulls which have been developed in the JIP, have between 800 and 1000 panels for seagoing container ships (L_{OA} between 320 m and 360 m). The Aframax tanker has 1200 panels.

In order to substantiate the claim that rough panel models suffice for RoPES, the $C04$ ship has been panellised with 972, 3514 and 14086 panels respectively. These models are defined as coarse, medium and fine for this discussion. Using fine panellisation for both passing and moored ship, in combination with a mirror wall as quay and a panel wall as opposite channel wall (see figure 7.2), the needed RAM memory exceeds the capacity of a 16GB laptop unit.

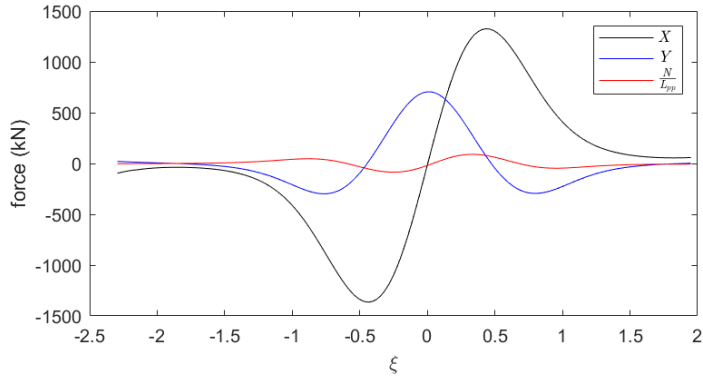

Figure 7.4: *RoPES simulation result moored ship 1 in channel; simulation with 5 m X 5 m panels (full lines); simulation with 10 m X 10 m panels (dashed lines).*

When modelling the ship-ship interaction without channel walls, it takes 10 seconds, 3 minutes and 2 hours 15 minutes to run the coarse, medium and fine mesh simulation respectively. Table 7.1 compares the peak forces given in the RoPES output. The differences between the ship mesh sizes have a larger impact than the panel size of the channel wall (figure 7.2). The differences are however still limited. Part of it can also be ascribed to a slight change in under water volume for the different mesh sizes.

Table 7.2 gives the comparison in peak forces for the interaction between a coarse passing $C04$ and moored $C04$ of different mesh sizes, in the channel configuration (figure 7.2). Running times for these simulations are 3 minutes, 11 minutes and 4 hours 20 minutes for the coarse, medium and fine ship mesh size. The results are comparable in magnitude with table 7.1.

Table 7.1: *Comparison peak forces (kN) from RoPES between coarse, medium and fine mesh sizes for moored and passing $C04$, no channel condition.*

	$X_{\max}$	$\lvert X_{\min}\rvert$	$Y_{\max}$	$\lvert Y_{\min}\rvert$	$\frac{N_{\max}}{L_{\mathrm{PP}}}$	$\lvert\frac{N_{\min}}{L_{\mathrm{PP}}}\rvert$
coarse(C)	560	575	1685	616	233	225
medium (M)	570	579	1686	612	236	226
fine (F)	572	577	1675	603	235	226
$\frac{\mathrm{M}-\mathrm{C}}{\mathrm{C}}\cdot 100(\%)$	1.9	0.8	0.1	-0.7	1.0	0.8
$\frac{\mathrm{F}-\mathrm{M}}{\mathrm{M}}\cdot 100(\%)$	0.3	-0.4	-0.7	-1.3	0.0	0.2

Table 7.2: *Comparison peak forces (kN) from RoPES between coarse, medium and fine mesh sizes for moored $C04$; channel is modelled.*

	$X_{\max}$	$\lvert X_{\min}\rvert$	$Y_{\max}$	$\lvert Y_{\min}\rvert$	$\frac{N_{\max}}{L_{\mathrm{PP}}}$	$\lvert\frac{N_{\min}}{L_{\mathrm{PP}}}\rvert$
coarse (C)	1296	1341	696	292	91	85
medium (M)	1309	1354	690	290	91	86
fine (F)	1311	1355	686	288	91	87
$\frac{\mathrm{M}-\mathrm{C}}{\mathrm{C}}\cdot 100(\%)$	1.0	1.0	-0.8	-0.8	0.7	1.5
$\frac{\mathrm{F}-\mathrm{M}}{\mathrm{M}}\cdot 100(\%)$	0.2	0.1	-0.6	-0.5	0.1	0.6

7.2.4 Sensitivity study distance to mirror wall

The moored ship is positioned close to the quay wall, which is numerically represented as a mirror wall in RoPES. In $PESCA$, the distance between tank wall and ship was 0.02 m, which means that for RoPES the (scaled) clearance of 1.6 m is present. The distance between a large portion of the ship's panels and the mirror wall is limited, compared to the panel size of the ship.

Two additional distances of the ship to the mirror wall are modelled, 0.6 m and 2.6 m. The X,Y en N are plotted in figure 7.5. The results show that the distance of the ship to the mirror has an impact, mostly for Y. A larger distance to the mirror wall results in an increase in Y, which is to be expected as a larger portion of the flow is present at the starboard side. No significant differences in magnitude and/or shape are however present. The mirror wall as implemented in RoPES is robust with respect to small clearances between ship and wall.

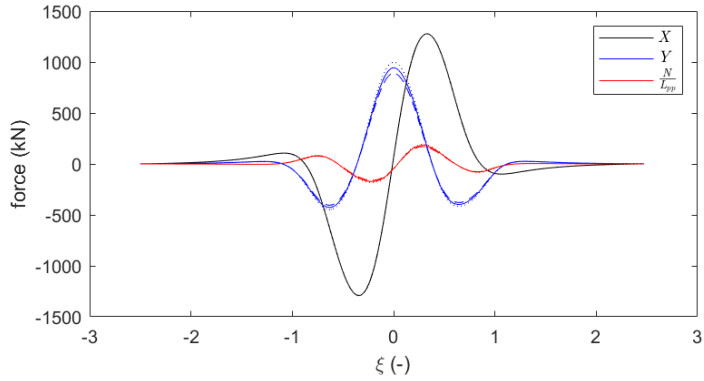

Figure 7.5: *RoPES simulation result moored $C0P$ (medium panel size) dashed line = 0.6 m to mirror wall, full line = 1.6 m to mirror wall (=$PESCA$), dotted line = 2.6 m to mirror wall.*

7.2.5 RoPES simulation set-up for systematic validation

Based on the discussion above, a choice is made on the RoPES set-up for the simulations which are going to be used to compare the results with $PESCA$. As passing distance, UKC and channel width

need to varied, as well as two combinations of moored and passing ship, acceptable calculation times range from 15 to 45 minutes for each simulation. The following set-up is chosen :

- Medium mesh size for all three ships, 3514, 1754 and 3376 panels for the $C04$, $C0P$ and $T0Y$ respectively.
- The full towing tank geometry is not modelled, only the channel walls, formed by a mirror wall and a panel wall are included in the model. The panel wall has a length of 2500 m and has 10 m X 10 m panel size approximately (exact size depends on water depth).
- The simulation time step is chosen according to the guidelines from [Pin14], proposing at least one data point every 10 m.
- The distance between ship starboard side panels and mirror wall is 1.6 m, as was the case in $PESCA$ (0.02 m times the scale factor of 80).

7.3 RoPES validation using $PESCA$ tests

In an ideal scenario, a numerical calculation is capable of exactly predicting the outcome of the real life flow problem. If all bodies have full scale dimensions, no scale effects are present, as is the case for physical scale model tests (section 6.3). As all numerical calculation techniques require some simplifications of the flow however, this perfect prediction is never possible. Despite scale effects being present, physical scale model tests are the most effective method to validate numerical packages.

Based on the discussion from sections 2.1.4.1 and 6.3, the differences between potential, double body, flow calculations (RoPES) and physical scale model tests ($PESCA$) can be identified. The schematic representation of figure 7.6 is used to support this discourse. The top figure (a) shows the flow system around the passing ship in RoPES, the middle figure (b) shows the same for the $PESCA$ flow (with simplified representation of the Kelvin pattern, only shown for the bow source). Figure (c) illustrates how the water level elevations caused by the primary wave system will compare between RoPES and $PESCA$. In $PESCA$, these can be physically measured using wave gauges. In RoPES, these would actually be representations of pressures, resulting from the potential flow calculation.

In potential flow, when a ship would be perfectly symmetrical, the pressure system surrounding it would be so as well (figure 2.5 (top wave system)). As expressed in section 6.3, the presence of boundary layers, which are more developed (thicker) at the aft ship, affect the pressure system. The fluid particles in this layer have already lost a part of their kinetic energy. According to potential flow, the aft ship is a zone of increased pressure; the kinetic energy of the particles in the boundary layer is insufficient to penetrate into this increased pressure zone, which causes a further deceleration and possibly unstable flow (vortices). As a result, less energy can be transformed into potential energy. In consequence, the high-pressure zone aft of the ship is reduced. Secondly, under the double body assumption, no free surface (Kelvin) waves are modelled, which in the real flow also take energy away from the system.

Both effects (boundary layer and Kelvin waves) lead to a smaller stern wave, which in turn leads to an asymmetry in the measured

forces on the moored ship. The first peaks in surge and sway are significantly higher than the subsequent peaks. This effect also becomes more prominent with increasing blockage. As boundary layers and surface waves are not present in RoPES, the force signals produced by RoPES are (nearly) symmetrical. Differences in hull shape between fore and aft ship cause some asymmetry in the wave system. It will be shown in section 7.4 that this is hardly visible in the measured forces.

The absence of the free surface in RoPES causes a second effect, namely that squat of the ships cannot be taken into account. As squat effects increase with higher blockage and passing speeds, this will decrease the flow section surrounding the ships. A small flow section leads in turn to an increase in flow speed and pressure changes. As a result, RoPES forces will generally be underpredicted at higher blockage and flow speed. For the first peak (surge, sway) this is always visible. When it comes to the second peak, the overestimation of the stern wave by RoPES, will counteract this effect. Both effects will thus partially cancel each other out. This is illustrated by figure 7.6 (c), for a passing ship showing significant squat. The RoPES pressure system is symmetrical (bow and stern pressure increase). In $PESCA$, the flow section is reduced, creating an increase in pressure difference. At the aft of the ship however, the system contains less energy compared to the bow. This could result in a similar pressure system in RoPES and $PESCA$, as two effects counteract each other. In section 7.5, where time series of RoPES and $PESCA$ forces are compared, this is further discussed.

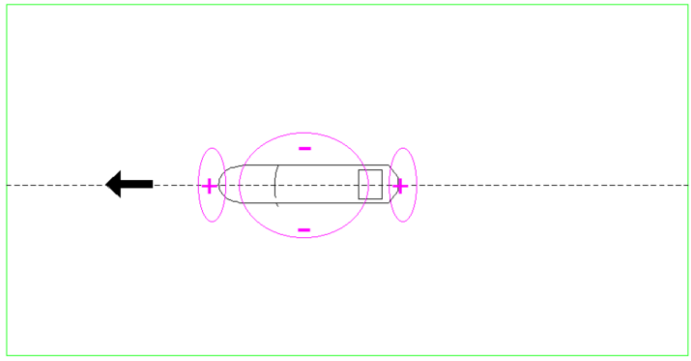

(a) Visualisation RoPES wave system

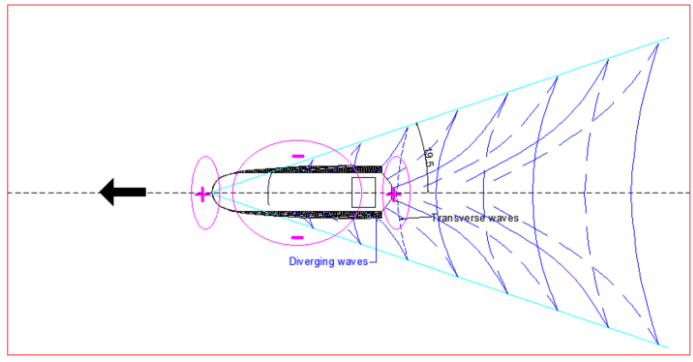

(b) Visualisation $PESCA$ wave system

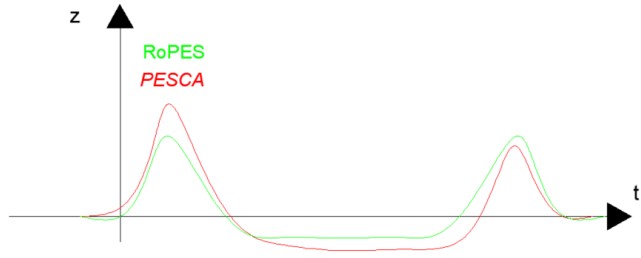

(c) Illustrative difference RoPES and $PESCA$ water level elevation

Figure 7.6: *Illustration of difference between wave system surrounding passing ship for RoPES (potential flow) and $PESCA$ (scaled turbulent flow)*

7.4 Comparison time series RoPES and *PESCA*

7.4.1 Analysis time series

RoPES provides as output the forces acting on the moored ship in 6DOF. The hull pressure distributions are not made available to the user. Force time series can however be compared with the $PESCA$ measurements as a validation effort for the numerical tool. The $PESCA$ measurements are again represented in the *Vlugmoor* axis system (appendix B), which coincides with the RoPES ship-fixed axis system. Two more actions are performed on the $PESCA$ time series :

- In $PESCA$ heave and trim motions are measured, RoPES gives a force and moment. Eq. 4.32 and 4.33 can be reversed to calculate the forces (Z, M) based on the measured motions (z, θ)
- All $PESCA$ forces need to be converted to their full scale equivalent. The scale factor (SF) for the seagoing ship program is 80, for the inland ship program 25. The forces (N) need to be multiplied by SF^3, the moments (Nm) by SF^4.

Similar to the work of [TB14], the force time series are compared for all force components, including roll, which was not analysed in [TB14]. The $PESCA$ time series were described in section 6.2.1, which are averaged high frequency measured signals, with one data point every 0.21 cm (model scale). In RoPES, at least one point every 10 m is available (section 7.2.5).

T0Y at quay, largest section Figure 7.7 shows the interaction forces for an event in the largest section which was modelled in $PESCA$, channel width of 10 B_{p} and UKC_{p} = 50%. The passing speed is 6 knots full scale. In this test, the effects of the confined section will be least visible compared to the other more shallow and/or more narrow sections. This case is seen as a benchmark to compare with the effect of confinement on the passing ship forces.

The left side of the figure shows surge, sway and yaw (horizontal plane); the right hand side shows heave, pitch and roll (vertical plane). RoPES time series are plotted in black, $PESCA$ time series in blue. The black and blue circles in the figures indicate the minimum and maximum value for the time series of RoPES and $PESCA$

respectively. For sway, the first and second minimum, located at approximately $\xi = -1$ and $\xi = 1$ respectively, are indicated separately. The reasoning behind this will become apparent further down this section.

The left side, forces in the horizontal plane, shows a very good agreement between RoPES and $PESCA$. The shape of the time series is well reproduced by the numerical model. The most significant difference lies in the value for the first (negative) peak in the surge force, which is underestimated by RoPES. The negative and positive RoPES peaks are -504 and +511 kN respectively, whereas $PESCA$ gives -550 and +494 kN as peak values. This effect follows from the analysis of scale effects in sections 6.3 and 7.3, where turbulent and free surface effects cause the stern wave of the passing ship to be lower than the bow wave. This effect cannot be predicted by RoPES. This has been further substantiated by letting the passing ship sail (forward) from the wave maker to the harbour (inland program, $E01$); leading to a larger first, positive, peak and smaller second, negative, peak. This was also observed by [Kri05], who stated that the ratio between second and first peak is 0.85. For the example here (-550 and 494 kN), this ratio is 0.89. Confinement of the section will lead to an even more pronounced difference between both peaks.

The forces in the vertical plane show larger differences between RoPES and $PESCA$. For heave, Z, the shape of the curve is similar, but the peak value is underestimated by RoPES. Before and after the passage ($\xi = -3$ and $\xi = 3$), the RoPES value does not go to zero, which is what we would expect, but shows an offset. A possible explanation would be that in the RoPES calculation of the resulting heave force, an offset is induced due to a difference in the weight which is given as input and the actual pressure integration by RoPES. Proving this without access to the RoPES calculation process is a tedious task. The next examples also show that the offset changes when for example the passing speed is altered, which means that a constant offset value is in fact not present.

The pitch moment can be reproduced successfully with RoPES, both regarding shape as well as magnitude. The roll response of the moored ship in quay configuration is low. The $PESCA$ signal seems to follow the ROPES result, the magnitude (500 - 1000 kNm full scale or 0.01 to 0.02 Nm in model scale) is however too low compared to

the accuracy of the measuring device.

T0Y at jetty, largest section Figure E.1 (appendix E) compares RoPES and $PESCA$ results for the $T0Y$ moored in jetty configuration, for the same passing event as discussed in the previous paragraph. Compared to figure 7.7, the surge force is lower, whereas the sway, yaw and roll are higher, which is to be expected when comparing quay and jetty mooring (figure 2.7). The first peak in surge is again significantly larger compared to the second peak. For sway, the positive peak is slightly underpredicted; the first and second negative peak show that in $PESCA$, the first peak is significantly higher than the second peak, whereas in RoPES, both peaks have a similar magnitude. This follows the observation for surge, caused again by the absence of turbulent and free surface effects in RoPES. For the remainder of this chapter, the first and second negative sway peak are treated separately.

T0Y at quay, reduced section Figure E.2 (appendix E) compares numerical and model test results for a channel width of 6 B_{p} and a UKC_{p} = 20%. The underestimation of the first surge peak becomes more pronounced, which will be analysed in detail in section 7.5. The sway and yaw force are actually slightly overestimated by RoPES. The $PESCA$ time series shows a smaller first negative peak (in absolute value), compared to the second peak. The roll moment is larger and can be captured accurately by the roll gauge, which was not the case in figure 7.7. The negative peak is significantly overpredicted in RoPES compared to what $PESCA$ measurements show.

T0Y at quay, reduced section, higher speed Figure E.3 (appendix E) shows results for the same section as Figure E.2, with a larger passing speed. The double body model is no longer able to predict the magnitudes of surge, as the differences become considerable; Again with the most significant increase in the first peak. The difference in sway force is limited; RoPES underestimates the (first) negative peak and overestimates the positive peak. The shape of the yaw moment is distorted, with comparable peak values. For heave, RoPES significantly underpredicts the peak value, yet the offset before and after the passage is also enlarged compared to

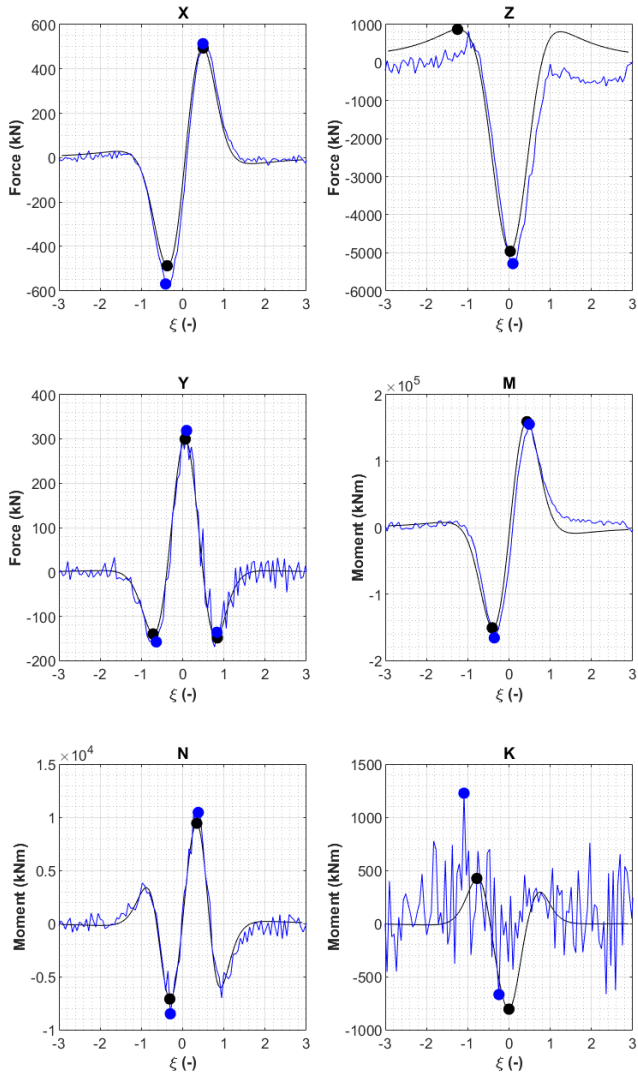

Figure 7.7: *Comparison RoPES (black) and $PESCA$ (blue) for 6DOF passing $C04$, moored $T0Y(Q)$, UKC_{p} = 50%, $\frac{d}{B_{\mathrm{p}}}$ = 2.0, $\frac{W}{B_{\mathrm{p}}}$ =10, V_{FS}= 6 kn*

figure E.2. RoPES underestimates the pitch moment, which follows the observation for surge.

T0Y at jetty, reduced section, large speed Figure E.4 (appendix E) shows the same passing case as Figure E.3, but with the ship moored at a jetty. The shape of the signals is matched well by RoPES for jetty mooring. All peak values are underestimated by RoPES. The difference in first and second negative peak in sway is prominent.

7.4.2 Summary

The comparison between calculated time series in RoPES and measured time series in $PESCA$ scale model tests, shows that overall RoPES performs well. The forces in the horizontal plane (surge, sway and yaw) measured in $PESCA$ are better matched by RoPES compared to the forces in the vertical plane (heave, pitch, roll). For heave, RoPES simulation show an offset from zero at the start and end of the simulation, which varies with passing speed and channel configuration. Further addressing this offset, by looking into the RoPES code, could provide a better estimate of the heave force. The measured roll moment in $PESCA$ is small, certainly when moored at the quay, leading to less accurate results in cases where the forces are low.

In $PESCA$, the second (third for sway) peak is lower compared to the first peak, as the stern wave of the primary wave system is lower compared to the bow wave. In RoPES, both peaks have similar magnitude, as a consequence of the double body potential flow.

For higher speeds and/or more confined sections, in jetty mooring, the force peaks of all 6DOF are underestimated by RoPES. For quay mooring, surge and pitch are underestimated. When the ship is moored at the quay, the reproduction of the shape of the signal is less good for yaw and roll, especially for higher speeds and/or confined sections.

7.5 Peak forces horizontal plane

Throughout this thesis, the emphasis has been on the forces (and equations) in the horizontal plane. For the RoPES validation, this path is continued. Additional motivation here is that from the analysis of the time series it follows that heave is difficult to compare, due to the presence of the offset which cannot be explained. The roll moment is also more difficult to compare, as the accuracy of the roll gauge did not allow small roll moments to be accurately measured. Moreover, in literature authors also tend to focus on the analysis of the horizontal plane.

When it comes to the validation of RoPES for passages in confined, rectangular channels, [TB14] forms the most important reference work (as was explained in section 7.1.3.1). They propose a correction factor F_{c} for the peak forces and moments coming from RoPES (see section 7.5.2). The factor expresses the more than quadratic dependency on passing speed for large passing speeds in confined channels.

Based on the discussion from section 7.1.3 and section 7.4 four hypotheses are formulated :

1. The effect of the passing distance is correctly represented in RoPES (section 7.5.1).

2. The correction factor, F_{c} proposed by Talstra and Bliek for high Froude depth numbers can be applied successfully (section 7.5.2).

3. The correction factor F_{c} needs to be applied to surge in quay mooring and to all forces in jetty mooring.

4. No authors have made a distinction between the different peak values for a given force component; The hypothesis is made that the correction factor F_{c} can be applied to all peaks.

7.5.1 Effect passing distance

[TB14] already commented that the RoPES results followed the ones from the model test, with in most cases an inverse relationship between passing distance and resulting force. The $PESCA$ analysis

revealed that an exponential relationship performs a bit better, although at small UKC, a power law relationship was preferred.

Figure 7.8 shows a comparison between $PESCA$ and RoPES forces, in function of passing distance, for passing distances between 0.3 and 1.2 m (0.5 to 2.0 times B_{p}). The circles represent the $PESCA$ measurement, the diamonds the RoPES simulation. For the negative sway force, the values for the second peak are represented by a purple cross and triangle for $PESCA$ and RoPES respectively. The stars represent the normalised difference between $PESCA$ and RoPES results, connected by a full line for visualisation purposes. For all data points, this offset is partly caused by the effect of passing speed and confinement, which is treated in the next section. A significant slope of the black curve would indicate that the passing distance is not correctly represented by RoPES. No such obvious trend is observed between $PESCA$ and RoPES results.

In figure E.5 (appendix E), results are shown for a passing distance between 0.6 and 3.0 m (1.0 to 5.0 times B_{p}). This figure does show a sloped full line, indicating an underestimation by RoPES which increases with larger passing distance. These results however need to be viewed under the following remarks :

- For large passing distances, the amplitude of the forces decreases. A lower amplitude means that the relative difference can become large due to the small value in the denominator.
- The measuring equipment is set to measure large interaction forces accurately, making them less accurate to capture small forces.
- For the largest passing distance (3.0 m), the effect of the secondary waves becomes more prominent, which is not captured by RoPES due to the nature of the numerical calculation. As the $PESCA$ peaks analysis automatically searches for the maximum in the time series, this might be the maximum reached due to the impact of the (high frequency) Kelvin waves.

Figure E.6 (appendix E) gives the dimensional difference between RoPES and $PESCA$ for the same case as figure E.5. The slope in the curve is less prominent, indicating that the observation made from figure E.5 is partly a result of non-dimensionalisation. However,

the conclusion remains that for large passing distances, the RoPES results should be treated with care, partly due to the absence of the effect of secondary waves in RoPES.

For passing distances ranging from (1.0 to 3.0 times B_{p}), which are the ones which are typically of most interest, the RoPES model provides a satisfactory estimate of the effect of passing distance on passing ship forces.

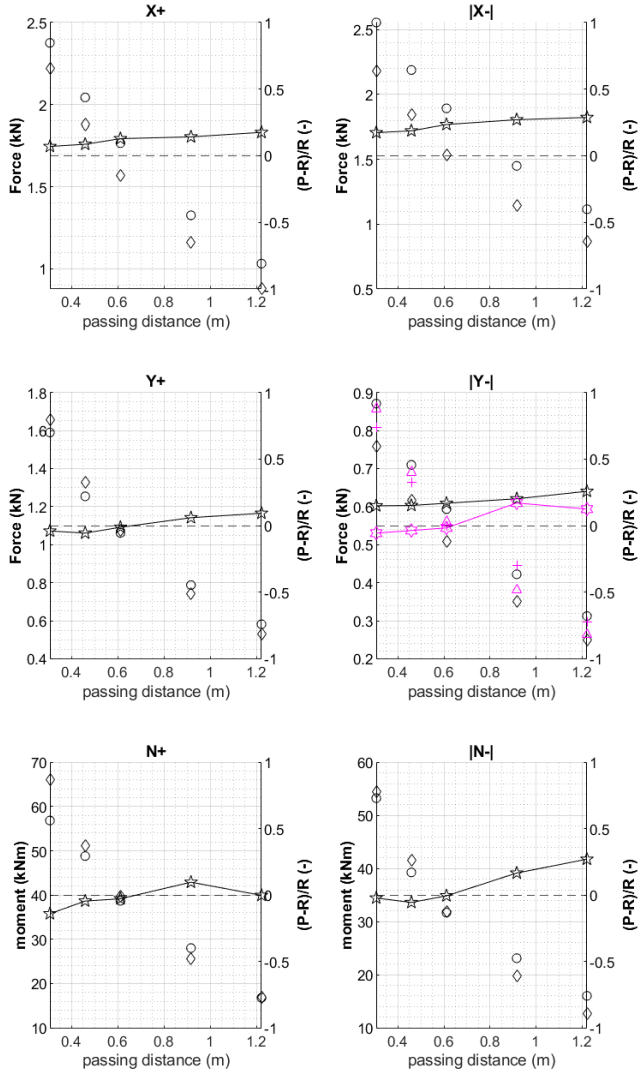

Figure 7.8: *Effect of passing distance on the peak forces.*
passing $C04$, moored $T0Y(Q)$, UKC_{p} = 10%, $\frac{W}{B_{\mathrm{p}}}$ = 10, V_{FS} = 8 kn
Left axis : $PESCA$ (circle,cross), RoPES (diamond, triangle)
Right axis : Relative difference $PESCA$ and RoPES (star, hexagon)

7.5.2 Validation of correction factor F_c

[TB14] derived the factor $F_{c,1Dtheory}$ based on a 1D flow (equal return flow and water level drop over the width of the section). Eq. 7.7 shows their proposed correction factor as a result of this 1D theory. V is the passing ship speed in m/s and c_w the critical wave speed in restricted water, linked to the wave celerity in shallow water c_{w0} by eq. 7.8.

They also propose a simplified formula ($F_{c,approx}$, eq.7.9), which does not require eq. 7.8 to be solved. In the paragraph of the paper explaining eq. 7.9, they state that the blockage needs to be calculated based on the section of moored and passing ship, which is not in line with their 1D theory, nor with how they formulated eq. 7.7. Therefore, m_P is here used in both formulas, calculating the blockage based on the cross section of the channel and the midship section of the passing ship.

The authors state that the formulae are accurate for $m_P < 0.25$. Figure 6.5 shows that, for the seagoing ships, all tests indeed fall in this region. For the remainder of this chapter, $F_{c,approx}$ is used in calculations, for which the notation is simplified to F_c

$$F_{c,1Dtheory} = 1 + \left(\frac{V}{c_w}\right)^2 \tag{7.7}$$

$$\frac{c_w}{c_{w0}} = \frac{2}{3}^{1.5} \cdot \left(1 - m_P + \frac{1}{2}\frac{c_w^2}{c_{w0}^2}\right)^{1.5} \tag{7.8}$$

$$F_{c,approx} \equiv F_c = 1 + (1 + 20 \cdot m_P)\left(\frac{V}{c_{w0}}\right)^2 \tag{7.9}$$

T0Y at quay, largest section Figure 7.9 compares the $PESCA$ measurement with the factor F_c. The $PESCA$ measurement is divided by V^2, which denotes the potential flow relationship. This number is normalised by the RoPES result (divided by V^2) at the lowest passing speed. Eq. 7.10 shows this representation, with i representing a passing speed, ordered from smallest to largest. This representation allows both the offset which might be present even at low speed, as well as the presence of a more than V^2 relationship in the

$PESCA$ measurements, to be visualised. For $Y-$, the purple colour (diamond) again indicates the second negative peak.

$$\frac{F_{\mathrm{i}}}{V_{\mathrm{i}}^2} norm. = \frac{\frac{F_{\mathrm{i},PESCA}}{V_{\mathrm{i}}^2}}{\frac{F_{1,\mathrm{RoPES}}}{V_1^2}} \tag{7.10}$$

The stars represent the proposed correction factor F_{c} by [TB14]. The following then holds :

- If the circles and stars show the same trend, F_{c} should be applied to correct the RoPES results.
- If the circles show steeper increase compared to the stars for increasing speeds, the factor F_{c} underestimates the speed effect.
- If the circles show less steep increase compared to the stars for increasing speeds, the factor F_{c} overestimates the speed effect.
- If the circles do not show any trend, then a correction of RoPES using F_{c} is not needed.

From figure 7.9, the factor F_{c} seems to represent the underestimation of $PESCA$ results by RoPES well for surge ($X+$ and $X-$). For the positive sway peak, the V^2 relationship holds, no correction is needed. For the negative peak, $Y-$, the first peak seems to follow F_{c} , whereas the second peak does not show a trend, thus indicating a correction would not be needed. Yaw does not show the need for a speed correction. The yaw moment peaks, both positive and negative, follow the quadratic relationship nicely.

T0Y at quay, reduced section Figure E.7 (appendix E) shows a similar trend to the largest section (figure 7.9). However, the $X+$ lies below the F_{c} factor, whereas the $X-$ peak is slightly higher than F_{c} for higher passing speeds. The first $Y+$ peak (black circle) shows an offset compared to the RoPES results, but no trend in function of the passing speed. The yaw moment relates more than quadratically to the passing speed, the trend is however not clear from the figure.

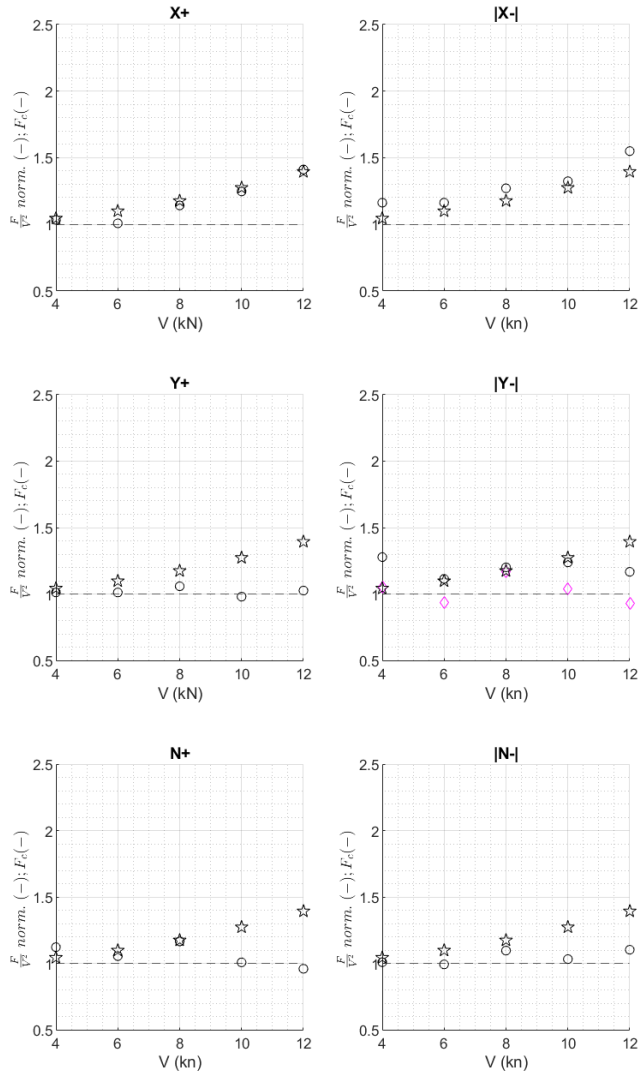

Figure 7.9: *Effect of speed on the peak force X, Y, N passing $C04$, moored $T0Y(Q)$, UKC_{p} = 50%, $\frac{W}{B_{\mathrm{p}}}$ = 10, $\frac{d_{\mathrm{pas}}}{B_{\mathrm{p}}}$ = 1.5 Normalised $PESCA$ peak (circle, diamond) and F_{c} (star)*

T0Y at quay, confined section Figure E.8 (appendix E) gives the passing ship forces for a blockage m_{p} of 0.227, which is near the upper limit where F_{c} should still be accurate. For $X-$, the correction factor indeed still performs well, for $X+$ however, there is no longer any correlation with the passing speed, so a correction factor is not required here. This also means that the difference between first and second force peak is considerable at high blockage.

The most interesting result is visible when looking at $Y-$, where both peaks seem to follow the trend of F_{c}. At the lowest speed (4 kn) considerable offsets are present between RoPES and PESCA however. RoPES significantly underestimates the first peak (factor 1.6), whereas the second peak in $PESCA$ is around 0.5 times the RoPES result. The yaw force is again less predictable, for large speed, a correction however seems to be needed for both $N+$ and $N-$.

T0Y at jetty, largest section Figure 7.10 shows that a correction factor representing the more than quadratic dependency, is needed for surge, sway and yaw, when a ship is moored in jetty configuration. The proposed factor F_{c} shows a good agreement with the plotted trend and can thus be used with confidence in these cases.

T0Y at jetty, reduced section Figure E.9 (appendix E), shows that the correction factor performs less well compared to the largest section. For $X+$ a trend which was present in figure 7.10 is no longer present, indicating that applying the correction factor F_{c} is in fact not needed. $X-$ follows the F_{c} trend nicely. The positive and first negative sway peak also follows the F_{c} correction nicely. The result for the second negative peak is less clear, as at first (4 to 8 kn) the quadratic dependency seems to hold; the values at 8 and 10 kn seem to jump above the proposed F_{c} factor. Additional plots, for other passing distances, could be used to further investigate this.

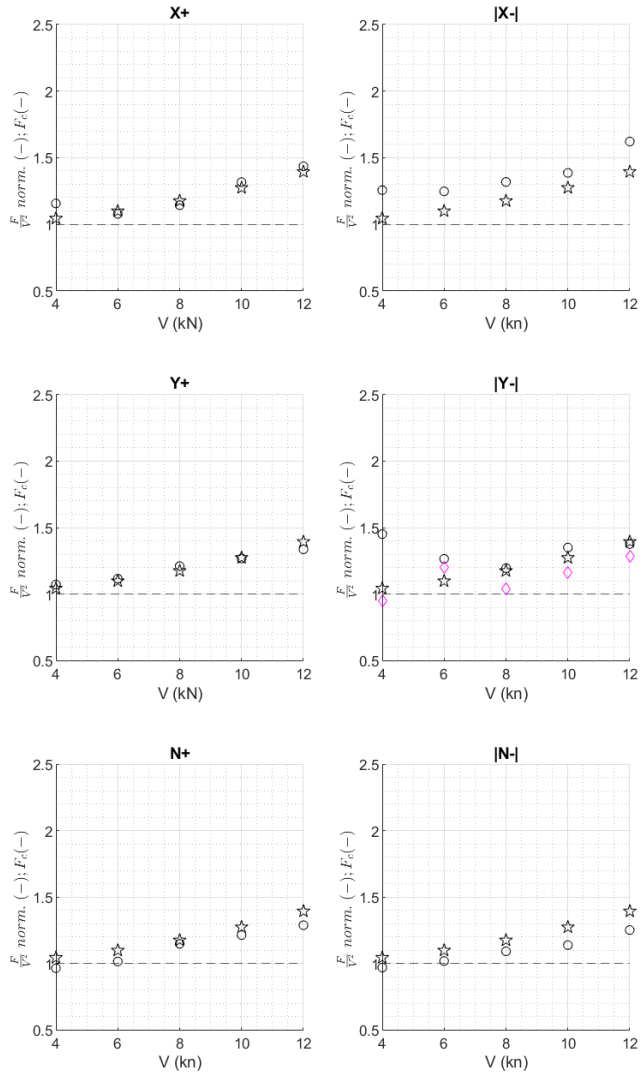

Figure 7.10: *Effect of speed on the peak force X, Y, N passing $C04$, moored $T0Y(J)$, UKC_{p} = 50%, $\frac{d_{\mathrm{pas}}}{B_{\mathrm{p}}}$ = 2.0, $\frac{W}{B_{\mathrm{p}}}$ = 10, Normalised $PESCA$ peak (circle, diamond) and F_{c} (star)*

Summarizing table Table 7.3 summarizes the need for application of F_c for surge, sway and yaw. The first half of the table expresses the observation by [TB14], stating the need to correct surge for quay mooring and all DOF for jetty mooring.

The second part shows the proposed correction needed for the different force components, based on cases discussed above. In case the trend is not fully conclusive, the assumption is made that F_c should be used as a conservative approximation. This assumption should be further refined based on the full $PESCA$ dataset.

In the bottom half of the table, a subdivision is made between positive and negative peak (surge, sway, yaw), and between first and second negative peak (sway). This can be generalised to first, second and third peak, with differences caused by the symmetry in RoPES peaks as a result of the double body potential flow. A differentiation is made between low to moderate blockage (indicated by $m_p \downarrow$) and high blockage ($m_p \uparrow$).

Table 7.3: *Preliminary analysis performance F_c based on a selection of quay wall and jetty passages for moored $T0Y$; P = based on $PESCA$, $m_p \downarrow$ = low blockage, $m_p \uparrow$ = high blockage.*

	X		Y			N	
[TB14] (Q)	F_c		/			/	
[TB14] (J)	F_c		F_c			F_c	
	X_1	X_2	Y_1*	Y_2*	Y_3	N_1	N_2
	$(X-)$	$(X+)$	(Y_{-1})	$(Y+)$	(Y_{-2})	$(N-)$	$(N+)$
P (Q), $m_p \downarrow$	F_c	F_c	F_c	/	/	/	/
P (Q), $m_p \uparrow$	F_c	/	F_c	F_c	/	F_c	F_c
P (J), $m_p \downarrow$	F_c	F_c	F_c	F_c	F_c	F_c	F_c
P (J), $m_p \uparrow$	F_c	/	F_c	F_c	F_c	F_c	F_c

** Due to the asymmetry in first and second negative peak which is not represented in RoPES, the Y_{-1} peak is always larger than what RoPES predicts, also at low speed*

7.5.3 Summary

This section started off by formulating four hypotheses, which were tested by comparing the $PESCA$ model test results with their numerical counterparts from RoPES. The answer to the hypotheses is formulated for each of the four statements, in the same order as presented above.

1. The effect of passing distance is correctly modelled by RoPES for the range of passing distances which are frequently observed in confined water. For larger passing distances, discrepancies are present. This is due to the smaller magnitude of forces, which makes it harder to measure them accurately in the towing tank. Second order wash waves also become prominent, which are measured in $PESCA$, but not modelled by RoPES.

2. The proposed factor F_{c} can be applied to correct RoPES simulations successfully. For the first negative peak in sway, an additional offset should be taken into account for confined water.

3. The subdivision into quay and jetty mooring, where F_{c} is only used to correct surge (horizontal plane) for quay mooring and used for surge, sway and yaw in case of jetty mooring, seems not to hold in all general cases. The analysis for low to moderate blockage is in line with [TB14], apart from the suggested correction of Y_1 for quay mooring. For high blockage, the trends deviate from what [TB14] observed, as will be discussed in the response to the fourth hypothesis.

4. The difference between the different peaks for the same force component becomes prominent for large blockage. Based on the analysis of the selected tests, the first peak in surge does not need correction for both quay and jetty mooring. For sway and yaw, the trend is no longer obvious and needs further investigation. For now, the author advises to use the correction factor for these cases, as this is a conservative approximation.

7.5.4 Future work : adding a second correction factor

The fourth point, regarding the need to correct all force peaks could be looked at from a different perspective. It has been shown that two effects occur:

1. RoPES underestimates forces on the moored ship for high passing speed and blockage.
2. RoPES cannot reproduce the asymmetry in force peaks, where the second (third) peak is always lower than the first peak in $PESCA$ tests (proven for surge and sway).

The first statement always holds, a correction factor F_{c} can generally be applied. In order to take into account the second point, a second correction factor $F_{\mathrm{c},2}$ can be applied to the second (surge), third (sway) force peak. Whereas F_{c} is strict larger than 1,$F_{\mathrm{c},2}$ will be strict lower than 1. A system like eq. 7.11 is then the result.

$$\begin{cases} F_{\mathrm{corr}} = F_{\mathrm{RoPES}} \cdot F_{\mathrm{c}} & \text{first peak} \\ F_{\mathrm{corr}} = F_{\mathrm{RoPES}} \cdot F_{\mathrm{c}} \cdot F_{\mathrm{c},2} & \text{second, third peak} \end{cases} \tag{7.11}$$

7.6 Tu_{m} to include confinement

The validation of the modified Tuck model Tu_{m} (eq. 6.19) showed that the effect of confined water on passing ship forces can be represented well by the Tu_{m} number. For the jetty mooring, the regression shows high R^2 values (0.91 and upwards, table 6.14); For quay mooring, the regression was further refined, by adding coefficients for UKC and channel width W.

The shortcoming of the very promising Tu_{m} model in fact was the general applicability over different combinations of moored and passing ships (section 6.7). Here, the power of RoPES and the mathematical model insights from chapter 6 can be combined to counter this aspect. If a RoPES simulation run is done with a given speed and blockage, the results for any passing speed and blockage can be calculated, under the assumption that the passing ship forces for both cases are a function of Tu_{m}. Eq. 7.12 represents this thought process, with $V_{\mathrm{a}}, m_{\mathrm{p,a}}$ and $V_{\mathrm{b}}, m_{\mathrm{p,b}}$ the two sets of speed and blockage.

$$F_{V_{\mathrm{b}},m_{\mathrm{p,b}}} = F_{V_{\mathrm{a}},m_{\mathrm{p,a}}} \cdot \frac{Tu_{\mathrm{m}}(V_{\mathrm{b}}, m_{\mathrm{p,b}})}{Tu_{\mathrm{m}}(V_{\mathrm{a}}, m_{\mathrm{p,a}})} \tag{7.12}$$

Figure 7.11 shows an application of this technique, where one RoPES calculation is run for V = 4 kn and m_{p} = 0.066 (which coincides with a channel width of 10 $B\mathrm{p}$ and UKC_{p} = 50%). Using eq. 7.12 gives the results for V = 6 to 12 kn, with m_{p} = 0.137. The stars (purple hexagon for the second negative sway peak) represent the value obtained from eq. 7.12, the circles (purple triangle for the second negative sway peak) are the corresponding $PESCA$ measurements. Both values are normalised using the technique from eq. 7.10.

The prediction for the largest peaks, $X-$ and $Y-$ is very good. $N+$ and $N-$ predictions are acceptable and conservative. For $X+$ and $Y+$, the model is not accurate. This follows from the observations above that with increase in confinement, the ratio between positive and negative peak changes, which is not covered by this approach.

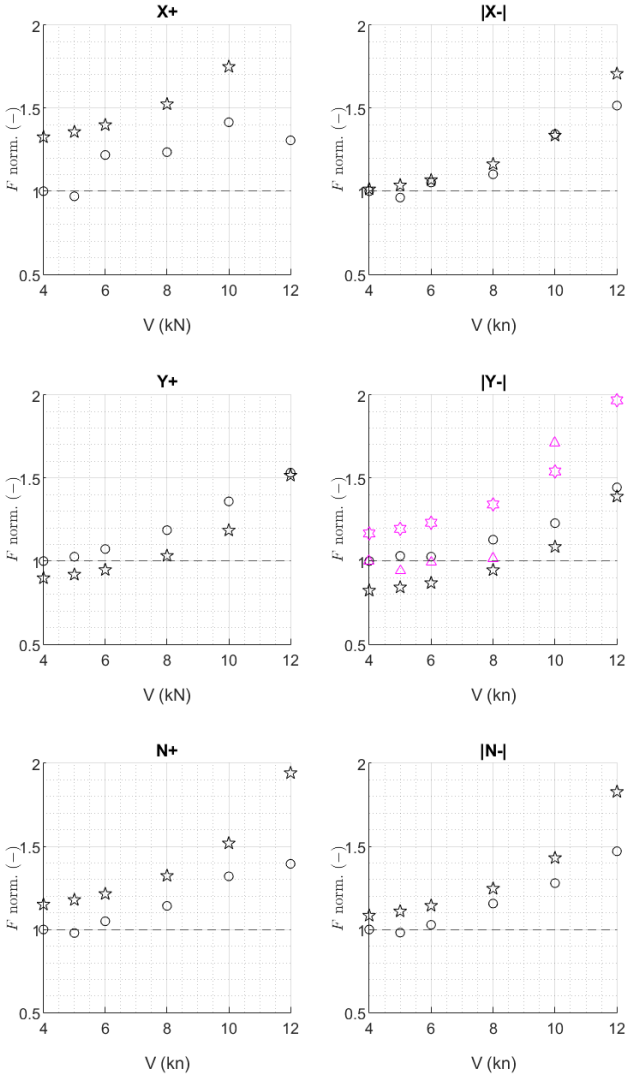

Figure 7.11: *Comparison modelled passing ship forces (eq. 7.12) (star, hexagon) with $PESCA$ measurements (circle, triangle)*
m_{p} = 0.137, passing $C04$, moored $T0Y(J)$, UKC_{p} = 20%, $\frac{d_{\mathrm{pas}}}{B_{\mathrm{p}}}$ = 1.0, $\frac{W}{B_{\mathrm{p}}}$ = 6

7.7 Summary

The $PESCA$ scale model test measurements have been used to validate the numerical model RoPES, which is a double body potential flow solver.

In order to accurately represent the $PESCA$ tests in the numerical RoPES environment, a sensitivity analysis has been performed, looking at the need to model the full towing tank, as well as the panel size of both channel and ship mesh.

The RoPES calculations deliver 6DOF forces in full scale, meaning that the $PESCA$ measurements need to be scaled up. The heave and pitch motion need to be converted to a heave force and pitch moment.

The analysis of the time series shows that the forces in the horizontal plane (surge, sway and yaw) are matched well by RoPES, concerning the shape of the signal as well as the magnitude of the peaks. For heave, an offset is present before and after the passage, which could not be explained without having access to the code. The pitch moment is modelled well; The roll moment can be reproduced well for jetty mooring, with less satisfying results for quay mooring.

The forces in the horizontal plane have been studied in detail. The effect of the passing distance is represented well in RoPES for low to moderate passing distance. When the passing distance is large, significant wash waves are measured in $PESCA$, which cannot be modelled with RoPES.

In confined water and/or at high speed, RoPES results need to be corrected, as proposed by [TB14], using their proposed factor F_{c}. This can indeed be used successfully. They indicated that for jetty mooring, the correction factor needs to be applied for all DOF, whereas for quay mooring, only surge needs to be corrected. The analysis of a few selected cases shows that the answer is more nuanced and is a function of the blockage. A subdivision between the different peaks for each DOF should also be made.

In case many different channel variations (width and water depth) need to be investigated, the correlation with Tu_{m} from chapter 6

can be used to predict peaks for different blockages. One RoPES simulation needs to be run, which is used to produce the force peaks for other passing speeds and blockages, based on the ratio between Tu_{m} parameters. This method shows potential. The addition of a factor which can represent the differences in positive and negative peak for surge, and first and second negative peak in sway, would increase the accuracy of this model.

References

[Del+12] G. Delefortrie et al. “The Effect of Shipping Traffic on Moored Ships”. In: *10th International Conference on Hydrodynamics*. St. Petersburg, Russia, 2012.

[HJ14] A.J. van der Hout and M.P.C. de Jong. “Passing ship effects in complex geometries and currents”. In: *PIANC World Congress*. San Francisco, USA, 2014.

[Kri05] D. Kriebel. *Mooring loads due to parallel passing ships*. Tech. rep. 2005.

[Pin04] J A Pinkster. “The influence of a free surface on passing ship effects”. In: *International Shipbuilding Progress* 61.4 (2004), pp. 313–338.

[Pin14] Pinkster Marine Hydrodynamics. *RoPES - Research on Passing Effects on Ships : User manual*. 2014, p. 38.

[PP14] J.A. Pinkster and H.J.M. Pinkster. “A fast, user-friendly, 3-D potential flow program for the prediction of passing vessel forces”. In: *PIANC World Congress*. San Francisco, USA, 2014.

[TB14] H. Talstra and A.J. Bliek. “Loads on moored ships due to passing ships in a straight harbour channel”. In: *PIANC World Congress*. San Francisco, USA, 2014, p. 19.

8

Concluding remarks and recommendations

8.1 Conclusions

The main goal of this thesis was to study and enhance the modelling of the response of moored ships in sheltered mooring locations. In order to do so, all elements of the mooring analysis were studied. The UGent in-house mathematical model *Vlugmoor* is at the heart of the mooring analysis.

The mooring configuration, the transfer function between ship and berth, is traditionally assessed based on guidelines for mooring line angles. As these guidelines cannot be applied successfully in some locations, e.g. mooring of a container ship at a quay berth with rail based gantry cranes, a novel approach was presented. In this method, the configuration is denoted by four so-called efficiency parameters, two for surge and two for the lateral direction. These parameters can be used to assess the configuration, spot weaknesses and estimate the impact of operational measures.

The elastic response of mooring lines determines to a large extent the ship's response. International standards however fail to incorpo-

rate elasticity parameters in their documents. A full scale mooring rope tension test at Bexco for three mooring ropes was executed and analysed to examine the difference in the elastic properties between lines, but also the change of the line response during cyclic loading. The more elastic lines showed significantly more impact of cyclic loading, on the stiffness of the line and the corresponding hysteresis. The calculated hysteresis energy production could be incorporated into the mathematical model, certainly when long simulation runs with cyclic loading are executed.

A variety of external disturbances can affect the ship, wind and passing ships being the prime sources in sheltered mooring locations. The wind effect is usually modelled using aerodynamic coefficients. A literature study of wind coefficients for (large) container ships highlights the impact of container stacking on these coefficients. A case study example shows that for rough environments, the reference wind pressure should be chosen higher than the one calculated at 10 m height, when the wind coefficients are determined for a smooth surface condition. An analytical method, based on Blendermann's research was validated using a CFD model for a limited number of wind directions.
Wind gusting has been implemented in *Vlugmoor*, based on the Von Karman power spectrum.

The impact of passing ships on moored ships can be assessed with numerous tools, including empirical relationships and numerical models. The effects of confined water are often not captured, or not correctly represented by these tools. Therefore, a dedicated model test program $PESCA$ was established, executed and analysed. A database of 1699 unique passing ship events were discussed in this thesis, for up to four channel widths and up to five UKC's.
The effect of passing distance, channel width and UKC was assessed using a regression analysis and compared with literature. Despite a fairly good agreement with literature, the need for a parameter which represents the effect of both channel width and UKC, became apparent. A novel empirical model, based on the modified Tuck number, was validated using the $PESCA$ tests. Whereas the modified Tuck model delivered optimal results for the prediction of surge peaks, extra terms, based on channel width and UKC, were added to fine-tune the model for sway and yaw in case of quay moored.

The $PESCA$ tests were also used to validate the potential flow solver RoPES. A good agreement was observed when comparing the time series. For heave, an unexpected offset was present in RoPES at the start and end of the simulation however. As RoPES' water surface boundary is fixed, the effect of confinement is underpredicted. The observations and proposed correction factor by Talstra and Bliek were validated, confirming the use of the factor. For very restricted sections, the use of the correction factor was further refined, as the impact of restricted water on the different peaks for each DOF differs.

The non-linear nature of the response of the moored ship requires a time domain calculation to be performed. Under the assumption of a quasi-static response, meaning that at each time step an equilibrium position is found, this system can be simplified and used for systematic calculations. This method was extended using impulse response functions (IRF), which represent the memory effect of the fluid.

The eigenperiods of the ship have been estimated based on a proposed analytical approach and compared with periods of external disturbances. The horizontal modes (surge, sway, yaw) are denoted by a large eigenperiod, in the range of long wave systems. Based on this comparison, the sensitivity of the equipment with respect to given external disturbances can be assessed, as well as impact of changes in mooring equipment on the eigenperiods.

Most moorings involve one moored ship, connected to the berth using her mooring equipment. In double-banking, two ships are moored adjacent to each other at one berth. A simplified moving quay wall model has been worked out and implemented in *Vlugmoor* to represent the relative movement of the ships with respect to each other.

The time domain solver gives time series of forces and ship motions as output. The interpretation of the motions depends on the type of loading , as well as the nature of the external disturbance (transient or cyclic). For some loading types, it is suggested to look at local motions, for example in extremities of the holds of bulk carriers or most forward or aft bays for container ships. For the latter, a method has been presented to come up with a safety limit for surge motions, considering the danger of potential collision between bridge/funnel and crane (spreader).

8.2 Recommendations

Despite the significant efforts from the author, the mooring analysis did not yet reveal all its secrets. Based on the discussions from the present work, the following recommendations for future research are made.

The time domain solver including the memory effect should be tested extensively in cases where cycling loading is modelled. This can be done in connection to the application of the wind gusting model.

The cyclic mooring line response curves, including hysteresis damping, could be implemented into *Vlugmoor*, to study the impact on long simulation runs of cycling loading. The same research could be done for fenders and included in the software.

The RoPES validation work should be extended, considering the full $PESCA$ test database. Certainly the inland ship interaction effect, for which tests with channel width three times the beam of the passing ship are available, should be validated. Such extensive parameter study could also be used to further confirm the applicability of the existing correction factor or to come up with a different expression.

The empirical model for passing ship effects proved to be lacking when used over all different passing and moored ship combinations. The influence of the ship shape and dimensions on the passing ship forces should be assessed further to refine the model. Modelling multiple ships and drafts in a physical scale model test however requires significant time and effort. Numerical simulations, using either potential or turbulent flow, could provide a faster alternative to gather an extensive dataset.

The method of assessing a mooring arrangement through its efficiency parameters can be further validated for different projects. Once enough validation work is available, this technique could be used in future projects, either in the first phase (prior to the time domain calculation) or to replace part of the simulation matrix.

A

Overview publications and mooring studies

A.1 Paper publications

T. Van Zwijnsvoorde, G. Delefortrie, E. Lataire; (2020) "Passing ship effects in shallow and confined water : open model test data for validation purposes". 6th MASHCON, 22-26 May, 2022, Glasgow, UK (preprint version 2.0)

T. Van Zwijnsvoorde, M.A. Tello Ruiz, G. Delefortrie, E. Lataire; (2019) "Sailing in shallow water waves with the DTC container carrier: open model test data for validation purposes". In: Candries, M. et al. 5th MASHCON International Conference on Ship Manoeuvring in Shallow and Confined Water with non-exclusive focus on manoeuvring in waves, wind and current, 19 - 23 May 2019, Ostend, Belgium. pp. 412-421

T. Van Zwijnsvoorde, K. Eloot, Vantorre, M, Lataire, E; (2019) "A mooring arrangement optimisation study". In : 11th International Workshop on Ship and Marine Hydrodynamics, Hamburg, Germany

T. Van Zwijnsvoorde, L. Donatini, W. Van Hoydonck, E. Lataire; (2019) "Wind modeling for large container vessels : a critical review of the calculation procedure". In : International Journal of Transport Development and Integration, Volume 3, number 4.

T. Van Zwijnsvoorde, L. Donatini, W. Van Hoydonck, E. Lataire; (2019) "Wind modeling for large container vessels : a critical review of the calculation procedure". In : Maritime Transport, Rome, Italy

T. Van Zwijnsvoorde, M. Vantorre, S. Ides, K. Eloot; (2019) "Safety of container ship (un)loading operations in the Port of Antwerp: Impact of passing shipping traffic". In : Maritime Business review, volume 4, issue 1.

T. Van Zwijnsvoorde, M. Vantorre; (2018) "Safety of container ship (un)loading operations: Impact of passing shipping traffic". In : WCTRS SIGA2 conference, Antwerp, Belgium.

T. Van Zwijnsvoorde, M. Vantorre, S. Ides; (2018) "Container ships moored at the port of Antwerp : Modelling response to passing vessels". In : Proceedings of teh 34th PIANC World Congress, Panama City, Panama.

T. Van Zwijnsvoorde, M. Vantorre; (2017) "Safe Mooring of Large Container Ships at Quay Walls Subject to Passing Ship Effects". In : International Journal of Maritime Engineering, 159(A4)

A.2 Mooring study I

Project title
Mooring analysis gas carrier in a restricted fairway
Project type
Design study new quay infrastructure, positioning of mooring points

type	(-)	gas carrier	n_{lines}	(-)	16
L_{OA}	(m)	245.0	MBL	(ton)	83.5
B	(m)	40.0	line type	(-)	HMPE + nylon
T_M	(m)	12.0	W	(m)	421.6
A_L	(m²)	5103	h	(m)	16.75
A_T	(m²)	1195	passing ship	(-)	oil tanker

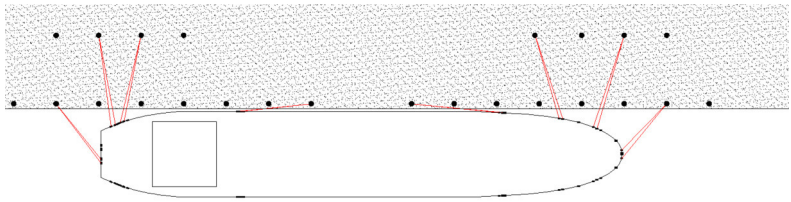

Challenges
(1) Design ship not yet built
(2) Large passing ship effect and wind effect
(3) Choice of fender type not yet made
Solution
(1) Scaling of smaller ship (fleet study) + discussion with client
(2) Custom mooring point arrangement
(3) Model of soft cylindrical fender + stiff quay wall
Vlugmoor adaptations
Mooring at quay modelled as series of high stiffness springs

A.3 Mooring study II

Project title
Mooring analysis container ship in restricted fairway
Project type
Study operational safety under ship passages

type	(-)	container	n_{lines}	(-)	16
L_{OA}	(m)	399.0	MBL	(ton)	140.0
B	(m)	59.0	line type	(-)	*Blank*
T_M	(m)	15.2	W	(m)	450.0
A_L	(m²)	*Blank*	h	(m)	18.0
A_T	(m²)	*Blank*	passing ship	(-)	container

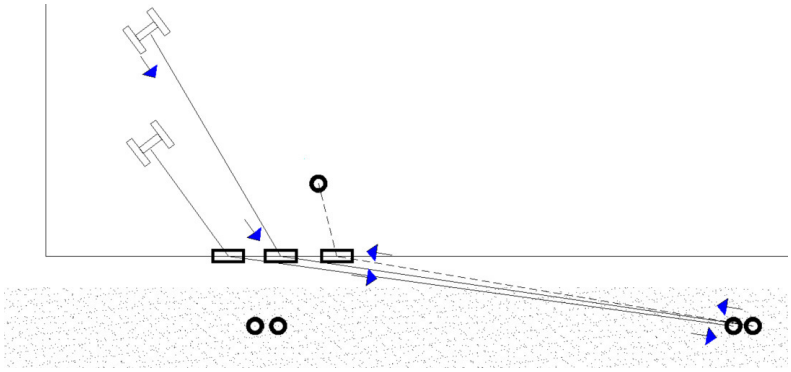

Challenges
(1) Small passing distance = large passing ship effect
(2) Mooring arrangement with limited surge capacity
Solution
(1) Systematic calculations to provide advice to pilots
(2) Double spring capacity by leading line back to bitt on board

A.4 Mooring study III

Project title
Mooring analysis bunker operation in confined waterway
Project type
Study operational safety under ship passages

type	(-)	inland tanker	n_{lines}	(-)	3-4
L_{OA}	(m)	110.0	MBL	(ton)	*Blank*
B	(m)	11.5	line type	(-)	*Blank*
T_M	(m)	3.5	W	(m)	450.0
A_L	(m²)	*Blank*	h	(m)	18.0
A_T	(m²)	*Blank*	passing ship	(-)	container

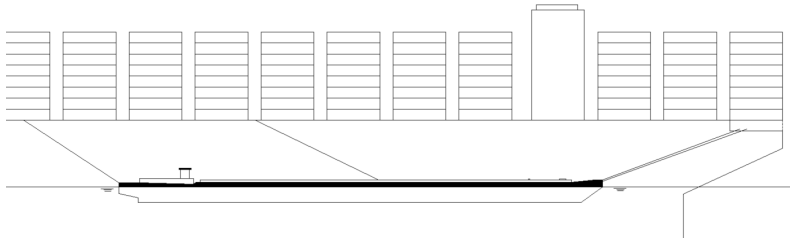

Challenges
(1) Representative mooring configuration for bunker operation
(2) Bunker ship moves relative to moored container ship
Solution
(1) Study of approach manoeuvre to determine configuration
(2) Moving quay wall model to represent moored container ship
Vlugmoor adaptations
Moving quay wall condition for mooring analysis bunker ship

A.5 Mooring study IV

Project title
Mooring analysis bulk carrier in waiting area under ship passage
Project type
Study of mooring incident

type	(-)	bulk carrier	n_{lines}	(-)	6
L_{OA}	(m)	225.0	MBL	(ton)	100
B	(m)	32.2	line type	(-)	*Blank*
T_M	(m)	13.8	W	(m)	*Blank*
A_L	(m²)	*Blank*	h	(m)	*Blank*
A_T	(m²)	*Blank*	passing ship	(-)	container

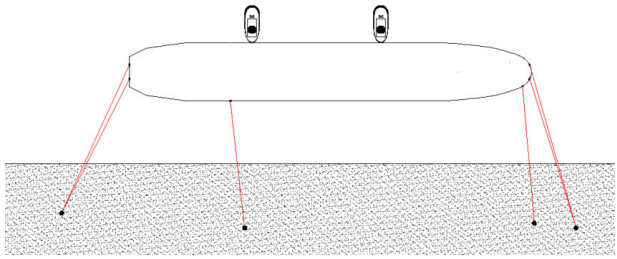

Challenges
(1) Determining ship and environment parameters (at time of incident)
(2) Representation of winch use on board in *Vlugmoor*
(3) Assessment the effect of tug boats pushing at side moored ship
Solution
(1) In-depth study AIS data, tidal charts and ship mooring configuration
(2) Study of model representing rendering winch
(3) Model of different push forces and application points
Vlugmoor adaptations
(1) Model of the effect of (multiple) pushing tug boats
(2) Rendering winch model

A.6 Mooring study V

Project title
Mooring analysis double banking oil tankers
Project type
Study operational safety under ship passages

Ship at berth

type	(-)	oil tanker	n_{lines}	(-)	16
L_{OA}	(m)	230.0	MBL	(ton)	72.0
B	(m)	32.0	line type	(-)	HMPE
T_M	(m)	14.5	W	(m)	*Blank*
A_L	(m²)	*Blank*	h	(m)	*Blank*
A_T	(m²)	*Blank*	passing ship	(-)	oil tanker

Ship alongside

type	(-)	oil tanker	n_{lines}	(-)	6
L_{OA}	(m)	145.0	MBL	(ton)	50
B	(m)	23.0	line type	(-)	polyester
T_M	(m)	10.0	W	(m)	*Blank*
A_L	(m²)	*Blank*	h	(m)	*Blank*
A_T	(m²)	*Blank*	passing ship	(-)	oil tanker

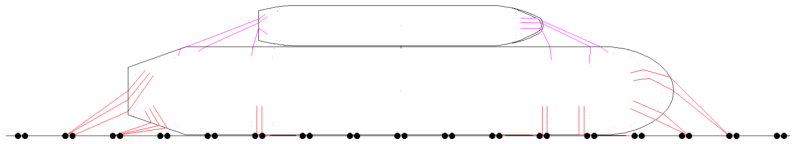

Challenges
(1) Determining mooring arrangement ship alongside
(2) Representation double banking in time domain simulation
Solution
(1) Study mooring equipment both ships + discussion with terminal
(2) Two step calculation ship at berth and ship alongside, moving quay wall
Vlugmoor adaptations
Moving quay wall application in *Vlugmoor*

A.7 Mooring study VI

Project title
Mooring analysis oil tanker at a jetty in a restricted waterway
Project type
Study operational safety under ship passages

type	(-)	oil tanker	n_{lines}	(-)	16
L_{OA}	(m)	274.2	MBL	(ton)	71
B	(m)	48.0	line type	(-)	steel + tail
T_M	(m)	15.5	W	(m)	*Blank*
A_L	(m²)	*Blank*	h	(m)	*Blank*
A_T	(m²)	*Blank*	passing ship	(-)	bulk carrier

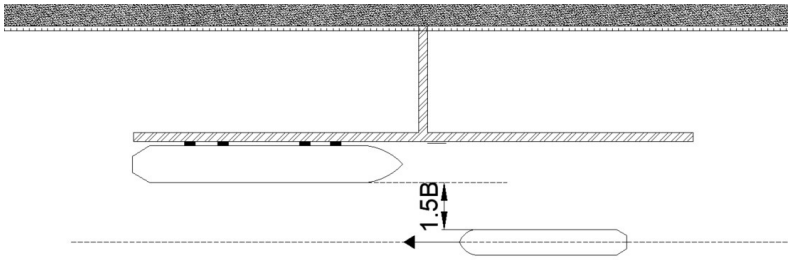

Challenges
(1) Large passing ship effects - various moored ship sizes
(2) Assessment requirement maintenance dredging
Solution
(1) Systematic matrix, variation moored ship - passing speed
(2) Inclusion of panellised bottom in RoPES software

A.8 Mooring study VII

Project title
Mooring analysis wind effects on container ships
Project type
Study operational measures in harsh wind conditions

type	(-)	container	n_{lines}	(-)	16
L_{OA}	(m)	399.0	MBL	(ton)	140.0
B	(m)	63.0	line type	(-)	*Blank*
T_M	(m)	14.0	W	(m)	*Blank*
A_L	(m²)	17721	h	(m)	19
A_T	(m²)	3569	passing ship	(-)	*Blank*

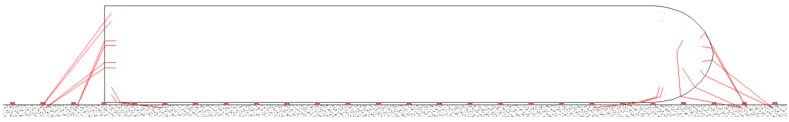

Challenges
(1) Selection of wind coefficients (container stacking)
(2) Relationship wind forecast and wind conditions at terminal
(3) Time varying wind speed for mooring analysis
Solution
(1) Literature study coefficients and stacking influence
(2) Analysis weather forecast, port and terminal measurement
(3) Inclusion of memory effects + study wind spectra
Vlugmoor adaptations
Generation of time series fluctuating wind (Von Karman spectrum)

A.9 Mooring study VIII

Project title
Mooring analysis bulk carrier during locking
Project type
Study mooring operation during water exchange (closed doors)

type	(-)	bulk carrier	n_{lines}	(-)	6
L_{OA}	(m)	259.9	MBL	(ton)	69.0
B	(m)	41.0	line type	(-)	polyester
T_M	(m)	12.5	W	(m)	*Blank*
A_L	(m²)	3049	h	(m)	*Blank*
A_T	(m²)	894	passing ship	(-)	*Blank*

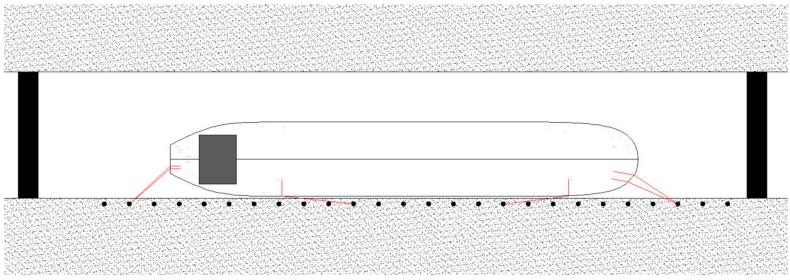

Challenges
(1) Representation of mooring operation during locking
(2) Mooring analysis time varying lock forces (obtained from scale model)
Solution
(1) Study of mooring equipment ships + discussions with pilots
(2) Lock forces as input and inclusion water level change
Vlugmoor adaptations
New object 'lock forces' and z-position variation mooring points

A.10 Mooring study IX

Project title
Mooring analysis oil tanker under wind (quay+jetty mooring)
Project type
Operational policy harsh wind conditions

---

type	(-)	oil tanker	n_{lines}	(-)	12
L_{OA}	(m)	185.0	MBL	(ton)	51.0
B	(m)	32.2	line type	(-)	polyester
T_M	(m)	6.5	W	(m)	*Blank*
A_L	(m²)	3796	h	(m)	*Blank*
A_T	(m²)	955	passing ship	(-)	*Blank*

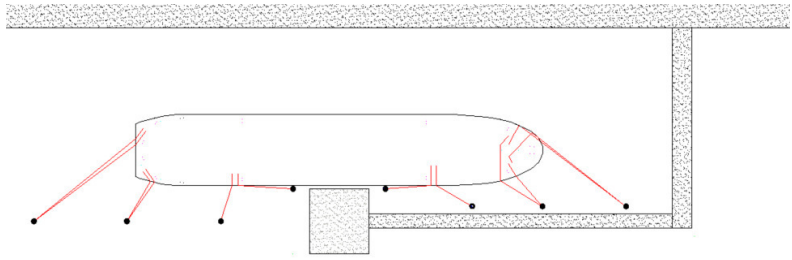

Challenges
(1) Selection of representative design ship for operational procedure
(2) Differentiation quay and jetty mooring
Solution
(1) Back-and-forth with client to obtain representative design ship
(2) Mooring analysis for both cases, separate mooring arrangement optimisation

A.11 Mooring study X

Project title
Mooring analysis container ship under ship passage
Project type
Bollard incident quay wall

type	(-)	container	n_{lines}	(-)	12
L_{OA}	(m)	332.0	MBL	(ton)	120.0
B	(m)	48.0	line type	(-)	nylon
T_M	(m)	11.7	W	(m)	*Blank*
A_L	(m²)	*Blank*	h	(m)	*Blank*
A_T	(m²)	*Blank*	passing ship	(-)	container + tanker

Challenges
(1) Estimation elongation curve nylon rope
(2) Study bollard loads
Solution
(1) Model of several curves, based on literature + standards
(2) Calculation total load on bollard (x,y,z,vector)
Vlugmoor adaptations
Bollard number related to mooring line number, calculation total bollard load

B

Axis system and convention

A consistent axis system definition is used throughout this thesis, which is in accordance with the definitions and conventions used in the mathematical model *Vlugmoor*. Six degrees of freedom (6DOF) are considered, see figure B.1. Table B.1 shows the corresponding notations. The axis system is a right-handed system, with origin at midships, on the waterline. The y-axis is defined positive to port side, the z-axis is positive upwards. Figure B.2 gives the ship positioned in the earth-fixed (inertial) axis system $O_{0x0y0z0}$. The ship-fixed axis system is defined as 0_{xyz}.

Table B.1: *Definition 6DOF in English and Nederlands (nl.).*

DOF	notation	force moment	motion rotation	velocity	acceleration
1	surge	X	x	u	$\dot{u}$
2	sway	Y	y	v	$\dot{v}$
3	heave	Z	z	w	$\dot{w}$
4	roll	K	ϕ	p	$\dot{p}$
5	pitch	M	θ	q	$\dot{q}$
6	yaw	N	ψ	r	$\dot{r}$

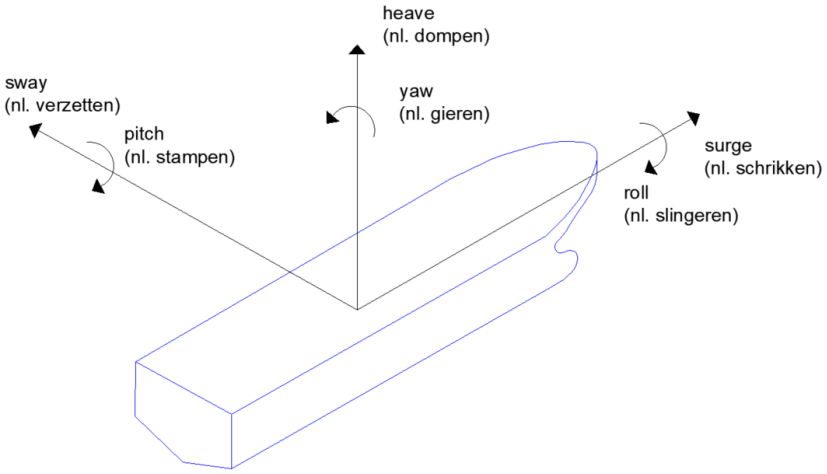

Figure B.1: *Definition 6DOF in English and Nederlands (nl.).*

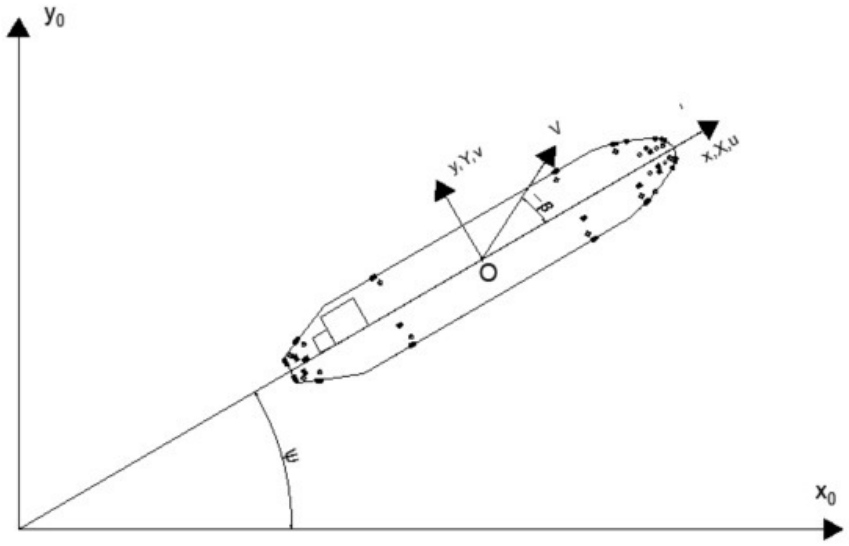

Figure B.2: *Axis system and conventions used in mathematical model Vlugmoor and throughout the thesis text. Ship (O_{xyz}) and earth inertial ($O_{0x0y0z0}$) system.*

When discussing mooring line angles and line lengths, the coordinates are expressed in the earth fixed axis system, which coincides with the starting position of the moored ship in the simulation run (figure B.3). The mooring points on the berth are denoted by the subscript b (berth) $x_{0\mathrm{b}}$, $y_{0\mathrm{b}}$, $z_{0\mathrm{b}}$, the point where the line leaves the ship, the fairlead, gets the subscript s (ship) $x_{0\mathrm{s}}$, $y_{0\mathrm{s}}$, $z_{0\mathrm{s}}$. Based on these coordinates, you get the line length l and line angles α,β. In the figure, an axis system $0_{0'x0'y0'z0'}$ is defined, which is a translation of the earth-fixed $O_{0x0y0z0}$ system to the attachment point of the mooring line on the berth.

In the $PESCA$ model tests, the positions of the ships during the experiments are defined in a earth-fixed axis system for the towing tank, which is denoted by adding the subscript t. There are three ships defined : one passing ship and two moored ships (fixed position $x_{0\mathrm{t}} = 23m$ and $x_{0\mathrm{t}} = 43m$ respectively for the moored ship). Note that this representation differs from the conventional towing tank axis convention, where the y-axis is defined positive to starboard and z-axis positive downwards. Appendix D elaborates on the transformation which is done for all data, to keep a consistent axis system for the discussion in this thesis. The ship-fixed axis system of each ship is denoted by a subscript p for the passing ship; the subscripts m1 and m2 are used to define the axis system of the moored ships.

Table B.2 summarizes the notations used for the axis systems.

Table B.2: *Axis system definitions .*

ship-fixed		earth-fixed	
general	O_{xyz}	general	$O_{0x0y0z0}$
passing	O_{xpypzp}	translated	$O_{0'x0'y0'z0'}$
moored 1	$O_{xm1ym1zm1}$	towing tank	$O_{0t0x0ty0tz0t}$
moored 2	$O_{xm2ym2zm2}$		

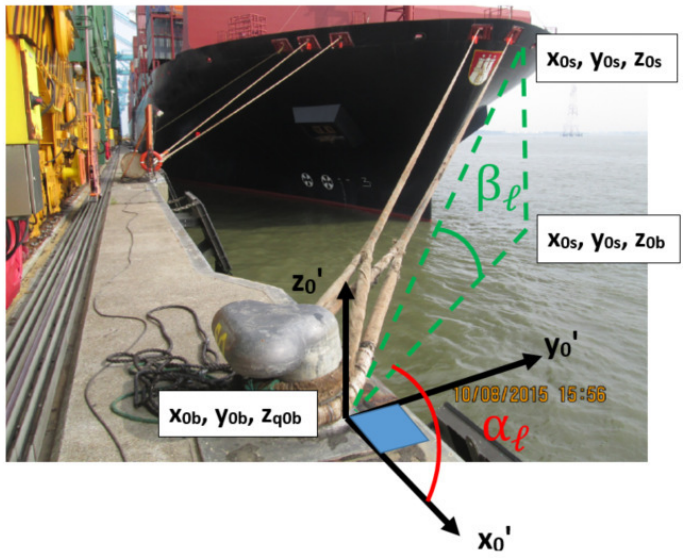

Figure B.3: *Mooring line coordinates b(berth) and s(ship) and definition mooring line angles* α_1 *and* β_1.

C

Wind : vertical profile, roughness, turbulence, spectrum

C.1 Vertical wind profile

C.1.1 General motion of wind

> "Wind, or the motion of air with respect to the surface, is fundamentally caused by variable solar heating of the earth's atmosphere. It is initiated by differences of pressure between points of equal elevation. " - from [SS96]

Wind will thus flow from high to low pressure locations, driven by the pressure gradient $\frac{\mathrm{d}p}{\mathrm{d}n}$. However, due to the rotation of earth, the path of a particle appears to be curved for an observer standing on earth. This apparent force is defined as the Coriolis force, which is stronger the closer you move to the polar regions. The combination of the pressure gradient and the Coriolis force generates an air flow along the lines of equal pressure, called isobars. The geostrophic wind, G (m/s), is expressed by eq. C.1, with ϕ_{G} being the latitude,

ω_{G} the spin rate of the earth and f_{c} the Coriolis parameter.

$$G = \frac{\frac{\mathrm{d}p}{\mathrm{dn}}}{2\rho\omega_{\mathrm{G}}\sin\phi_{\mathrm{G}}} = \frac{\frac{\mathrm{d}p}{\mathrm{dn}}}{\rho f_{\mathrm{c}}} \tag{C.1}$$

C.1.2 Surface friction

Eq. C.1 is valid for undisturbed mean wind flow at great heights, where no energy is added or removed from the system. Due to the presence of the earth's surface however, friction is generated, which causes the flow to lose energy and thus slow down near the surface, resulting in an atmospheric boundary layer, which is denoted here as δ_a. In this boundary layer there is variation of mean wind speed, wind direction and turbulence with the height above the surface.

These three considerations are very important to make. The variation in (mean) wind speed with height causes different wind pressures along the ship's structure. For large container vessels, where the top of the bridge is located up to 50 m above the water surface, the wind speed will be much larger at this top point compared to the main deck level. The turbulence causes the wind velocity to fluctuate in time and space, denoted by a general energy balance between turbulent eddies of various sizes.

C.1.3 Logarithmic velocity profile

The wind field in a homogeneous boundary layer can be described as eq. C.2 (for the x-direction and corresponding velocity mean velocity U).

$$G - U(z) = -\frac{1}{\rho f_{\mathrm{c}}}\frac{\partial \tau_v}{\partial z} \tag{C.2}$$

Here G is the geostrophic wind (boundary condition), $U(z)$ longitudinal velocity in function of height, $\frac{\mathrm{d}\tau_v}{\mathrm{d}z}$ the variation in frictional force and f_{c} the Coriolis parameter. The solution of equation C.2 is not straightforward. A popular approach is assuming that the boundary layer is defined into an outer layer and a surface layer, for which the solutions of the equations should match in the overlap region.

Without going into further detail, based on these assumptions and eq. C.2, the logarithmic law can be described (eq. C.3). u_* (m/s) is the shear velocity (eq. C.4), defined as the ratio between the surface

shear and the density of the air. Another profile commonly used in wind modelling is the power law (eq. C.5), for which the power α can be found in several literature sources. Often, the 1/7 power law is used.

$$U(z) = \frac{1}{\kappa} u_* \ln \frac{z}{z_0} \tag{C.3}$$

$$u_* = \sqrt{\frac{\tau_0}{\rho}} \tag{C.4}$$

$$U(z_1) = U(z_2) \left(\frac{z_1}{z_2} \right)^{\alpha} \tag{C.5}$$

C.1.4 Inclusion of thermal convection

In the above discussion, the assumption is made that there is no thermal mixing present, in which case the stratification is denoted as neutral. Due to temperature differences between land/sea and air, the atmosphere can become stable / unstable, which slightly alters the wind profile, as shown by Monin and Obukhov in eq. C.6. ψ_{mu} and L_{mu} are the Monin-Obukhov function and length respectively. For further details, reference is made to [CWH96] and [Van+90]. For L = ∞ and ϕ = 0 , expression C.6 reduces to equation C.3, as it should.

$$U(z) = \frac{1}{\kappa} u_* \left(\ln \frac{z}{z_0} - \psi_{\mathrm{mu}} \frac{z}{L_{\mathrm{mu}}} \right) \tag{C.6}$$

C.1.5 Roughness sea wind profile

In chapter 5 of the thesis, the definition and influence of terrain roughness, z_0, has already been discussed. For open sea, this roughness varies in function of the wind field on the specific location, but also from remote wind fields, generating swell. The wave climate determines the roughness of the surface. Charnock derived an expression for z_0 in function of the shear velocity (eq. C.7), described in [CWH96], with α equalling 0.0144 for fully developed seas.

$$z_0 = \alpha \frac{u_*^2}{g} \tag{C.7}$$

[SS96] gives expressions to calculate a surface drag coefficient C_{d} (eq. C.8), based on the mean wind speed at 10 m height which is

subsequently translated into a surface roughness (eq. C.9).

$$C_{\mathrm{d}} = 5.1\,(U(10))^{0.46}\,10^{-4} \tag{C.8a}$$

$$C_{\mathrm{d}} = (7.5 + 0.67U(10))10^{-4} \tag{C.8b}$$

$$C_{\mathrm{d}} = 0.0015\left[1 + exp\left(-\frac{U(10) - 12.5}{1.56}\right)\right]^{-1} + 0.00104 \tag{C.8c}$$

$$z_0 = \frac{10}{e^{\left(\frac{\kappa}{\sqrt{C_d}}\right)}} \tag{C.9}$$

Table C.1 gives the calculated values for z_0 and u_* based on eq. C.7 and eq. C.9, for a 10 m/s wind speed at 10 m height above the surface.

Table C.1: *Calculation of shear velocity u_* and roughness length z_0 based on empirical formula, for a wind speed of 10 m/s at 10 m height.*

	eq C.7	eq C.8a	eq C.8b	eq C.8c
$z_0(10^{-4})$ (m)	2.008	2.954	2.455	1.466
u_* (m/s)	0.370	0.384	0.377	0.360

C.2 Atmospheric turbulence

When an anemometer reading is analysed, a continuous fluctuation of the wind speed around the mean velocity U(z) for a given value of the height z will be observed. This is caused by turbulence or time-dependent fluctuations in the air flow (given that the anemometer has a fixed position in space). Having a good understanding of the theory behind turbulence is needed to comfortably use wind power spectra, used to generate time series of wind speeds as input for a mooring analysis. Note that turbulence occurs in all directions; Longitudinal turbulence is focussed on here, as this defines the shape of the wind spectrum which is used to generate the wind time series U_{ref} (section 5.14).

C.2.1 Turbulence intensity

Turbulence intensity (I_z) is often expressed relative to the mean wind speed (eq. C.10). σ_u is the variance of the turbulent spectrum. Different expressions for σ_u exist. In chapter 5 of the thesis, eq. 5.17, a relationship dependent on the height above the surface (z) was presented. Eq. C.11 is another expression used to evaluate σ_u, based on the friction velocity u_* and a parameter β_u (for values see [SS96], table 2.3.1), where the variance is assumed to be independent of the height.

$$I(z) = \frac{\sigma_u}{U(z)} \tag{C.10}$$

$$\sigma_u = \beta_u u_* \tag{C.11}$$

C.2.2 Integral scales of turbulence

Velocity fluctuations in time can be written as a superposition of eddies passing in one point. These turbulent motions have varying sizes, which are defined similar to travelling waves, by a wave number. The average size of eddies is denoted as 'integral scales of turbulence'. For each direction (x,y,z) these scales can be calculated. Including cross terms, there are nine such scales in total. The turbulence length L_u^x (m), the longitudinal turbulence caused by the longitudinal air flow, is expressed by eq. C.12.

$$L_u^x = \frac{1}{\sigma_u^2} \int R_{u1u2}(x) \mathrm{d}x \tag{C.12}$$

In this expression, R_{u1u2} is the cross-correlation function of the longitudinal velocity component. These scales can be compared with critical dimensions of the vessel, which can be beam/length or dimensions of structures on deck. In the assumption that flow disturbances travel with the mean speed (Taylor's hypothesis of frozen turbulence), eq. C.12 can be rewritten as eq. C.13.

$$L_u^x = \frac{1}{\sigma_u^2} \int R_u(x) \mathrm{d}x \tag{C.13}$$

Estimations of this turbulent scale are made based on measurement campaigns. Empirical formula for turbulence scales are derived from said measurements. [SS96] reports turbulence lengths between 36 m (z = 16 m, z_0 = 1.00 m) and 82 m (z = 15 m, z_0 = 0.01 m) indicating that for typical large container ships these eddies may have length scales close to the dimension of the ship's beam. Several empirical formula have been developed to estimate L_u^x. Eq. C.14 ([SS96]) gives an expression for the large scale turbulence in function of parameters C and z_{m}.

$$L_u^x = \mathrm{C} z_{\mathrm{m}} \tag{C.14}$$

[Bec10] defines eq. C.15.

$$L_u^x = 300 \left(\frac{z}{350}\right)^{\frac{1}{k}} with\ 1/k = 0.437 + 0.153 \log z_0 \tag{C.15}$$

In [LG97] reference is made to ESDU - Engineering Sciences Data Unit , defining expressions eq. C.16. eq. C.15 and C.16a are similar in shape, with slightly different expressions for k. eq. C.16a is the expression used in *Vlugmoor* (chapter 5, eq. 5.18).

$$L_u^x = 300 \left(\frac{z}{300}\right)^{\frac{1}{k}} with\ 1/k = 0.46 + 0.074 \ln z_0 \tag{C.16a}$$

$$L_u^x = 25 z^{0.35} z_0^{-0.063} \tag{C.16b}$$

In [Yan+12], an empirical formula for the integral length scale is derived based on measurements at Beijing meteorological tower (eq. C.17), valid for wind speeds above 8 m/s (measured at z = 47 m). Below this value, the integral length scale increases with increasing wind speeds. The authors give no estimation of z_0: as it is a city environment, the surface is considered to be rough.

$$L_u^x = \begin{cases} 90 \left(\frac{z}{30}\right)^{0.55} & z > 30 \\ 90 & z \leq 30 \end{cases} \tag{C.17}$$

Table C.2 compares the values for L_u^x based on the different expressions listed above. There is no good agreement between measured data and the empirical formula. This can be expected as the expressions are derived based on specific data sets, which are extrapolated for different heights. One thing to note is that a rough surface leads to smaller integral length scales. The average eddy size for wind coming from sea is thus larger than from land.

Table C.2: *Turbulence length L_u^x based on measured data and empirical formula.*

	meas.	eq. C.14	eq. C.15	eq. C.16a	eq. C.16b
$z = 15\ z_0 = 0.01$	82	198	196	117	86
$z = 16\ z_0 = 1.00$	36	78	106	78	66

C.3 Theoretical shape wind spectrum

In many cases, actual wind measurements at the site for which the mooring analysis needs to be performed are not available. Even when this data is present, the processing time and effort is often not available to generate a representative time series of wind speeds. This is why in many projects, predefined power spectra for wind are used to define a fluctuating wind field. Many authors have proposed different spectra, leaving the user a choice. In most occasions this preference is more 'historically grown', without considering which approximation is best suited for a given project. This section aims at providing some background on the general shape of wind spectra.

C.3.1 Kolmogorov's hypotheses

A turbulent wind field consists of eddies of different sizes, defined by their wavelength (λ_e) or wave number (k_e). In general, the largest eddies transfer their energy to the smaller eddies, which end up dissipating the energy. These large eddies show directional dependency (hence different length scales), however at smaller scales, Kolmogorov formulated a hypothesis of local anisotropy.

> "When the flow is characterized by sufficiently high Reynolds numbers, the small scale turbulent motions are isotropic", from [Bak05]

Small scale eddies can thus be represented solely based on the energy received from the large eddies (ϵ_e, energy transfer rate) and the viscous dissipation (ν). This leads to Kolmogorov's first similarity hypothesis.

> "When the Reynolds numbers characterizing the flow are sufficiently high, the form of the smallest eddies is uniquely described by ϵ_e and ν", from [Bak05]

The energy transfer from larger to smaller eddies is more predominant then the viscous energy dissipation, which leads to a eddy representation solely based on ϵ_e, leading to the following second hypothesis.

"When the Reynolds number characterizing the flow are sufficiently high, the form of the eddies is uniquely described by ϵ_e." , from [Bak05]

C.3.2 Power spectrum in the inertial sub-range

Based on the first hypothesis and dimensional analysis, eq. C.18 represents the shape of spectral energy distribution (based on [SS96] and [Bak05]) in the inertial sub-range.

$$\frac{nS(n)}{\sigma_u^2} = Cf^{-2/3}\ with f = \frac{nz}{U} \tag{C.18}$$

n is the frequency, $S(n)$ the power spectrum, σ_u^2 the variance, f the Monin similarity constant and C a constant. This spectrum shape is often encountered in power spectra in literature.

C.3.3 Boundary condition wind spectrum

The expression for the spectral shape in the inertial sub-range, equation C.18, is often used to represent the spectrum over the whole domain. In [SS96] shows that the spectrum in its limit for low frequencies, should obey eq. C.19. Eq. C.18 does however not comply with these boundary conditions, meaning that the energy representation in the limit of the distribution will deviate from the theoretical assessment.

$$S(0) = 4\frac{\sigma_u^2 L_u^x}{U} \tag{C.19a}$$

$$\left.\frac{\mathrm{d}S(n)}{\mathrm{d}n}\right|_{n=0} = 0 \tag{C.19b}$$

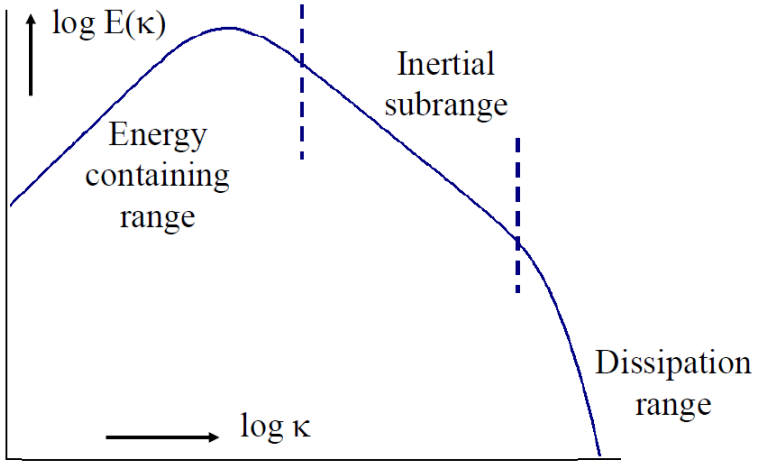

Figure C.1: *Spectral energy distribution wind field (longitudinal turbulence), figure taken from [Bak05].*

C.4 Power spectra used in practice

Several power spectra are available in literature, which are based on wind measurements and the theory which is described above. Notations and definitions often change between sources, even for the same wind spectrum. The candidate has attempted to use uniform definitions wherever possible. A subdivision is made in between height dependent and independent spectra.

C.4.1 Height dependent spectra

Batchelor The Batchelor spectrum, eq. C.20 [Yan+12], satisfies the spectral shape for the inertial sub-range.

$$\frac{nS_u(z,n)}{u_*^2} = \alpha f^{-2/3} \tag{C.20}$$

This shape indeed matches the general expression for the energy distribution in the inertial sub-range (eq. C.18). In expression C.18, the variance of the signal (σ_u) is included in the denominator, whereas in C.20, the shear velocity is used. This could lead to large errors in the spectral amplitudes when overlooking this important difference in notation. Therefore, the spectrum is reformulated (eq. C.21), using the expression for u_* from eq. C.10.

$$\frac{nS_u(z,n)}{\sigma_u^2} = \frac{\alpha}{\beta_u} f^{-2/3} \tag{C.21}$$

Von Karman spectrum Eq. C.22 gives the spectrum defined by Von Karman ([Yan+12]):

$$\frac{nS_u(z,n)}{\sigma_u^2} = \frac{\frac{4nL_u^x}{z}}{\left(1+\frac{70.8nL_u^{x^2}}{z^2}\right)^{\frac{5}{6}}} \tag{C.22}$$

In eq. C.22, the integral length scale for the turbulence, L_u^x is used (see section C.2.2). The boundary definitions in C.19 are met in this case. Note that for low frequencies, S(n) is nearly constant. In other words, the energy contained in the large eddies is overestimated.

Another way of representing this spectrum is based on the definition of a new dimensionless coordinate f_u (eq. C.23), leading to the

spectral representation from eq. C.24, which is the one included in *Vlugmoor* (chapter 5, eq. 5.15).

$$f_u = \frac{nL_u^x}{U} \tag{C.23}$$

$$\frac{nS_u(z,n)}{\sigma_u^2} = \frac{4f_u}{(1+70.8f_u^2)^{5/6}} \tag{C.24}$$

Solari In the American Wind Code, a spectrum very similar to the one given in equation C.24 is given, with different numerical constants (eq. C.25), from [Yan+12].

$$\frac{nS_u(z,n)}{\sigma_u^2} = \frac{6.868f_u}{(1+10.302f_u)^{5/3}} \tag{C.25}$$

The similarity between equations C.25 and C.24 becomes obvious as $(f_u)^{2^{(5/6)}} = f_u^{5/3}$.

Simiu Simiu developed an expression which again follows the theoretical shape in the inertial sub-range. In [Bec10] and [SS96], the shear velocity u_* is included in the spectral representation, implicitly assuming a value for β_u (u_* and σ_u are related through eq. C.11. Eq. C.26 represents the more general representation of the energy distribution.

$$\frac{nS_u(z,n)}{\sigma_u^2} = \frac{33.33f}{(1+50f)^{5/3}} \tag{C.26}$$

The values for S(0) and $\left.\frac{dS(n)}{dn}\right|_{n=0} = 0$ are not consistent with the boundary conditions in this case. The energy in the lower end of the spectrum will be underpredicted using expression C.26.

Kaimal The Kaimal spectrum is very similar to the Simiu spectrum, with slightly different coefficients, but the same general shape of the curve, obeying the theoretical derivation for the inertial subrange. The same remarks hold as for the Simiu spectrum.

$$\frac{nS_u(z,n)}{\sigma_u^2} = \frac{17.5f}{(1+33f)^{\frac{5}{3}}} \tag{C.27}$$

Qinqsham et al. In [Yan+12], they fit a spectrum to measured wind data, following the general spectral representation from eq. C.28.

$$\frac{nS_u(z,n)}{\sigma_u^2} = \frac{4f_u(1+a_u \cdot f_u)}{(1+b_u f_u^{\gamma_u})^{\frac{13}{5\gamma_u}}} \tag{C.28}$$

This equation satisfies the boundary condition at S(0), while the derivative is a constant, meaning that S(n) is a linear function for low frequencies. The parameters a_u, b_u and γ_u need be chosen based on observed wind fields.

C.4.2 Height independent spectra

Height independent spectra are the easiest to use in practice, as they assume a single spectral spreading of the energy, independent of the height. This simplification comes with the advantage that only two parameters need to be defined : The mean wind speed at 10 m ($U(10)$) and the turbulent energy σ_u. Two examples of height independent models given here are the widely used Davenport model and the Harris spectrum.

Davenport The Davenport wind spectrum is used in many engineering applications, including the modelling of wind fields on vessels. Eq. C.29 represents this spectrum, with $f_{u\mathrm{D}}$ expressed by eq. C.30

$$\frac{nS_u(n)}{\sigma_u^2} = \frac{\frac{2f_{u\mathrm{D}}^2}{3}}{\left(1+f_{u\mathrm{D}}^2\right)^{\frac{4}{3}}} \tag{C.29}$$

$$f_{u\mathrm{D}} = \frac{1200\ n}{U(10)} \tag{C.30}$$

Similarity between equation C.23 and C.30 implies that Davenport used a turbulent length scale, L_u^x of 1200 m, at 10 m height, which is high when looking at the discussion in section C.2.2 (table C.2).

Harris The Harris spectrum is analogous to the Davenport spectrum, with a slight deviation in the shape of the spectral curve (eq. C.31).

$$\frac{nS_u(n)}{\sigma_u^2} = \frac{\frac{2f_{u\mathrm{H}}}{3}}{\left(1+f_{u\mathrm{H}}^2\right)^{\frac{5}{6}}} \tag{C.31}$$

The notation $f_{u\mathrm{H}}$, is similar to $f_{u\mathrm{D}}$, with a definition which differs in the assumption of the integral length scale for turbulence, which is 1800 m here, compared to 1200 m for Davenport.

$$f_{u\mathrm{H}} = \frac{1800n}{U(10)} \tag{C.32}$$

References

[Bak05] A. Bakker. *Lecture 9 - Kolmogorov's Theory Applied Computational Fluid Dynamics*. 2005.

[Bec10] J. Bec. "Influence of wind spectrum formula choice on footbridge response". In: *The 5th International Symposium on Computational Wind Engineering (CWE)*. Chapel Hill, USA, 2010.

[CWH96] J.P. Coelingh, A.J.M. van Wijk, and A.A.M Holtslag. "Analysis of wind speed observations over the North Sea". In: *Journal of Wind Engineering and Industrial Aerodynamics* 61 (1996), pp. 51–69.

[LG97] D. Lungu and P. van Gelder. "Characteristics of wind turbulence with applications to wind codes". In: *Proceedings of the 2nd European & African Conference on Wind Engineering*. Genova, Italy, 1997, pp. 1271–1277.

[SS96] E. Simiu and R. H. Scanlan. *Wind effects on structures : Fundamentals and applications to design*. 1996.

[Van+90] A.J.M. Van Wijk et al. "Evaluation of stability corrections in wind speed profiles over the North Sea". In: *Journal of Wind Engineering and Industrial Aerodynamics* 33 (1990), pp. 551–566.

[Yan+12] Q. Yang et al. "Statistical spectrum model of wind velocity at Beijing Meteorological Tower". In: *The s-7th International Colloqium on Bluff Body Aerodynamics and Applicatoin (BBAA7)*. Shanghai, China, 2012.

D

$PESCA$ test set-up details

The $PESCA$ scale model tests have been discussed in chapters 6 and 7. This attachment forms an extension to the content of both chapters.

- Section D.1 gives the characteristics of the ship models as tested, as well as a representation of the under water body of the ship.
- Section D.2 elaborates on the structure of the output files (.DPT) from the towing tank (Zeeman software). The axis system conversion which is performed to be consistent with the *Vlugmoor* system is discussed.
- Section D.3 elaborates on peak selection in case of significant secondary wave presence.
- Section D.4 lists the $PESCA$ tests which were not discussed in the main body of the thesis, yet are available in .DPT format for further processing.
- Section D.5 includes two tables on the repeatability analysis.
- Section D.6 lists the lessons learned by the candidate when executing towing tank tests.

D.1 Ship models

D.1.1 $C04$

Table D.1: *Characteristics $C04$ ship model.*

$C04$			
var	unit	MS	FS
L_{OA}	(m)	4.414	353.1
L_{PP}	(m)	4.367	349.4
B	(m)	0.611	48.9
T_{M}	(m)	0.190	15.2
m	(m)	320.6	1.64E+08
x_{G}	(m)	-0.048	-3.84
z_{G}	(m)	-0.003	-0.24
I_{xx}	(kgm²)	11.9	3.90E+10
I_{yy}	(kgm²)	367.4	1.20E+12
I_{zz}	(kgm²)	385.8	1.26E+12
$\overline{GM_{\mathrm{T}}}$	(m)	0.090	7.7
$\overline{GM_{\mathrm{L}}}$	(m)	*Blank*	*Blank*
A_{w}	(m²)	2.469	15799
C_{M}	(-)	0.983	0.983
C_{B}	(-)	0.632	0.632

(a)

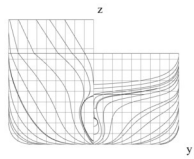

(b)

Figure D.1: *Linesplan $C04$*

D.1.2 $C0P$

Table D.2: *Characteristics $C0P$ ship model.*

$C0P$			
var	unit	MS	FS
L_{OA}	(m)	4.615	369.2
L_{PP}	(m)	4.350	348.0
B	(m)	0.610	48.8
T_{M}	(m)	0.190	15.2
m	(m)	326.2	1.70E+08
x_{G}	(m)	-0.114	-9.12
z_{G}	(m)	0.002	0.16
I_{xx}	(kgm²)	11.2	3.67E+10
I_{yy}	(kgm²)	396.6	1.30E+12
I_{zz}	(kgm²)	376.1	1.23E+12
$\overline{GM_{\mathrm{T}}}$	(m)	0.105	8.4
$\overline{GM_{\mathrm{L}}}$	(m)	8.495	679.6
A_{w}	(m²)	2.289	14649
C_{M}	(-)	0.990	0.990
C_{B}	(-)	0.647	0.647

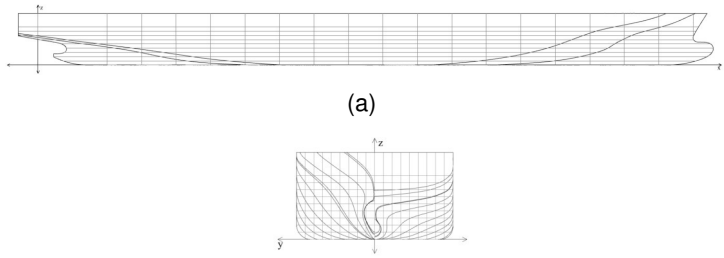

(a)

(b)

Figure D.2: *Linesplan $C0P$*

D.1.3 $T0Y$

Table D.3: *Characteristics $T0Y$ ship model.*

$T0Y$			
var	unit	MS	FS
L_{OA}	(m)	3.160	252.8
L_{PP}	(m)	3.067	245.4
B	(m)	0.560	44.8
T_{M}	(m)	0.188	15.0
m	(m)	247.3	1.27E+08
x_{G}	(m)	0.110	8.8
z_{G}	(m)	-0.002	-0.16
I_{xx}	(kgm²)	8.3	2.72E+10
I_{yy}	(kgm²)	148.5	4.87E+11
I_{zz}	(kgm²)	153.9	5.04E+11
$\overline{GM_{\mathrm{T}}}$	(m)	0.048	3.9
$\overline{GM_{\mathrm{L}}}$	(m)	3.650	292.0
A_{w}	(m²)	1.492	9549
C_{M}	(-)	0.997	0.997
C_{B}	(-)	0.766	0.766

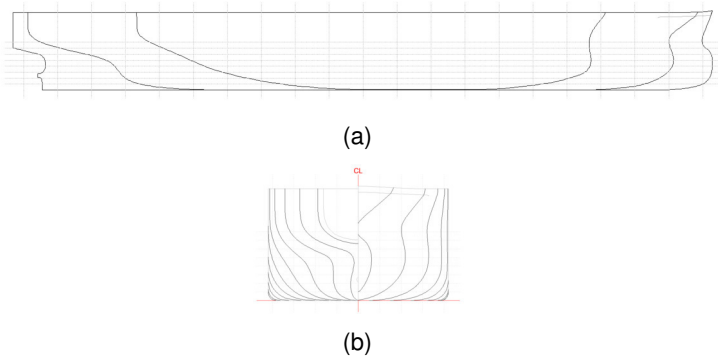

(a)

(b)

Figure D.3: *Linesplan $T0Y$*

D.1.4 $T0H$

Table D.4: *Characteristics $T0H$ ship model.*

$T0H$			
var	unit	MS	FS
L_{OA}	(m)	2.316	185.3
L_{PP}	(m)	2.215	177.2
B	(m)	0.295	23.6
T_{M}	(m)	0.100	8.0
m	(m)	54.3	3.30E+07
x_{G}	(m)	0.01	0.8
z_{G}	(m)	-0.028	-2.24
I_{xx}	(kgm²)	0.9	2.95E+09
I_{yy}	(kgm²)	17.6	5.77E+10
I_{zz}	(kgm²)	18.8	5.83E+10
$\overline{GM_{\mathrm{T}}}$	(m)	0.049	3.9
$\overline{GM_{\mathrm{L}}}$	(m)	*Blank*	*Blank*
A_{w}	(m²)	0.560	3584
C_{M}	(-)	0.983	0.983
C_{B}	(-)	0.830	0.830

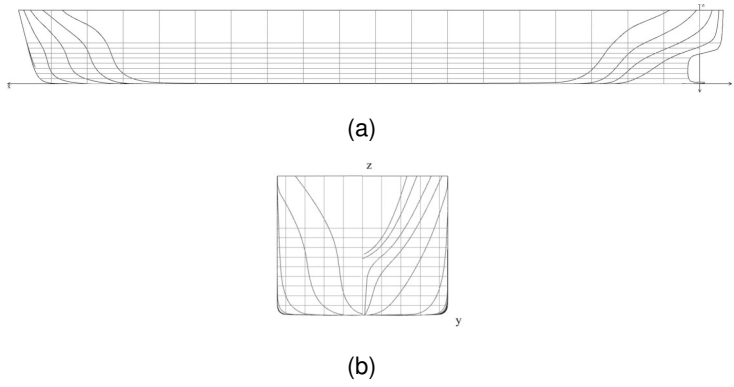

(a)

(b)

Figure D.4: *Linesplan $T0H$*

D.1.5 $E01$

Table D.5: *Characteristics $E01$ ship model.*

$E01$			
var	unit	MS	FS
L_{OA}	(m)	4.377	109.4
L_{PP}	(m)	4.334	108.4
B	(m)	0.684	17.1
T_{M}	(m)	0.140	3.5
m	(kg)	342.7	5.35E+06
x_{G}	(m)	0.060	1.5
z_{G}	(m)	0.002	0.1
I_{xx}	(kgm²)	16.9	1.65E+08
I_{yy}	(kgm²)	355.2	3.47E+09
I_{zz}	(kgm²)	379.6	3.71E+09
$\overline{GM_{\mathrm{T}}}$	(m)	0.219	5.5
$\overline{GM_{\mathrm{L}}}$	(m)	*Blank*	*Blank*
A_{w}	(m²)	2.749	1718
C_{M}	(-)	0.993	0.983
C_{B}	(-)	0.826	0.826

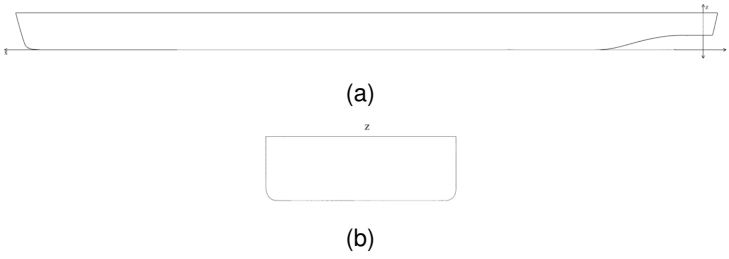

Figure D.5: *Linesplan $E01$*

D.1.6 $B01$

Table D.6: *Characteristics $B01$ ship model*

$B01$			
var	unit	MS	FS
L_{OA}	(m)	4.398	109.95
L_{PP}	(m)	4.393	109.8
B	(m)	0.458	11.5
T_{M}	(m)	0.140	3.5
m	(m)	249.4	3.90E+06
x_{G}	(m)	0.051	1.3
z_{G}	(m)	-0.012	-0.3
I_{xx}	(kgm²)	6.9	6.74E+07
I_{yy}	(kgm²)	275.0	2.69E+09
I_{zz}	(kgm²)	278.2	2.72E+09
$\overline{GM_{\mathrm{T}}}$	(m)	0.074	1.8
$\overline{GM_{\mathrm{L}}}$	(m)	*Blank*	*Blank*
A_{w}	(m²)	1.942	1213
C_{M}	(-)	0.998	0.998
C_{B}	(-)	0.885	0.885

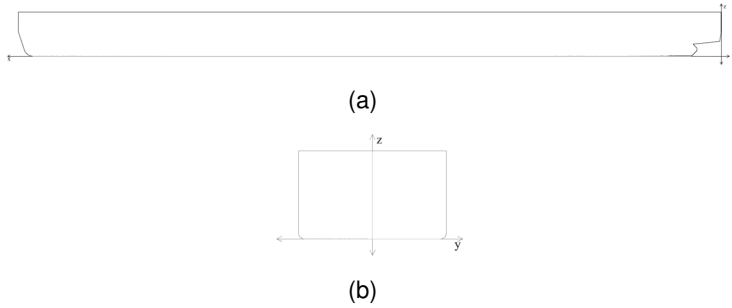

(a)

(b)

Figure D.6: *Linesplan $B01$*

D.1.7 $D03D04$

Table D.7: *Characteristics $D03D04$ ship model.*

$D03D04$			
var	unit	MS	FS
L_{OA}	(m)	3.076	76.9
L_{PP}	(m)	3.017	75.4
B	(m)	0.912	22.8
T_{M}	(m)	0.140	3.5
m	(m)	365.8	5.72E+06
x_{G}	(m)	-0.088	-2.2
z_{G}	(m)	0.001	0.0
I_{xx}	(kgm²)	38.0	3.71E+08
I_{yy}	(kgm²)	205.4	2.01E+09
I_{zz}	(kgm²)	236.9	2.31E+09
$\overline{GM_{\mathrm{T}}}$	(m)	0.445	11.1
$\overline{GM_{\mathrm{L}}}$	(m)	*Blank*	*Blank*
A_{w}	(m²)	2.722	1701
C_{M}	(-)	1.000	1.000
C_{B}	(-)	0.950	0.950

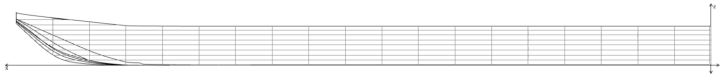

(a)

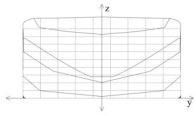

(b)

Figure D.7: *Linesplan $D03$, $D04$*

D.2 Output $PESCA$ - axis system conversion

D.2.1 Position measuring equipment

On moored and passing ships, measurement equipment is positioned to measure forces (load cells, LC) and motions (potentiometers, P). Wave gauges (WG) are installed to measure water level changes. The position of the equipment is given in figure D.8 (passing ships), figure D.9 (moored, seagoing) and figure D.10 (moored, inland). The values of x_i and y_j are given in table D.8 (passing ships) and table D.9 (moored ships).

Table D.8: *Position LC and P for passing ships : $C04$ and $E01$ (m) (figure D.8).*

distance	$C0P$	$E01$
$\|x_1\|$	1.137	1.450
$\|x_2\|$	1.004	1.002
$\|x_3\|$	0.998	0.995
$\|y_1\|$	0.295	0.327

Table D.9: *Position LC,P,WG for moored ships (m) (figure D.9 and D.10).*

distance	$C0P$	$T0H$	$T0Y$ (Q)	$T0Y$ (J)	$B01$	$D03D04$
$\|x_1\|$	1.140	0.629	1.530	1.530	1.530	1.350
$\|x_2\|$	0.700	0.610	0.835	0.835	0.835	0.835
$\|x_3\|$	0.050	0.050	0.050	0.050	0.050	0.050
$\|x_4\|$	1.000	1.000	1.000	1.000	1.000	1.000
$\|x_5\|$	N.A.	N.A.	0.075	0.075	N.A.	N.A.
$\|y_1\|$	0.050	.0.50	0.050	0.050	0.050	0.050
$\|y_2\|$	0.020	0.020	0.020	0.978	0.020	0.020

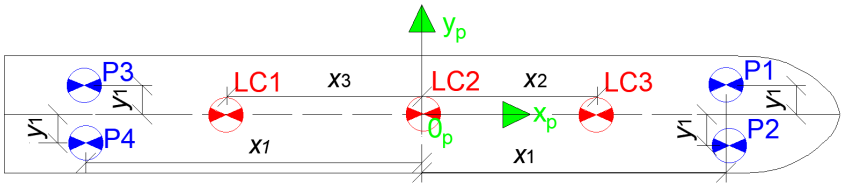

(a) $C04$

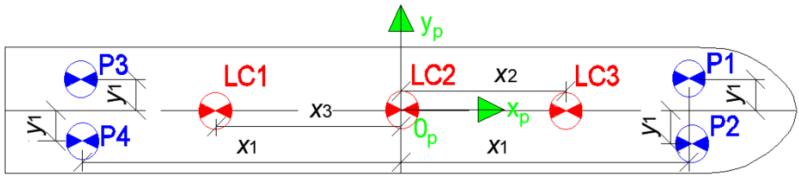

(b) $E01$

Figure D.8: *Position measuring equipment on passing ships, LC = load cell, P = potentiometer.*

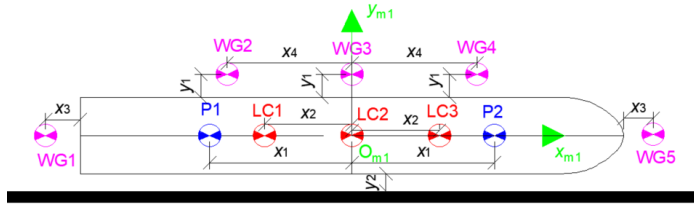

(a) $C0P$

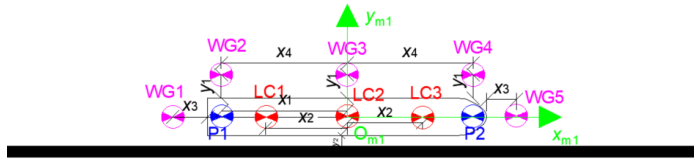

(b) $T0H$

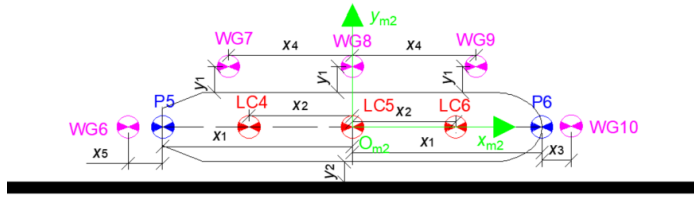

(c) $T0Y$ quay

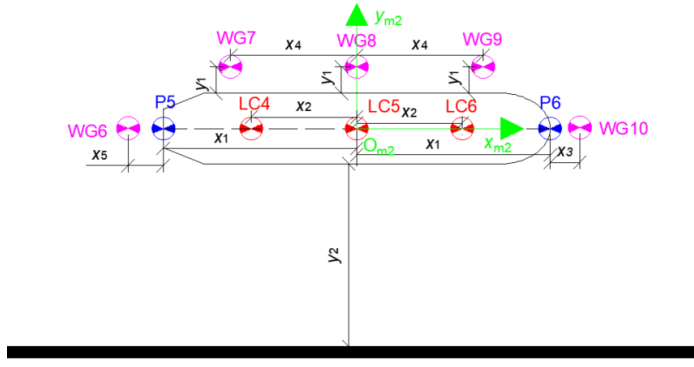

(d) $T0Y$ jetty

Figure D.9: *Position measuring equipment on moored, seagoing ships, LC = load cell, P = potentiometer, WG = wave gauge.*

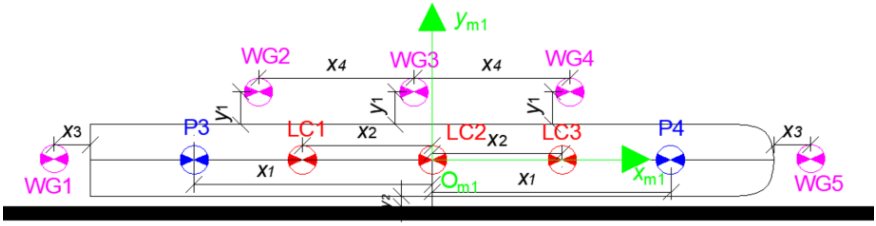

(a) $B01$

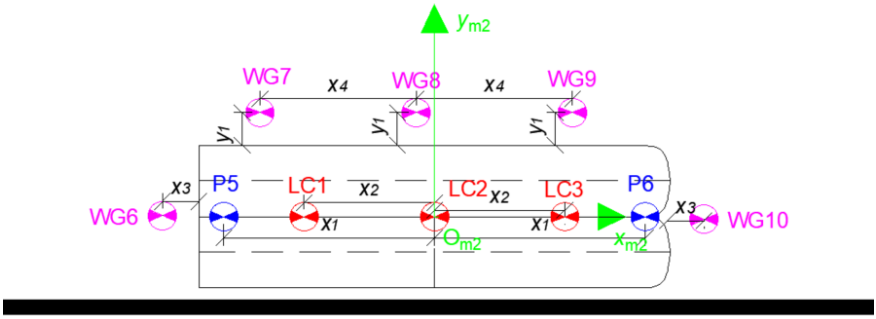

(b) $D03D04$

Figure D.10: *Position measuring equipment on moored, inland ships, LC = load cell, P = potentiometer, WG = wave gauge.*

D.2.2 DPT output file *Zeeman*

The raw measured data is processed using the dedicated software package *Zeeman*. Using this software, the measured signals (up to 100 Hz) are processed to workable formats, including converting the force and motion measurements to $6DOF$ representations. Table D.10 shows the content of the 56 data columns, using *MS EXCEL* column definitions. The passing ship (attached to the carriage) and wave gauge properties are part of the standard *DPT* structure; The data measured on the moored ships is added for the $PESCA$ test series.

D.2.3 Post-processing on DPT

D.2.3.1 Force and motion representation

The measurements on the moored ships are the values registered at the respective load cells and potentiometers and they still need conversion to $6DOF$ forces and motions, as was done automatically for the passing ship. The following equations are used to process the load cell and potentiometer data.

$$\begin{cases} X = X_{\mathrm{LC3}} + X_{\mathrm{LC1}} \\ Y = Y_{\mathrm{LC3}} + Y_{\mathrm{LC1}} \\ N = Y_{\mathrm{LC3}} \dot{|} x_2 | + Y_{\mathrm{LC1}} \cdot -|x_2| \\ z = \dfrac{z_{\mathrm{P1}} \dot{|} x_3 | + z_{\mathrm{P2}} \cdot -|x_3|}{2 \cdot |x_3|} \\ trim = \dfrac{z_{\mathrm{P1}} - z_{\mathrm{P2}}}{2 \cdot |x_3| \cdot 1000} \end{cases} \tag{D.1}$$

D.2.3.2 Axis system conversion

The default towing tank axis convention, which is used for both moored as well as passing ship has its origin at midships, waterline, with the z-axis positive downwards. In *Vlugmoor*, as well as throughout the whole thesis, the axis system is defined with the z-axis positive upwards (origin also midships, on the waterline). This means that the values from the *.DPT* files need to be converted to be compliant with the thesis axis system. If 'axTT' is the axis system system definition used in the towing tank (and thus *.DPT* file) and 'axVL' is the thesis

Table D.10: *Structure towing tank .DPT output file, $MSExcel$ columns A - BD.*

passing ship (carriage)					
A	test name	()	K	$\dot{u}$	(m/s²)
B	test type	()	L	$\dot{v}$	(m/s²)
C	$x_{0\mathrm{t}}$	(m)	M	$\dot{p}$	(°/s²)
D	$y_{0\mathrm{t}}$	(m)	N	$\dot{r}$	(°/s²)
E	ϕ	(°)	O	X	(N)
F	ψ	(°)	P	Y	(N)
G	u	(m/s)	Q	z	(mm)
H	v	(m/s)	R	K	(Nm)
I	p	(°/s)	S	trim	(mm/m)
J	r	(°/s)	T	N	(Nm)
U-AC reserved for rudder/propeller*					
wave gauges AD-AP are 13 wave gauges (mm)					
moored ship 1					
AQ	X_{LC3}	(N)	AU	z_{P2}	(mm)
AR	X_{LC1}	(N)	AV	z_{P1}	(mm)
AS	Y_{LC1}	(N)	AW	K	(Nm)
AT	Y_{LC3}	(N)			
moored ship 2					
AX	X_{LC3}	(N)	BB	z_{P2}	(mm)
AY	X_{LC1}	(N)	BC	z_{P1}	(mm)
AZ	Y_{LC1}	(N)	BD	K	(Nm)
BA	Y_{LC3}	(N)			

* $PESCA$ *tests are performed without rudder / propeller.*

axis system (=*Vlugmoor* axis system), then the following conversion applies :

$$\begin{cases} X_{\mathrm{axVL}} = X_{\mathrm{axTT}} \\ Y_{\mathrm{axVL}} = -Y_{\mathrm{axTT}} \\ N_{\mathrm{axVL}} = -N_{\mathrm{axTT}} \\ z_{\mathrm{axVL}} = -z_{\mathrm{axTT}} \\ trim_{\mathrm{axVL}} = -trim_{\mathrm{axTT}} \\ K_{\mathrm{axVL}} = K_{\mathrm{axTT}} \end{cases} \tag{D.2}$$

D.3 Secondary waves & slack in load cell

In the main thesis text, the distinction between primary and secondary (Kelvin) wave systems was already discussed, with the effect of the primary wave system on the moored ship being dominant due to this longer periodicity. For most tests, the amplitude of the primary wave system is also higher compared to the secondary system (e.g. figure 6.18).

Figure D.11 shows an example of the forces measured in the inland ship program. The peak value for Y is actually measured as a result of Kelvin wave action, which is in a way to be expected for a fast passage at large passing distance. The signal however shows many oscillations, with the primary passage (for Y two negative and one positive peak) hardly captured. This seems to be partly caused by slack in the connection of the load cell, which also causes the cell to oscillate. This inaccuracy in the load cell positioning was observed for the inland ship program, for the moored ship at position one, after which extra care and extra inspections reduced this unwanted oscillation in the load cell.

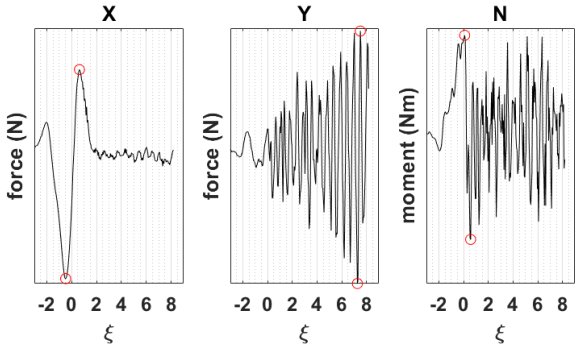

Figure D.11: *Selection positive and negative peak value from model test signal, passing $E01$, moored ship $B01(Q)$, UKC_{p} = 20%, $\frac{d}{B_{\mathrm{p}}}$ = 4.0, $\frac{W}{B_{\mathrm{p}}}$ = 11.46, V_{FS} = 14 km/h.*

D.4 Repeatability of model tests

Results repeatability analysis for force measurement moored ship 2 $x_{0\mathrm{t}}$ = 43 m (table D.11) and for wave gauge readings (table D.12).

Table D.11: *Test repeatability analysis for moored ship at position $x_{0\mathrm{t}}$ = 43 m, ratio standard deviation over the average for force peaks.*

		$\sigma/\mu(\%)$							
n	ship	$X-$	$X+$	$Y-$	$Y+$	$N-$	$N+$	$K-$	$K+$
11	$T0Y$	1.2	1.0	1.9	2.7	3.2	5.2	9.9	7.1
12	$T0Y$	0.8	0.9	1.3	2.2	1.9	2.7	11.7	12.6
12	$T0Y$	1.1	1.1	6.7***	8.6***	11.7	8.6	15.3	13.3
11	$T0Y$	0.5	0.5	3.1	3.0	2.1	3.8	10.0	8.5
13	$T0Y$	*N.A.*	*N.A.*	*N.A.*	*N.A.*	*N.A.*	*N.A.*	*N.A.*	*N.A.*
13	$T0Y$	*N.A.*	*N.A.*	*N.A.*	*N.A.*	*N.A.*	*N.A.*	*N.A.*	*N.A.*
12	$T0Y$	*N.A.*	*N.A.*	*N.A.*	*N.A.*	*N.A.*	*N.A.*	*N.A.*	*N.A.*
13	$T0Y$	1.0	1.5	0.7	1.6	1.7	1.5	8.3	7.3
13	$T0Y$	1.0	0.9	0.9	1.5	1.3	1.0	5.7	8.2
13	$T0Y$	0.7	1.1	0.9	1.8	1.1	1.4	1.9	7.2
11	$T0Y$	1.0	2.1	2.3	2.0	3.3	2.3	3.5	4.3
11	$T0Y$	1.5	1.6	1.4	2.3	1.7	2.1	2.5	7.2
10	$D03D04$	*N.A.*	*N.A.*	*N.A.*	*N.A.*	*N.A.*	*N.A.*	*N.A.*	*N.A.*
13	$D03D04$	*N.A.*	*N.A.*	*N.A.*	*N.A.*	*N.A.*	*N.A.*	*N.A.*	*N.A.*
15	$D03D04$	1.6	1.2	2.5	2.5	4.5	2.5	6.3	10.0
12	$D03D04$	1.6	4.5	6.7	7.0	7.3	6.6	3.5	16.4
12	$D03D04$	1.3	0.9	2.5	2.4	2.9	2.4	2.9	11.0
13	$D03D04$	0.5	0.6	1.9	0.9	2.7	1.1	2.5	8.0

*** *Time series repetition tests shown in figure 6.15*

Table D.12: *Test repeatability analysis for wave gauges, ratio standard deviation over the average for maximum wave gauge measurement.*

	$\sigma/\mu(\%)$												
n	1	2	3	4	5	6	7	8	9	10	11	12	13
11	0.9	1.1	1.4	1.7	1.9	1.1	1.7	1.2	1.7	4.6	2.4	2.5	2.9
12	2.2	1.4	1.3	2.8	2.5	2.2	1.9	0.9	1.3	0.9	2.2	4.2	1.5
12	0.6	1.1	1.0	*N.A.*	1.2	1.2	0.8	1.1	1.7	1.1	1.0	1.3	0.9
11	0.4	0.4	0.5	0.6	0.4	0.7	1.5	0.5	1.0	0.6	0.5	0.6	0.7
13	0.8	0.5	0.5	0.5	0.9	*N.A.*	*N.A.*	*N.A.*	*N.A.*	*N.A.*	1.2	0.5	*N.A.*
13	0.8	1.1	1.1	1.1	0.9	*N.A.*	*N.A.*	*N.A.*	*N.A.*	*N.A.*	2.1	7.0	*N.A.*
12	0.9	1.6	1.5	1.3	1.1	*N.A.*	*N.A.*	*N.A.*	*N.A.*	*N.A.*	1.2	1.7	*N.A.*
13	3.6	4.6	4.7	2.4	3.5	3.0	2.4	2.0	2.2	3.1	4.1	4.1	6.3
13	1.7	1.6	2.2	1.4	1.8	1.5	1.2	1.2	2.0	2.7	2.8	1.9	3.0
13	2.0	2.1	2.2	2.3	2.8	2.4	1.9	1.6	1.9	2.8	2.1	2.1	3.1
11	3.4	3.6	4.0	3.6	3.3	1.6	2.7	2.3	2.0	2.6	3.5	5.4	5.1
11	3.5	1.1	1.2	1.6	1.5	1.0	1.1	1.8	1.3	1.0	0.6	1.0	1.1
10	4.0	4.7	5.2	6.6	4.2	*N.A.*	*N.A.*	*N.A.*	*N.A.*	*N.A.*	7.5	5.9	*N.A.*
13	1.5	1.3	1.9	1.8	1.3	*N.A.*	*N.A.*	*N.A.*	*N.A.*	*N.A.*	1.9	1.3	*N.A.*
15	1.7	1.9	1.7	1.7	2.2	2.4	1.6	1.5	1.6	1.5	2.7	3.0	4.6
12	3.5	2.8	2.5	2.8	3.9	3.2	2.4	2.6	7.7	3.6	3.8	5.1	4.9
12	1.1	0.7	0.6	0.9	1.2	1.0	1.5	1.9	0.9	0.8	1.2	0.9	0.8
13	0.8	0.5	0.5	0.5	0.9	1.7	0.5	0.7	0.5	0.6	1.2	0.5	0.6

D.5 $PESCA$ tests not discussed in thesis

In chapter 6, 1699 parameter combinations for passing ship effects were discussed, as part of the $PESCA$ model test program. Two more test types were executed as part of the $PESCA$ series, however they have not yet been analysed in the same detail as was done for the 1699 tests which were discussed extensively.

Section D.5.1 elaborates on the tests where the passing ship was sailing with a non-zero drift angle. Section D.5.2 presents tests where the moored $T0Y$ was moored at a discontinuous quay section of various sizes.

D.5.1 $PESCA$ tests with drift angles

Tests with drift angles have only been performed for six environments, where the $C04$ passes the moored $C0P$ and $T0Y$ (Q). Depending on the passing speed and passing distance, three possible sets of drift angles were tested (in degrees). (1) [-2.5, 2.5] (2) [-5.0 -2.5 2.5 5.0] (3) [-10.0 -5.0 -2.5 2.5 5.0 10.0] or 26 parameter combinations.

[Van20] provides a first assessment of these model tests. In most cases, a non-zero drift angle causes larger passing ship forces, compared to tests with the zero-drift angle (for the same y_{0t} position at midships of the passing ship, see figure D.12). The author defined an equivalent passing distance, for which the test with non-zero drift gives the same result as the test with zero-drift angle. He observed that such parameters need to be determined separately for the different DOF. Regression results however were suboptimal and an extension of this research would be needed to obtain an equivalent passing distance (or to define another method).

D.5.2 $PESCA$ tests with discontinuous quay

At the end of the test program, a discontinuous quay element was built into the towing tank, at the position x_{0t} = 43.0 m, moored $T0Y$. Figure D.13 shows the different lengths of the discontinuous quay which were constructed in the towing tank (8 different configurations). All these configurations were tested for a channel width of 6

Table D.13: *Test environment : channel width W, UKC, number of unique parameter combinations tested with a non-zero drift angle for each environment,* N.A. *= environment is not tested.*

				$UKC(\%)$				
Pas	Moor	$x_{0\mathrm{t}}$ (m)	$W/B_{\mathrm{p}}(-)$	50	40	30	20	10
$C04$	$C0P$(Q)	23	10	16	N.A.	N.A.	34	12
			6	46	N.A.	N.A.	N.A.	N.A.
			4	18	N.A.	N.A.	N.A.	8
$C04$	$T0Y$(Q)	43	10	16	N.A.	N.A.	34	12
			6	46	N.A.	N.A.	N.A.	N.A.
			4	18	N.A.	N.A.	N.A.	8

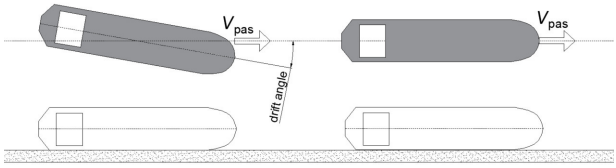

Figure D.12: *Passing events with (left) and without (right) drift angle, for the same passing distance, defined by the trajectory of the midship of the passing ship.*

B_{p} and a UKC of 20%. For each environment, 19 parameter combinations were assessed, for 152 parameter combinations in total.

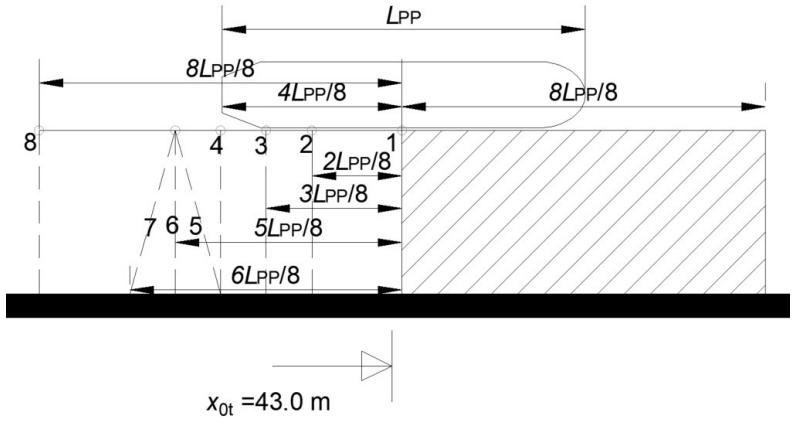

Figure D.13: *Schematic representation moored $T0Y$ with discontinuous quay wall, indication of different set-ups of the discontinuous quay (number 1 to 8).*

Table D.14: *Test environment (envir.) discontinuous quay ; figure D.13.*

envir.	pos $\frac{x}{8} \cdot \frac{L_{\mathrm{PP}}}{8}$ (angle)	envir.	pos $\frac{x}{8} \cdot \frac{L_{\mathrm{PP}}}{8}$ (angle)
DQ1	$0(0\,\mathrm{deg})$	DQ5	$5(-21.8\,\mathrm{deg})$
DQ2	$2(0\,\mathrm{deg})$	DQ6	$5(0\,\mathrm{deg})$
DQ3	$3(0\,\mathrm{deg})$	DQ7	$5(21.8\,\mathrm{deg})$
DQ4	$4(0\,\mathrm{deg})$	DQ8	$8(0\,\mathrm{deg})$

D.6 Lessons learned

This section highlights some of the lessons learned by the candidate whilst performing the towing tank tests. The main suggestion of the candidate is to keep a detailed daily diary which can be in the form of an $MS\ EXCEL$ sheet, with for example references to more extensive memos and/or reports whenever necessary.

- The water level in the towing tank is regulated by several pumps and valves. An overflow valve is present to keep the level constant, as there is constant water inflow to compensate for water evaporation. In case of a power cut, the pump needs to be manually restarted. Water levels are monitored at the wave maker, the harbour and the overflow valve; at the harbour, a manual check can be performed. These systems should be checked at regular time intervals, to get a correct physical water level at all times, certainly at low UKC.

- The position of the tank wall in the tank axis system is $y_0 = 3.5$. There are deviations from this ideal tank wall in practice. At the position of the moored ships $x_0 = 23$ and $43m$, the deviation was up to + 3 mm and -2 mm respectively.

- Wave gauges are sensitive measurement devices, so careful handling and correct calibration are a necessity. It is advised to check the readings at regular intervals, for example after each test batch. Gauges could show a linear deviation over a large time scale. This does not influence the quality of the test, yet it could trigger an alarm signal, as it thinks that the water level is much higher/lower than it is in reality, causing the carriage to stop.

- During the tests, magnetic interference between the engines of the carriage and the measurement equipment could occur. Prior to the attachment of the ship, it is good to run through the tank to see if any of these effects are present. During these trials, a noise band of at most ± 0.4 mm on water levels measurements has been observed. For some of the gauges, there is a 'jump' in the signal at a specific x_0 location, indicating some electromagnetic interference. The magnitude of this is also in the order of 0.3 mm, but cannot be allocated to noise, as it is still visible when a low pass filter is applied.

- The data transfer from gauges to the main pc is done through a PIOC - Parallel Input/Output Controller - system. As with every data transmission system, errors can occur, e.g. when one data step is counted incorrectly. Restarting the system solves this issue. For $PESCA$, due to the spread of equipment throughout the tank, moored ships and water level gauges, *PIOCs* were connected to different electric circuits, which need to be restarted individually.
- In Zeeman, where the test setup is done, safety checks to avoid contact with objects in the tank are made. For the ship attached to the carriage, a safety rectangle is defined around the ship. For $PESCA$, this was set to a minimum, as some passages were at minimal passing distance. A low speed run is advised to check that no equipment could be damaged; Camera wiring, water level gauges, potentiometers,...
- The moored ships are attached to a custom built frame and were altered throughout the test program. When calibration of the force gauges is performed, it is important to check if there is any "crosstalk", e.g. when a force is applied strictly in the x-direction, the gauge in the y-direction should not measure a trend. In practice, there will always be some crosstalk, but this should be limited compared to the actual force range you are interested in.
- The standard waiting time in between two tests is 2000 s in batch mode, allowing for any long (standing) waves to dissipate. For most tests, this proved to be sufficient. For the runs with smallest channel section however, the standing wave was present for a longer time. Waiting time was increased to 3000 s for these tests.

References

[Van20] J. Vanden Bulcke. "Effect of passing ships with a drift angle on moored ships : analysis scale model test results". Msc Thesis. Ghent University, 2020.

E

RoPES validation details

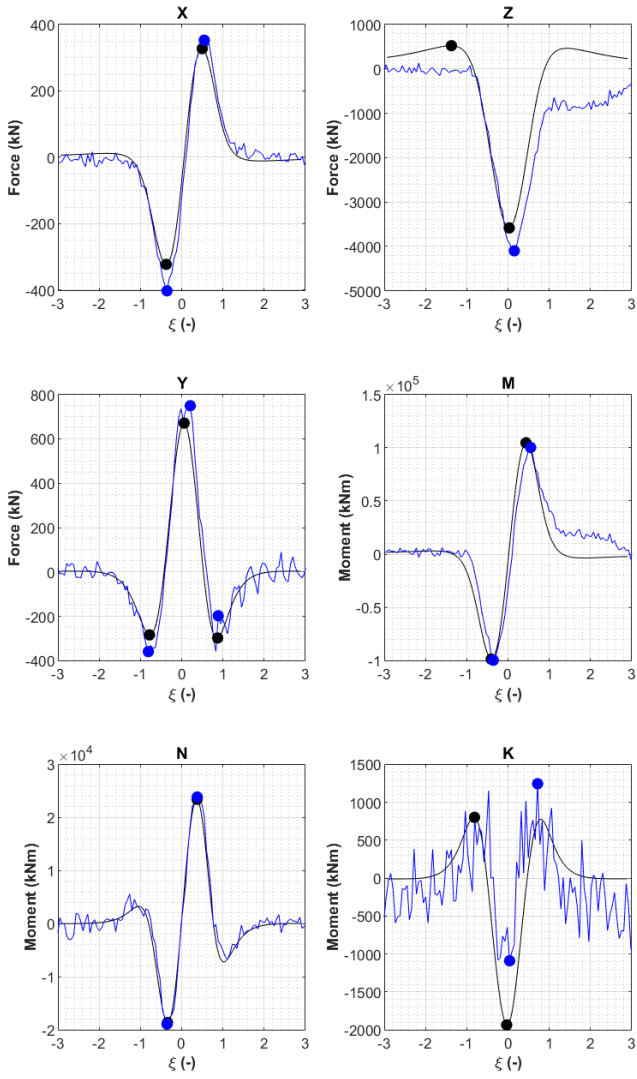

Figure E.1: *Comparison RoPES (black) and PESCA (blue) for 6DOF passing C04, moored T0Y(J),* UKC_{p} *= 50%,* $\frac{d}{B_{\mathrm{p}}}$ *= 2.0,* $\frac{W}{B_{\mathrm{p}}}$ *= 10,* V_{FS} *= 6 kn*

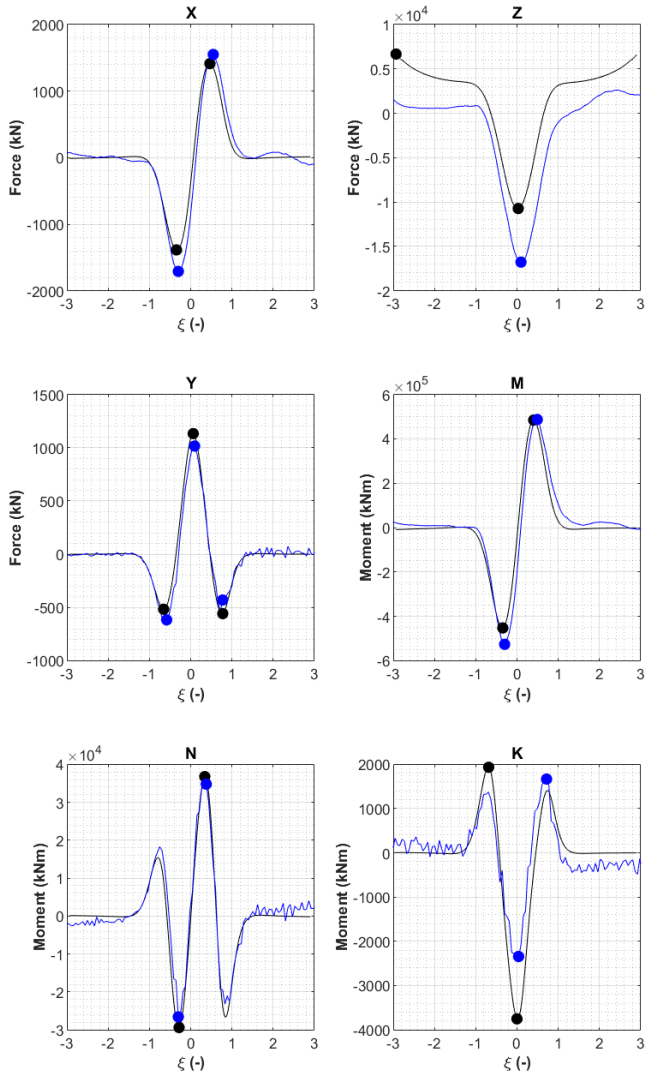

Figure E.2: *Comparison RoPES (black) and PESCA (blue) for 6DOF passing C04, moored T0Y(Q), UKC_{p} = 20%, $\frac{d}{B_{\mathrm{p}}}$ = 1.0, $\frac{W}{B_{\mathrm{p}}}$ = 6, V_{FS} = 6 kn*

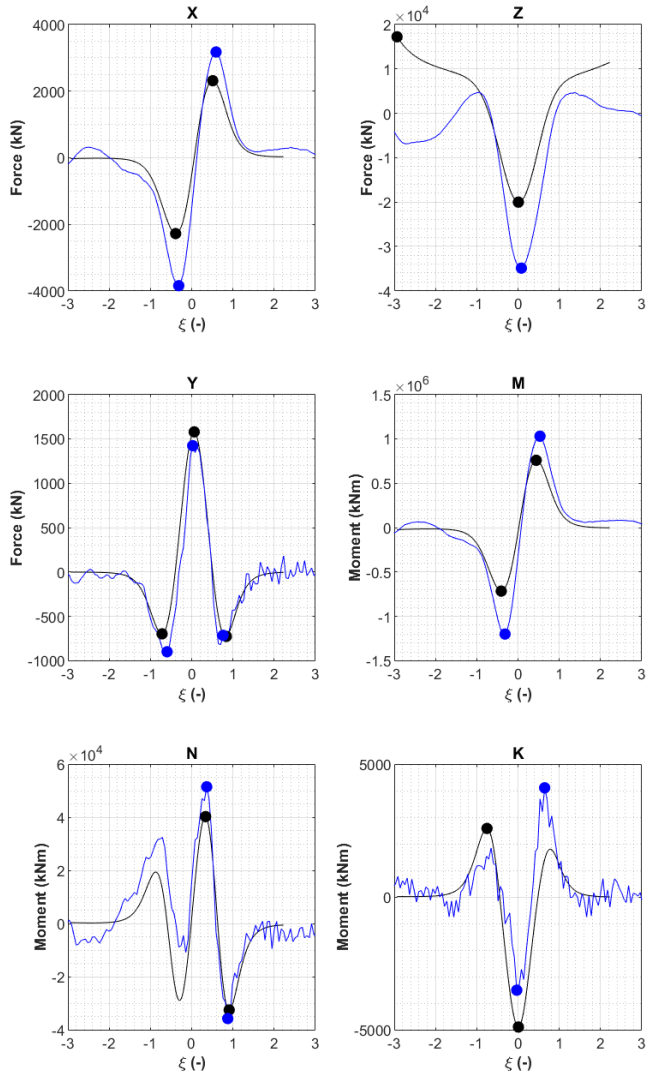

Figure E.3: *Comparison RoPES (black) and $PESCA$ (blue) for 6DOF passing $C04$, moored $T0Y(Q)$, UKC_{p} = 20%, $\frac{d}{B_{\mathrm{p}}}$ = 2.0, $\frac{W}{B_{\mathrm{p}}}$ = 6, V_{FS} = 10 kn*

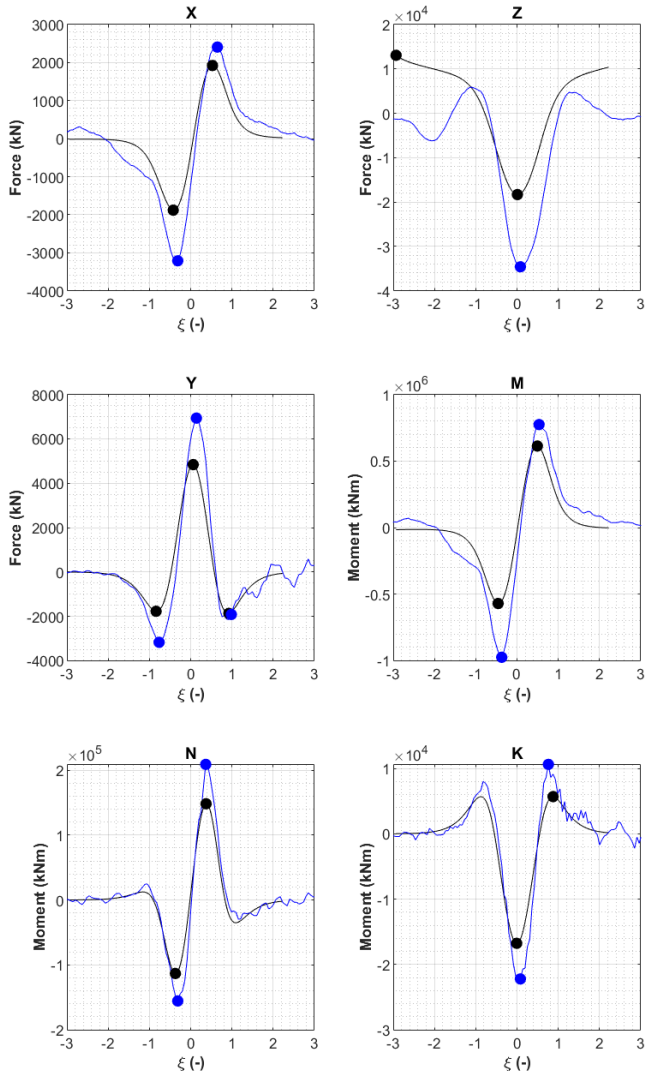

Figure E.4: *Comparison RoPES (black) and PESCA (blue) for 6DOF passing C04, moored T0Y(J),* UKC_{p} *= 20%,* $\frac{d}{B_{\mathrm{p}}}$ *= 2.0,* $\frac{W}{B_{\mathrm{p}}}$ *= 6,* V_{FS} *= 10 kn*

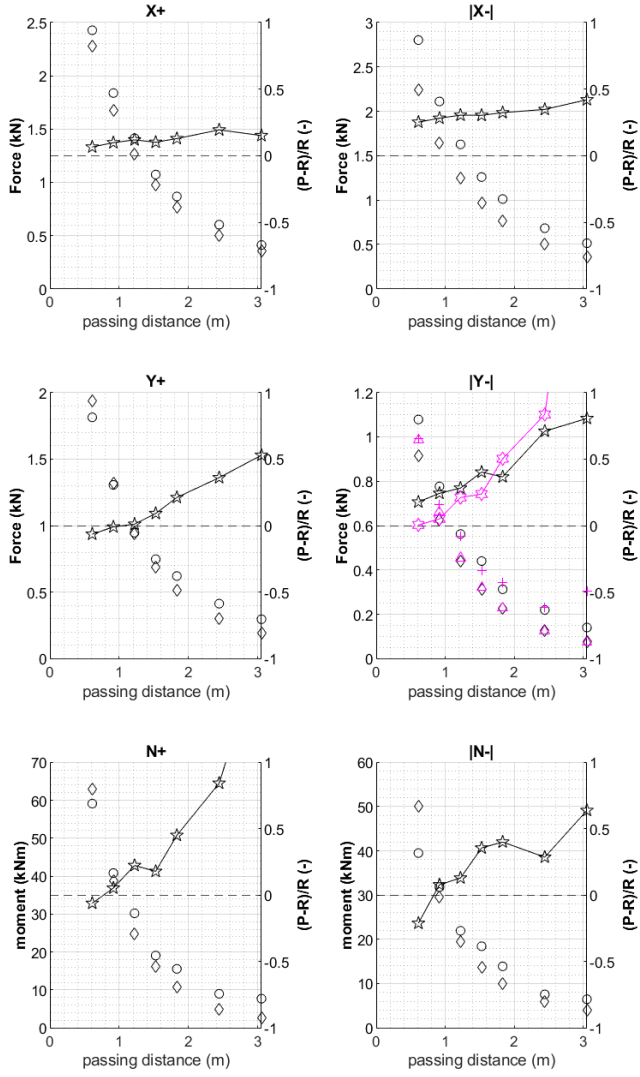

Figure E.5: *Effect of passing distance on the peak force X, Y, N passing $C04$, moored $T0Y(Q)$, UKC_{p} = 20%, $\frac{W}{B_{\mathrm{p}}}$ = 10, V_{FS} = 8 kn*
Left axis : $PESCA$ (circle,cross), RoPES (diamond,triangle)
Right axis : Relative difference $PESCA$ and RoPES (star,hexagon)

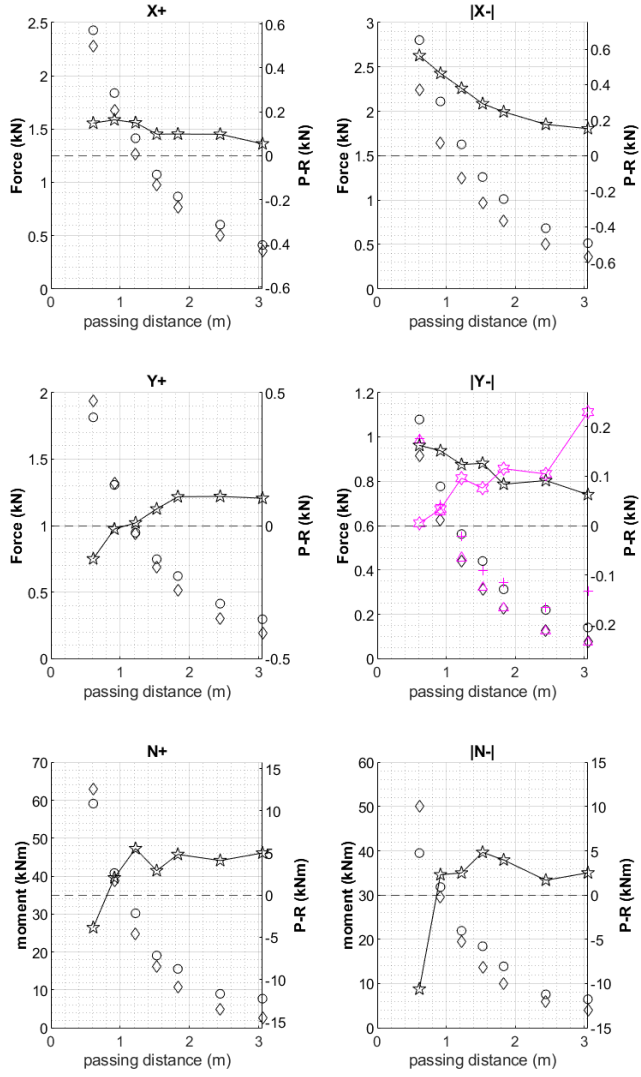

Figure E.6: *Effect of passing distance on the peak force X, Y, N passing $C04$, moored $T0Y$ (Q), UKC_{p} = 20%, $\frac{W}{B_{\mathrm{p}}}$ = 10, V_{FS} = 8 kn*
Left axis : $PESCA$ (circle,cross), RoPES (diamond,triangle)
Right axis : Difference $PESCA$ and RoPES (star,hexagon)

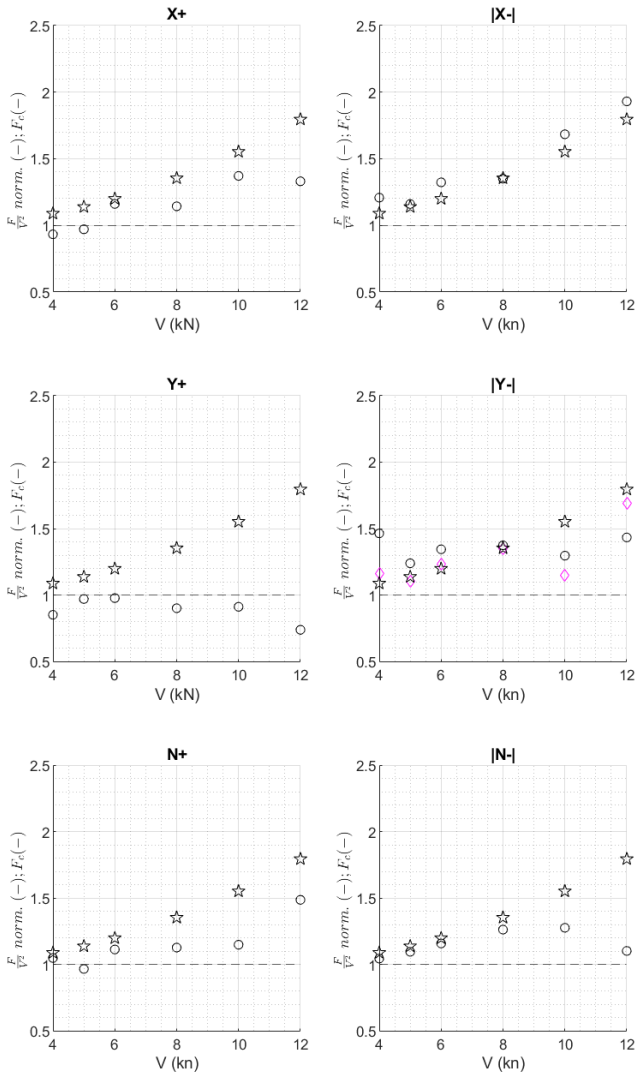

Figure E.7: *Effect of speed on the peak force X, Y, N passing $C04$, moored $T0Y$ (Q), UKC_{p} = 20%, $\frac{d_{\mathrm{pas}}}{B_{\mathrm{p}}}$ = 2.0, $\frac{W}{B_{\mathrm{p}}}$ = 6 Normalised $PESCA$ peak (circle, diamond) and F_{c} (star)*

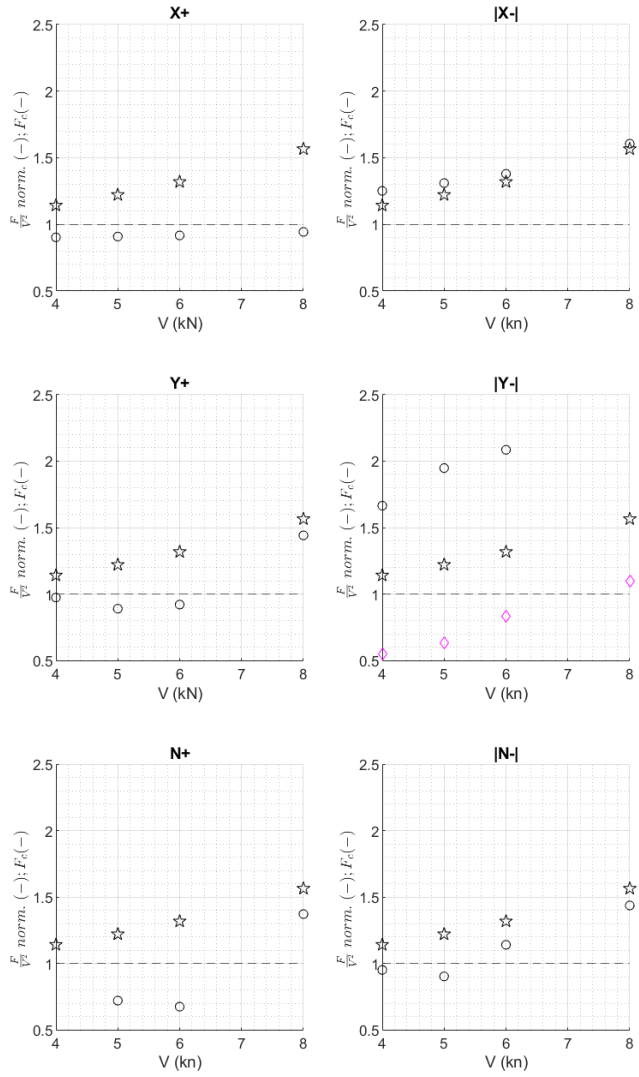

Figure E.8: *Effect of speed on the peak force X, Y, N, passing $C04$, moored $T0Y(Q)$, UKC_{p} = 10%, $\frac{d_{\mathrm{pas}}}{B_{\mathrm{p}}}$ = 1.0, $\frac{W}{B_{\mathrm{p}}}$ = 4 Normalised $PESCA$ peak (circle, diamond) and F_{c} (star)*

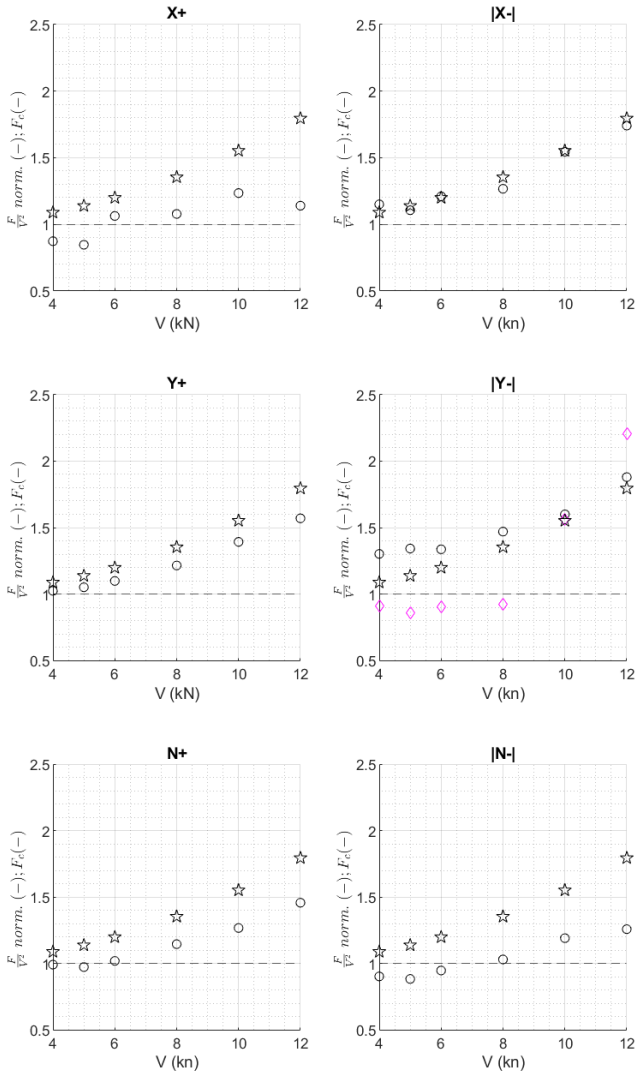

Figure E.9: *Effect of speed on the peak force X, Y, N passing $C04$, moored $T0Y$ (J) , UKC_{p} = 20%, $\frac{d_{\mathrm{pas}}}{B_{\mathrm{p}}}$ = 1.0, $\frac{W}{B_{\mathrm{p}}}$ = 6 Normalised $PESCA$ peak (circle, diamond) and F_{c} (star)*

F

Case study examples

F.1 $T0Y$

The $T0Y$ ship is an Aframax type tanker. The main hull characteristics are taken from the full scale representation of the ship model tested in the $PESCA$ program (table D.3). The mooring equipment is determined based on available data of ships of similar sizes.

The application of the $T0Y$ ship model within $PESCA$ is not discussed here. The use of $T0Y$ to illustrate certain aspects of ship mooring, with the emphasis on mooring equipment and configuration, is summarized in the present appendix. Throughout the thesis text, the $T0Y$ case is discussed in the following sections:

- Table 6.2 and table D.3 give the main characteristics of the ship hull. These are repeated in the present appendix, table F.1.
- Section 2.2.3 shows the moored $T0Y$ at a (dedicated) jetty and a quay berth, explaining the differences in mooring configuration.
- Section 2.5 discusses the *Vlugmoor* application, with large surge motions of the moored $T0Y$.

- Section 3.2 elaborates on the mooring equipment found on board of such oil tankers and makes a comparison with prescribed international standards.
- Section 4.2 (figure 4.1) gives the added mass and damping coefficients in the frequency domain (diagonal terms), for 20 % UKC.
- Section 4.3.3.6 gives the eigenperiods for the $T0Y$, moored at the quay type berth, for 20 % UKC.

F.1.1 Hull and mooring parameters

Table F.1 summarizes the relevant hull and mooring equipment characteristics, as well as the calculated eigenperiods for the quay berth mooring arrangement (figure F.2), at 20 % UKC (figure F.3).

Table F.1: *Characteristic parameters hull and mooring equipment $T0Y$.*

hull characteristics			
L_{OA} (m)	252.8	A_{w} (m²)	9549
L_{PP} (m)	245.4	I_{xx} (kgm²)	2.72E+10
B (m)	44.8	I_{yy} (kgm²)	4.87E+11
T_M (m)	15.0	I_{zz} (kgm²)	5.04E+11
Δ (kg)	1.27E08	H (m)	28.4
$\overline{GM}_{\mathrm{T}}$ (m)	3.90		
mooring equipment			
MBL (ton)	81.0*	n_{l}	16*
eigenperiods (quay config. figure F.2)			
$T_{\mathrm{n}x}$	78.1	$T_{\mathrm{n}\phi}$	12.3
$T_{\mathrm{n}y}$	71.2	$T_{\mathrm{n}\theta}$	13.5
$T_{\mathrm{n}z}$	16.2	$T_{\mathrm{n}\psi}$	245.1

* Based on data 2 ships of similar size

F.1.2 Mooring configurations

Two mooring arrangements are discussed for the $T0Y$, a jetty berth type (figure F.1 and a quay berth type F.2). The mooring line param-

eters for the quay berth type are given in table F.2.

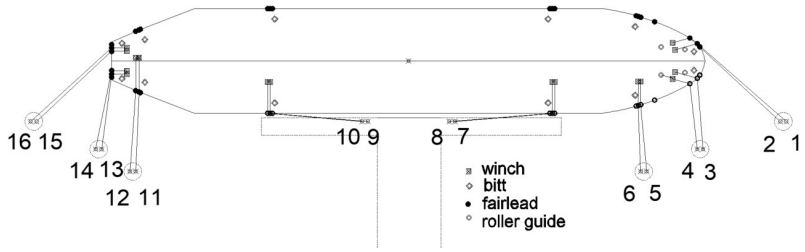

Figure F.1: *Mooring configuration $T0Y$ at jetty berth conform OCIMF.*

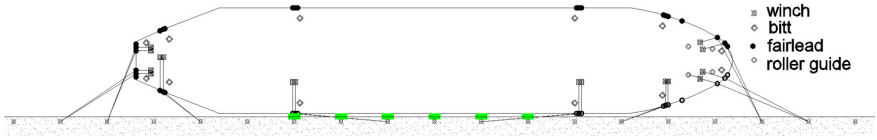

Figure F.2: *Mooring configuration $T0Y$ at multi-purpose berth.*

Table F.2: *Mooring line angles, mooring line lengths and efficiency parameters $T0Y$, multi-purpose berth mooring configuration (figure F.2).*

line n°	α	β	θ	l_{bf}	l_{fw}
1	138	13	137	54	7.6
2	137	14	136	50	9.9
3	131	27	127	27	9.9
4	140	26	134	28	7.6
5	160	30	146	25	9.9
6	162	29	147	25	10.2
7	5	16	21	45	13.3
8	5	16	17	44	13.3
9	175	17	18	42	13.3
10	175	17	18	43	13.3
11	72	43	105	18	14.7
12	79	42	99	18	14.1
13	59	27	118	27	6.4
14	60	26	118	28	6.4
15	43	15	136	46	6.4
16	44	15	135	47	6.4

F.1.3 Ship hydrodynamics

The hydrodynamic parameters added mass (a) and (radiation) damping (b) were calculated using Hydrostar, for 20 % UKC, figure F.3.

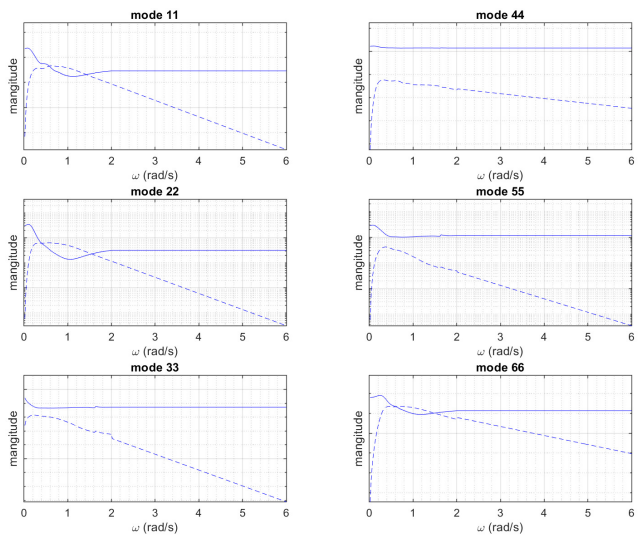

Figure F.3: *Hydrodynamic coefficients diagonal terms a and b matrix for $T0Y$, 20% UKC.*

F.2 $ULCS$

The $ULCS$ of Ultra Large Container Ship represents a generic container ship of length 400.0 m. Her properties are largely derived from the UASC Barzan, as described in *RINA Significant Ships of the year 2015*, figure F.4. This case was presented in two papers published by the candidate. [Van+19a] presents the effect of the mooring arrangement on the ship's response under ship passages. [Van+19b] gives a critical review on the wind force calculation on ships.

In the thesis text, the case is discussed in the following sections :

- Section 3.2 elaborates on the mooring equipment found on board of such container ships and makes a comparison with prescribed international standards.
- Section 4.3.4 discusses the use of efficiency parameters to describe the mooring arrangement. The $ULCS$ case study is used to illustrate the potential of the efficiency parameter definition. This section is based on [Van+19a].
- Section 5.3 elaborates on the wind force calculation based on wind coefficients for large container ships. The $ULCS$ case is used to quantify the effect of a rough wind profile on the calculation of wind forces.

F.2.1 Hull, superstructure and mooring parameters

The hull characterises, mooring equipment and superstructure parameters which are relevant for the case study example are given in table F.3.

F.2.2 Mooring configurations

In order to evaluate the theory behind the efficiency parameters, several mooring configurations were defined and compared for the $ULCS$. Figure F.5 is the mooring arrangement which is considered as the standard configuration when mooring at a container berth. The mooring line angles and lengths, as well as efficiency parameters, are given in table F.4

Figure F.4: *Container ship UASC Barzan, used as basis for the generic $ULCS$ ship case study.*

Table F.3: *Characteristic parameters hull and mooring equipment $ULCS$.*

Hull and superstructure characteristics			
L_{OA} (m)	400.0	Δ (ton)	228861
L_{PP} (m)	383.0	H (m)	56.1
B (m)	58.6	$\bar{H}$ (m)	44.0
T_M (m)	14.5	A_{f} (m²)	3146
D (m)	30.6	A_{l} (m²)	17583
Mooring equipment			
MBL (ton)	148.7*	n_{l}	16*

* Based on data 37 ships of similar size

Figures F.6 and F.7 give all mooring configuration which were discussed in [Van+19a].

- **MC0, L2+NL1** illustrates the benefits of using stiff HMPE lines (L2) in combination with elastic tails (NL1) to replace the medium elastic lines (L1).
- **MC1, L1** shows the effect of changing the line length of one of the aft springs (figure F.6 (a))
- **MC2, L1** shows the effect crossing the aft lines (figure F.6 (b))
- **MC3, L1** shows the effect crossing the fore lines (figure F.6 (c))
- **MC4, L1** shows that crossing of fore and aft lines results in more efficient mooring lines (figure F.6 (d))
- **MC5, L1** moves the winches from the (higher) forecastle deck to a lower mooring deck on the same level as the aft mooring deck (figure F.6 (e))
- **MC6, L1** addition of winches at funnel and accommodation position in order to add two pairs of spring lines (figure F.7 (a)-(b))
- **MC7, L1** combination of MC4,MC5,MC6, with stiff lines + tail in order to see how much improvement is theoretically possible given the proposed optimisation steps (figure F.7 (c)-(d))

F.2.3 Efficiency parameter summary

The efficiency parameters, $\mathrm{e}_{X\mathrm{p}}$ and $\mathrm{e}_{X\mathrm{n}}$, for all $ULCS$ mooring arrangements MC0-MC7, are given in table F.5. Figure 4.12 compares the prediction using efficiency parameters with the surge motion calculated by *Vlugmoor* (quasi-static), as an extension of figure F.8 from the main text.

Figure F.5: *Mooring arrangement MC0, $ULCS$*

Table F.4: *Mooring line angles, mooring line lengths and efficiency parameters $ULCS$, MC0 (figure F.5).*

line n°	α	β	θ	l_{bf}	l_{fw}	e_{Xi}	e_{Yi}
1	45	6	144	71.3	5.0	0.36	0.36
2	41	6	141	66.5	5.8	0.43	0.33
3	50	9	131	46.9	5.8	0.43	0.60
4	44	9	134	42.5	5.8	0.57	0.55
5	65	17	112	24.5	5.8	0.30	1.38
6	55	22	113	18.8	5.0	0.66	1.36
7	176	10	94	42.4	45.8	-0.61	0.00
8	176	10	94	39.2	12.0	-1.05	0.01
9	20	27	110	28.1	23.6	0.76	0.10
10	21	20	110	37.4	7.2	0.97	0.14
11	102	40	138	19.5	22.9	-0.04	0.73
12	74	27	76	28.2	6.2	0.10	1.20
13	137	17	135	44.1	7.0	-0.53	0.47
14	131	15	128	48.7	7.0	-0.40	0.53
15	143	11	141	67.8	6.2	-0.46	0.27
16	142	8	52	85.9	7.7	-0.36	0.22

Table F.5: *Efficiency parameters $ULCS$ for MC0 to MC7.*

Config	Action	line type	$\mathrm{e_{X}}_p$	$\mathrm{e_{X}}_n$	$\mathrm{e'_{X}}_p$	$\mathrm{e'_{X}}_n$
MC0	Ref config	L1	4.60	3.44	4.60	3.44
MC0	Stiff lines	L2 +NL1	4.60	3.44	10.92	8.16
MC1	Spring change	L1	4.50	3.47	4.50	3.47
MC2	Cross aft	L1	4.69	3.53	4.69	3.53
MC3	Cross fore	L1	4.61	4.15	4.61	4.15
MC4	Cross all	L1	4.70	4.25	4.70	4.25
MC5	Lower deck	L1	5.64	4.60	5.64	4.60
MC6	added springs	L1	6.50	5.52	6.50	5.52
MC7	MC2+MC5+MC6	L2 +NL1	7.68	6.84	18.66	16.62

(a) $ULCS$, MC1

(b) $ULCS$, MC2

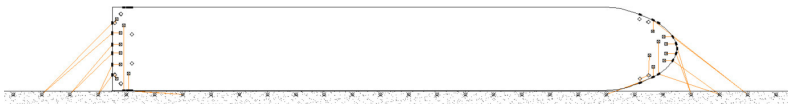

(c) $ULCS$, MC3

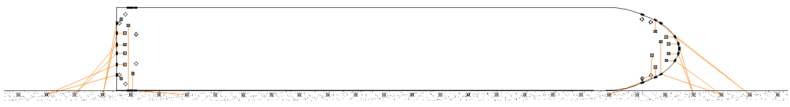

(d) $ULCS$, MC4

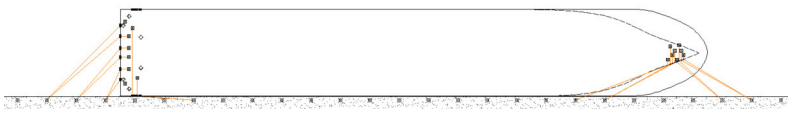

(e) $ULCS$, MC5

Figure F.6: *Mooring arrangements $ULCS$, part I.*

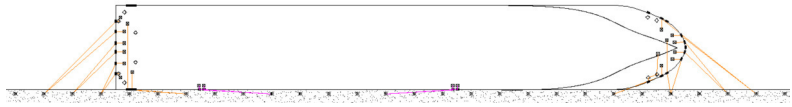

(a) $ULCS$, MC6, top view

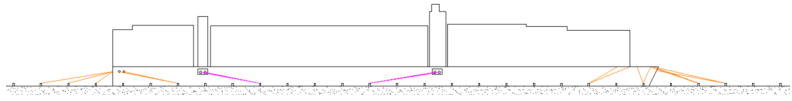

(b) $ULCS$, MC6, side view

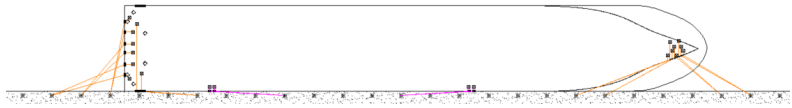

(c) $ULCS$, MC7, top view

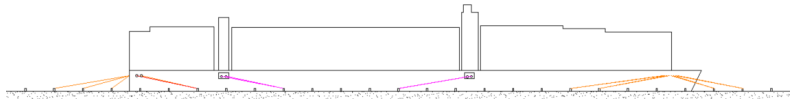

(d) $ULCS$, MC7, side view

Figure F.7: *Mooring arrangements $ULCS$, part II,, orange lines = 16 mooring lines as present on the $ULCS$ study example, purple = addition of two sets of springs.*

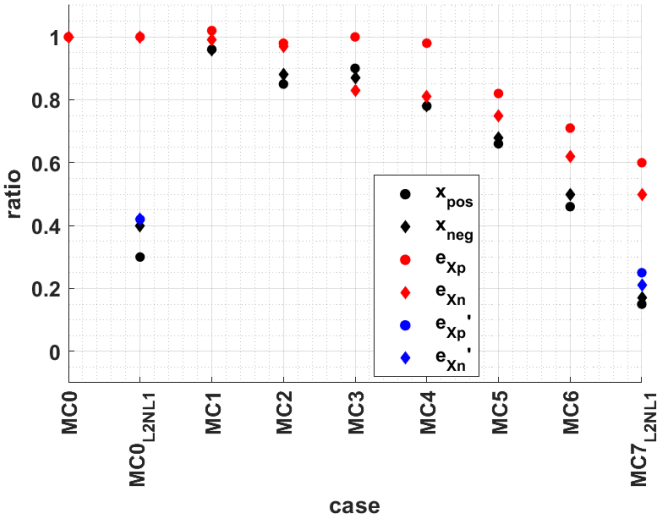

Figure F.8: *Longitudinal ship motion calculated using Vlugmoor and efficiency parameter ratios, made non-dimensional with the values for the reference configuration (MC0). Expanded version of figure 4.12, MC1, MC2 and MC3 were added.*

F.2.4 Wind surfaces

The wind surfaces (frontal and lateral)for the $ULCS$ at T_{M} = 14.5 m are given in figure F.9.

(a) A_{f} (b) A_{l}

Figure F.9: *Definition wind surfaces $ULCS$*

References

[Van+19a] T. Van Zwijnsvoorde et al. “A mooring arrangement optimisation study”. In: *11th International Workshop on Ship and Marine Hydrodynamics*. Hamburg, Germany, 2019.

[Van+19b] T. Van Zwijnsvoorde et al. “Wind modeling for large container vessels: a critical review of the calculation procedure”. In: *International Journal of Transport Development and Integration* 3.4 (2019), pp. 369–381.

List of Figures

List of Tables

Hutchison Ports ECT Rotterdam.